CNGB1 MUTATION IN PAPILLON DOGS: THE IDENTIFICATION, CHARACTERIZATION AND CURE

By

Paige A. Winkler

A DISSERTATION

Submitted to
Michigan State University
in partial fulfilment of the requirements
for the degree of

Genetics – Doctor of Philosophy

2015

PUBLIC ABSTRACT

CNGB1 MUTATION IN PAPILLON DOGS: THE IDENTIFICATION, CHARACTERIZATION AND CURE

By

Paige A. Winkler

Progressive retinal atrophy (PRA) is an inherited retinal dystrophy that affects over 100 breeds of dogs. Typically the disease begins with loss of dim-light vision and then progresses to total blindness. The loss of dim-light vision is due to a mutation in a gene that is necessary for rod photoreceptor development, maintenance or function. PRA is the canine equivalent of a human disease, retinitis pigmentosa (RP), which affects about 1 in 4000 people. Mutated genes that cause PRA in dogs are often the same genes that cause RP in humans. Information gleaned from PRA can be used to help understand RP in humans.

Papillon dogs are one of the 100 breeds of dogs that are affected with PRA. In this dissertation, I have identified a mutation in the gene *CNGB1* which accounts for 70% of the PRA in the Papillon dogs. The *CNGB1* gene codes for a protein that is necessary for rod phototransduction and olfactory transduction. Human patients with RP type 45 also have mutations in the *CNGB1* gene.

The *CNGB1* affected dogs have abnormal and decreased rod function at the earliest age tested. Normal day light (cone photoreceptor) vision is maintained until cone function decreases between 4 and 5.5 years of age. However, dogs maintain navigational day-light vision for many more years. These functional data, coupled with *in vivo* and *ex vivo* histological data, show that the disease results in a slow retinal degeneration that will eventually lead to complete blindness.

Gene replacement therapy is a method of supplying a cell with the means to produce a normal protein in place of the abnormal or absent protein caused by a mutation in a gene. Gene therapy has been proven successful in research and clinical settings, especially in the context of retinal degenerations. We used a viral vector to introduce a copy of the normal dog *CNGB1* gene back into the rod photoreceptors in the *CNGB1* affected dogs. The gene therapy was able to rescue rod function and the rescue was maintained until the last data point was collected 9 months after injection.

The olfactory involvement of the *CNGB1* mutation was investigated in the *CNGB1* affected dogs. The olfactory epithelium and the olfactory bulbs were abnormal in the *CNGB1* affected dogs when compared to control dogs. I developed a behavioral test that could assess olfactory function in the *CNGB1* dogs with very little training. The *CNGB1* affected dogs had decreased but not absent olfactory function.

The detailed descriptions of the retinal and olfactory phenotypes, in addition to the successful gene replacement therapy trial, in the *CNGB1* affected dogs have laid the ground work for future studies including working with clinicians to advance gene replacement therapy trials in human patients with mutations in the *CNGB1* gene.

ABSTRACT

CNGB1 MUTATION IN PAPILLON DOGS: THE IDENTIFICATION, CHARACTERIZATION AND CURE

By

Paige A. Winkler

Progressive retinal atrophy (PRA) is an inherited retinal dystrophy that affects over 100 breeds of dogs. It is characterized by a bilateral retinal degeneration commonly resulting in blindness. Affected dogs typically present with loss of dim light vision, attenuation of retinal blood vessels and tapetal hyperreflectivity. The purpose of this study was to identify the underlying cause of PRA in Papillon dogs and to characterize the phenotype at the cellular and molecular levels.

I identified a mutation in the gene *CNGB1* which accounts for 70% of the PRA in the Papillon dogs. The *CNGB1* mutation involves a 6 base pair insertion and a 1 base pair deletion resulting in exon skipping and a premature stop codon cause by a frameshift. *CNGB1* encodes the β-subunit of a cyclic nucleotide-gated ion (CNG) channel. *CNGB1* has multiple splice variants expressed in rod photoreceptors, olfactory sensory neurons and other tissues. CNG channels are directly involved in rod phototransduction and olfactory transduction.

The retinal phenotype of the *CNGB1* affected dogs was characterized by *in vivo* and *ex vivo* analyses. Electroretinograms (ERGs) and behavioral vision testing were conducted to assess retinal function throughout the course of the disease. The *CNGB1* affected dogs had decreased and abnormal rod function at the earliest age tested but cone function was preserved until 5.5 years of age. Histological analyses showed that

the morphology of rod photoreceptors deteriorate slowly over the first ~1.5 years of life while cone photoreceptor morphology is preserved for longer.

Adeno-associated viral (AAV) vector therapy was used to treat five *CNGB1* affected dogs with a wild-type copy of canine *CNGB1* cDNA. One eye was injected with a low titer ($1x10^{12}$) of an AAV vector delivering *CNGB1* cDNA, six eyes were injected with a higher titer ($5x10^{12}$) and one eye was injected with a GFP-expressing construct as a vehicle and procedural control. All dogs treated with the AAV vector containing the wild-type copy of *CNGB1* showed rescue of rod function that was maintained throughout the time course of the study (9 months).

The *CNGB1* affected dog olfactory phenotype was investigated using *in vivo* and *ex vivo* techniques. The olfactory epithelium and the olfactory bulbs were abnormal in the *CNGB1* affected dogs when compared to control dogs. I developed a behavioral test that could assess olfactory function in the *CNGB1* dogs. The *CNGB1* affected dogs had decreased but not absent olfactory function.

The detailed descriptions of the retinal and olfactory phenotypes, in addition to the successful gene replacement therapy trial, in the *CNGB1* affected dogs have laid the ground work for future studies including working with clinicians to advance gene replacement therapy trials in human patients with mutations in the *CNGB1* gene.

Copyright by
PAIGE A. WINKLER
2015

This dissertation is dedicated to the dogs.
Their contribution was not taken lightly.

ACKNOWLEDGMENTS

I would like to thank my advisors, Dr. Simon Petersen-Jones and Dr. Patrick Venta. I am profoundly grateful for the countless hours they spent mentoring me. Most importantly for having confidence in me when I didn't have it in myself.

I would also like to thank my committee members: Dr. Hans Cheng, Dr. Stephan Carey and Dr. Colleen Hegg. I truly do not think I could have made it through the past 5 years without such patient and amazing mentors.

There are so many people who had a strong impact on me and this dissertation:

- Dr. Cathy Ernst, director of the Genetics Program; Dr. Brian Schutte, associate director of the Genetics Program; Dr. Barb Sears, former director of the Genetics Program; Jeannine Lee and Cindy Robinson.
- Dr. Vilma Yuzbasiyan-Gurkan, the VYG lab (past and present) and the Comparative Medicine and Integrative Biology community
- Ethan Dawson-Baglien and Dr. Laurence Occelli, my partners in crime.
- Dr. Andrea Minella and Dr. Marianna Bacellar, labmates and friends.
- Janice Querbin. The most amazing person on earth and without whom no puppies would have been born and no ERGs would have been run.
- Dr. Erika Sikina and Jennifer Davis, who spent many hours doing olfaction testing
- Christine Harman, Kristen Kohl and Michelle Fritz, for keeping all the PIs under control

- Lisa Allen, Kim Williamson and the rest of the vivarium staff for taking care of my dogs daily.
- The Papillon Club of America, Leona Domino and Sandy Vaillancourt. The Papillon Club of America has provided funding and support for this dissertation. Leona and Sandy flew to Sweden to pick up our foundation stock for this project. They opened their hearts and their homes to the dogs that started everything.
- All the breeders, owners and dogs that contributed samples to this project.
- The Myers-Dunlap Endowment Fund, Michigan State University College of Veterinary Medicine Endowed Research Funds, College of Natural Science Fellowships and Portuguese Water Dog Club of America for all the financial support.
- My parents, Mike and Cathy Winkler. Who gave me monetary and emotional support when I needed it and took care of my dogs whenever I needed a break.
- My brother and sister-in-law, Ross and Norah Winkler. For being supportive, teaching me how to peel a mango and for being ninjas.
- Josh Smith, for thinking that dating a grad student was a good idea, never ending support and for giving me a reason to graduate.

TABLE OF CONTENTS

LIST OF TABLES

LIST OF FIGURES

KEY TO ABBREVIATIONS

kb – kilobases

bp – base pairs

SNPs – single nucleotide polymorphisms

GWAS – genome wide association studies

PRA – progressive retinal atrophy

RP – retinitis pigmentosa

OS – outer segments

IS – inner segments

ONL – outer nuclear layer

ERG – electroretinography or electroretinogram

OCT – spectral domain-optical coherence tomography

CNG – cyclic nucleotide-gated

CNGB1 – cyclic nucleotide-gated ion channel beta subunit

CNGA1 – cyclic nucleotide-gated ion channel alpha subunit

OE – olfactory epithelium

OSN – olfactory sensory neurons

OB – olfactory bulb

AAV – adeno-associated virus

IHC – immunohistochemistry

CHAPTER 1

INTRODUCTION

1.1 Domestication of the dog and development of dog breeds

1.1.1 Domestication of dogs

In the thousands of years that dogs have been man's best friend they have provided aid in day to day activities and companionship. While we know that dogs have been at our sides for a very long time the actual timeframe and location of canine domestication is a hotly debated topic between evolutionary geneticists, archaeologists and paleontologists [1]. There does seem to be a consensus that modern day canines are descendants of gray wolves but the widespread distribution of wolves throughout Eurasia does not aid in pinpointing a location for domestication [2-5]. Archaeologists have found dog bones buried with human remains dated to 12,000 years ago in the Middle East and 16,000 years ago in Eurasia [1]. Dog-like remains were found in Europe that date to over 30,000 years ago indicating a much earlier date of domestication than previous archaeological studies [5,6]. While archaeological evidence is hard to dispute, the skeletal differentiation between domesticated dog and wild wolf could bias the timeframe. It is possible that dogs were domesticated well before their skeletal/morphological divergence from wolves [5].

Molecular genetic data has been utilized in the attempt to identify a timeframe and location. Mitochondrial DNA studies of dogs and other canid species have suggested that canine domestication could have started over 100,000 years ago in multiple locations throughout Eurasia [3,7]. However, other studies using mitochondrial DNA have provided evidence that a single dog domestication event happened less than 16,300 years ago in China [2]. Studies involving genomic DNA, which removes the maternal bias from the previous studies, have shown significant influences of Middle

Eastern wolves on the domesticated dog genome [5]. The likely continued intermixing of domesticated dogs and wild wolf populations has created a tangled web of genetic diversity that researchers are still trying to sort out [5]. Despite the controversy behind the time and location of the domestication of the dog there is little disagreement on the impact this event had on humans.

1.1.2 Development of dog breeds

Ancient art and descriptions of types of dogs have implicated the existence of 'breeds' for thousands of years. Early dogs were bred selectively to enhance certain behaviors to aid humans in their work. Herding and hunting 'proto-breeds' are examples of the result of strong behavioral selection [4,8]. Dogs were also selected for morphological traits (physical characteristics, coat color/length and size). In the mid-1800s, defined breed standards started to emerge [8]. The formation of breed clubs, and the rules and competition involved, created the reproductively isolated breeds that we are familiar with today [9]. One of the rules of breed clubs is the breed barrier rule that requires that a dog's parents must be registered in order for a dog to be registered. This creates the genetic isolation of breeds from one another [9]. The result of the breed barrier rule has created hundreds of breeds that are highly phenotypically variable. To date, the American Kennel Club recognizes 184 dog breeds and the Federation Cynologique Internationale (an international federation of kennel clubs) recognizes 343 dog breeds (www.akc.org, www.fci.be). Using a molecular approach, breeds can be clustered together in two main groups; ancient breeds and modern breeds. Ancient breeds include Asian breeds (e.g. Akita, Shiba Inu and Chow Chow), African breeds (e.g. Basenji), Arctic breeds (e.g. Siberian Husky and Alaskan Malamute) and the

Middle Eastern sighthounds (e.g. Afghan Hound and Saluki) [8,9]. The modern breeds include all other breeds known which can be further clustered into four main groups; the mastiff/terrier breeds, herding/sighthound breeds, hunting breeds and mountain breeds [8,9]. The clustering of these breeds used a combination of genetic techniques made possible with the high quality sequencing and publication of the canine genome.

1.2 The canine genome

Dogs have 39 pairs of chromosomes; 38 pairs of autosomes and one pair of sex chromosomes. The 38 autosomes are telocentric, meaning that their centromere is near the end of the chromosome [10,11]. In 2005, a high quality draft of the canine genome was compiled by Lindblad-Toh *et al.* at the Broad Institute of MIT and Harvard. The genome was sequenced using a whole-genome shotgun approach resulting in 7.5X coverage of the canine genome. A female boxer was sequenced; the dog was chosen because of its low genetic variability, which made assembly of the genome easier because, for example, segmental duplications were easier to detect [4].

The most highly studied mammalian genomes (human, chimpanzee, mouse and rat) only represent two Orders of placental mammals. The dog belongs to a third Order and the publication of the canine genome allows for comparative genomics between the three Orders [4]. The dog genome has about 2.5 billion base pairs of DNA, similar to that of humans (2.9 billion) and mouse (2.6 billion) [4,12,13]. Dogs have ~19,300 protein coding genes, almost all of these genes have orthologs to human genes. Humans have about 22,000 genes and mice have ~23,000, with the differences in gene numbers being primarily due to large expansions of particular gene families [4,12,14].

Dog population structure is unique because there is less variation within breeds and more variation across breeds than is seen in many other types of animals. Intrabreed linkage disequilibrium (LD) is nearly 100X longer than interbreed LD [4]. The LD within a breed is on the order of megabases while the LD across breeds is on the order of kilobases (kb), similar to what is seen in European human populations where LD is (<100 kb) [4,15]. Although LD varies between intra/interbreed dogs and humans,

the density of single nucleotide polymorphisms (SNPs) is comparable (1/900 intrabreed; 1/1,600 interbreed; 1/1,000 human) [4,16].

1.3 Canine models of inherited diseases

In population genetics there are three key factors upon which I will focus, due to their context in canine genetics, which can modulate genetic drift within a species; effective population size, selection and founder events. Genetic drift is defined as a process of evolutionary change involving the random sampling of alleles from the parental population and the passing of those alleles on to the next generation [17,18]. Understandably, the size of the parental population (and the frequency of the allele) has a strong effect on the probability of an allele being passed from one generation to the next. However, it is not the census size of the population that determines this; it is the number of individuals that actually pass their genetic information on to the next generation. This is the basis of the concept of effective population size. The individuals who do not successfully reproduce do not have any influence on the next generation. Factors such as unequal numbers of the sexes and inbreeding can have large impact on the effective population size [19]. Inbreeding increases the likelihood of the same allele being inherited by an offspring by decreasing the number of available alleles that can undergo selection [17,18].

The degree to which individuals pass their genetic information can be influenced by natural selection (the individual is more fit due to their combination of alleles and is therefore more likely to successfully reproduce) or artificial selection (breeding of plants and animals and the propagation of desired traits controlled by humans).

The frequencies of alleles in a population can also be influenced by founder or bottleneck events. A founder event occurs when a small part of a population breaks away from a larger population thereby losing some of the genetic variation of the

original population [18]. A population bottleneck occurs when the effective population size decreases drastically [18]. An example of this is the importation of a breed recognized in Europe to America. A small group of dogs will be brought overseas and that small group will be used to create an American population. It is easy to appreciate the loss of genetic diversity in the future American dogs by starting a new population with only a select few dogs from Europe. The creation of the breed barrier rule created a founder event resulting in all dogs that exist within a breed today are from an original set of registered dogs.

A small effective population size with strong selection (artificial or natural) can have a huge effect on genetic drift [18]. The development of dog breeds is a prime example of artificial selection, where physical characteristics and behaviors have been selected and fixed within breeds by humans. In artificial selection, humans would not knowingly select for a disease causing allele. However, it is possible that a deleterious allele could be linked to a positive trait that is being selected. In addition, a popular animal (e.g. a winner of a dog show), which is a carrier for a deleterious mutation, could be used to produce many offspring, increasing the frequency of that deleterious allele within the breed [18].

Putting these genetic concepts in the context of dog breeds and breeding, it is not surprising that rare alleles can increase in frequency within a breed. Humans selectively breed for certain characteristics and behaviors in their dogs, complying with a strict breed standard. Occasionally, a highly successful dog will be bred to produce hundreds or thousands of descendants because that dog stands out as an excellent representative of the breed [20]. The excessive use of one individual can result in

founder events within a breed. A group investigated the population structure and effective population size of 10 breeds registered in the United Kingdom Kennel Club. They found that in some breeds, one popular sire could produce over 1,000 offspring. Additionally, they found that the effective population size of the breeds was very low due to inbreeding and the use of popular dogs. Golden retrievers had a registration population of over 31,000 animals but the calculated effective population size was 67 individuals [20]. Boxers, mentioned previously to have been chosen for genomic sequencing due to the low genetic variability of one member, had a registration population size of 44,000 and an effective population size of 45 [20]. These breeds both had an extensive use of popular sires and dams, meaning that from one generation to the next only a fraction of the potential parental dogs were used to produce the next generation.

These features of the canine population structure make dogs ideal for disease research. The publication of the high quality draft sequence of the genome in 2005, the advances of tools for genome wide association studies (GWAS) and next generation sequencing has allowed canine models to emerge as useful models of human disease [21]. Breeders and owners are concerned with the health and welfare of their dogs and many breed clubs require health tests that dogs must pass in order to be bred. This is a useful approach for catching early- and mid-age diseases. However, a dog may no longer get the health tests after they are retired from breeding. If disease occurs at a young age in a breeding animal, the dog is not used for breeding and these types of mutations can be removed from the gene pool. Recessive and late onset deleterious diseases can be carried through the generations unnoticed. Due to inbreeding and the

use of popular dogs the likelihood that an offspring will inherit two copies of these deleterious alleles increases. Because of the population and breeding structure within dog breeds, most Mendelian diseases identified have locus and allelic homogeneity, meaning that a majority of diseases found within a breed are caused by an identical mutation in one gene, generally descended from a single founder. There are, however, a few instances of locus heterogeneity identified in dog breeds, progressive retinal atrophy being a prime example [22].

The extent of LD and availability of variable SNPs reduces the number of SNPs needed for GWAS compared to outbred populations such as humans. Some researchers predicted that only ~10,000 SNPs are needed to map traits [4]. However, an Illumina High Density Canine SNP bead array has been developed that utilizes over 170,000 SNPs spaced across the canine genome is available for researchers to use in their GWAS studies.

Studying canine diseases can benefit both dog and man. Identifying a disease causing mutation can allow the development of a genetic test for breeders to utilize in their breeding program and provides the potential to virtually extinguish a disease in only a few generations. Approximately 80% of canine genetic diseases have a corresponding human genetic disease [21]. Understanding how a disease manifests and progresses can be studied extensively in dogs which can lead to a better understanding of the comparable disease in humans [23]. For example, canine cancer has a similar etiology to human cancers and they have a similar response to treatments. Certain breeds are predisposed to certain types of cancer which implies a genetic basis for the disease [23]. Additionally, a mutation has been identified in Golden retrievers

that results in Duchenne X-linked muscular dystrophy. The canine disease matches the human disease so closely that therapies are being tested in affected dogs in hopes of developing a therapy for affected humans [21,23].

Therapies derived for the canine disease can often lead to clinical trials for the human disease. A particularly relevant example of this is the mutation in the *RPE65* gene in Briard dogs. This mutation causes an autosomal recessive retinal degeneration in the dog. The human analog of this disease is Leber congenital amaurosis in which children are born blind or become blind at a very early age. Acland *et al.* used gene replacement therapy to insert a working copy of the *RPE65* gene and provided the long term rescue of vision in the dog model [24]. Just a few years after this pivotal study, gene replacement therapy trials in humans were initiated with positive results [25].

1.4 Inherited retinal dystrophies in dogs

Inherited retinal dystrophies in dogs include progressive retinal atrophy (PRA), achromatopsia and Leber congenital amaurosis models. Canine achromatopsia (Ach) is a retinal dystrophy that is stationary, i.e. there is little change in vision during the course of the patient's life. Ach is caused by mutations in cone specific proteins (*CNGA3*, *CNGB3*) resulting in non-functional cones but the rods are unaffected [26,27]. The dogs are not able to see using cone-mediated (day-light and bright-light) vision but can see in dimmer light settings when the rods are functioning. Canine models of Leber congenital amaurosis (LCA) show retinal dysfunction very early in life and progress slowly if it progresses at all. A well-known canine LCA model, the *RPE65-/-* briard dog were originally described to have congenital stationary night blindness but were later reclassified because there is histological evidence of a very slow retinal degeneration [27].

1.4.1 Progressive retinal atrophy in dogs

PRA is a genetically heterogeneous retinal dystrophy reported in over 100 breeds of dog [28]. All forms of PRAs have a similar clinical presentation but the age of onset, the effect on the ERG and the progression differ depending on the underlying gene mutation. Typically PRA presents as an initial loss of night and peripheral vision and with progression day vision is also effected eventually leading to complete blindness in most instances. The entire retina degenerates over time which leads to attenuation of the retinal blood vessels and hyperreflectivity of the tapetum lucidum (Figure 1.1). The most common forms of PRA are recessively inherited but X-linked and

dominantly inherited forms have been identified [27].To date there are mutations in 19 genes that cause retinal dystrophies in dogs (Table 1.1) [22,27,29,30].

Figure 1.1. Canine fundus images. Left, 6 month old dog affected with PRA. At this early stage of the disease, the fundus looks normal. Right, 3.5 year old dog affected with PRA; note the tapetal hyperreflectivity, attenuation of retinal vasculature and the atrophy of the optic nerve head.

Identification of casual mutations in PRA affected dogs can be challenging due to the genetic heterogeneity of the disease [22]. It is becoming increasingly recognized that more than one gene mutation causing PRA can be segregating within a single breed [27,31-33]. However, the population structure and well-kept pedigrees of purebred dogs can aid in identifying family groups to study increasing the possibility of focusing on one locus at a time. Additionally, age of onset, the type of cell that is dysfunctional in early stages of the disease (determined by ERG) and the rate of progression of the disease are all features that can be used to characterize and classify the phenotype. While end-stage PRA due to any gene mutation looks similar both ophthalmoscopically and electroretinographically, studying dogs at early stages and careful phenotyping of the disease can be very valuable to identify candidate genes and/or potential instances of locus heterogeneity.

PRA is homologous to the human diseases retinitis pigmentosa (RP) and for the early onset forms, Leber congenital amaurosis. Because of the similarities of PRA to RP and LCA, PRA affected dogs can be used as models for studying inherited retinal degenerations. Dogs are diurnal and share the same environment as their human counterparts which allows for the study of any environmental factors that might be involved in a disease. Dog and human eyes are similar in size and shape which aids in optimizing translational therapies. Dogs have a region of higher photoreceptor density (the *area centralis*) which is comparable to a human macula. Dogs are ideal models for studying eye diseases for a better understanding of the progression of the disease and development of future therapies.

PRA can subdivided into rod-cone dysplasias, rod-cone degenerations or cone-rod dystrophies as determined by retinal functional testing by electroretinography (ERG) and by histological investigation. Each of these forms of photoreceptor dystrophy show different histological and ERG characteristics and the age of onset can vary considerably. Classical PRA is a rod-led degeneration in which the rods either fail to develop normally and degenerate (rod-cone dysplasias) or they mature normally but then degenerate (rod-cone degenerations). Dogs with rod-cone dysplasia may have an abnormal rod ERGs at a very young age and the ERGs may never fully develop. With the rod-cone degenerations function develops normally but then the amplitudes of the ERG decreases over time paralleling the loss of rods. A retinal dystrophy is classified as a cone-rod dystrophy when the cone photoreceptors are affected either prior or simultaneously with the rod photoreceptors. This effect on cone photoreceptors manifests as decreased daylight vision and abnormal or diminished cone ERGs.

Understanding which photoreceptor type is initially involved, and whether there is dysfunction prior to degeneration can suggest potential candidate genes for the condition. Table 1.1 shows a list of known retinal dystrophies in dogs.

Table 1.1. Genes associated with inherited retinal dystrophies in dogs

Gene	Breed(s)	Inheritance[1]	Human Disease[2]	Ref
ADAM9	Glen of Imaal terrier	aR	CORD	[34]
c1orf36	Collie	aR	arRP	[35]
c2orf71	Multiple breeds	aR	arRP	[33,36]
CCDC66	Schapendoes	aR	arRP	[37]
CNGA1	Shetland sheepdogs	aR	arRP	[38]
CNGA3	German shepherd dogs	aR	Ach	[39]
CNGB1	Papillons	aR	arRP	[31]
CNGB3	Alaskan malamute, German shorthaired pointer	aR	Ach	[26]
FAM161A	Tibetan terrier, Tibetan spaniel	aR	arRP	[40]
IQCB1	Pit bull terrier	aR	CORD	[41]
NPHP4	Standard wirehaired dachshund	aR	CORD	[42]
PDE6A	Cardigan welsh corgi	aR	arRP	[43]
PDE6B	Irish setter, sloughi, American Staffordshire terrier	aR	arRP	[41,44, 45]
PRCD	Multiple breeds	aR	arRP	[46]
RHO	Mastiff	aD	adRP	[47]
RPE65	Briard	aR	LCA	[48]
RPGR	Siberian Husky, Mixed breed	X	XRP	[49]
RPGRIP1	Miniature longhaired dachshund	aR	CORD	[50]
SAG	Basenji	aR	arRP	[51]
SLC4A3	Golden Retriever	aR	arRP	[32]
STK381	Norwegian elkhound	aR	arRP	[52]
TTC8	Golden Retriever	aR	arRP	[22]

1. Mode of inheritance: aR, autosomal recessive; aD, autosomal dominant; X, X-linked.
2. Associated human disease: arRP, autosomal recessive retinitis pigmentosa; adRP, autosomal dominant retinitis pigmentosa, XRP, X-linked retinitis pigmentosa; LCA, Leber congenital amaurosis; CORD, cone-rod dystrophy; Ach, achromatopsia.

1.5 Inherited retinal dystrophies in humans

Inherited retinal dystrophies are genetically and phenotypically heterogeneous disorders. Mutations in 238 genes have been identified that cause some form of inherited retinal dystrophy (https://sph.uth.edu/Retnet/home.htm). Over 80 of these genes have visual impairment as part of a syndrome in which multiple tissues in the body are affected; these are termed syndromic retinopathies and will not be discussed further. Retinal dystrophies can have an autosomal dominant, recessive or X-linked mode of inheritance. Some retinal dystrophies have been associated with multiple modes of inheritance based on the severity of the mutation in the gene responsible for the disease [53]. To complicate matters, different mutations within one gene can result in different retinal dystrophies depending on the part of the gene mutated and the effect of the mutation. All of these factors combined make clinical and genetic classification challenging to obtain [53,54]. While all forms of retinal dystrophies are important I will be focusing on three progressive inherited retinal dystrophies which are homologous to PRA in dogs; retinitis pigmentosa (RP), LCA and cone-rod dystrophies (CORD). Table 1.2 shows a compiled list of genes in which mutations have been identified and cause one of these diseases.

Table 1.2. Inherited retinal dystrophy genes and associated type organized by proposed involvement in the retina

Gene	Type[1]	Inheritance[2]
Phototransduction cascade		
CNGA1	RP49	aR
CNGB1	RP45	aR
GUCA1A	CORD14	aD
GUCA1B	RP48	aD
GUCY2D	LCA1, CORD6	aR, aD
KCNJ13	LCA16	aR
PDE6A	RP43	aR
PDE6B	RP40	aR
PDE6G	RP57	aR
RHO	RP4	aR, aD
SAG	RP47	aR
Vitamin A metabolism/visual cycle		
ABCA4	RP19, CORD3	aR, aD
LRAT	jRP, LCA14	aR
RBP3	RP66	aR
RDH12	RP53, LCA13	aR
RGR	RP44	aR
RLBP1	naRP	aR
RPE65	RP20, LCA2	aR
Structural or cytoskeletal		
CRB1	RP12, LCA8	aR
FSCN2	RP30	aD
PRPH2	RP7, LCA18	aR, aD
RDS	LCA18, RP7	aR, aD
RP1	RP1	aR, aD
TULP1	RP14, LCA15	aR
RNA intron-splicing factors		
PRPF3	RP18	aD
PRPF31	RP11	aD
PRPF4	RP70	aD
PRPF6	RP60	aD
PRPF8	RP13	aD
RP9	RP9	aD
CACNA1F	CORDX3	X
CLRN1	RP61	aR
RIMS1	CORD7	aD

Table 1.2. cont'd

RP2	RP2	X
SEMA4A	RP35, CORD10	aR, aD
USH2A	RP39	aR
Photoreceptor morphogenesis		
CDHR1	RP65, CORD15	aR
PROM1	RP41, CORD12	aR
AIPL1	jRP, LCA4, naCORD	aR, aD
ARL6	RP55	aR
C2orf71	RP54	aR
CEP290	LCA10	aR
IFT172	RP71	aR
KIZ	RP69	aR
LCA5	LCA5	aR
RPGR	RP3, RP15, CORDX1	X
RPGRIP1	LCA6, CORD13	aR
TTC8	RP51	aR
Retinal development and/or maintenance		
CRX	LCA7, CORD2	aR, aD
GDF6	jRP, LCA17	aR
NR2E3	RP37	aR
NRL	RP27	aR
RAX2	CORD11	aD
ZNF408	naRP	aR
ZNF513	RP58	aR
Intracellular trafficking		
RAB28	CORD18	aR
RD3	LCA12	aR
RP2	RP2	aD
TOPORS	RP31	aD
Other		
ADAM9	CORD9	aR
BEST1	RP50	aD
c8orf37	RP64, CORD16	aR
CA4	RP17	aD
CERKL	RP26	aR
DHDDS	RP59	aR
DRAM2	CORD21	aR
EMC1	naRP	aR
EYS	RP25	aR

Table 1.2. cont'd

FAM161A	RP28	aR
GPR125	naRP	aR
HGSNAT	naRP	aR
IDH3B	RP46	aR
IMPDH1	RP10, LCA11	aD
IMPG2	RP56	aR
KIAA1549	naRP	aR
KLHL7	RP42	aD
MAK	RP62	aR
MERTK	RP38	aR
NEK2	RP67	aR
NMNAT1	LCA9	aR
PITPNM3	CORD5	aD
POC1B	CORD20	aR
PRCD	RP36	aR
SLC7A14	RP68	aR
SPATA7	jRP, LCA3	aR
TTLL5	CORD19	aR

1. Type identified by http://omim.org. RP, retinitis pigmentosa; jRP, juvenile retinitis pigmentosa; naRP, no RP type has been assigned (in literature); CORD, cone-rod dystrophy; naCORD, no CORD type has been assigned (in literature); LCA, Leber congenital amaurosis. Table modified from [55,56].
2. Mode of inheritance identified by http://omim.org or from reference listed. aR, autosomal recessive; aD, autosomal dominant; X, X-linked

1.5.1 Retinitis pigmentosa

Retinitis pigmentosa is an inherited retinal degeneration that occurs in humans. It is the leading cause of inherited blindness affecting about 1 in 4000 people [55]. Non-syndromic RP is restricted to phenotypes involving the eye. The age of onset of RP is variable but typically rod-mediated and peripheral vision starts to deteriorate in adolescence or young adulthood. The loss of peripheral vision continues often resulting in tunnel vision. Cone-mediated vision decreases, causing loss of central vision and visual acuity and patients are usually diagnosed as legally blind in their 40s. In addition

to the loss of vision, the fundus (posterior segment of the eye) of RP patient shows attenuation of retinal blood vessels, optic disc pallor and pigment deposits in the peripheral retina (Figure 1.2).

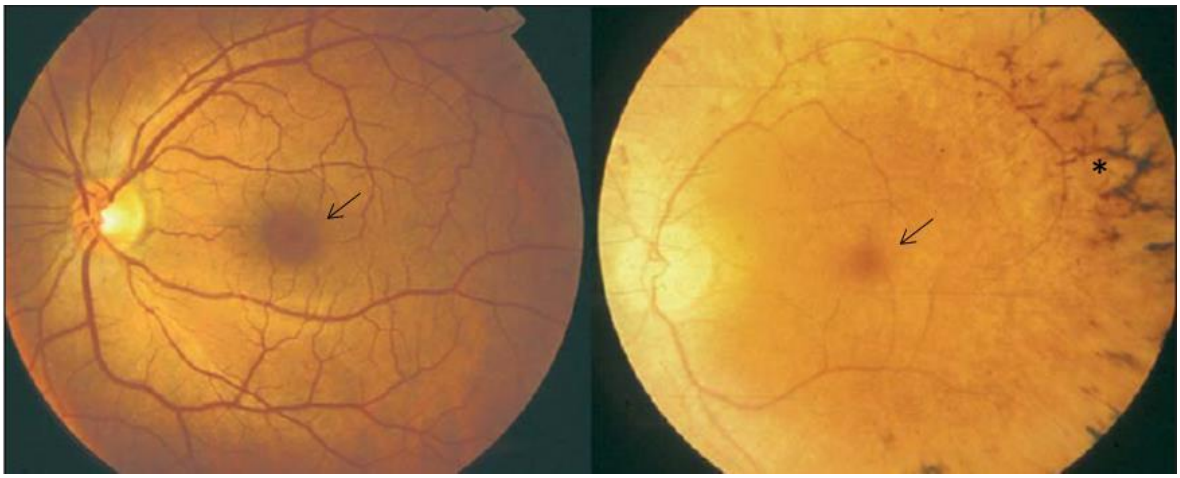

Figure 1.2. Human fundus images. Normal human (left) and RP patient (right) fundus images. Black arrows point to the fovea in each fundus; note the shrinking macula, attenuation of retinal vessels and the optic nerve pallor. The * in the RP fundus shows the pigment deposits that give RP its name. Figure modified from [55].

RP is a genetically heterogenous disease with identified mutations in over 50 genes [57]. RP types are denoted as RP 1-71 and are classified by their causal mutation (http://omim.org/). Like PRA, RP is most commonly recessively inherited (arRP) but dominant and X-linked inherited forms also occur. Mutations that cause RP are found in genes that are involved in photoreceptor structure and function, photoreceptor support cells, cell-cell interactions, RNA intron-splicing factors and cell development and maintenance as well as a group of genes with protein localization in the retina but of unknown function. There are mutations in over 40 genes that result in arRP (Table 1.2) (http://omim.org/, https://sph.uth.edu/Retnet/home.htm). Many arRP mutations have been identified by homozygosity mapping (via SNP arrays) or

sequencing family groups in which RP is segregating. Commercially available microarrays are available for screening for known mutations, however the efficacy of this method is questionable due to the genetic heterogeneity of RP [58]. Next generation whole genome sequencing and exome sequencing, while more expensive, are becoming the method of choice for screening for arRP.

1.5.2 Leber congenital amaurosis

LCA is a retinal dystrophy affecting 1/30,000 to 1/81,000 children [59,60]. As the name implies, children are often born with visual impairments or show symptoms by one year of age. LCA accounts for about 20% of children enrolled in schools for the blind [56].

LCA is phenotypically variable but three main characteristics must be present. The patient must have severe and early visual deficits. The patient must have reduced or absent pupillary responses. The patient must have abnormal or non-recordable electroretinograms. Additional findings include variable abnormal fundus appearance, photophobia, bone spicule shaped pigment and inability to focus on an object [56].

LCA patients also show variation in the progression of the disease. In a summary of studies, 90 patients were examined and 15% showed deterioration of visual acuity, 75% showed no change in visual acuity (from first diagnosis) and 10% showed improved visual acuity [56]. The variability seen in phenotype is attributable to the gene in which the mutation occurs and the severity of the effects of the mutation [56]. LCA has an autosomal dominant or recessive mode of inheritance. There have been mutations described in 18 genes that result in a diagnosis of LCA (Table 1.2). Many of these genes have also been implicated in RP and cone rod dystrophies.

1.5.3 Cone-rod dystrophies

Cone-rod dystrophies (CORD) affect about 1/40,000 people [54]. In contrast to RP, CORDs begin with cone abnormalities either prior to or simultaneously with rod defects. This means that daylight and central vision is affected first while dim light and peripheral vision is retained for longer. CORD symptoms are often described in two stages [54].

The first stage includes reduced visual acuity and photophobia. The macula is a region of the retina with a very high density of cones and is used for high acuity vision (e.g. reading and facial recognition). Because cones are the first photoreceptors affected in CORDs, the macula is the location where the first signs of degeneration occur. During the first stage, there are generally no complaints of night blindness. Retinal vessels show little to no attenuation but bone spicule shaped pigment deposits can be seen in the macular region. Additionally, there may be dyschromatopsia (altered color vsion). Patients usually begin to show signs of visual impairment at a young age [54]. Although central vision is impaired during this stage the patients can still ambulate without aid because their peripheral vision is still useful.

The second stage of the disease occurs when the rods begin to degenerate. At this point, dim light vision decreases and peripheral vision deteriorates and patients become legally blind. The rate of progression and age of legal blindness varies but in general occurs earlier than what is seen in RP patients [54].

CORDs can have an autosomal dominant, autosomal recessive or X-linked mode of inheritance. Table 1.2 shows a list of genes with mutations associated with CORD.

1.6 Retinal structure and function

The eye is an organ that is highly specialized to take visual information from the outside world and transmit that information to the brain. Light is refracted by the cornea then passes through the pupil and is further refracted by the lens to be focused at the back of the eye on the retina (Figure 1.3). Light photons travel through the cell layers of the retina to the photoreceptors where they are converted into a neuronal response that then travels anteriorly through the retina to be transmitted through the optic nerve to the brain. Some animals, particularly ones adapted to dim light and/or night vision, have a tapetum lucidum. The tapetum lucidum is a reflective tissue within the inner choroidal layer that reflects light that is not absorbed by the photoreceptors back to the photoreceptors increasing the chances of light absorption [61-63].

1.6.1 Retinal anatomy

The retina is composed of 10 organized layers that receive and amplify the signal from photons entering the eye (Figure 1.4):

a) Retinal pigment epithelium
b) Photoreceptor layer
c) External limiting membrane
d) Outer nuclear layer
e) Outer plexiform layer
f) Inner nuclear layer

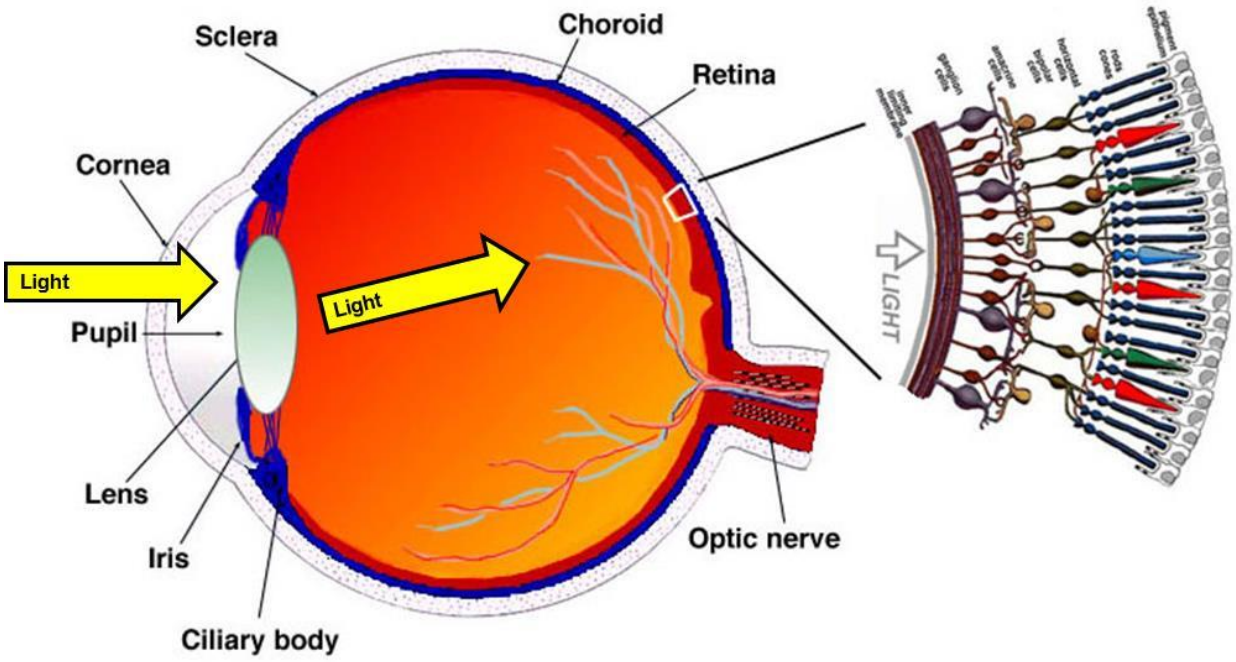

Figure 1.3. Gross anatomy of the human eye. Light enters the eye through the pupil and the lens focuses the light to the retina at the back of the eye. Light then passes through the multiple cell layers of the retina to the photoreceptors where the photons are turned into a neuronal signal that is propagated anteriorly through the retina to the ganglion cells and then to the brain. Figure modified from [63].

g) Inner plexiform layer

h) Ganglion cell layer

i) Nerve fiber layer

j) Internal limiting membrane

These will be examined in detail in the following subsections.

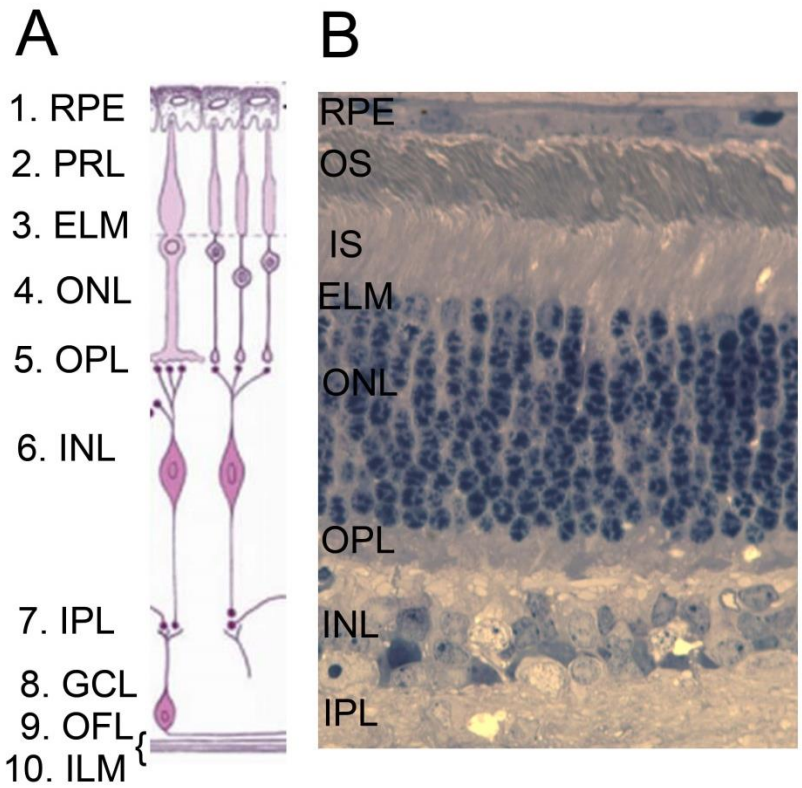

Figure 1.4. Layers of the retina. The 10 layers of the retina are labeled in A) a simplified schematic of retinal cells and layers and B) a histological section of a canine retina, nuclei are stained dark blue. (A) modified from [64]. RPE – retinal pigment epithelium, PRL – photoreceptor layer, OS – photoreceptor outer segment, IS – photoreceptor inner segment, ELM – external limiting membrane, ONL – outer nuclear layer, OPL – outer plexiform layer, INL – inner nuclear layer, IPL – inner plexiform layer, GCL – ganglion cell layer, OFL – optic nerve fiber layer, ILM – inner limiting membrane.

1.6.1.a Retinal pigment epithelium

The retinal pigment epithelium layer consists of a single layer of retinal pigment epithelial (RPE) cells. These cells are positioned between the outer segments (OS) of the photoreceptors and the choroid. These non-neuronal cells support the photoreceptors and are instrumental in vision. RPE cells in the tapetal fundus are not actually pigmented, as this would defeat the purpose of having a tapetum. The pigment granules in the non-tapetal RPE absorb scattered light, protecting the eye from photo-

oxidation. RPE cells form a barrier between the photoreceptor OS and the choroid. Therefore, the RPE cells are necessary for the transport of nutrients from the choroidal blood vessels to the photoreceptors and to transport waste out of the photoreceptors. The RPE cells are also responsible for phagocytosis of the photoreceptor OS disks that are shed from the tips of the photoreceptor outer segments. During a process known as the visual cycle the RPE cells convert the retinoid, all-trans retinol, into the chromophore 11-*cis* retinal that is transported to the photoreceptors to combine with opsin and form the active visual pigment of the photoreceptor. Following phototransduction all-trans retinol is produced and is transported back to the RPE for conversion back to 11-*cis* retinal for transport to the photoreceptors. Mutations in genes expressed in the RPE cells can lead to photoreceptor degeneration and vice versa indicating how closely these cells rely on one another [62,65-68].

1.6.1.b Photoreceptor layer

The photoreceptor layer consists of the inner segments (IS) and OS of the rod and cone photoreceptor cells. The rod photoreceptors are cells that are used for dim light vision. They have stacks of disks in their OS that are pinched off from the membrane and are densely packed with the visual pigment rhodopsin. Cone photoreceptors are used in daylight and color vision and their disks are invaginations of the outer membrane. Cones have different opsins which differ in the wavelength of light they absorb. The OS of the photoreceptors are the site of phototransduction; where light energy is turned into a neuronal response to be propagated through the rest of the retina and onward to the brain [62,66,69-71]. Photoreceptor anatomy and the phototransduction cascade will be discussed in detail later in this chapter.

1.6.1.c External limiting membrane

The external limiting membrane consists of the Müller cell connections to the rods and cones. The Müller cells provide metabolic and structural support to the photoreceptors. The processes of the Müller cells contribute to the matrix of the external limiting membrane helping to create a structure and a barrier to the inner retina [62,66,71].

1.6.1.d Outer nuclear layer

The outer nuclear layer (ONL) contains the cell bodies of the photoreceptors. In the healthy human central retina, the ONL is 6-8 nuclei thick while in dogs the central retina ONL is 10-12 nuclei thick and loss of nuclei in the ONL results from photoreceptor death [62,66,71]

1.6.1.e Outer plexiform layer

The outer plexiform layer is the location of the synapses between the photoreceptors and the second order neurons, which are the bipolar and horizontal cells. The rod and cone photoreceptors release a neurotransmitter, L-glutamate, in an inverse graded response to light (i.e. in the dark the photoreceptors release L-glutamate, and light stimulation decreases the amount of L-glutamate release). The connections between the photoreceptors and the horizontal and bipolar cells are a site of visual integration which organizes the information based on contrast of the object being seen in comparison to its surroundings. Horizontal cells form synapses with photoreceptors and bipolar cells and are able to supply information to both types of cells. Horizontal cells are involved in lateral information transfer while the bipolar cells

are involved in the vertical transmission of signal through the retina towards the brain. In humans there are 11 types of bipolar cells; 1 type that forms synapses with rod photoreceptors and 10 that form synapses with cone photoreceptors. Each type of bipolar cell responds differently to the input supplied by its connecting photoreceptor which aids in the integration of the visual signals. The cone bipolar cells are divided into two types: ON and OFF bipolar cells. The ON bipolar cells depolarize in response to light while OFF bipolar cells hyperpolarize [66,72]. One rod bipolar cell will synapse with multiple rod cells creating an amplification of signal [62,66,72].

1.6.1.f Inner nuclear layer

The inner nuclear layer houses the nuclei and cell bodies of the bipolar, Müller, horizontal and amacrine cells. These nuclei do no form the clear, organized rows seen in the ONL [62,66,71].

1.6.1.g Inner plexiform layer

The inner plexiform layer is the location of the synapses between bipolar cells and the amacrine and ganglion cells. The amacrine cells provide feedback to both the bipolar and ganglion cells in a lateral manner while the bipolar to ganglion synapses are involved in vertical information transfer [62,66,71].

1.6.1.h Ganglion cell layer

The ganglion cell layer holds the nuclei and cell bodies of the ganglion cells. The ganglion cells receive the information that the rest of the retina has accumulated and organized and transmits this information to the brain [62,66,71].

1.6.1.i Nerve fiber layer

The axons of the ganglion cells converge together and form nerve bundles that group together at the lamina cribrosa (a perforated plate region of the sclera) to form the optic nerve connecting the eye to the brain. The nerve fiber layer runs parallel to the retinal surface [62,66,71].

1.6.1.j Internal limiting membrane

The internal limiting membrane is the basement membrane of the retina which is formed by a matrix of the inner ends of the Müller cell processes [62,66,71].

1.6.2 Photoreceptor anatomy

Photoreceptors are the cells that receive the photons of light and turn this signal into an electrical response. Photoreceptor cells are specialized, sensory ciliated cells that consist of four key features (Figure 1.5):

a) Outer segment
b) Inner segment
c) Connecting cilium
d) Cell body
e) Synaptic terminals

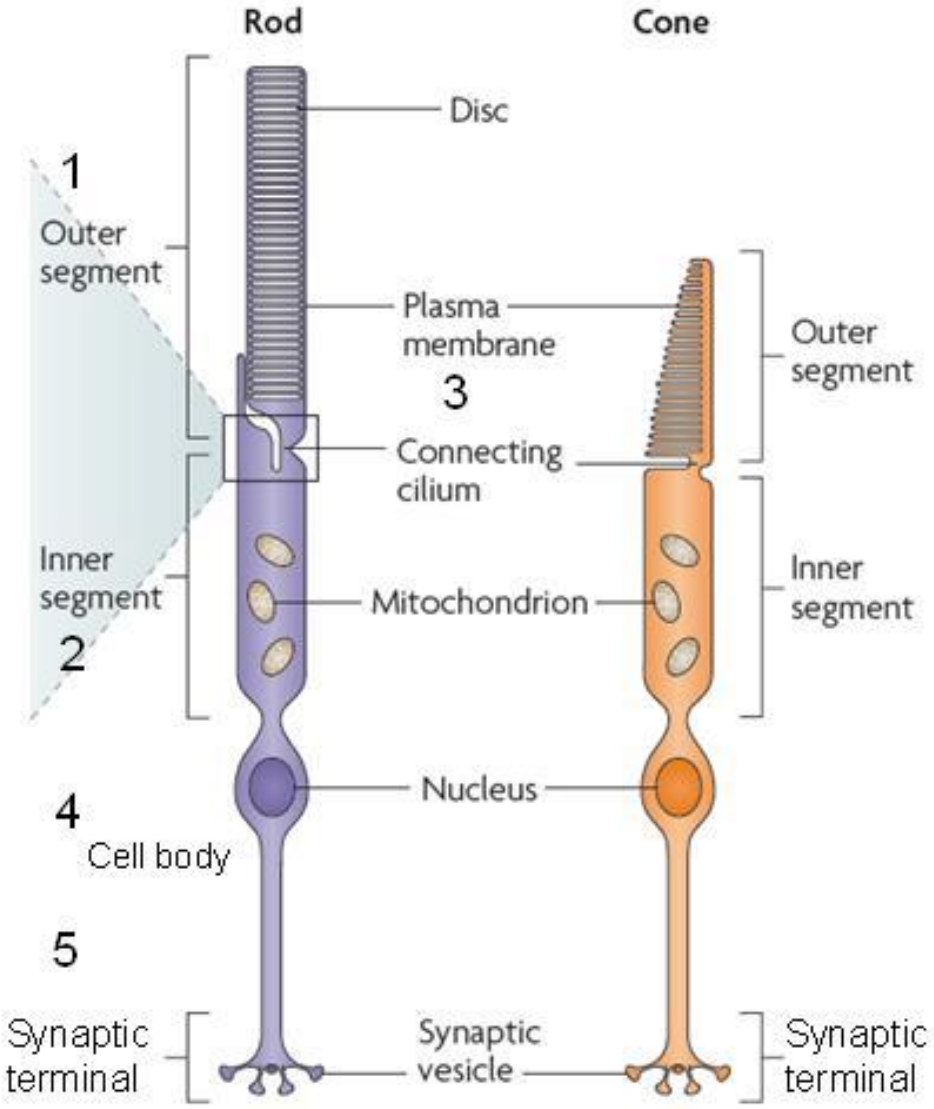

Figure 1.5. Rod and cone photoreceptor anatomy schematic. The photoreceptors consist of 1) the outer segments, 2) the inner segments, 3) the connecting cilium 4) the cell body and 5) the synaptic terminal. Disks in rods are pinched off from the membrane while they are invaginations of the plasma membrane in cones. Phototransduction occurs on the disk membranes in the photoreceptor outer segments. The inner segment houses the cellular organelles and supplies the outer segments via the connecting cilium. The cell body contains the nucleus and has long processes reaching from to the inner and outer segments and to the synaptic terminal. The synaptic terminal synapses with second order neurons to propagate the signal through the retina. Modified from [73]

1.6.2.a Outer segment

The OS is composed of stacked membrane disks where the opsin, or light reactive molecule, and the phototransduction machinery are housed. The disks contain high concentrations of the visual pigment (the opsin conjugated with 11-*cis* retinal) and the disks at the distal ends of the OS are phagocytosed and recycled by the RPE cells [62,66,69-71,74].

1.6.2.b Inner segment

The inner segment is the site of the metabolic and synthetic machinery of the cell. Photoreceptors require a large amount of energy (~90,000 ATP molecules per second per cell). The inner segment houses the mitochondria at the distal end near the base of the OS to supply the cell with the energy it needs. In addition to the normal maintenance of the cell, the endoplasmic reticulum and the golgi apparatus are responsible for packaging the opsin-filled vesicles that are constantly being transported to the OS to replace the disks that are being recycled by the RPE cells [62,66,69-71,73].

1.6.2.c Connecting cilium

The connecting cilium connects the inner segment to the OS and supplies the machinery for intracellular transport. The cilium is constructed of microtubules and microfilaments. The microtubules form doublets that extend from the inner segment to the OS but once in the OS they become singlets. These singlet microtubules are referred to as the axoneme and provide structural support and transportation to the distal end of the OS. The microtubules use kinesins and dynein motors for anterograde and retrograde cellular transport. Microtubules are also used for transport from the

endoplasmic reticulum to the golgi apparatus to the connecting cilium. In addition to the microtubules, the connecting cilium contains microfilaments. Microfilaments also provide structural support and transport [62,66,69-71].

1.6.2.d Cell body

The cell body of the photoreceptor contains the nucleus and is located in the ONL of the retina. Long processes extend basally from the cell body to the inner and outer segments and apically to the synaptic terminal. The cell bodies of the cone photoreceptors are located closest to the external limiting membrane. The basal process is relatively short while the apical process must extend through the entire ONL to the outer plexiform layer where the synaptic terminal is located. The rest of the ONL consists of the cell bodies of the rod photoreceptors. The basal and apical processes are variable in length, depending on where in the ONL the cell body is located. The rod cell body apical processes also extend to the outer plexiform layer where the synaptic terminals are located [62,66,69-71,73].

1.6.2.e Synaptic terminal

The synaptic terminals of the rods and cones are called spherules and pedicules, respectively. The synaptic vesicles, filled with L-glutamate, are released when the photoreceptor membrane is depolarized. This means that in the dark-state, the cells are releasing the neurotransmitter to the secondary neurons. When the cells become light activated, L-glutamate release is reduced [75,76].

1.6.3 Phototransduction

Phototransduction in rods and cones is similar but our principal understanding of phototransduction is the result of studies performed in rods. This section will focus on rod phototransduction [62,66,69-71,74].

1.6.3.a Phototransduction cascade in rods

Rhodopsin is a membrane bound protein combined with a retinoid that is located on the disks of the rod photoreceptor OS. Rhodopsin is the visual pigment of rods and is a G-coupled protein receptor. 11-*cis* retinal (a chromophore) is cross-linked within rhodopsin; this relationship between rod opsin and 11-*cis* retinal makes the light sensitive version of the protein, rhodopsin. When the chromophore is hit by a photon, it isomerizes to form all-*trans* retinal. This change in shape of the chromophore causes it to dissociate from rhodopsin resulting in a series of conformational change in rhodopsin resulting in an 'activated' rhodopsin, also known as metarhodopsin. Metarhodopsin is able to interact with and activate the G-protein transducin (Figure 1.6, 1). Transducin is composed of three subunits; alpha, beta and gamma. The alpha subunit of transducin binds GDP but activation causes GDP to dissociate and GTP binds in its place. The beta-gamma subunits dissociate and the activated alpha subunit of transducin then interacts with a cGMP-phosphodiesterase (PDE6) (Figure 1.6, 2). The PDE6 protein has four subunits, one alpha (A), one beta (B) and two gammas (Y). Two activated transducins bind, one to each of the two Y subunits of PDE6 and the complex dissociates from the PDE6A/B, no longer inhibiting the catalytic properties of PDE6A/B. PDE6A/B hydrolyzes cGMP to 5'-GMP (Figure 1.6, 3). The hydrolysis of cGMP causes

the closure of the cyclic nucleotide gated ion (CNG) channels in the plasma membrane of the outer segment (*not* on the disks) (Figure 1.6, 4).

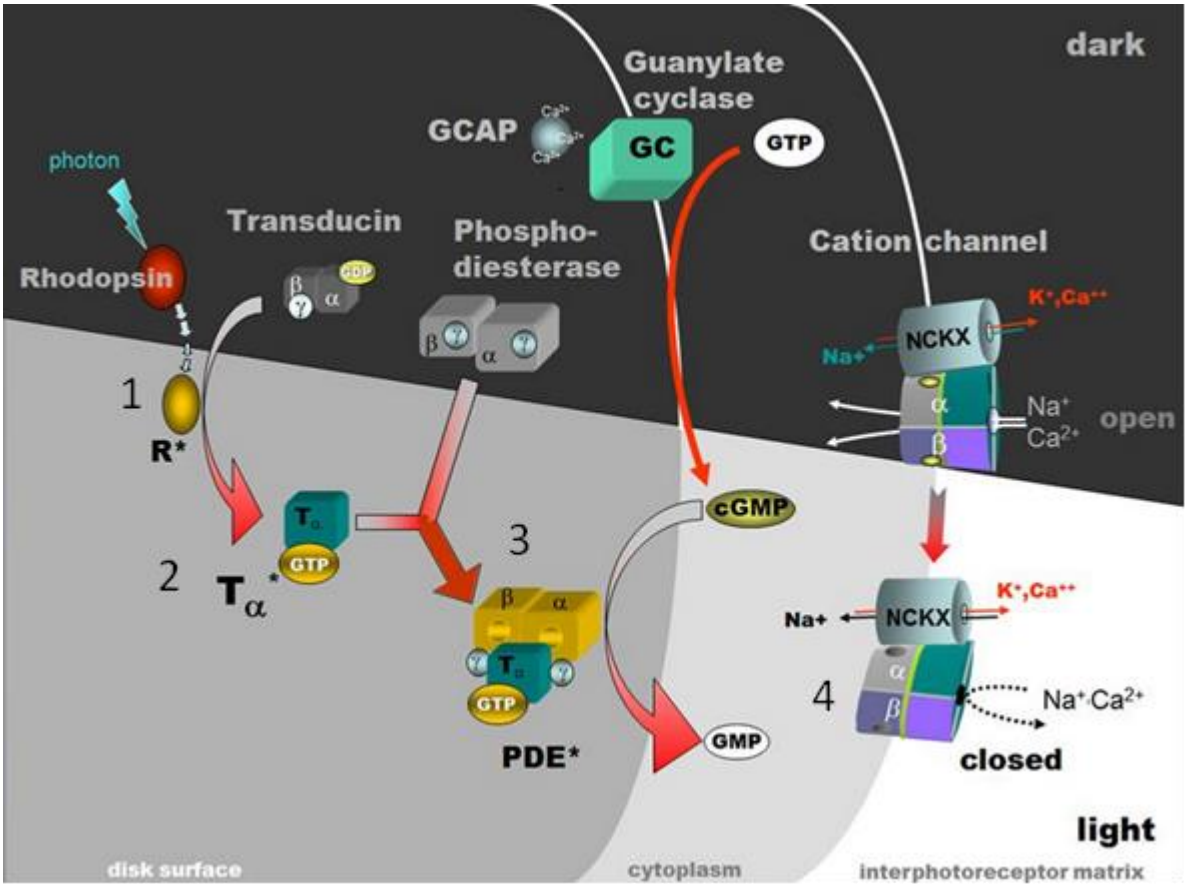

Figure 1.6. Phototransduction in the rod photoreceptor. In the dark, transducin and the phosphodiesterase are inhibited and cGMP is bound to the CNG channels allowing for the slight depolarization of the photoreceptor (top). Light enters the rod photoreceptor and causes a conformational change in rhodopsin (1). Metarhodopsin activates transducin (2). Transducin activates the cGMP phosphodiesterase which hydrolyzes cGMP (3), closing the CNG gated channel (4). Figure modified from [70].

In the dark rod photoreceptors are slightly depolarized because a low proportion of CNG channels are open allowing for the steady influx of cations (Na^+ and Ca^{2+}) into the cell, this is called the dark current. The rods are kept from complete depolarization by Na^+/ Ca^{2+}- K^+ exchangers that pump ions out of the cell. Interestingly, only about 1% of CNG channels are open in the dark [77]. In the depolarized state, the photoreceptor releases

L-glutamate from the synaptic terminal. Upon exposure to light the phototransduction cascade reduces the levels of cGMP leading to closure of the CNG channels stopping the influx of cations into the OS. The closure of the CNG channels, in combination with the still active Na^+/ Ca^{2+}- K^+ exchangers, causes a hyperpolarization of the photoreceptor (i.e. the cell becomes more negative). Hyperpolarization of the cell results in a graded decrease in L-glutamate release from the synaptic terminals [62,66,69-71,74].

1.6.3.b Inactivation of phototransduction cascade

Rhodopsin is deactivated by two mechanisms. First, it is phosphorylated by a protein called rhodopsin kinase. This decreases its activity but does not inactivate the chromophore. Complete inactivation comes via binding of arrestin. Arrestin stays bound to rhodopsin until the chromophore is reduced and transported to the RPE cells for recycling.

Transducin alpha is deactivated by the hydrolysis of the bound GTP to GDP. This causes the dissociation of transducin alpha from PDE6. Transducin has internal hydrolase activity which, in conjunction with a GTPase activating protein, allows for self-limiting activity. Transducin alpha rebinds the transducin beta-gamma subunits.
The deactivated transducin dissociates from the PDE6Y subunits. With the PDE6Y subunits free, they are able to rebind to and inhibit the PDE6A/B subunits.

After hyperpolarization due to CNG channel closure of the cell, the cell must return to its depolarized state. This occurs by the above mechanisms to inactivate proteins that aid in the hydrolysis of cGMP. However, cGMP still must be restored to open the CNG channels. This occurs due to the activity of guanylate cyclase (GC). GC

is inhibited by guanylate cyclase-activating proteins in the presence of high intracellular Ca^{2+} but the closure of CNG channels causes the Ca^{2+} concentration in the cell to decrease enough for dissociation and activation of GC. GC activity is necessary to restore cGMP levels and open CNG channel for restoration of the depolarized resting state of the rod photoreceptor [62,66,69-71,74].

1.7 The electroretinogram

The electroretinogram (ERG) is a method of measuring the retina's response to light stimuli. While the first recorded realization that the eye elicits an electrical response to light was in 1865, it was not until the early 1900s that the individual components of the ERG started to become elucidated. Initial ERG studies showed three waves, a fast negative wave (the a-wave) followed by a positive wave (the b-wave), and third slow positive wave (the c-wave) [68,69].

There are two types of current that travel through the eye. There is a local current that travels through the retina. The remote current travels through the retina, to the vitreous, to the cornea and then back to the retina via the choroid and RPE cells. ERGs can be measured locally or remotely. A locally measured ERG uses microelectrodes placed within the retina at specific cell layers. This is invasive but useful for measuring the isolated responses of certain cell types. Measuring an ERG remotely involves placing an electrode in the vitreous or on the cornea (usually attached via a special contact lens). A remote ERG is the result of a summation of electrical currents in all radial cell types in the retina (photoreceptors, bipolar cells and Müller cells), this ERG can be measured by placing an electrode on the cornea. The horizontal and amacrine cells have little to no effect on the ERG because they are arranged laterally and the signals cancel each other out. The corneal ERG is not invasive and is common practice in clinical and research settings [68,69].

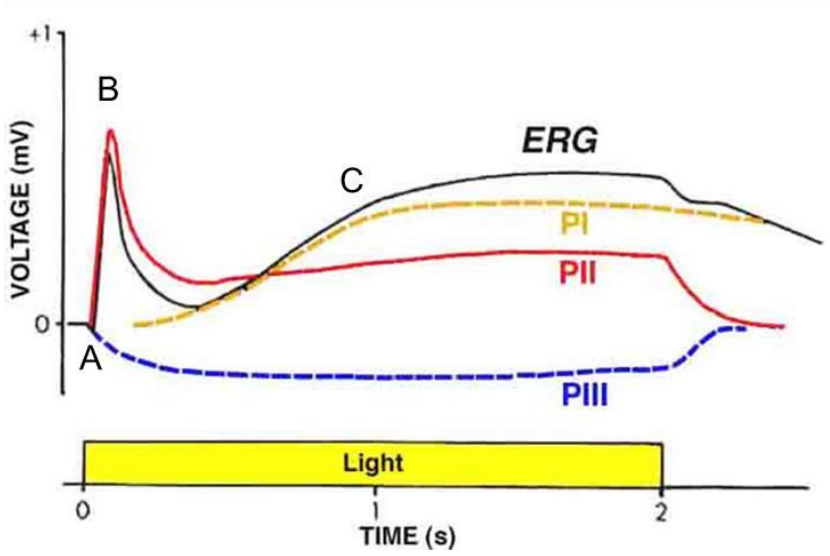

Figure 1.7. The three components of the ERG. Deepening levels of anesthesia were used to identify the three components that summate to form the ERG waveform. The PI component is the first to disappear, followed by PII and then PIII. The PI component (yellow line) originates from RPE cell membrane potentials. PII (red line) is due to the depolarization of the ON-bipolar cells. PIII component (blue line) is the result of photoreceptor hyperpolarization. The black line is the typical ERG measured which is the combined wave of all three components; the a-wave (A), b-wave (B) and c-wave (C) are labeled. Figure modified from [68,78].

In 1933, Ragnar Granit identified three components (PI, PII, PIII) of the ERG that disappeared in turn when the depth of anesthesia was increased (Figure 1.7). The PI component is a slow positive response and is the first to disappear under anesthesia. The second component is PII and has a fast positive peak that decreases to an intermediate positive wave that is sustained during the light exposure. The final component of the ERG is PIII which consists of a fast negative response peak (faster than the response in PII) which is maintained for the duration of the light flash. These three components combine to form the composite ERG tracing that is measured under no or normal levels of anesthesia, and encompass the three waves (a-, b- and c-waves) that had been described earlier in the century [68,69].

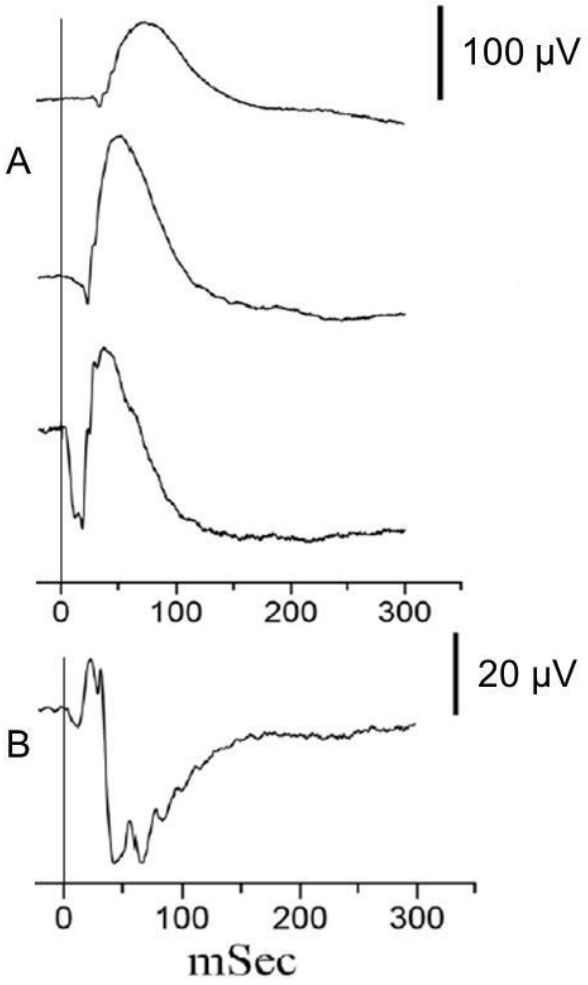

Figure 1.8. Representative canine ERG tracings. 10 week old normal dog ERG tracing. A) Dark adapted (scotopic) ERGs with light flashes of -2.4, -1.2 and 0.4 log cdS/m^2 after 20 minutes dark adaptation. B) Photopic ERG with a light flash of 0.4 log cdS/m^2 after 10 minutes light adaptation. Figure modified from [31].

The a-wave is the fast, negative wave of the PIII component (Figure 1.7 and Figure 1.8). The negativity of the wave is the result of the reduction of the dark current during phototransduction in response to light. Specifically, it is the result of the cells becoming hyperpolarized (more negative) due to the closure of CNG channels in the photoreceptor OS. To dissect out the different cell types that contribute to the ERG waves, cellular antagonists or agonists can be injected into the eye. When L-glutamate was identified as the neurotransmitter released from the photoreceptors researchers

were able to use an L-glutamate antagonist, 2-amino-phosphonobutyric acid (APB), to block synaptic transmission of the photoreceptors to bipolar cells. Doing this did not affect the a-wave but all subsequent waves were no longer present, indicating that the a-wave is the result of a change in current *before* the message is passed to bipolar cells, i.e. the a-wave is generated by the photoreceptors. The PIII component has a slow positive response that is not seen in normal ERGs because it is occluded by the PI component. By extracting the retina away from the RPE cells and blocking L-glutamate release from the photoreceptors (i.e. removing the PI and fast PIII components), it has been determined that the slow positive PIII response is due to changes in the Müller cell membrane potentials [68,69].

The origin of the b-wave has a long history of debate as to whether it originates from the Müller cells or the ON-bipolar cells but the current consensus is that the b-wave originates from the latter. The ON-bipolar cells depolarize in response to light giving rise to the positive PII component (Figure 1.7 and Figure 1.8). As described earlier, APB blocks photoreceptor synaptic transmission to bipolar cells and doing so completely removes the b-wave. Additional studies in the mGluR6 knockout mouse (which do not have the ON-bipolar cell L-glutamate receptor) showed that without the ability of the ON-bipolar cell to receive signal from the photoreceptor the mice have no b-wave. Exposure of Müller cells to barium blocks their K^+ permeability and therefore blocks a change in their membrane potential. ERGs that were recorded after barium was injected into the vitreous showed an increase of the b-wave amplitude. This led to the conclusion that Müller cells do not contribute to and they might actually counteract

the production of the b-wave. Blockage of OFF-bipolar cells and third order neurons also enhance the b-wave [68,69].

The c-wave is the final wave of the ERG and is produced by the PI component. This wave is not seen in normal flash ERG protocols in humans or dogs (Figure 1.7 and Figure 1.8) [68,69,79]. To see this wave, there must be an extended light exposure and DC recording perform (the normal flash ERG is recorded by AC recording). The c-wave is generated from the RPE cells. The origin of the c-wave was elucidated by studying retinas with destroyed photoreceptors (c-wave is unaffected), destroyed glial cells (c-wave remains unchanged) and recording a retinal ERG after removal of the RPE cells (loss of c-wave). The membrane potential change in RPE cells that is responsible for the c-wave is dependent on phototransduction. Therefore, analysis of the c-wave can give insight to photoreceptor and the RPE health and the relationship between the two [68,69].

There are standard ERG protocols for clinicians set by the International Society of Clinical Electrophysiology of Vision (ISCEV) for humans and the European College of Veterinary Ophthalmologists (ECVO) for dogs [79,80]. Generally, these include a dark-adapted (scotopic) recorded ERG and a light-adapted (photopic) ERG. These protocols also include detailed standards for every aspect of the ERG to create consistency between patients and clinics.

Researchers often use more extensive ERG protocols than the standard ISCEV and ECVO recommended protocols. There are many factors that can affect ERGs and these must be accounted for in analysis but utilizing these factors can lead to a better understanding of the ERG. One of the main factors affecting the ERG is light

adaptation. In most settings, putting the patient in the dark for 20-60 minutes before starting the ERG dark-adapts the retina. The dark-adapted state is very sensitive to dim light stimuli and is a way to measure rod-driven vision. The ERG starts with a very dim light flash and the intensity of the flash will increase. Increasing the light flash intensity brings about mixed rod and cone response. After the scotopic protocol, the patient is light adapted (a background light is turned on) for at least 10 minutes. Then, a series of flashes, in increasing brightness, is applied over the background light. The presence of constant light saturates the rods so the photopic ERG is a cone-only ERG. Only about 5% of the photoreceptors are cones and they have a much faster response, so the resultant ERG will have smaller wave amplitudes but the response times will be quicker. Dark- and light-adapted ERGs are part of the standard ERG protocols listed previously [68,69,79,80].

As eluded to in the previous paragraph, the intensity of the light flash is a variable factor. Most protocols use a series of very dim to very bright light flashes. During a scotopic ERG, the very dim flashes elicit mainly rod responses and the amplitudes are often low because of the graded release of L-glutamate. As the flashes increase in intensity, more rods and, above certain intensities, cones are activated resulting in a larger amplitude response. In the bright flashes of a scotopic ERG, the waves are the result of mixed rod and cone responses. In the photopic ERG, there is a background light that saturates the rods and only a cone response is recorded. The flashes are superimposed on the background light. In the scotopic protocol the time between flashes must be increased as the brightness of the flash increases. This allows the cells an appropriate amount of time to recover to the dark-adapted state after the flash

stimulus. An intensity series for dark- and light- adapted ERGs is an optional test that maybe added onto the standard protocols listed previously but researchers may have more advanced protocols (i.e. more flashes or more range in the intensities) [68,69,79,80].

The standard ERG protocol uses flashes of white light. However, altering the color of the light flashes can help differentiate between contributions from rods and cones. Peak rod sensitivity occurs at about 500 nm (blue/green color spectrum). Rods are about 1000 times more sensitive than cones to blue light so a dark-adapted ERG using blue flashes can be used to elicit rod-only responses. Cones and rods are similarly sensitive to red/orange light flashes but the timing of rod and cone responses is different. Using a red flash will produce two distinct components in the b-wave, the faster being from cones and the slower from rods. This method can be useful for investigating the degree of rod function. Different colored light flashes are not generally used in the clinical setting but can be useful for researchers [68,69,79,80].

The frequency of the light flashes is also a factor used to separate cone and rod responses. A flicker frequency of higher than 15 Hz is used to investigate cone-only responses. This utilizes the temporal properties of the different photoreceptors. Cones respond to and recover from light exposure quickly while rods are slower to recover. Thirty Hz flicker ERGs to assess cone function are included in standard protocols but researchers may opt to choose additional frequencies in their studies [68,69,79,80].

1.7.1 Measuring and analysis of electroretinograms

The standard ERG protocols include sections that describe how to measure and report ERGs [79,80]. The amplitudes of the waves and the time to the peak amplitude of

the waves (implicit time) are measured and reported. Figure 1.9 is a diagram of the points that are measured on the ERG. The a-wave amplitude is measured from baseline (ERG recording amplitude before a light flash, set to zero) to the lowest point of the a-wave curve. The b-wave amplitude is the response increase from the lowest point in the a-wave to the peak of the b-wave. A- and b-wave amplitudes will be smaller for dimmer light flashes and will increase as the light flashes become brighter. Implicit time to each wave is measured from the time of the flash of light (set to zero) to the peak of the wave. Implicit time will decrease as the light flashes become brighter. Comparing wave amplitudes and implicit times of affected and breed/age matched normal controls can give insight to the tracings of an abnormal ERG [62,68,79,80].

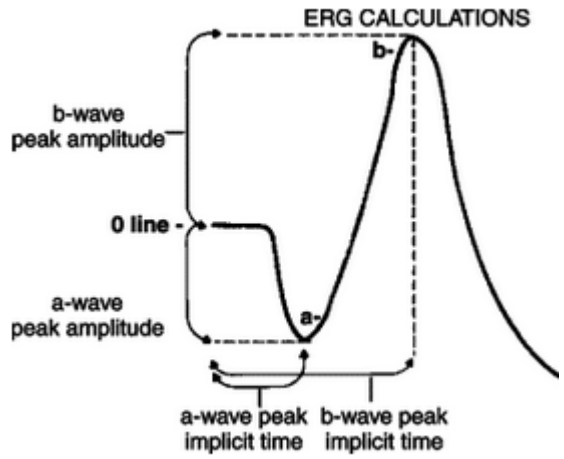

Figure 1.9. Measuring the ERG. The implicit time of the a- and b-waves are measured from the time of the light flash to the time of the wave peak. A-wave amplitude is measured from baseline to the lowest point of the wave. B-wave height is measured from the a-wave trough to the peak of the b-wave. Figure from [62]

Another parameter that can be assessed from an appropriate ERG study is the response threshold. In a scotopic ERG, the threshold is determined when the first a- or

b-wave is measurable. Increased threshold is indicative of abnormal rod function. Altered photopic ERG thresholds would imply abnormal cone responses [62,68,79,80].

Measuring and analyzing ERGs in these ways provides a consistent and objective measurement for comparisons of ERGs between individuals. Each component of the ERG can give insight into the mechanisms of retinal dysfunction.

1.8 Progressive retinal atrophy in Papillon dogs

PRA was first reported in Papillon dogs in 1995 [81]. Starting in the early 2000s, the Comparative Ophthalmology (CO) lab at Michigan State University began collecting DNA samples from Papillons affected with PRA and their relatives. This was the start of a mutually beneficial relationship with the CO lab and the Papillon Club of America (PCA). In 2009, the PCA arranged for a breeding of two European Papillons affected with PRA. The pregnant female was brought to the United States and produced two affected puppies. These three affected Papillons were the start of a research colony now maintained by the CO lab. The ability to study affected puppies at an early age and at consistent time points during the early stages of their PRA was instrumental in identifying the causal mutation. Figure 1.10, A-C shows fundus images of one of the affected Papillon puppies at 6, 10 and 14 months of age compared to the affected mother at 3.5 years old (Figure 1.1-, D). The fundic photographs taken during the first ~1.5 years of life show the beginning stages of PRA in the affected dog.

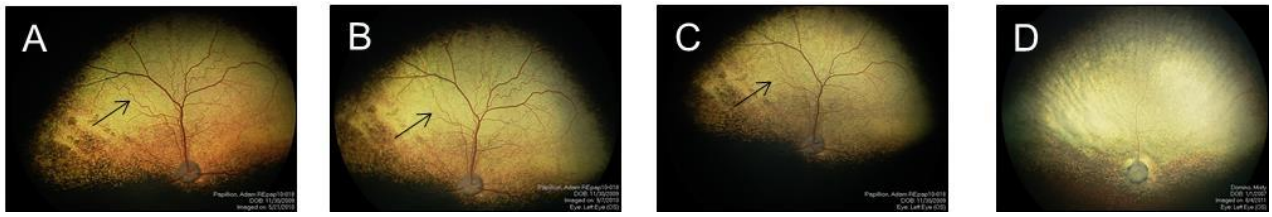

Figure 1.10. Fundus image series of PRA affected Papillon dogs. Images from a male affected Papillon at 6, 10 and 14 months of age (A-C) and an affected female at 3.5 years of age (D). The black arrow marks attenuation of retinal vasculature. Note the increasing of reflectivity of the tapetum in the fundic images.

While the image series in Figure 1.10 shows convincing evidence of the beginning stages of PRA, please appreciate the subtlety of the changes if the dog were to be only

examined once during this time period. It is standard breeding practice, recommended by the PCA, to have yearly eye exams conducted on breeding animals starting at 2 years of age (www.pcagenetics.com).

In 2011, a mutation was identified in the gene *CNGB1* that accounts for approximately 70% of PRA in Papillon dogs [31]. The details of initial phenotyping, identification of the mutation and functional data supporting the identified causal mutation are included in Chapter 2 of this dissertation.

1.9 Cyclic nucleotide-gated ion channels

Cyclic nucleotide-gated ion (CNG) channels are nonselective cation channels that are members of the voltage-gated ion channel family. Like other members of this family, the individual subunits of the channel consist of 6 membrane spanning segments (S1-S6) with the N-terminal and C-terminal ends of the protein projecting into the cytoplasmic side of the cell membrane. The subunits contain a cNMP binding domain near the C-terminal end. The CNG channel is a heterotetrameric protein, consisting of a combination of alpha and beta subunits [82,83].

The CNG channels allow the influx of Na^+, K^+ and Ca^{2+} cations into the cell. While the channels are nonselective, it is their role in Ca^{2+} cation influx that is integral to cellular processes involved in signal transduction in sensory cells [82,83].

1.9.1 Gene structure

CNG channel proteins are encoded by two gene subfamilies (Figure 1.11). The alpha subunits are transcribed from the *CNGA1*, *CNGA2*, *CNGA3* and *CNGA4* genes (A1-A4). The sequence similarity between the A1-A3 genes is over 75% but the A4 sequence deviates from the subfamily [82]. The genomic structure of the N-terminal of the A subfamily is highly conserved up to the exon encoding the second transmembrane segment (S2). In the A1-A3 genes the S2 through the C-terminal is conserved and consists of only one large exon but the A4 gene is poorly conserved in this region. The A3 gene encodes multiple splice variants expressed in different tissues [82].

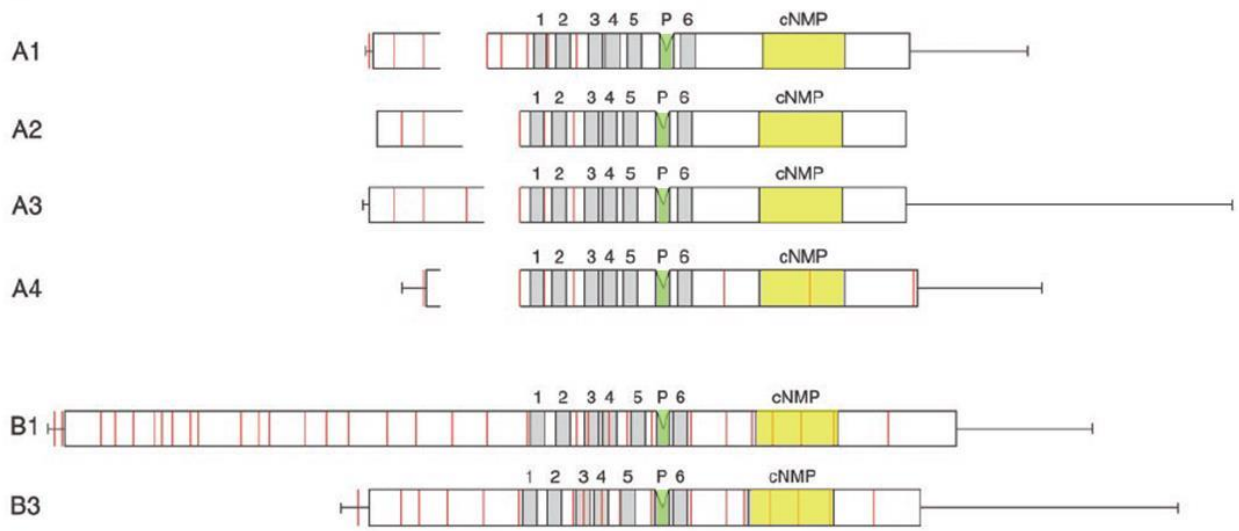

Figure 1.11. Cyclic nucleotide-gated ion channel subfamilies. The alpha (A) subunit families are transcribed from the genes *CNGA1*, *CNGA2*, *CNGA3* and *CNGA4*. The beta (B) subunits are transcribed from the *CNGB1* and *CNGB3* genes. Exon boundaries are marked with red lines. Transmembrane domains S1 through S6 are marked with gray boxes. The pore region and the cyclic nucleotide binding domain are marked with green and yellow boxes, respectively. Figure modified from [82].

The beta subunits are transcribed from the *CNGB1* and *CNGB3* genes (B1, B3). The gene originally designated as *CNGB2* is now called *CNGA4* [84]. Though quite different from the A subfamily, the B genes are similar to one another sharing about 67% sequence similarity [82]. The genomic structure of the B subfamily is conserved consisting of 12 exons that encode the S2 to C-terminal portion of the protein. The N-terminal portion of the B genes varies drastically and is probably the result of a different gene fused to the N-terminal *CNGB1* original gene [82]. The *CNGB1* gene produces multiple splice variants. There are multiple *CNGB1* splice variants described; three expressed in the retina, one in olfactory epithelium and two in testes and the flagellum of sperm [85-87]. The retinal variants consist of various combinations of the glutamic

acid-rich protein (GARP) exons and a full length *CNGB1* (CNGB1a) transcript. The olfactory epithelium transcript (CNGB1b) is a shorter form of CNGB1a, lacking the GARP-region [88]. The variants expressed in the testes lack the GARP regions and are very similar in their sequences differing only in their N-terminal region [82,85].

1.9.2 Protein structure and functional domains

The general CNG subunit consists of six transmembrane segments with the N-terminal and C-terminal ends of the proteins extending into the cytoplasm. In addition to the common transmembrane topology, all CNG subunits have a voltage sensitive motif, a pore region and a cyclic nucleotide binding domain (CNBD) [82]. The A subunits have a carboxy-terminal leucine zipper (CLZ) domain [89].

The voltage sensitive motif is a charged amino acid sequence located within the S4 transmembrane segment. In voltage-gated ion channels this segment rotates to open the channel in response to depolarization. CNG channels are not voltage sensitive but still contain the motif. It is possible that the amino acids in the CNG channel motif enable the channel to be constitutively open under physiological conditions. This would remove the voltage sensitivity of the CNG channel and leave the gating of the channel under cyclic nucleotide control [82,90].

The pore sequence is linked between the S5 and S6 transmembrane domains by amino acid linker sequences. While the pore S5 and S6 sequences are conserved there is considerable variability between the channels in different tissues in regards to their Ca^{2+} affinity. This variability arises from the linker sequences between the S5-pore-S6 region [91]. The selectivity filter is located in the pore loop.

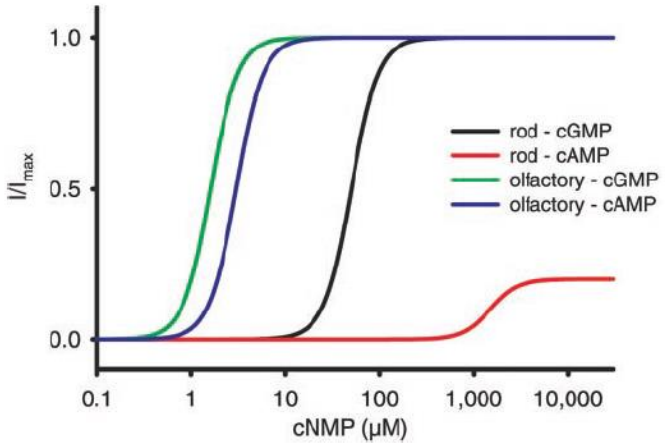

Figure 1.12. Channel reactivity to cNMP binding. Olfactory sensory neurons are similarly responsive to cGMP and cAMP and much more sensitive to these cNMPs than rod photoreceptors. Rod photoreceptors are much more sensitive to cGMP than to cAMP. This graph displays normalized current to cNMP concentration; the concentration of cNMP is on a log scale [82].

It is a highly conserved glutamate residue (E363) that binds Ca^{2+} and holds the divalent cation in the pore, blocking monovalent cation entry [91]. CNG subunits are arranged with their pore and S6 regions exposed to one another to allow the formation of the channel [92].

All CNG subunits have a CNBD located near the C-terminal domain. The CNBD consists of an 80-100 amino acid sequence. Cyclic nucleotides bind to this sequence in a series of polar and non-polar interactions. The binding of the cyclic nucleotides results in a conformational change that opens the channel [93]. All cyclic nucleotides can bind to the CNBD region but the opening of the channel due to a bound cyclic nucleotide can vary in different cell types. For example, photoreceptors preferentially bind cGMP and the ability of cGMP to open photoreceptor channels is three orders of magnitude greater than cAMP (Figure 1.12) [82]. In contrast, olfactory sensory neurons respond equally

well to both cAMP and cGMP and lower concentrations of the cyclic nucleotides are needed for these channels to open [82].

The CLZ domain is located only on the A subunits of CNG channels. This domain is important for subunit binding and stoichiometry [89]. It has been shown that CNGA1 and CNGA3 fragments containing the CLZ domains form trimers in solution by forming a 3-helix coiled-coil complex [89,94]. Carefully conducted experiments have shown that CNGA1 and CNGA3 subunits form trimers first and then the high affinity of B subunits to A subunits controls the binding of one B subunit [89,94].

1.9.3 Channel composition and functional properties

CNG channels are heterotetrameric complexes consisting of A and B subunits. In expression systems, A subunits can form functional homomeric channels but the channels do not show native channel characteristics. Native channel characteristics include Ca^{2+} permeability, sensitivity to blockage by L-cis-diltiazem (a pharmacological CNG channel blocker) and Ca^{2+}-dependent regulation. Homomeric A subunit channels have decreased Ca^{2+} permeability, carry less single channel current and are not as sensitive to channel blockage by L-cis-diltiazem or Ca^{2+}-dependent regulation [82,95,96]. The B subunits cannot form homomeric channels. It has been convincingly shown that rod photoreceptor CNG channels consist of a 3:1 CNGA1:CNGB1a ratio of subunits and the common olfactory sensory neuron CNG channels contain a 2:1:1 CNGA2:CNGA4:CNGB1b subunit composition [82,89,94,97,98] . Cone photoreceptor channels have not been studied as intensely as rods but recent reports have shown that CNGA3 CLZ domains form trimers in solution, indicating that the cone CNG channel has a 3:1 A:B stoichiometry like the rods and the olfactory sensory neurons [89,94]. The

additional CNG channel in OSNs has not been studied but a 3:1 CNGA3:CNGB stoichiometry has been proposed [82].

1.9.4 CNG channels in photoreceptors

CNG channels are located in the plasma membrane of the photoreceptors. The GARP region of the CNGB1a subunit (in rods) interacts with peripherin/rds in the disk membranes [99]. The interaction between these two proteins in the two different membranes results in an organized distribution of CNG channels around the membrane of the OS. The A subunits of CNG channels interact with the Na^+/ Ca^{2+}- K^+ exchangers, allowing the close proximity of the channels. The influx of Na^+ and Ca^{2+} ions into the cell via the open CNG channels results in the depolarized state of the photoreceptors in the dark, i.e. the “dark current”, and the activity of the Na^+/ Ca^{2+}- K^+ exchangers prevent the cell from complete depolarization. In the dark, L-glutamate is released from the photoreceptor in a graded state. The CNG channels are the sole source of Ca^{2+} influx into the photoreceptor. When a photon is absorbed by the photoreceptor the phototransduction cascade is initiated and the CNG channels close creating a hyperpolarization of the cell and a decrease in L-glutamate release.

1.9.5 CNG channels in olfactory sensory neurons

The olfactory epithelium (OE) of the nasal cavity is the location of sensory transduction for the sense of smell. The olfactory sensory neurons (OSNs) are bipolar neurons. The dendrite of the OSN extends to the apical side of the OE and the axon extends to the olfactory bulb (OB). On the tip of the OSN dendrite there are 20-50 cilia. The cilia contain the machinery for sensory transduction. Olfactory signal transduction

will be discussed in detail later in this chapter. There are two main populations of OSNs that contain CNG channels. The most common type of OSN uses cAMP as the channel activator. This channel has a 2:1:1 CNGA2:CNGA4:CNGB1b subunit composition and this is the best understood pathway. The less common type of OSN uses cGMP as the channel activator. This channel contains the CNGA3 subunit and a B subunit but it is still unclear which B subunit is utilized. While the stoichiometry of this channel has not been studied, a 3:1 CNGA3:CNGB has been proposed [82]. The CNG channels are closely associated with Ca^{2+}-activated Cl^- channels and Na^+-$2Cl^-$-K^+ cotransporters.

1.9.6 Olfactory system anatomy

The olfactory system is a specialized system that is designed for the intake of air containing odorants and sending the olfactory information to the brain. The olfactory system consists of three main features (Figure 1.13):

a) Nasal cavity and the olfactory epithelium
b) Olfactory sensory neurons
c) Olfactory bulb

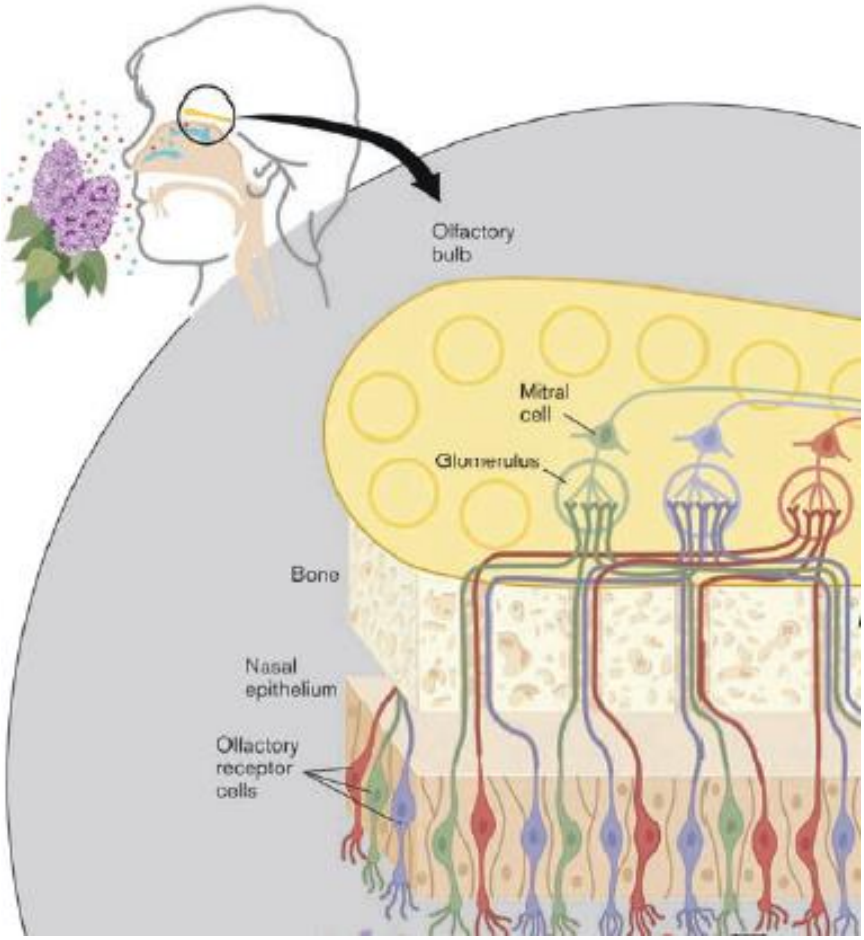

Figure 1.13. The olfactory system. The olfactory system is composed of three main features. The nasal cavity and olfactory epithelium are circled in the image in the upper left and displayed in pink in the bottom of the enlarged image. The olfactory sensory neurons (OSNs) are in red, blue and green; representing groups of OSNs with differing olfactory receptors. The axons of the OSNs extend through the cribriform plate to the olfactory bulb where they form synapses with mitral cells in the glomeruli. Modified from [100].

1.9.6 a Nasal cavity and the olfactory epithelium

Air enters the nasal cavity through the nostrils in the nose. The nasal cavity acts as both an olfactory and respiratory reservoir. Inside the nasal cavity, there are scroll-like bones called turbinates. Lining these thin bones are the respiratory and olfactory epithelia. Some turbinates have a combination of the two epithelia while some contain

solely respiratory or olfactory epithelium. The turbinates have two functions. One function is to warm, humidify and filter the air before it goes to the lungs; this is the respiratory function of the nasal cavity and will not be discussed further [101]. The other function is to expose the OE to incoming odorants.

The OE contains three types of cells (Figure 1.14). There are supporting cells, the OSNs (discussed in the next section) and the basal cells. The supporting cells (or the sustentacular cells) are columnar cells that provide physical and metabolic support to the OSNs. The supporting cells produce the odorant-binding proteins necessary for the trafficking of the incoming odorant to the olfactory receptor. There are two types of basal cells; the globose basal cells and the horizontal basal cells. The globose basal cells are the cells that are responsible for differentiating and maintaining the olfactory epithelium while the horizontal cells replenish the globose cells [102,103]. The neuroepithelium, consisting of the OSNs and sustentacular cells, is exposed to the outside environment necessitating that damaged cells are repaired and replaced. The OSNs in neuroepithelium are one of the few types of nerve cells that can be replaced by cell division during post-natal life. In fact, OSNs have a cellular life span of about one month, so the activity of the globose basal cells is instrumental in the maintenance of the neuroepithelial tissue [101]. The OE contains olfactory glands, also called Bowman’s glands. These glands are below the basal lamina but have ducts that extend through the OE to the surface of the tissue. The glands continuously secrete the mucus that coats the olfactory tract. The secretion holds the odorant-binding proteins produced by the support cells and aids in trapping and trafficking odorants inspired through the nose [101,104].

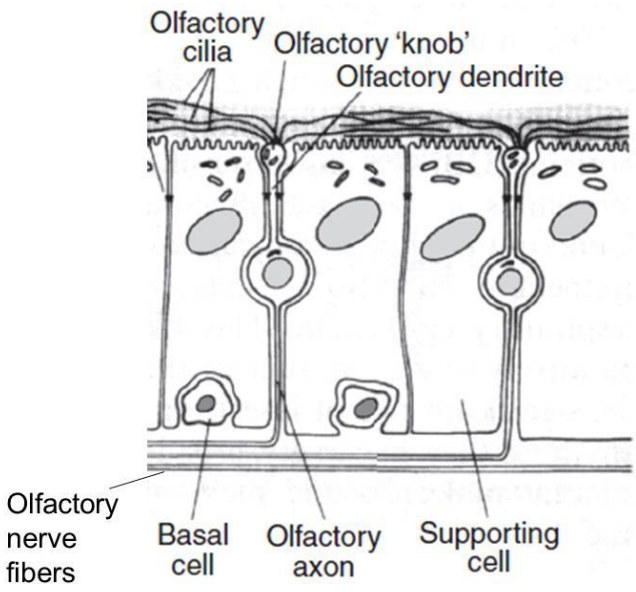

Figure 1.14. The olfactory epithelium. The olfactory epithelium (OE) consists of three types of cells; supporting cells, olfactory sensory neurons (OSNs) and basal cells. The cilia are connected to the dendrite of the OSNs and are exposed to the external environment on the apical side of the OE. The axons of the OSNs extend below the basal lamina and group together to form nerve fiber bundles which extend from nasal cavity through the cribriform plate to the olfactory bulb. Modified from [101].

1.9.6.b Olfactory sensory neurons

OSNs are bipolar neurons with an apical knob extending towards the surface of the OE and the axon extending to the OB. The knob of the OSN contains the nonmotile cilia where olfactory transduction occurs. The unmyelinated axons of the OSNs converge into nerve bundles below the basal lamina and the bundles travel together through the cribriform plate to the olfactory bulb. The bundled axons make up the olfactory nerve [104-107].

The cilia are key structures in the olfactory system. They greatly increase the surface area of the OSN that is exposed to the environment and incoming odors. The cilia are long and narrow projections that hold the olfactory transduction machinery. The olfactory receptors are located in the cilia. The olfactory receptors are a member of the

seven transmembrane G-protein-coupled receptor family and are similar to the opsin genes in the photoreceptors. In humans, there are over 300 functional genes that encode different olfactory receptors while dogs have over 800 functional genes; each species has numerous pseudogenes as well. Each gene produces a receptor that recognizes a set of similar molecules and each OSN (and associated cilia) contain only that one type of olfactory receptor. Additionally, all OSNs that express the same receptor converge in the same glomeruli in the OB [104-107].

The cilia have three major functions in olfactory transduction. First, the cilia take the chemical information from the environment and, through the steps that lead to depolarization of the OSN, turn that message into an electrical response. Second, the small volume of an individual cilium allows a minor local change in ion concentration that can result in depolarization of the cell. This minor change in the cilia is amplified to produce a large neural response. Finally, the cilia aids in adaptation or desensitization of the odor response. The second or continued exposure to an odorant, in a short period of time, produces a decreased response compared to the initial exposure response (see Olfactory Signal Transduction, section 1.8.7, for more details) [104-107].

1.9.6.c Olfactory bulb

The axons of the OSNs form nerve bundles and exit the nasal cavity through the cribriform plate to the OB. The OB is composed of five layers; the nerve fiber layer, the glomerular layer, external plexiform layer, the mitral cell layer and the inner plexiform layer (Figure 1.15) [106,108].

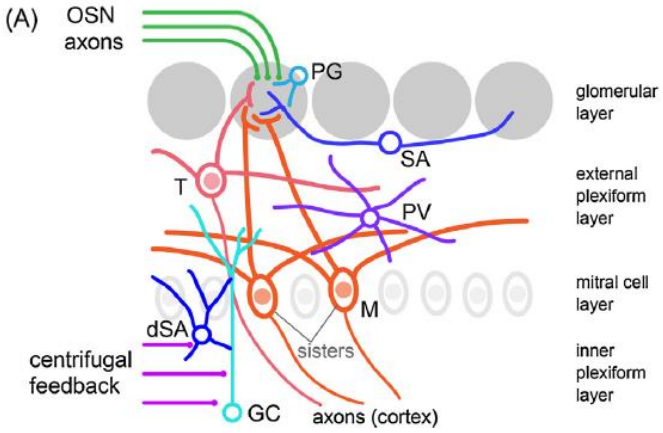

Figure 1.15. The layers of the olfactory bulb. The layers of the olfactory bulb starting from the outside, (where the OSNs form glomeruli with the tufted and mitral cells) the glomerular layer, to the inner plexiform layer. T-tufted cells, M-mitral cells, SA-short axon cells, PG-periglomerular cells. Reproduced from [108].

The outer most layer of the OB is the nerve fiber layer. The axons from the OSNs form a complex web surround the outside of the OB. The axons of the OSNs travel through these networks before terminating in the glomeruli. In the glomerular layer the OSN axons form synapses with post-synaptic mitral and tufted cells. A glomerulus, a spherical area of synaptic transmission in the OB, may contain up to 1000 OSN axons. Tufted cells are secondary neurons that receive excitatory messages via the neurotransmitter glutamate, from the OSNs and project their axons to the olfactory cortex (a region of the brain that receives olfactory input). Mitral cells receive most of their excitatory information from tufted cells but some synapse with OSNs. There are inhibitory cells in the glomerular layer, the periglomerular cells and the short axon cells, which synapse with OSNs, tufted and mitral cells and aid in information processing [106,108].

The external plexiform layer contains the cell bodies and dendrites of some secondary neurons. The tufted and mitral cell dendrites expand laterally and synapse

with inhibitory parvalbumin-expressing interneurons which aid in controlling global gain of the neurons with which they synapse. Granule cell dendrites extend to the external plexiform layer and synapse with mitral and tufted cells to mediate inhibition [106,108].

The mitral cell layer contains the cell bodies of the mitral cells. Mitral cells extend their dendrites to the glomeruli and the external plexiform layer while their axons extend through the inner plexiform layer to the olfactory cortex. Although all OSNs expressing a certain olfactory receptor converge in the same glomeruli, mitral and tufted cells extend to different regions of the olfactory cortex [106,108].

The inner plexiform layer is the inner most part of the OB. This layer consists of granule cells, deep short axon cells and the dendrites of mitral and tufted cells. Granule cells and deep short axon cells provide inhibitory information from the brain to the mitral and tufted cells, this is termed centrifugal feedback. The dendrites from the mitral and tufted cells branch into many regions of the olfactory cortex. The determined location of the dendrites based on the initial input from the glomeruli is not clearly understood [108,109].

1.9.7 Olfactory signal transduction

The majority of OSNs in the OE use CNG channels for signal transduction. There are two major pathways that utilize CNG channels. One pathway utilizes cGMP and a channel with a proposed stoichiometry of 3:1 (CNGA3:CNGB) and the B subunit is yet to be determined. There is not much known about this pathway but there seems to be a consensus that it is used for only certain types of odors, specifically natriuretic peptide hormones. As this is a minor pathway that is not fully understood, it will not be discussed further.

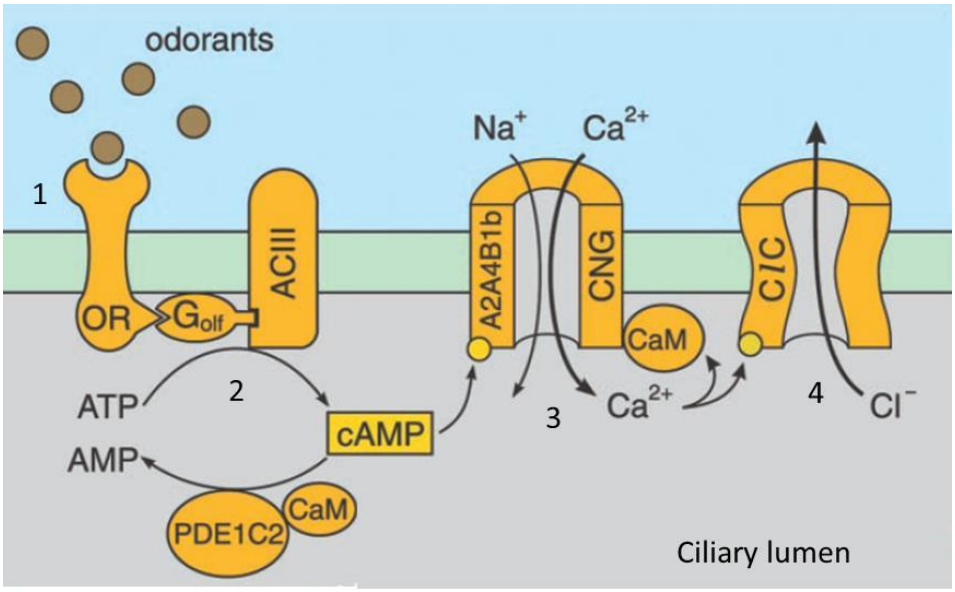

Figure 1.16. Olfactory signal transduction. Olfactory transduction in the olfactory sensory neuron cilium (modified from Kaupp and Siefert 2002). 1) The odorant binds to the olfactory receptor (OR), 2) the G_{olf} protein activates adenylyl cyclase III (ACIII) converting ATP to cAMP. 3) Binding of cAMP to the CNG channel allows the influx of cations. 4) Ca^{2+} binds to and opens the Cl^- channel for complete depolarization of the cell. Figure modified from [82].

The signal transduction pathway that applies to the majority of OSNs utilizes the CNG channel with CNGB1b. The stoichiometry of this channel is 2:1:1 CNGA2: CNGA4:CNGB1b. The CNG channels and olfactory receptors are localized to the cilia of the OSNs which extend out of the OE and into the mucosa of the olfactory tract. When an odorant binds to an olfactory receptor it activates a G protein (G_{olf}) (Figure 1.16, 1). G_{olf} then activates adenylate cyclase III which converts ATP to cAMP (Figure 1.16, 2). cAMP binds to and opens the CNG channels allowing for the influx for cations, depolarizing the cell (Figure 1.16, 3). The increase in local Ca^{2+} opens a nearby Ca^{2+}-dependent Cl^- channel which expels Cl^- which further depolarizes the cell, in fact 80% or more of the depolarization of the cell is due to these Cl^- channels (Figure 1.16, 4)

[82,105]. The depolarization of the OSN triggers the release of an action potential sending an electrical response to the glomeruli in the OB.

During repeat exposures to a scent over a short period of time, the electrical response to that odor reduces. The adaptation mechanisms work directly through the CNG channels in the OSN [110]. Calcium/calmodulin (Ca^{2+}/CaM) is the inhibitory factor involved. The influx of Ca^{2+} into the cell is important for the initial signal transduction and the cell's ability to adapt to an odor. The Ca^{2+} binds to CaM and the Ca^{2+}/CaM complex binds to the CNGA2 subunits and inhibits the channel [110]. CaM also activates the olfactory phosphodiesterase which converts cAMP to AMP, which decreases the amount of available cAMP to open CNG channels and limits the response of the odorant [82,105,110].

1.9.8 CNG channelopathies

Mutations in CNG channels lead to numerous disorders most of which manifest in the photoreceptors. Mutations in CNG genes in humans and animal models have enabled us to improve our understanding of the roles of each of the CNG subunits.

Mutations in the cone CNG channel subunits (*CNGA3* and *CNGB3*) result in achromatopsia (total color blindness). The cones have abnormal to no function but the rods function normally. However rod function only provides a very low level of visual acuity. Human achromatopsia patients have been identified with mutations in either *CNGA3* or *CNGB3*. Canine models have been identified with mutations in the *CNGB3* gene [26,111]. A mouse model for *CNGA3* has been developed as well [112]. A *CNGA3* mutant sheep has been identified and has been used as a large animal model in preliminary gene therapy trials [113,114].

CNGA1 subunit mutations result in RP 49 [115]. Mutations in this gene account for about 1% of arRP patients. These patients have typical RP symptoms. *CNGA1* knockout mice are not yet available but a mutation in the *CNGA1* gene was found in Shetland sheepdog resulting in PRA [38,95].

Olfactory deficits in humans due to CNG channels have yet to be reported but mouse knockout models of the subunits have been studied in detail. Four mouse models have been developed for the study of the CNGA2 subunit [116-119]. These mice have decreased olfactory ability and have a high neonatal mortality rate because mouse pups rely on their sense of smell to find the mother to nurse and the affected mice appear to have reduced ability to locate the mother. While the mice are not anosmic, they do have abnormal development of the OE and OB. In *CNGA4* knockout mice the olfactory system develops normally and there is no apparent difference in morphology between mutants and wild-types. These mice have differences in odor adaptation and cAMP affinity [120,121].

1.9.8.a CNGB1 mutations

CNGB1 mutations have been identified in humans resulting in RP 45, which is reported to result in about 4% of RP cases [55]. The affected patients present with night blindness and decrease peripheral vision by 20 years of age. Their day vision decreases slowly throughout their life resulting in blindness around the age of 60 [122,123]. Patients with CNGB1 mutations and their clinicians are enthusiastic about starting clinical gene therapy trials to restore vision (Drs. Stephen Tsang and Alex Levin, personal communications). Mouse models have been generated to study the impact of *CNGB1* mutations.

The N-terminal mouse knockout was created by removing exons 1 and 2 from the *CNGB1* gene that results in a complete knockout of all rod-specific splice variants. The retinal degeneration is severe and is associated with developmental structural abnormalities in the rod OS. CNGA1 subunits still localize to the OS and the rods still have some abnormal function [124]. While informative, this model does not accurately recapitulate the phenotype of human patients with RP 45.

The C-terminal mouse knockout (*cngb1X-26*) removes exon 26 from the *CNGB1* gene, resulting in a premature stop codon in the full length retinal *CNGB1* transcript and also the olfactory *CNGB1* transcript but the GARP regions are unaffected. These mice have an abnormal visual and olfactory phenotype. There is no recordable rod ERG and single cell rod recording showed very little individual rod response to light. Immunohistochemistry labeling for CNGA1 and full length CNGB1 showed that neither protein was expressed at normal levels (CNGB1 was absent and CNGA1 was expressed at very low levels). The lack of CNGB1 in this mouse model leads to a disruption of phototransduction and results in retinal degeneration. At about 6 months of age, the mice have about 50% of their ONL still present and the photoreceptor OS are shortened. By 11 months of age, only 1 layer of nuclei remained in the ONL [125]. These mice have been used in initial gene therapy trials which have had successful results, partially restoring their vision [126].

The *cngb1X-26* mice also have an olfactory deficit because the mutation occurs in a region of the gene that also affects the CNGB1b transcript. *Cngb1X-26* mice had a higher than normal postnatal mortality and a decrease in body weight because they had difficulty in locating the mother to nurse. In buried food tests, the mice were able to find

food but it took them about 3 times longer than wild-type controls [127]. The OE is slightly thinner in affected mice compared to wild-type mice but the morphology was similar. Immunohistochemistry labeling showed that CNGA2 and CNGA4 channels formed but were not targeted to the cilia and therefore were mislocalized to the cell membrane of the cell body. These channels are still active and may explain the delayed olfactory responses in the mice because it would take the cAMP longer to diffuse to the channels outside of the cilia to open the channel [127].

1.10 Gene therapy

Gene therapy is a method of introducing new or different genes into an organism to reduce or cure disease symptoms. Gene therapy can be used for gene supplementation therapy (used where a mutation causes loss-of-function of a gene) or gene silencing/knockdown therapy (used in conditions in which a mutation results in a gain-of-function or has a toxic product). There are multiple approaches for delivery of a therapeutic gene and these can be divided into non-viral methods and those that utilize viral vectors. Non-viral approaches consist of therapeutic DNA which may or may not be combined with a delivery aid (i.e. physical or chemical) and are introduced to the tissue or cells of interest [128]. Non-viral vectors are relatively safe and have little limitations on size of the gene that can be delivered but they are sensitive to cellular barriers (physical and functional) which must be overcome [128]. While non-viral vectors continue to be developed and optimized, viral vectors are the most commonly utilized and in this chapter I will focus on viral vector methods of gene delivery.

1.10.1 Gene therapy vectors

Viruses have evolved to overcome the host physical and functional barriers. Researchers exploit these features to develop a vector from the virus that will deliver the therapeutic transgene to the target tissue and lead to expression of the therapeutic gene. The most commonly utilized viral vectors (at least in the context of retinal gene therapy) are lentivirus, adenovirus and adeno-associated virus vectors [128].

Lentiviruses are single-stranded RNA retroviruses. Lentiviral vectors can integrate their sequence into the chromosomes of dividing or non-dividing cells, allowing

for long term expression of a transgene. However, the ability to integrate into the host cell chromosomes is cause for some concern. If the lentivirus inserts its genome into a necessary gene or regulatory unit, it could result in insertional mutagenesis with potential adverse consequences. The lentivirus vector can hold up to 8 kb of modification sequence. A major drawback of the lentiviral vector is that it is relatively large in size (80-100 nm) which makes delivery to photoreceptors difficult [128].

Adenoviruses are double-stranded DNA viruses. These viruses infect non-dividing cells and do not incorporate their DNA into the host chromosome (i.e. they exist as episomes within the cell) so insertional mutagenesis is not a concern. These viruses have a very large packaging capacity being able to hold up to 37 kb of DNA sequence. Unfortunately, the virus is up to 100 nm in size, creating difficulty in photoreceptor transduction. Furthermore, the adenoviral vectors can elicit host immune responses that deactivate adeno-modified cells [128]. Methods are being used to modify the adenovirus in such a way that decreases the host immune responses to allow for long-term expression of the transgene [128].

Adeno-associated viral (AAV) vectors are single-stranded DNA viruses that can only replicate in the presence of a helper virus (i.e. with the aid of an adeno or herpes virus). These are small viruses (25 nm) which hold about 4.7 kb of DNA, which limits the size of the gene that can be introduced using the AAV vector [128,129]. While a majority of human beings have been exposed to adeno-associated viruses, there is no disease associated with the virus although a recent report indicates that AAV2 may be involved in some hepatocellular carcinomas [130]. There is also little concern for insertional mutagenesis because the AAV vector persists long term as episomes and

very rarely incorporate into the host genome. The small particle size, ability to transfect non-dividing cells and the ease of viral modifications have placed these vectors at the forefront of retinal gene therapy [128,129].

1.10.2 Wild-type AAV structure and cellular integration

The wild-type AAV can only cause infection with a helper virus; in the absence of the helper virus it exists either as an episome within the host cell or is incorporated into the host genome until activated by a helper virus [129]. The wild-type AAV consists of two inverted terminal repeats (ITRs), two open reading frames and three promoters (Figure 1.17). The three promoters (p5, p19 and p40) code for four replication proteins (*rep*) and three capsid proteins (*cap*). The AAV capsid is the particle that holds the single- stranded DNA. It consists of only 60 polypeptides. The capsid can be modified to increase vector efficacy and decrease immune response (this will be considered in more detail below).

The AAV binds to a receptor on the membrane of the host cell and is endocytosed into the cell by a clathrin-coated pit (Figure 1.18). The AAV then goes through a series of endosomal processing steps, necessary for proper integration of the virus [131]. The endosomal processing results in conformational changes to the capsid proteins exposing nucleus localization signals and a phospholipase domain located on the capsid [129]. The viral vector then enters the nucleus and the capsid is removed in a process called viral uncoating. Once the vector genome is released within the nucleus it must become double-stranded.

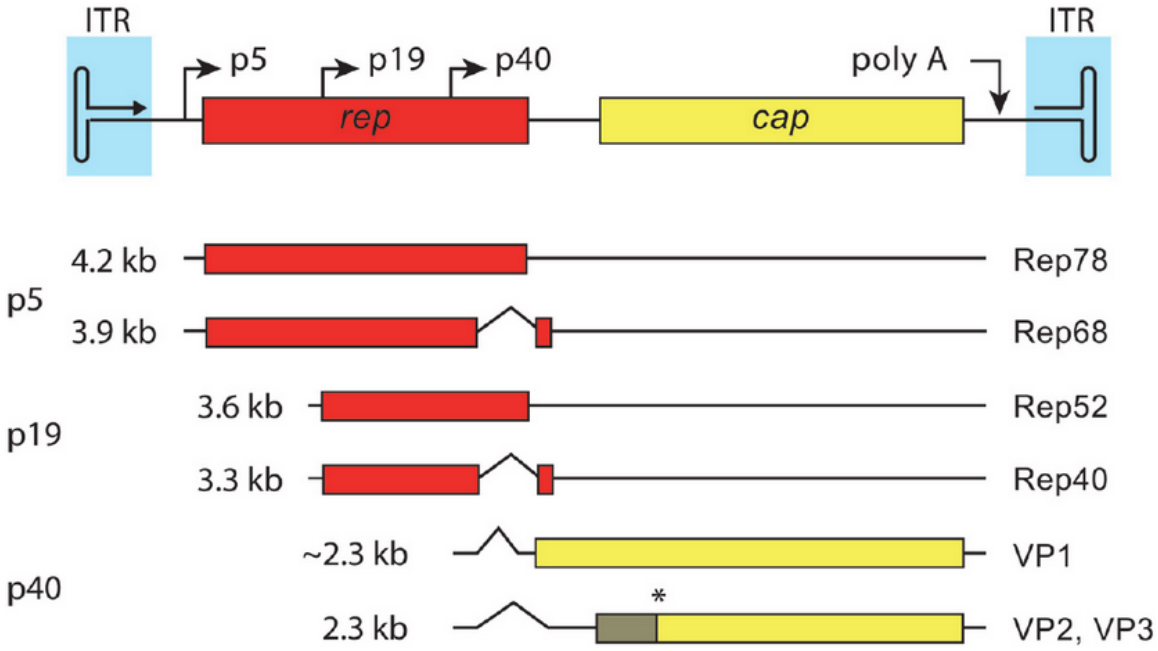

Figure 1.17. Wild-type adeno-associated viral genome. The adeno-associated viral (AAV) genome consists of two inverted terminal repeats (ITR), three promoters (p5, p19 and p40), two open reading frames (*rep* and *cap*) and a poly A tail. The p5 promoter produces two larger replication proteins Rep78 and 68 while the p19 promoter produces the smaller replication proteins Rep52 and 42. P40 produces the capsid proteins VP1, 2 and 3. The promoters, *rep* and *cap* open reading frames can be removed and replaced with a different coding sequence, assisting in gene therapy. Figure reproduced from [129].

The genome becomes double-stranded either by DNA repair mechanisms of the host cell or by annealing of complimentary single-stranded vector genomes. Once it is double-stranded it concatamerizes with the ITR sequences of different additional double-stranded genomes to form the circular structures. The longer the cell is exposed to treatment, the larger the concatamerized episome becomes [128,131]. Risk of AAV integration is low (one integration per 10^3-10^4 vector particles) but still needs to be monitored [132]. Vector integration is random and is very low in non-dividing cells [128,129,131].

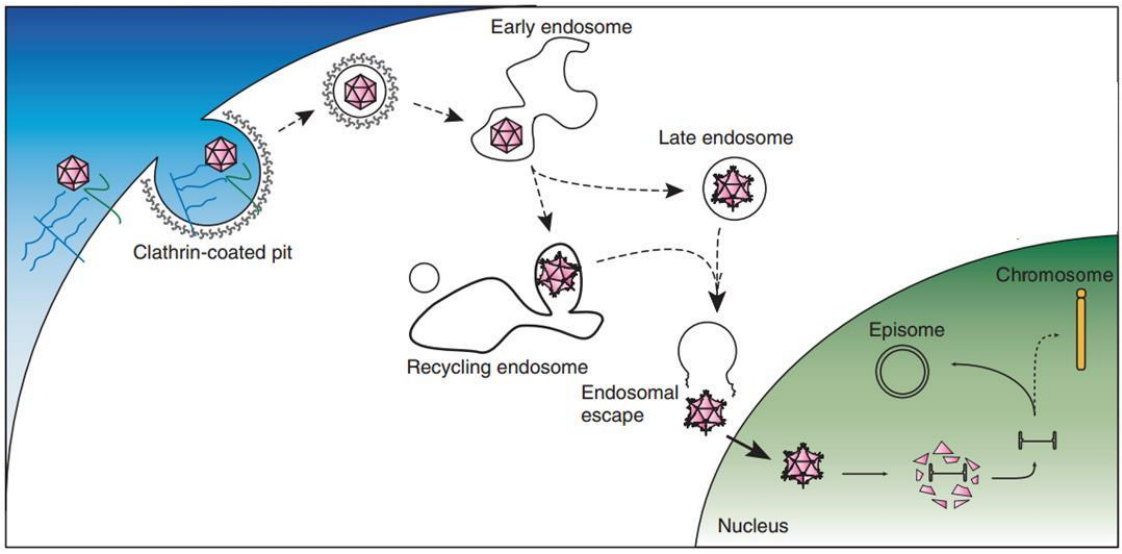

Figure 1.18. Viral entry into the cell. The virus binds to a receptor on the cell surface. The specific receptor is dependent on the vector capsid composition and serotype. The virus enters the cell via a clathrin-coated pit. The virus is processed through an endosome causing a conformational change in the capsid and endosomal escape. The virus is then able to enter the nucleus and expose its genome. The single-stranded viral genome becomes double-stranded and forms episomes for long lasting transduction. Rarely, the viral genome integrates into the host genome at random locations. Modified from [128].

1.10.3 Vector modification

AAV vectors attach to a receptor on the cell surface and then enter the cell via endocytosis. The receptor that the AAV binds to is dependent on the capsid sequence of the vector. This different AAV serotypes have different capsid sequences. The AAV serotype influences which cell type it is able to transduce. Understanding the cellular tropism of vectors can help researchers choose the best vector to target the cell type that is to be modified. AAV vector transduction efficiency can be modified by altering the serotype of the vector. For example, a hybrid vector can be created that takes the genome from one vector (most commonly used is AAV2) and packages it inside a capsid of another serotype (a process known as pseudotyping). For example if it is

packages into an AAV5 capsid it creates an AAV2/5 vector. Pseudotyping may increase transduction efficiency of a desired cell type.

The ITRs are the origins for DNA replication, packaging signals and chromosome maintenance. Recombinant AAV vectors (rAAV) need only these ITR sequences *in cis* for transduction, the *rep* and *cap* sequence can be removed and replaced with a gene and promoter of interest. The coding sequence of the gene can be packaged within the cell as long as the entire coding sequence is less than 5 kb [128,129,131]. The ideal promoter to package within the vector will depend on the target cell type. Promoters can be ubiquitous or cell type specific. The use of a cell type specific promoter decreases the likelihood that the protein of interest is produced in the incorrect cell type (reducing off target effects) [128,129,131].

The capsid sequence can also be modified. Altering conserved capsid tyrosine residues and replacing them with phenylalanine residues has been shown to increase transduction efficiencies (by allowing the vectors to escape ubiquitination) and can decrease immune response [128,129,131]. Some groups have modified capsids with a known ligand for a receptor on their cell of interest [131].

1.10.4 Retinal gene therapy

Gene therapy in the retina has been very successful in animal models and human clinical trials. The eye is an external organ that can be monitored non-invasively and is immune privileged [128]. A subretinal injection (in which the vector is injected between the retina and the RPE) creates a focal retinal detachment often referred to as a “bleb” [128,133]. Within these blebs, the vector is exposed directly to photoreceptors and retinal pigment epithelial cells. This is the most efficient delivery route to target the

outer retinal cells (RPE and photoreceptors). Most vectors used for retinal gene therapy will transduce RPE cells but transduction efficiency in the photoreceptors varies between AAV serotypes and between different capsid modifications. The most commonly utilized vectors for photoreceptor transduction are AAV2 pseudotypes (specifically, AAV2/5, AAV2/8 and AAV2/9) [128]. Vectors can also be delivered intravitreally but the transduction efficiency of photoreceptors is not as high as with subretinal delivery route, most likely due to poor penetration through the inner limiting membrane of the retina [128].

As mentioned earlier, a huge advance in retinal gene therapy was made when gene supplementation therapy using an AAV2 vector delivered by subretinal injection led to sustained transgene expression and rescue of visual function in dogs with marked visual impairment due to a mutation in the *RPE65* gene [24]. This proof of principle study was adapted to human patients [134]. The results from these Phase I/II clinical studies have shown that the AAV2/2 vector is safe in human subjects and holds promising results. However, follow up studies have shown that with older-treated patients there may be long term visual improvement but the retina continues to degenerate [128]. Since these pivotal proof of concept studies in animal models and human patients, at least five additional clinical trials are underway for gene replacement therapy in the retina and even more preclinical trials are starting [135].

1.11 Conclusion

The identification of animal models to study diseases is necessary to understand the biology and mechanisms of a disease. Mouse models are commonly used but there are some drawbacks to using the mouse models, especially for vision research. Mice have small eyes and they are nocturnal, so they have a rod-dominated retina. They do not have a region of high cone/photoreceptor density as seen in the macula of humans. Additionally, many mouse models are engineered and have relatively homogenous genetic background.

Large animal models, specifically dogs, are important for development of therapies of retinal diseases. Dogs have a similar eye shape and morphology to humans. They have a photoreceptor-dense region of the eye called the *area centralis* which is similar in location and function to the human macula. Studying multiple species can highlight species differences in the diseases which can further our understanding of the disease.

In the following chapters I describe the identification and detailed phenotype of the *CNGB1* affected dog. Furthermore, I present the preliminary results of the first successful gene therapy trial in the *CNGB1* affected dog.

REFERENCES

REFERENCES

1. Grimm D (2015) Dawn of the dog. Science 348: 274-279.

2. Pang JF, Kluetsch C, Zou XJ, Zhang AB, Luo LY, et al. (2009) mtDNA data indicate a single origin for dogs south of Yangtze River, less than 16,300 years ago, from numerous wolves. Molecular Biology and Evolution 26: 2849-2864.

3. Freedman AH, Gronau I, Schweizer RM, Ortega-Del Vecchyo D, Han E, et al. (2014) Genome sequencing highlights the dynamic early history of dogs. PLoS Genetics 10: e1004016.

4. Lindblad-Toh K, Wade CM, Mikkelsen TS, Karlsson EK, Jaffe DB, et al. (2005) Genome sequence, comparative analysis and haplotype structure of the domestic dog. Nature 438: 803-819.

5. Vila C, Leonard, J. A. (2012) Canid Phylogeny and Origin of the Domestic Dog. In: Ostrander EA, Ruvinsky A., editor. Genetics of the Dog. 2 ed. Wallingford, Oxon, GBR: CABI Publishing.

6. Germonpre M, Sablin MV, Stevens RE, Hedges REM, Hofreiter M, et al. (2009) Fossil dogs and wolves from Palaeolithic sites in Belgium, the Ukraine and Russia: osteometry, ancient DNA and stable isotopes. Journal of Archaeological Science 36: 473-490.

7. Vila C, Savolainen P, Maldonado JE, Amorim IR, Rice JE, et al. (1997) Multiple and ancient origins of the domestic dog. Science 276: 1687-1689.

8. Parker HG, Kim LV, Sutter NB, Carlson S, Lorentzen TD, et al. (2004) Genetic structure of the purebred domestic dog. Science 304: 1160-1164.

9. Parker HG (2012) The History and Relationships of Dog Breeds. In: Ostrander EA, Ruvinsky A., editor. Genetics of the Dog. 2 ed. Wallingford, Oxon, GBR: CABI Publishing.

10. Breen M, Langford CF, Carter NP, Holmes NG, Dickens HF, et al. (1999) FISH mapping and identification of canine chromosomes. Journal of Heredity 90: 27-30.

11. Selden JR, Moorhead PS, Oehlert ML, Patterson DF (1975) The Giemsa banding pattern of the canine karyotype. Cytogenetics and Cell Genetics 15: 380-387.

12. Venter JC, Adams MD, Myers EW, Li PW, Mural RJ, et al. (2001) The sequence of the human genome. Science 291: 1304-1351.

13. Waterston RH, Lindblad-Toh K, Birney E, Rogers J, Abril JF, et al. (2002) Initial sequencing and comparative analysis of the mouse genome. Nature 420: 520-562.

14. Guenet JL (2005) The mouse genome. Genome Research 15: 1729-1740.

15. Sutter NB, Eberle MA, Parker HG, Pullar BJ, Kirkness EF, et al. (2004) Extensive and breed-specific linkage disequilibrium in Canis familiaris. Genome Research 14: 2388-2396.

16. Nachman MW (2001) Single nucleotide polymorphisms and recombination rate in humans. Trends in Genetics 17: 481-485.

17. Charlesworth B (2009) Fundamental concepts in genetics: effective population size and patterns of molecular evolution and variation. Nature Reviews: Genetics 10: 195-205.

18. Hedrick PW (2011) Genetics of populations. Sudbury, Massachusetts: Jones and Bartlett Learning.

19. Wright S (1965) The Interpretation of Population Structure by F-Statistics with Special Regard to Systems of Mating. Evolution 19: 395-420.

20. Calboli FC, Sampson J, Fretwell N, Balding DJ (2008) Population structure and inbreeding from pedigree analysis of purebred dogs. Genetics 179: 593-601.

21. Shearin AL, Ostrander EA (2010) Leading the way: canine models of genomics and disease. Disease Models and Mechanisms 3: 27-34.

22. Downs LM, Hitti R, Pregnolato S, Mellersh CS (2014) Genetic screening for PRA-associated mutations in multiple dog breeds shows that PRA is heterogeneous within and between breeds. Veterinary Ophthalmology 17: 126-130.

23. Parker HG, Shearin AL, Ostrander EA (2010) Man's best friend becomes biology's best in show: genome analyses in the domestic dog. Annual Review of Genetics 44: 309-336.

24. Acland GM, Aguirre GD, Ray J, Zhang Q, Aleman TS, et al. (2001) Gene therapy restores vision in a canine model of childhood blindness. Nature Genetics 28: 92-95.

25. Bainbridge JW, Mehat MS, Sundaram V, Robbie SJ, Barker SE, et al. (2015) Long-term effect of gene therapy on Leber's congenital amaurosis. New England Journal of Medicine 372: 1887-1897.

26. Yeh CY, Goldstein O, Kukekova AV, Holley D, Knollinger AM, et al. (2013) Genomic deletion of CNGB3 is identical by descent in multiple canine breeds and causes achromatopsia. BMC Genetics 14: 27.

27. Miyadera K, Acland GM, Aguirre GD (2012) Genetic and phenotypic variations of inherited retinal diseases in dogs: the power of within- and across-breed studies. Mammalian Genome 23: 40-61.

28. Whitley RD (1988) Focusing on eye disorders among purebred dogs. Veterinary Medicine 83: 50-62.

29. Petersen-Jones SM, Komaromy AM (2015) Dog models for blinding inherited retinal dystrophies. Human Gene Therapy Clinical Development 26: 15-26.

30. Mellersh CS (2014) The genetics of eye disorders in the dog. Canine Genetics and Epidemiology 1: 1-14.

31. Winkler PA, Ekenstedt KJ, Occelli LM, Frattaroli AV, Bartoe JT, et al. (2013) A Large Animal Model for CNGB1 Autosomal Recessive Retinitis Pigmentosa. PLoS One 8: e72229.

32. Downs LM, Wallin-Hakansson B, Boursnell M, Marklund S, Hedhammar A, et al. (2011) A Frameshift Mutation in Golden Retriever Dogs with Progressive Retinal Atrophy Endorses SLC4A3 as a Candidate Gene for Human Retinal Degenerations. PLoS One 6: e21452

33. Svensson M, Olsen L, Winkler PA, Petersen-Jones SM, Bergstrom T, et al. (2015) Progressive retinal atrophy in the Polski Owczarek Nizinny dog: a clinical and genetic study. Veterinary Ophthalmology.

34. Goldstein O, Mezey JG, Boyko AR, Gao C, Wang W, et al. (2010) An ADAM9 mutation in canine cone-rod dystrophy 3 establishes homology with human cone-rod dystrophy 9. Molecular Vision 16: 1549-1569.

35. Kukekova AV, Goldstein O, Johnson JL, Richardson MA, Pearce-Kelling SE, et al. (2009) Canine RD3 mutation establishes rod-cone dysplasia type 2 (rcd2) as ortholog of human and murine rd3. Mammalian Genome 20: 109-123.

36. Downs LM, Bell JS, Freeman J, Hartley C, Hayward LJ, et al. (2013) Late-onset progressive retinal atrophy in the Gordon and Irish Setter breeds is associated with a frameshift mutation in C2orf71. Animal Genetics 44: 169-177.

37. Dekomien G, Vollrath C, Petrasch-Parwez E, Boeve MH, Akkad DA, et al. (2010) Progressive retinal atrophy in Schapendoes dogs: mutation of the newly identified CCDC66 gene. Neurogenetics 11: 163-174.

38. Wiik AC, Ropstad EO, Ekesten B, Karlstam L, Wade CM, et al. (2015) Progressive retinal atrophy in Shetland sheepdog is associated with a mutation in the CNGA1 gene. Animal Genetics 46: 515-521.

39. Tanaka N, Dutrow EV, Miyadera K, Delemotte L, MacDermaid CM, et al. (2015) Canine CNGA3 Gene Mutations Provide Novel Insights into Human Achromatopsia-Associated Channelopathies and Treatment. PLoS One 10: e0138943.

40. Downs LM, Mellersh CS (2014) An Intronic SINE insertion in FAM161A that causes exon-skipping is associated with progressive retinal atrophy in Tibetan Spaniels and Tibetan Terriers. PLoS One 9: e93990.

41. Goldstein O, Mezey JG, Schweitzer PA, Boyko AR, Gao C, et al. (2013) IQCB1 and PDE6B mutations cause similar early onset retinal degenerations in two closely related terrier dog breeds. Investigative Ophthalmology & Visual Science 54: 7005-7019.

42. Wiik AC, Wade C, Biagi T, Ropstad EO, Bjerkas E, et al. (2008) A deletion in nephronophthisis 4 (NPHP4) is associated with recessive cone-rod dystrophy in standard wire-haired dachshund. Genome Research 18: 1415-1421.

43. Petersen-Jones SM, Entz DD, Sargan DR (1999) CGMP phosphodiesterase-alpha mutation causes progressive retinal atrophy in the Cardigan Welsh corgi dog. Investigative Ophthalmology & Visual Science 40: 1637-1644.

44. Dekomien G, Runte M, Godde R, Epplen JT (2000) Generalized progressive retinal atrophy of Sloughi dogs is due to an 8-bp insertion in exon 21 of the PDE6B gene. Cytogenetics and Cell Genetics 90: 261-267.

45. Suber ML, Pittler SJ, Qin N, Wright GC, Holcombe V, et al. (1993) Irish setter dogs affected with rod/cone dysplasia contain a nonsense mutation in the rod cGMP phosphodiesterase beta-subunit gene. Proceedings of the National Academy of Sciences of the United States of America 90: 3968-3972.

46. Zangerl B, Goldstein O, Philp AR, Lindauer SJ, Pearce-Kelling SE, et al. (2006) Identical mutation in a novel retinal gene causes progressive rod-cone degeneration in dogs and retinitis pigmentosa in humans. Genomics 88: 551-563.

47. Kijas JW, Cideciyan AV, Aleman TS, Pianta MJ, Pearce-Kelling SE, et al. (2002) Naturally occurring rhodopsin mutation in the dog causes retinal dysfunction and degeneration mimicking human dominant retinitis pigmentosa. Proceedings of the National Academy of Sciences of the United States of America 99: 6328-6333.

48. Veske A, Nilsson SE, Narfstrom K, Gal A (1999) Retinal dystrophy of Swedish briard/briard-beagle dogs is due to a 4-bp deletion in RPE65. Genomics 57: 57-61.

49. Zhang Q, Acland GM, Wu WX, Johnson JL, Pearce-Kelling S, et al. (2002) Different RPGR exon ORF15 mutations in Canids provide insights into photoreceptor cell degeneration. Human Molecular Genetics 11: 993-1003.

50. Mellersh CS, Boursnell ME, Pettitt L, Ryder EJ, Holmes NG, et al. (2006) Canine RPGRIP1 mutation establishes cone-rod dystrophy in miniature longhaired dachshunds as a homologue of human Leber congenital amaurosis. Genomics 88: 293-301.

51. Goldstein O, Jordan JA, Aguirre GD, Acland GM (2013) A non-stop S-antigen gene mutation is associated with late onset hereditary retinal degeneration in dogs. Molecular Vision 19: 1871-1884.

52. Goldstein O, Kukekova AV, Aguirre GD, Acland GM (2010) Exonic SINE insertion in STK38L causes canine early retinal degeneration (erd). Genomics 96: 362-368.

53. Sohocki MM, Daiger SP, Bowne SJ, Rodriguez JA, Northrup H, et al. (2001) Prevalence of mutations causing retinitis pigmentosa and other inherited retinopathies. Human Mutation 17: 42-51.

54. Hamel CP (2007) Cone rod dystrophies. Orphanet Journal of Rare Diseases 2: 7.

55. Hartong DT, Berson EL, Dryja TP (2006) Retinitis pigmentosa. Lancet 368: 1795-1809.

56. Chacon-Camacho OF, Zenteno JC (2015) Review and update on the molecular basis of Leber congenital amaurosis. World Journal of Clinical Cases 3: 112-124.

57. Hebrard M, Manes G, Bocquet B, Meunier I, Coustes-Chazalette D, et al. (2011) Combining gene mapping and phenotype assessment for fast mutation finding in non-consanguineous autosomal recessive retinitis pigmentosa families. European Journal of Human Genetics 19: 1256-1263.

58. van Huet RA, Pierrache LH, Meester-Smoor MA, Klaver CC, van den Born LI, et al. (2015) The efficacy of microarray screening for autosomal recessive retinitis pigmentosa in routine clinical practice. Molecular Vision 21: 461-476.

59. Koenekoop RK (2004) An overview of Leber congenital amaurosis: a model to understand human retinal development. Survey of Ophthalmology 49: 379-398.

60. Stone EM (2007) Leber congenital amaurosis - a model for efficient genetic testing of heterogeneous disorders: LXIV Edward Jackson Memorial Lecture. American Journal of Ophthalmology 144: 791-811.

61. Smith CUM (2008) The Human Eye. Biology of Sensory Systems: John Wiley & Sons, Ltd. pp. 281-314.

62. Maggs DJ, Miller PE, Ofri R, Slatter DH (2008) Slatter's fundamentals of veterinary ophthalmology. Philadelphia, PA: Saunders Elsevier.

63. Kolb H (1995) Gross Anatomy of the Eye. In: Kolb H, Fernandez E, Nelson R, editors. Webvision: The Organization of the Retina and Visual System. Salt Lake City UT.

64. Remington L (2005) Retina. Clinical Anatomy and Physiology of the Visual System. 2 ed. St. Louis, Missouri: Butterworth-Heinemann.

65. Strauss O (2005) The retinal pigment epithelium in visual function. Physiological Reviews 85: 845-881.

66. Smith CUM (2008) The Retina. Biology of Sensory Systems: John Wiley & Sons, Ltd. pp. 315-351.

67. Strauss O (1995) The Retinal Pigment Epithelium. In: Kolb H, Fernandez E, Nelson R, editors. Webvision: The Organization of the Retina and Visual System. Salt Lake City UT.

68. Perlman I (1995) The Electroretinogram: ERG. In: Kolb H, Fernandez E, Nelson R, editors. Webvision: The Organization of the Retina and Visual System. Salt Lake City UT.

69. Arden GB, Heckenlively JR (2006) Principles and Practice of Clinical Electrophysiology of Vision. Cambridge, Mass: MIT Press.

70. Kolb H (1995) Photoreceptors. In: Kolb H, Fernandez E, Nelson R, editors. Webvision: The Organization of the Retina and Visual System. Salt Lake City UT.

71. Kolb H (1995) Simple Anatomy of the Retina. In: Kolb H, Fernandez E, Nelson R, editors. Webvision: The Organization of the Retina and Visual System. Salt Lake City UT.

72. Nelson R, Connaughton V (1995) Bipolar Cell Pathways in the Vertebrate Retina. In: Kolb H, Fernandez E, Nelson R, editors. Webvision: The Organization of the Retina and Visual System. Salt Lake City UT.

73. Wright AF, Chakarova CF, Abd El-Aziz MM, Bhattacharya SS (2010) Photoreceptor degeneration: genetic and mechanistic dissection of a complex trait. Nature Reviews: Genetics 11: 273-284.

74. Fu Y (1995) Phototransduction in Rods and Cones. In: Kolb H, Fernandez E, Nelson R, editors. Webvision: The Organization of the Retina and Visual System. Salt Lake City UT.

75. Kolb H (1995) Neurotransmitters in the Retina. In: Kolb H, Fernandez E, Nelson R, editors. Webvision: The Organization of the Retina and Visual System. Salt Lake City UT.

76. Falk GaRS (2006) Synaptic Transmission: Sensitivity Control Mechanisms. In: Arden JRHaGB, editor. Principles and Practice of Clinical Electrophysiology of Vision. 2 ed. Cambridge: MIT. pp. 79-90.

77. Yau KW (1994) Phototransduction mechanism in retinal rods and cones. The Friedenwald Lecture. Investigative Ophthalmology & Visual Science 35: 9-32.

78. Granit R (1933) The components of the retinal action potential in mammals and their relation to the discharge in the optic nerve. Journal of Physiology 77: 207-239.

79. Ekesten B, Komaromy AM, Ofri R, Petersen-Jones SM, Narfstrom K (2013) Guidelines for clinical electroretinography in the dog: 2012 update. Documenta Ophthalmologica 127: 79-87.

80. McCulloch DL, Marmor MF, Brigell MG, Hamilton R, Holder GE, et al. (2015) ISCEV Standard for full-field clinical electroretinography (2015 update). Documenta Ophthalmologica 130: 1-12.

81. Hakanson N NK (1995) Progressive retinal atrophy in papillon dogs in Sweden: A clinical survey. Veterinary & Comparative Ophthalmology: 83-87.

82. Kaupp UB, Seifert R (2002) Cyclic nucleotide-gated ion channels. Physiological Reviews 82: 769-824.

83. Biel M (2009) Cyclic Nucleotide-regulated Cation Channels. Journal of Biological Chemistry 284: 9017-9021.

84. Bradley J, Frings S, Yau KW, Reed R (2001) Nomenclature for ion channel subunits. Science 294: 2095-2096.

85. Wiesner B, Weiner J, Middendorff R, Hagen V, Kaupp UB, et al. (1998) Cyclic nucleotide-gated channels on the flagellum control Ca2+ entry into sperm. Journal of Cell Biology 142: 473-484.

86. Ardell MD, Bedsole DL, Schoborg RV, Pittler SJ (2000) Genomic organization of the human rod photoreceptor cGMP-gated cation channel beta-subunit gene. Gene 245: 311-318.

87. Sautter A, Zong X, Hofmann F, Biel M (1998) An isoform of the rod photoreceptor cyclic nucleotide-gated channel beta subunit expressed in olfactory neurons. Proceedings of the National Academy of Sciences of the United States of America 95: 4696-4701.

88. Bonigk W, Bradley J, Muller F, Sesti F, Boekhoff I, et al. (1999) The native rat olfactory cyclic nucleotide-gated channel is composed of three distinct subunits. Journal of Neuroscience 19: 5332-5347.

89. Zhong H, Molday LL, Molday RS, Yau KW (2002) The heteromeric cyclic nucleotide-gated channel adopts a 3A:1B stoichiometry. Nature 420: 193-198.

90. Quandt FN, Nicol GD, Schnetkamp PPM (1991) Voltage-dependent gating and block of the cyclic-GMP-dependent current in bovine rod outer segments. Neuroscience 42: 629-638.

91. Seifert R, Eismann E, Ludwig J, Baumann A, Kaupp UB (1999) Molecular determinants of a Ca2+-binding site in the pore of cyclic nucleotide-gated channels: S5/S6 segments control affinity of intrapore glutamates. European Molecular Biology Organization Journal 18: 119-130.

92. Higgins MK, Weitz D, Warne T, Schertler GFX, Kaupp UB (2002) Molecular architecture of a retinal cGMP-gated channel: the arrangement of the cytoplasmic domains. European Molecular Biology Organization Journal 21: 2087-2094.

93. Zagotta WN, Olivier NB, Black KD, Young EC, Olson R, et al. (2003) Structural basis for modulation and agonist specificity of HCN pacemaker channels. Nature 425: 200-205.

94. Shuart NG, Haitin Y, Camp SS, Black KD, Zagotta WN (2011) Molecular mechanism for 3:1 subunit stoichiometry of rod cyclic nucleotide-gated ion channels. Nature Communications 2:457.

95. Biel M, Michalakis S (2009) Cyclic nucleotide-gated channels. Handbook of experimental pharmacology: 111-136.

96. Korschen HG, Illing M, Seifert R, Sesti F, Williams A, et al. (1995) A 240 kDa protein represents the complete beta subunit of the cyclic nucleotide-gated channel from rod photoreceptor. Neuron 15: 627-636.

97. Zheng J, Zagotta WN (2004) Stoichiometry and assembly of olfactory cyclic nucleotide-gated channels. Neuron 42: 411-421.

98. Zheng J, Trudeau MC, Zagotta WN (2002) Rod cyclic nucleotide-gated channels have a stoichiometry of three CNGA1 subunits and one CNG131 subunit. Neuron 36: 891-896.

99. Poetsch A, Molday LL, Molday RS (2001) The cGMP-gated channel and related glutamic acid-rich proteins interact with peripherin-2 at the rim region of rod photoreceptor disc membranes. Journal of Biological Chemistry 276: 48009-48016.

100. Axel R (2005) Scents and sensibility: a molecular logic of olfactory perception (Nobel lecture). Angewandte Chemie International Edition 44: 6110-6127.

101. Ross MH, Pawlina W (2011) Histology: a text and atlas : with correlated cell and molecular biology. Philadelphia: Wolters Kluwer/Lippincott Williams & Wilkins Health.

102. Leung CT, Coulombe PA, Reed RR (2007) Contribution of olfactory neural stem cells to tissue maintenance and regeneration. Nature Neuroscience 10: 720-726.

103. Caggiano M, Kauer JS, Hunter DD (1994) Globosee basal cells are neuronal progenitors in the olfactory epithelium: a lineage analysis using a replication-incompetent retrovirus. Neuron 13: 339-352.

104. Smith CUM (2008) Olfaction. Biology of Sensory Systems: John Wiley & Sons, Ltd. pp. 219-243.

105. Pifferi S MA, Kurahashi T. (2010) Signal transduction in vertebrate olfactory cilia. In: A. M, editor. The Neurobiology of Olfaction. Boca Raton (FL): CRC Press.

106. Leinwand SG, Chalasani SH (2011) Olfactory networks: from sensation to perception. Current Opinion in Genetics & Development 21: 806-811.

107. Kleene SJ (2008) The electrochemical basis of odor transduction in vertebrate olfactory cilia. Chemical Senses 33: 839-859.

108. Imai T (2014) Construction of functional neuronal circuitry in the olfactory bulb. Seminars in Cell & Developmental Biology 35: 180-188.

109. Lundstrom JN, Boesveldt S, Albrecht J (2011) Central Processing of the Chemical Senses: an Overview. ACS Chemical Neuroscience 2: 5-16.

110. Trudeau MC, Zagotta WN (2003) Calcium/calmodulin modulation of olfactory and rod cyclic nucleotide-gated ion channels. Journal of Biological Chemistry 278: 18705-18708.

111. Sidjanin DJ, Lowe JK, McElwee JL, Milne BS, Phippen TM, et al. (2002) Canine CNGB3 mutations establish cone degeneration as orthologous to the human achromatopsia locus ACHM3. Human Molecular Genetics 11: 1823-1833.

112. Biel M, Seeliger M, Pfeifer A, Kohler K, Gerstner A, et al. (1999) Selective loss of cone function in mice lacking the cyclic nucleotide-gated channel CNG3. Proceedings of the National Academy of Sciences of the United States of America 96: 7553-7557.

113. Banin E, Gootwine E, Obolensky A, Ezra-Elia R, Ejzenberg A, et al. (2015) Gene Augmentation Therapy Restores Retinal Function and Visual Behavior in a Sheep Model of CNGA3 Achromatopsia. Molecular Therapy 9:1423-33.

114. Reicher S, Seroussi E, Gootwine E (2010) A mutation in gene CNGA3 is associated with day blindness in sheep. Genomics 95: 101-104.

115. Dryja TP, Finn JT, Peng YW, McGee TL, Berson EL, et al. (1995) Mutations in the gene encoding the alpha subunit of the rod cGMP-gated channel in autosomal recessive retinitis pigmentosa. Proceedings of the National Academy of Sciences of the United States of America 92: 10177-10181.

116. Baker H, Cummings DM, Munger SD, Margolis JW, Franzen L, et al. (1999) Targeted deletion of a cyclic nucleotide-gated channel subunit (OCNC1): biochemical and morphological consequences in adult mice. Journal of Neuroscience 19: 9313-9321.

117. Brunet LJ, Gold GH, Ngai J (1996) General anosmia caused by a targeted disruption of the mouse olfactory cyclic nucleotide-gated cation channel. Neuron 17: 681-693.

118. Zheng C, Feinstein P, Bozza T, Rodriguez I, Mombaerts P (2000) Peripheral olfactory projections are differentially affected in mice deficient in a cyclic nucleotide-gated channel subunit. Neuron 26: 81-91.

119. Zhao H, Reed RR (2001) X inactivation of the OCNC1 channel gene reveals a role for activity-dependent competition in the olfactory system. Cell 104: 651-660.

120. Kelliher KR, Ziesmann J, Munger SD, Reed RR, Zufall F (2003) Importance of the CNGA4 channel gene for odor discrimination and adaptation in behaving mice. Proceedings of the National Academy of Sciences of the United States of America 100: 4299-4304.

121. Munger SD, Lane AP, Zhong H, Leinders-Zufall T, Yau KW, et al. (2001) Central role of the CNGA4 channel subunit in Ca2+-calmodulin-dependent odor adaptation. Science 294: 2172-2175.

122. Bareil C, Hamel CP, Delague V, Arnaud B, Demaille J, et al. (2001) Segregation of a mutation in CNGB1 encoding the beta-subunit of the rod cGMP-gated channel in a family with autosomal recessive retinitis pigmentosa. Human Genetics 108: 328-334.

123. Kondo H, Qin MH, Mizota A, Kondo M, Hayashi H, et al. (2004) A homozygosity-based search for mutations in patients with autosomal recessive retinitis pigmentosa, using microsatellite markers. Investigative Ophthalmology & Visual Science 45: 4433-4439.

124. Zhang YW, Molday LL, Molday RS, Sarfare SS, Woodruff ML, et al. (2009) Knockout of GARPs and the beta-subunit of the rod cGMP-gated channel disrupts disk morphogenesis and rod outer segment structural integrity (vol 122, pg 1192, 2009). Journal of Cell Science 122: 1927-1927.

125. Huttl S, Michalakis S, Seeliger M, Luo DG, Acar N, et al. (2005) Impaired channel targeting and retinal degeneration in mice lacking the cyclic nucleotide-gated channel subunit CNGB1. Journal of Neuroscience 25: 130-138.

126. Koch S, Sothilingam V, Garcia Garrido M, Tanimoto N, Becirovic E, et al. (2012) Gene therapy restores vision and delays degeneration in the CNGB1(-/-) mouse model of retinitis pigmentosa. Human Molecular Genetics 21: 4486-4496.

127. Michalakis S, Reisert J, Geiger H, Wetzel C, Zong XG, et al. (2006) Loss of CNGB1 protein leads to olfactory dysfunction and subciliary cyclic nucleotide-gated channel trapping. Journal of Biological Chemistry 281: 35156-35166.

128. Trapani I, Puppo A, Auricchio A (2014) Vector platforms for gene therapy of inherited retinopathies. Progress in Retinal and Eye Research 43: 108-128.

129. Muzyczka N (2010) Adeno-associated Viral (AAV) Vectors. In: Zolotukhin S, Herzog RW, editors. Guide to Human Gene Therapy. River Edge, NJ, USA: World Scientific Publishing Co. pp. 415.

130. Nault JC, Datta S, Imbeaud S, Franconi A, Mallet M, et al. (2015) Recurrent AAV2-related insertional mutagenesis in human hepatocellular carcinomas. Nature Genetics 47: 1187-1193.

131. Schultz BR, Chamberlain JS (2008) Recombinant adeno-associated virus transduction and integration. Molecular Therapy 16: 1189-1199.

132. Russell DW, Miller AD, Alexander IE (1994) Adeno-associated virus vectors preferentially transduce cells in S-phase. Proceedings of the National Academy of Sciences of the United States of America 91: 8915-8919.

133. Petersen-Jones SM, Bartoe JT, Fischer AJ, Scott M, Boye SL, et al. (2009) AAV retinal transduction in a large animal model species: comparison of a self-complementary AAV2/5 with a single-stranded AAV2/5 vector. Molecular Vision 15: 1835-1842.

134. Cideciyan AV (2010) Leber congenital amaurosis due to RPE65 mutations and its treatment with gene therapy. Progress in Retinal and Eye Research 29: 398-427.

135. Boye SE, Boye SL, Lewin AS, Hauswirth WW (2013) A comprehensive review of retinal gene therapy. Molecular Therapy 21: 509-519.

CHAPTER 2

A LARGE ANIMAL MODEL FOR *CNGB1* AUTOSOMOAL RECESSIVE RETINITIS PIGMENTOSA

Winkler PA, Ekenstedt KJ, Occelli LM, Frattaroli AV, Bartoe JT, Venta PJ, Petersen-Jones SM. A large animal model for *CNGB1* autosomal recessive retinitis pigmentosa. *PLoS ONE*. PMID: 23977260

Author Contributions

Conceived and designed the experiments: PAW, SMP-J, PJV, JTB, KJE. Performed the experiments: PAW, LMO, SMP-J. Analyzed the data: KJE, AVF, PAW, LMO, PJV, SMP-J. Wrote the paper: PAW, SMP-J. Provided input for writing the manuscript: KJE, AVF, PJV, JTB

2.1 Abstract

Retinal dystrophies in dogs are invaluable models of human disease. Progressive retinal atrophy (PRA) is the canine equivalent of retinitis pigmentosa (RP). Similar to RP, PRA is a genetically heterogenous condition. We investigated PRA in the Papillon breed of dog using homozygosity mapping and haplotype construction of single nucleotide polymorphisms within a small family group to identify potential positional candidate genes. Based on the phenotypic similarities between the PRA-affected Papillons, mouse models and human patients, *CNGB1* was selected as the most promising positional candidate gene. *CNGB1* was sequenced and a complex mutation consisting of the combination of a one basepair deletion and a 6 basepair insertion was identified in exon 26 (c.2387delA;2389_2390insAGCTAC) leading to a frameshift and premature stop codon. Immunohistochemistry (IHC) of pre-degenerate retinal sections from a young affected dog showed absence of labeling using a C-terminal CNGB1 antibody. Whereas an antibody directed against the N-terminus of the protein, which also recognizes the glutamic acid rich proteins arising from alternative splicing of the CNGB1 transcript (upstream of the premature stop codon), labeled rod outer segments. CNGB1 combines with CNGA1 to form the rod cyclic nucleotide gated channel and previous studies have shown the requirement of CNGB1 for normal targeting of CNGA1 to the rod outer segment. In keeping with these previous observations, IHC showed a lack of detectable CNGA1 protein in the rod outer segments of the affected dog. A population study did not identify the *CNGB1* mutation in PRA-affected dogs in other breeds and documented that the *CNGB1* mutation accounts for ~70% of cases of Papillon PRA in our PRA-affected canine DNA bank. *CNGB1* mutations are one cause

of autosomal recessive RP making the *CNGB1* mutant dog a valuable large animal model of the condition.

2.2 Introduction

Retinitis pigmentosa (RP) is the leading cause of inherited blindness in humans affecting about 1 in 4,000 people [1]. It can be inherited in a dominant, recessive or X-linked fashion and shows considerable locus heterogeneity, with mutations in over 40 genes identified as causing non-syndromic RP (RetNet: https://sph.uth.edu/retnet/sum-dis.htm). Proteins encoded by these genes are necessary for a variety of functions within photoreceptors and their supporting cells. The age at onset and rate of progression of RP vary such that some patients have a history of night blindness from childhood while others may not notice symptoms until they are adults. The variability depends on the gene involved and the effect of the mutation on gene function, but there is also variability between patients with the same mutation [2,3]. Rod photoreceptors are affected initially, resulting in loss of night (rod-mediated) vision and constriction of the visual fields. Loss of cone-mediated (daytime and color) vision may occur secondarily to rod-loss, even when RP is caused by a mutation of a gene exclusively expressed in rods, and can lead to complete blindness.

Retinal dystrophies analogous to RP occur in dogs, with reports of such conditions in over 100 different breeds [4]. The canine RP equivalent is known as progressive retinal atrophy (PRA) [5,6]. The gene mutations underlying several forms of PRA have been identified and many have proven to be in genes analogous to those known to cause RP [7-13] or in some instances have suggested new candidate genes for investigation in RP patients [14-16].

Spontaneously occurring retinal dystrophies in canine models are of particular interest because the canine eye is similar in size to the human eye. This morphological

similarity allows for identical surgical approaches for intravitreal and subretinal injection of therapeutic agents and testing for approaches such as implantation of intravitreal sustained-release devices. An additional advantage of canine models over rodent models is that the canine eye has regions of higher photoreceptor density (of both rods and cones), namely the area centralis and the visual streak that are somewhat analogous to the human macula [17]. In contrast, the retina of laboratory rodents lacks an equivalent region having an even density of photoreceptors across the retina [18]. Dogs with spontaneous mutations resulting in retinal dystrophies have proven to be important in preclinical assessment of therapies destined for use in human patients. For example, dogs with a mutation in *RPE65* as a model for Leber congenital amaurosis type II were crucial for preclinical proof-of-concept gene therapy trials [19] which led to phase 1/2 human clinical trials [20-22]. The RPE65 mutant dog and other dog retinal dystrophy models have subsequently been used in several other preclinical trials for retinal gene and drug therapy [19,23-31]. Identification of the gene mutations underlying other forms of canine PRA may provide additional spontaneous canine models to allow study of disease mechanisms and proof-of-concept therapy trials.

The Papillon breed of dog was initially reported to have PRA in 1995 [32]. Studies of the phenotype of affected dogs suggested loss of rod electrophysiological responses but maintenance of cone-driven responses at least until late in the disease process [33,34]. Our unpublished studies of PRA in Papillons show a wide range in age of onset. This phenotypic variability could either suggest within-breed locus heterogeneity or could merely be the result of background genetic or environmental influences.

In this study we report a frameshift mutation in *CNGB1* that is the cause of one form of PRA in Papillon dogs providing a large-animal model of autosomal recessive RP (RP45) due to *CNGB1* mutations.

2.3 Materials and methods

2.3.1 Ethics statement

All procedures were in compliance with the ARVO statement for the Use of Animals in Ophthalmic and Vision Research and approved by the Michigan State University Institutional Animal Care and Use Committee (AUF number 05/11-106-00; Institutional NIH/PHS Animal Welfare Assurance number A3955-01).

2.3.2 Electroretinography

To assess rod and cone photoreceptor function, electroretinograms (ERGs) were recorded using a modification of a previously described technique [26]. Briefly, ERGs were recorded using an Espion E2 Electrophysiology system with ColorDome Ganzfeld (Diagnosys LLC, Lowell, MA) and bandpass set between 0.5 and 500 Hz. Dogs were dark-adapted for one hour and anesthetized with injectable propofol (10 mg/kg PropoFlo, Abbott Animal Health, North Chicago, IL), intubated and maintained on inhaled 1 to 2% isoflurane (Isoflo, Abbott Laboratories, North Chicago, IL) delivered in oxygen. The ERG assessment consisted of three dark-adapted flash intensities at -2.4, -1.2 and 0.4 log cdS/m^2 to record rod and mixed rod-cone responses. This was followed by light adaptation at 30 cd/m^2 for 10 minutes and recording of a light-adapted response to a 0.4 log cdS/m^2 flash and then 33 Hz flicker responses to the same intensity both superimposed on the same background light.

2.3.3 Spectral domain-optical coherence tomography

Assessment of retinal morphology was performed by Spectral Domain-Optical Coherence Tomography (SD-OCT; Spectralis OCT+HRA Heidelberg Engineering Inc., Heidelberg, Germany). Dogs were anesthetized as described for ERG, the pupil dilated with 1% topical tropicamide (Mydriacyl, Alcon Laboratories, Honolulu, HI, USA), a lid speculum fitted and the eye positioned in primary gaze using a stay suture in the inferior perilimbal conjunctiva. High-resolution cross-section images obtained by line and volume scanning and images from the same region of the central retina of affected and control (wild-type) Papillons were assessed.

2.3.4 Animal use and sample collection

A pregnant female Papillon dog that had been diagnosed with PRA and had been mated with a PRA-affected Papillon stud dog was donated to the Michigan State University Comparative Ophthalmology laboratory with the consent of the owner to allow the study of the phenotype of PRA in the breed. This female and her offspring were used to establish a small breeding colony of dogs. The colony was kept under standard laboratory housing with 12:12hr light:dark cycles.

Blood samples from client-owned Papillon dogs were donated with owner consent. DNA was extracted from blood samples using a commercial DNA extraction kit with a modified protocol (Qiagen Sciences, Germantown, MD). Briefly, a red blood cell lysis buffer (0.32 M sucrose, 10 mM Tris, 5 mM $MgCl_2$) was added in a 2 step fashion to whole blood (3X volume and then 2X volume, respectively). Cell lysis solution (Qiagen Sciences, Germantown, MD) was added to lyse the white blood cells followed by

addition of protein precipitation solution (Qiagen Sciences, Germantown, MD), isopropanol DNA precipitation and a 70% ethanol wash step.

The retina from a mixed breed dog was dissected from an enucleated eye and placed in an RNA stabilization buffer (RNAlater, Qiagen Sciences, Germantown, MD) and stored in a -80° C freezer until RNA extraction. RNA was extracted using an RNEasy kit according to manufacturer's protocol (Qiagen Sciences, Germantown, MD). cDNA was made from mRNA using a 3' RACE kit according to manufacturer's protocol (Invitrogen, Carlsbad, CA).

2.3.5 Genome-wide association mapping

Twenty-four Papillons (9 cases, 15 controls) were genotyped for 173,662 single nucleotide polymorphisms (SNPs) using Illumina Canine HD BeadChips. Initial genome-wide association analysis was conducted using the genome analysis toolset PLINK [35]. SNPs with a minor allele frequency (MAF) of <5% and with missing genotype calls of >10% were removed from the analysis. The final data set consisted of 116,235 markers. All 24 individuals genotyped successfully for over 90% of the SNPs and were retained in the analysis. One of the control dogs was removed from the PLINK analysis but was used in the run of homozygosity analysis. The final genotyping rate was >99.8%. Chi-square association mapping was conducted in PLINK, and correction for multiple testing was achieved using the Max(T) permutation procedure (10,000 permutations) in PLINK.

2.3.6 Custom sorting program and haplotype construction

Homozygosity mapping was performed using a custom sorting program. An algorithm was written to search for blocks of SNPs where there was a difference in the

calls between the affected and unaffected dogs. The high quality SNP data, generated from PLINK, was imported to a Microsoft SQL Server 2008R2 database (Microsoft Corporation, Redmond, WA) to take advantage of its efficient set theory based querying mechanism. The received data was formatted with dog identifiers as columns and SNPs as rows. Indexing the data provided a method to measure continuity. The query used scalar-valued functions to assess the criteria described below and attached a flag to each row identified. For each individual SNP, if the affected dogs shared the same homozygous genotype, then the unaffected dogs were compared and rows identified where 95% of the unaffected dogs did not share the same genotype as the affected dogs. Upon those criteria being met, the affected and unaffected groups were considered 'different' by the algorithm. Identified SNPs were then sorted into groups formed by having a level of adjacency of at most four SNPs apart. Only sections with 6 or more SNPs meeting the above criteria were marked for further analysis. These regions were then sorted by size of the region and all regions 1.5 MB or larger were inspected for arRP candidate genes using the University of California, Santa Cruz (UCSC) Genome Browser [36] (http://genome.ucsc.edu/). Four regions of particular interest (on CFA2, CFA4, CFA7, and CFA12) were then subjected to haplotype construction, using fastPHASE [37]. Haplotypes were manually examined for shared regions in related affected family members.

2.3.7 DNA sequencing

The UCSC Genome Browser (http://genome.ucsc.edu/) CanFam2.0 was used in conjunction with the cDNA sequences to identify the exons for the *CNGB1* gene. Primers (Supplemental Table 2.S1) were designed flanking the entire exon and the

splice sites using Primer3 (http://frodo.wi.mit.edu/). Sanger dideoxy-sequencing was done by an ABI 3730 Genetic Analyzer (Applied Biosystems, Inc., Foster City, CA) at Michigan State University's Research Technology Support Facility.

2.3.8 *CNGB1* genotyping assay

A restriction enzyme digest was designed to quickly screen dogs for the mutation in *CNGB1* (see supplemental methods). This assay was used to test for the presence of the mutation in 139 Papillon dogs, 33 PRA affected dogs from 8 different breeds and 66 unaffected dogs from 9 different breeds.

2.3.9 Immunohistochemistry

A PRA-affected female Papillon from the research colony and an unaffected mixed breed female control dog were humanely euthanized at 8 weeks of age. The eyes were enucleated and the right eye was fixed in paraformaldehyde following a previously describe protocol [38].

Frozen sections were immunolabeled with either a rabbit anti-mouse CNGB1 N-terminal (kindly provided by Dr. Stephen Pittler), rabbit anti-human CNGB1 C-terminal (Sigma-Aldrich, St Louis, MO) or mouse monoclonal CNGA1 ([39] kindly provided by Dr. Bob Molday) antibody. Sections were blocked with 10% horse serum (Sigma-Aldrich, St Louis, MO) for 2 hours at room temperature and labeled with primary antibodies (dilutions of: N-terminal CNGB1 1:100, C-terminal CNGB1 1:300 and CNGA1 1:10) overnight at 4°C. Secondary antibodies (anti-rabbit or anti-mouse Alexa Fluor 488, 1:500) (Invitrogen Molecular Probes, Carlsbad, CA) were placed on the sections for 2

hours at room temperature. All sections were counterstained with the nuclear stain DAPI (Invitrogen Molecular Probes, Carlsbad, CA).

Sections were imaged using a fluorescent microscope (Nikon Eclipse 80i, Nikon Instruments Inc., Melville NY) using commercial image capture software (MetaVue, Molecular Devices, Sunnyvale CA).

2.4 Results

2.4.1 Phenotypic description

DNA samples were collected from 23 PRA-affected Papillons and 119 unaffected Papillons. The dogs had all been examined by a veterinary ophthalmologist. For the affected dogs an ophthalmoscopic diagnosis was made between 10 months and 13 years of age (data not shown). A small breeding colony of PRA-affected Papillons was established, consisting of an affected female and two affected offspring. Electroretinography (ERG) showed markedly reduced or absent rod-mediated ERG responses from an early age with preservation of cone photoreceptor responses (Figure 2.1). Spectral Domain-Optical Coherence Tomography (SD-OCT) performed on PRA-affected Papillons (confirmed to have the *CNGB1* mutation described in this paper) showed that at the time the canine retina reaches maturity (approximately 8 weeks of age [40]) retinal layer thicknesses were comparable to a normal control (Figure 2.2A and 2.2B) and that affected dogs have a progressive thinning of the outer nuclear layer with age (Figure 2.2C & D).

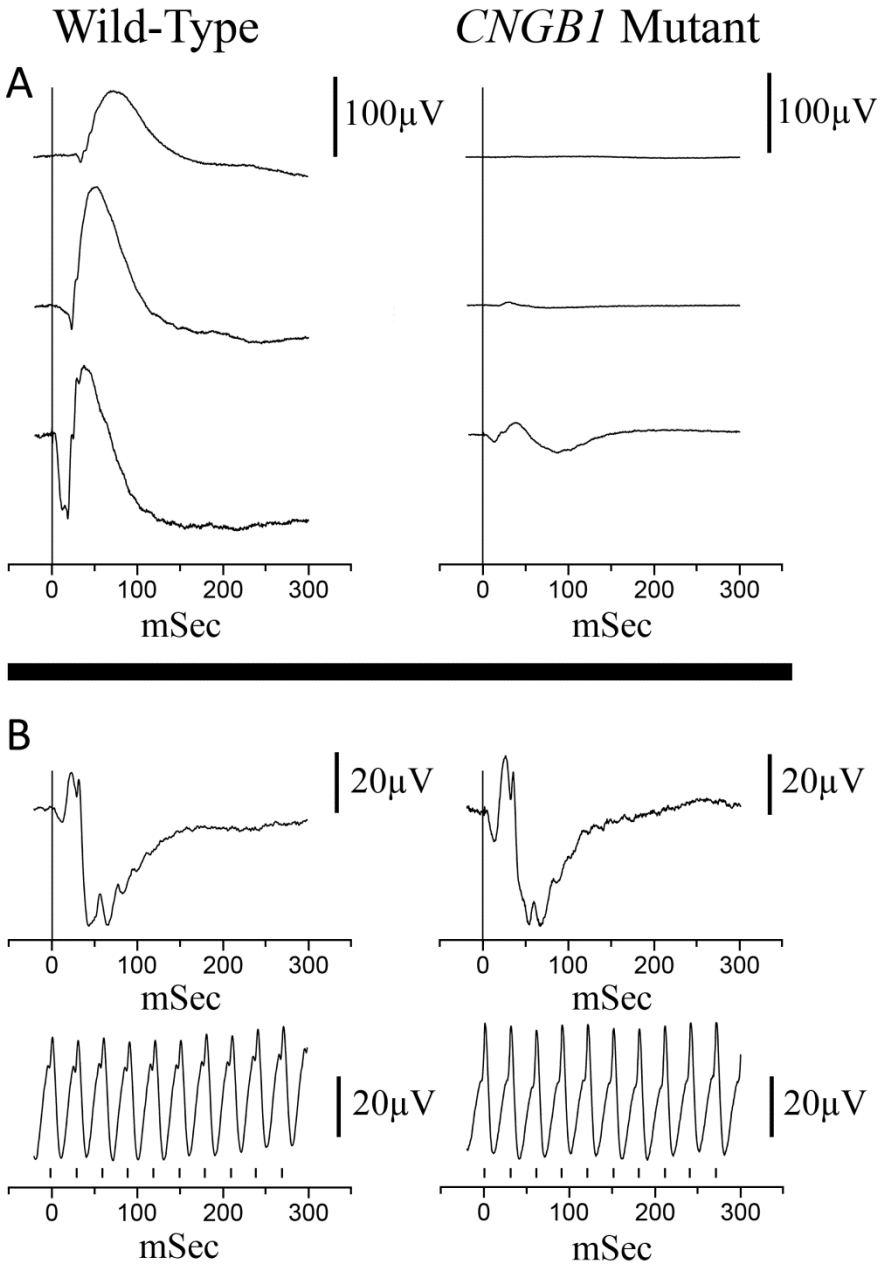

Figure 2.1. Representative ERG tracings from a normal control Papillon and a PRA-affected Papillon, both 10 weeks of age. A. Dark-adapted ERG recordings at -2.4, -1.2 and 0.4 log cdS/m^2. B. Light-adapted flash and flicker (33Hz) ERG tracings. Background white light of 30 cd/m^2 and flash intensity of 0.4 log cdS/m^2. The vertical bars on the flicker ERG indicates the flash timing.

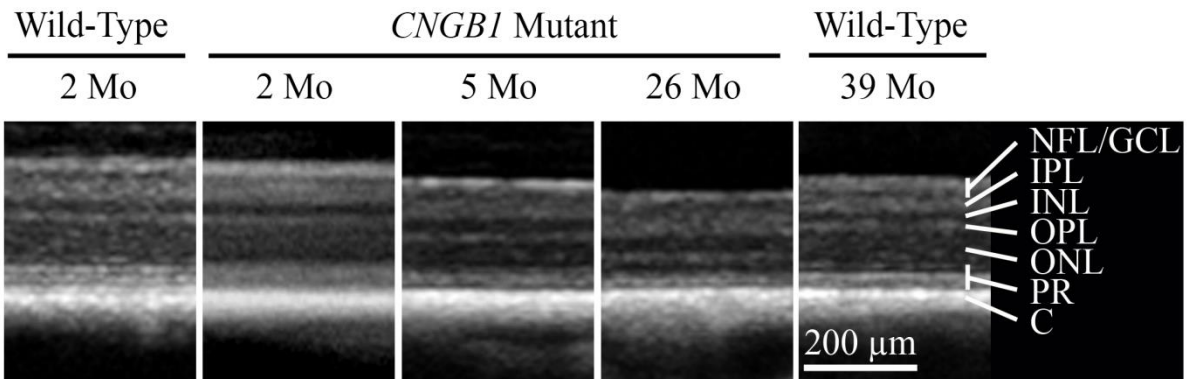

Figure 2.2. SD-OCT cross sectional images of the central retina from *CNGB1* mutant Papillons and wild-type controls. Note the progressive thinning of the outer nuclear layer of the retina in the affected animals. NFL/GCL – nerve fiber layer/ganglion cell layer; IPL – inner plexiform layer; INL – inner nuclear layer; OPL – outer plexiform layer; ONL – outer nuclear layer; PR – photoreceptor inner and outer segments; C – choroid. (Note the retinal pigment epithelium is not labeled).

2.4.2 Mapping of the Papillon PRA locus

An initial genome-wide association analysis performed using PLINK software [35] and including the genotypes from 23 Papillons (9 cases, 4 obligate carriers and 10 controls) yielded no significant associations (data not shown). Because within breed locus heterogeneity for PRA in dogs is a common occurrence, and because we and others had noted a wide range of age of onset [32] between the affected dogs, we suspected that more than one form of PRA may be segregating in the Papillon breed. Therefore, we analyzed the genotyping data from a small family group of 3 affected dogs within our breeding colony that we felt were very likely to share the same gene mutation (pedigree in Figure 2.3). We compared the genotyping results of the 3 affected dogs with that of 2 obligate carriers from the family and 11 control dogs (an additional control was included in this analysis). Our pedigree analysis supported an autosomal recessive mode of inheritance (data not shown) so we performed homozygosity mapping using a custom written computer program. The program was set

to identify regions of homozygosity containing runs of at least six SNPs in the cases and for which the control animals did not share homozygosity (see Materials and Methods). This revealed 13 such regions of homozygosity greater than 1.5 Mb but only 4 of these regions contained obvious positional autosomal recessive RP candidate genes; *CNGB1* (CFA2)*, RBP3* and *RGR* (CFA4)*, RD3* and *CRB1*(CFA7) and *TULP1* (CFA12) (Table 2.1).

Figure 2.3 shows a section of the run of homozygosity surrounding *CNGB1* and the *p*-values for each marker, resulting from a chi-square association test corrected for multiple testing (the full region of homozygosity is shown in Supplementary Table 2.S4). These four regions were then subjected to haplotype construction, and haplotypes were examined within the small family group (data not shown). Only in the CFA2 region did the affected dogs from this family have a unique extended haplotype which was not present in the homozygous state in control (non-obligate carrier) dogs. Obligate carrier dogs each possessed one copy of this haplotype. Furthermore, after comparing the phenotype of the PRA-affected dogs in our colony with that reported for human families and mouse models with *CNGB1* mutations, *CNGB1* was considered the strongest candidate. Based on the haplotype analysis and phenotypic information, *CNGB1* was selected to screen first for mutations.

Table 2.1. Regions of homozygosity above 1.5 MB from small Papillon family

Chr	Start Position[1]	End Position[1]	Size of Region (bp)	arRP Candidate Genes[2]	Location of Candidate Genes[1]
6	3,330,209	12,765,968	9,435,759	-	-
28	10,867,526	19,744,585	8,877,059	-	-
4	34,171,819	42,900,776	8,728,957	*RGR*	ch4:37,501,028-37,504,555
4	34,171,819	42,900,776	8,728,957	*RBP3*	ch4:38,165,164-38,175,385
21	19,922,213	28,084,112	8,161,899	-	-
7	7,812,042	14,771,908	6,959,866	*CRB1*	chr7:8,233,979-8,375,413
7	7,812,042	14,771,908	6,959,866	*RD3*	chr7:12,835,467-12,835,739
2	37,571,313	43,948,453	6,377,140	-	-
12	3,051,458	8,579,562	5,528,104	*TULP1*	chr12:7,639,870-7,647,308
7	3,000,316	7,077,039	4,076,723	-	-
37	23,673,475	26,349,135	2,675,660	-	-
14	8,954,008	11,562,422	2,608,414	-	-
32	11,212,687	13,539,152	2,326,465	-	-
2	60,980,617	62,826,928	1,846,311	*CNGB1*	chr2:61,454,476-61,520,336
14	37,878,684	39,484,021	1,605,337	-	-

1. Locations are all in respect to UCSC Genome Browser CanFam2.0 (http://genome.ucsc.edu)
2. arRP - autosomal recessive retinitis pigmentosa. Gene abbreviations: *RBP3* - retinol binding protein 3, *RGR* - retinal G protein coupled receptor, *RD3* - retinal degeneration protein 3, *CRB1* - crumbs homolog 1, *TULP1* - tubby like protein 1, *CNGB1* - cyclic nucleotide gated channel beta 1

SNP Name	Chr	Base Position	Pval	A1	A2	A3	C1	C2	U1	U2	U3	U4	U5	U6	U7	U8	U9	U10	U11
BICF2P544910	2	61,179,425	0.0022	AA	AA	AA	AB	AB	AB	BB	BB	BB	BB	BB	BB	BB	BB	AB	AB
BICF2P348907	2	61,182,288	0.0022	BB	BB	BB	AB	AB	AB	AA	AA	AA	AA	AA	AA	AA	AA	AB	AB
BICF2P1349008	2	61,198,715	0.0022	AA	AA	AA	AB	AB	AB	BB	BB	BB	BB	BB	BB	BB	BB	AB	AB
BICF2S23137837	2	61,206,318	0.0022	BB	BB	BB	AB	AB	AB	AA	AA	AA	AA	AA	AA	AA	AA	AB	AB
BICF2S23035024	2	61,341,337	0.0022	BB	BB	BB	AB	AB	AB	AA	AA	AA	AA	AA	AA	AA	AB	AB	AB
BICF2S23238410	2	61,420,765	0.0022	BB	BB	BB	AB	AB	AB	AA	AA	AA	AA	AA	AB	AA	AA	AA	AA
BICF2P309315	2	61,428,709	0.0022	BB	BB	BB	AB	AB	AB	AA	AA	AA	AA	AA	AA	AA	AA	AA	AA
BICF2P606415	2	61,556,283	0.0022	BB	BB	BB	AB	AB	AB	AA	AA	AB	AA	AA	AB	AA	AB	AA	AA
BICF2P548237	2	61,563,742	0.0022	BB	BB	BB	AB	AB	AB	AA	AA	AB	AA	AA	AB	AA	AB	AA	AA
BICF2S23117344	2	61,604,057	0.0022	BB	BB	BB	AB	AB	AB	AA	AA	AB	AA	AA	AB	AA	AB	AB	AB
BICF2S23119288	2	61,608,201	0.0022	AA	AA	AA	AB	AB	AB	BB	BB	AB	BB	BB	AB	BB	AB	AB	AB
BICF2P75954	2	61,645,929	0.0022	AA	AA	AA	AB	AB	AB	BB	BB	AB	BB	BB	BB	BB	BB	AB	AB
BICF2S23730507	2	61,656,330	0.0022	BB	BB	BB	AB	AB	AB	AA	AA	AB	AA	AA	AA	AA	AB	AB	AB
BICF2P52239	2	61,677,919	0.0022	BB	BB	BB	AB	AB	AB	AA	AA	AB	AA	AA	AB	AA	AB	AB	AB
BICF2S23740273	2	61,700,423	0.5756	BB	BB	BB	BB	BB	BB	BB	BB	AB	BB	BB	AB	BB	AB	BB	BB
BICF2P57790	2	61,719,834	0.0022	AA	AA	AA	AB	AB	BB	BB	BB	AB	BB	BB	BB	BB	AB	AB	AB
BICF2P1445705	2	61,736,588	0.0022	AA	AA	AA	AB	AB	BB	BB	BB	BB	BB	BB	BB	BB	AB	BB	BB
BICF2P651283	2	61,761,135	0.0022	BB	BB	BB	AB	AB	AA	AA	AA	AB	AA	AA	AA	AA	AA	AA	AA
BICF2P1201761	2	61,781,060	0.5858	BB	BB	BB	BB	BB	BB	BB	BB	AB	BB	BB	BB	BB	BB	AB	AB
BICF2S23256057	2	61,792,733	0.0022	AA	AA	AA	AB	AB	BB	BB	BB	BB	BB	BB	BB	BB	BB	BB	BB
BICF2P705841	2	61,822,011	0.0022	AA	AA	AA	AB	AB	BB	BB	BB	BB	BB	BB	BB	BB	BB	BB	BB
BICF2S23730081	2	61,830,410	1	BB	BB	BB	BB	BB	BB	BB	BB	AB	BB	BB	AB	BB	BB	BB	BB

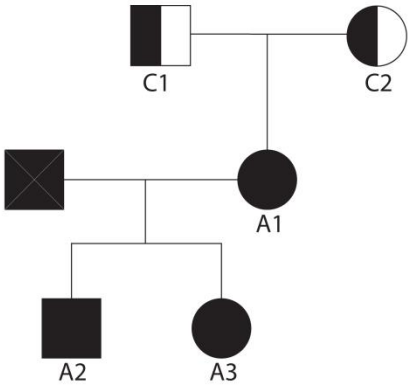

Figure 2.3. SNP analysis in the *CNGB1* region using a small family group of affected and unaffected Papillons. The SNPs are located in a 1.84 Mb region of homozygosity among the affected dogs (Only SNPs near the center of the region are shown). *CNGB1* is located at chr2:61,454,476-61,520,336 in the reference genome (canFam2.0). SNP genotypes are given in columns for each dog, with the family group data displayed to the left of the black back and all others to the right of the black bar. All affected dogs (1-3) share the same haplotype, obligate carriers (C1-2) each have one copy of the haplotype seen in the affected dogs and none of the unaffected dogs (U1-11) possess the haplotype seen in the affected dogs. A-Major allele, B-minor allele, as designated by Illumina (Illumina Inc, San Diego, CA).

2.4.3 Genomic structure of canine *CNGB1*

To establish the genomic structure of canine *CNGB1* we sequenced cDNA from a control canine retinal library and genomic DNA from a control Papillon and compared these to the published canine genomic sequence for this region (CanFam2.0). From these comparisons we deduced the intron/exon boundaries for *CNGB1* (Table 2.2) which differed from the predicted structure seen on the University of California, Santa Cruz (UCSC) Genome Browser [36] (http://genome.ucsc.edu/).

2.4.4 Sequence analysis of *CNGB1*

The full coding region of canine *CNGB1* was sequenced from the cDNA of a control canine retinal library (cDNA sequence submitted to GenBank KC527595). Sequencing cDNA from the control dog revealed three single nucleotide variants (SNVs), at locations c.3378C>A, c.3440T>C and c.3534G>A, and one previously reported single nucleotide polymorphism (SNP) at location c.151G>A (rs22870569). *CNGB1* exons and exon/intron boundaries were sequenced from genomic DNA from control and affected Papillons. This revealed the same SNVs and SNP as seen in the sequenced cDNA but also contained two additional variants; a previously described SNP (c.27G>A, rs22870567) and a SNV allele that segregates with the affected phenotype (c.215C>T; p.P72L). PolyPhen-2 predicts that this is a benign change in amino acid (HumVar 0.412) [41].

The affected Papillon had a frameshift mutation in exon 26. This consisted of a 1 bp deletion (chr2: 61,502,597; c.2387delA) and a 6 bp insertion (between chr2:61,502,599-61,502,600; c. 2389_2390insAGCTAC).

This mutation (c.2387delA;2389_2390insAGCTAC, which for simplicity we will refer to as *CNGB1-fs26*) is predicted to result in a premature stop codon, 17 bp downstream and is present in affected Papillons but not in unaffected Papillons or in the canine reference genome (UCSC Genome Browser CanFam2.0) (Figure 2.4).

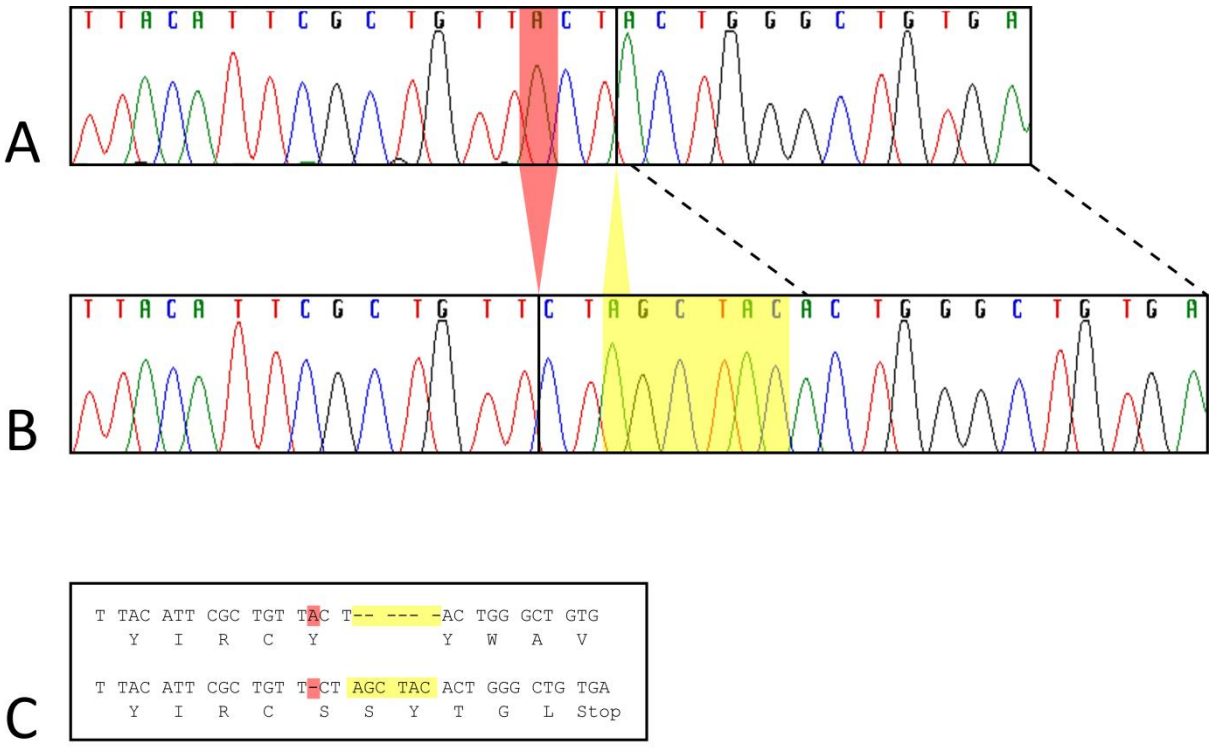

Figure 2.4. Papillon mutation in *CNGB1* exon 26. Sanger dideoxy-sequencing traces for part of *CNGB1* exon 26 are shown for an unaffected (A) and an affected (B) Papillon. Panel C shows the codon and amino acid alignment inferred from the traces in panels A and B, for the unaffected sequence (top) and affected Papillon mutation sequence (bottom). The complex Papillon mutation includes a 6 bp AGCTAC insertion between reference bases chr2:61,502,599-61,502,600 (yellow highlight in panel C and within yellow box in panel B) and an adenine deletion at chr2: 61,502,597 (red highlight in panel C and red triangle in panel B). The deletion causes a frameshift and premature stop codon within seven residues, including the two new, inserted codons.

Table 2.2. Intron and exon boundaries for canine *CNGB1* gene

	Location on Chr2[1]	Donor[2]	Intron (size)	Acceptor[2]	
Exon 1	61,454,476-61,454,528	ATCTGAGCAAgtaagtcagg	1 (2533bp)	tgtcctacagGTGTCGGGAT	Exon 2
Exon 2	61,457,062-61,457,243	GGACTCCCTGgtaagagaat	2 (2069bp)	aaccttccagCCACCTGAAG	Exon 3
Exon 3	61,459,313-61,459,364	GGCCCTCAGGgtgagtgccg	3 (288bp)	tcttttccagAAATCCAGGA	Exon 4
Exon 4	61,459,653-61,459,725	AAGTGAACAGgtaccacacc	4 (772bp)	tgtccctcagCAGTTCCAAC	Exon 5
Exon 5	61,460,498-61,460,618	CCCTGCTCAGgtacttctga	5 (89bp)	gtcctggcagGCAGGAGCAC	Exon 6
Exon 6	61,460,708-61,460,750	GGGAGCTCAGgtgaggccag	6 (184bp)	ttcttctcagATGGACTTGG	Exon 7
Exon 7	61,460,935-61,460,965	GGGACACCGGgtgagtcctc	7 (1283bp)	ccctgtgcagGTCTGGGCCC	Exon 8
Exon 8	61,462,249-61,462,324	AACCTCCAAGgtaagtcaaa	8 (352bp)	tctgatctagGACCAGAGAG	Exon 9
Exon 9	61,462,677-61,462,716	TTGGACACAGgtacagggag	9 (365bp)	tgctgcttagAGCCCCCTGG	Exon 10
Exon 10	61,463,082-61,463,241	ACCCTGCCAGgtgagccccc	10 (852bp)	ccacttgcagGTTGATGGCT	Exon 11
Exon 11	61,464,094-61,464,169	CAGGGAGCAGgtctgttctg	11 (1686bp)	tcccatgcagGAGCCTGACT	Exon 12
Exon 12	61,465,856-61,465,892	GTGCAGACCAgtaagtgcct	12 (6320bp)	tcccctgcagTCTGCATCCT	Exon 13
Exon 13	61,472,213-61,472,375	AGATGCCCAGgtgggagcca	13 (1405bp)	ctcaactcagGAAGCTGCCC	Exon 14
Exon 14	61,473,781-61,473,861	AGGAGGCAAAgtaaggtgct	14 (5744bp)	ggggtcacagTGTCCTGCTG	Exon 15
Exon 15	61,479,606-61,479,693	CTCCCAGCAGgtacggagcg	15 (685bp)	ttgtctgcagGAGCTGCAGG	Exon 16

Table 2.2. cont'd

Exon 16	61,480,379-61,480,415	AGCCCAGAAGgtaggtgtgc	16 (5435bp)	tctctccaagTGCCTGCTAC	Exon 17
Exon 17	61,485,851-61,486,010	GAACAGAAAGgtcacctttt	17 (2502bp)	gtccttgcagGAAGAGGCTG	Exon 18
Exon 18	61,488,513-61,488,620	AAGGCACTGAgtgagtgggg	18 (2472bp)	gtgtccacagTGGCCAGGAT	Exon 19
Exon 19	61,491,093-61,491,250	CCAAAGCCCTgtgagtccag	19 (1047bp)	catcccacagCCCCGGCCAA	Exon 20
Exon 20	61,492,298-61,492,456	CCGCTGACCAgtgagtcctg	20 (883bp)	ctccctgcagACCTGATGTA	Exon 21
Exon 21	61,493,340-61,493,548	AGACATCATTgtgagtcccg	21 (723bp)	tttctttcagACAGACAAAA	Exon 22
Exon 22	61,494,272-61,494,322	TCGCTTTAAGgtgcgcgctg	22 (273bp)	gggatttcagATGGACATGC	Exon 23
Exon 23	61,494,596-61,494,682	CTGTTTGAAGgtaggcttcc	23 (1879bp)	ttcttcccagTACATGGCCT	Exon 24
Exon 24	61,496,562-61,496,626	ATGTTTACAGgtgagacaca	24 (808bp)	tctcccgcagGGTCATCAGG	Exon 25
Exon 25	61,497,435-61,497,557	TGGGAAACAGgtgagccagt	25 (5025bp)	ctctctctagTTACATTCGC	Exon 26
Exon 26	61,502,583-61,502,724	GATCGGACAGgtagctgggt	26 (704bp)	ttgcccctagATGAGAGACG	Exon 27
Exon 27	61,503,429-61,503,588	GGCATGCTGGgtaagatggg	27 (1872bp)	tcctttccagACGAGTCAGA	Exon 28
Exon 28	61,505,461-61,505,558	TCTCTTCCAGgtatggcccc	28 (100bp)	ttggggacagGGCTGTGACC	Exon 29
Exon 29	61,505,659-61,505,742	GTGCAAGAAGgtgagtggcc	29 (3003bp)	tctgtttcagGGGGAGATAG	Exon 30
Exon 30	61,508,746-61,508,864	GAGAAATAAGgtcagagggg	30 (258bp)	tctaccccagCTTACTGGCT	Exon 31

Table 2.2. cont'd

Exon 31	61,509,123-61,509,269	AGAAGGCCAGgtacattttt	31 (6620bp)	tttctttcagGCGCATGCTG	Exon 32
Exon 32	61,515,890-61,516,109	GCTGGAACAGgtaagatggt	32 (2609bp)	tggattttagGCCAAGAGCT	Exon 33
Exon 33	61,518,719-61,519,006	GGCCGAGTGA - 3'UTR			

1. Locations are all in respect to UCSC Genome Browser CanFam2.0 (http://genome.ucsc.edu)
2. Capital letters are exonic DNA sequences and lower case bases are intronic regions

End of coding region marked in Exon 33 row by underlined TGA

Table 2.3. Single nucleotide variant (SNV) locations in genomic Papillon *CNGB1*

Location	Position on Chr2[1]	cDNA change	Reference allele[2]	Variant allele[3]	cDNA bp	Protein change[4]	SNP number[5]
Exon 2	61,457,096	c.27G>A	G	A	G	-	rs22870567
Exon 2	61,457,220	c.151G>A	G	A	A	p.E69K	rs22870569
Exon 3	61,459,353	c.215C>T	C	T	C	p.P72L	-
Exon 33	61,518,754	c.3378C>A	C	A	A	-	-
Exon 33	61,518,816	c.3440T>C	T	C	C	p.L1165P	-
Exon 33	61,518,910	c.3534G>A	G	A	A	-	-

1. Locations are all in respect to UCSC Genome Browser CanFam2.0 (http://genome.ucsc.edu)
2. Reference allele from UCSC Genome Browser CanFam2.0
3. Variant allele from sequenced gDNA of Papillons
4. Protein change due to the SNV found in either Papillons and/or cDNA. Change is in respect to CanFam2.0
5. SNP number from Broad Institute SNP collection (http://www.broadinstitute.org/mammals/dog/snp2)

Table 2.3 shows the SNVs and SNPs detected and Supplemental Figure 2.S1 shows the predicted canine protein amino acid sequence and alignment with other species. Primers for sequencing canine gDNA and cDNA are supplied in Supplementary Table 2.S1 and Table 2.S2, respectively.

A genotyping assay for the mutation was developed (supplemental methods). The assay was used to genotype 20 Papillons that had been diagnosed by a veterinary ophthalmologist to have PRA (not including purpose-bred colony dogs) and 119 Papillons whose owners reported no abnormal vision (Table 2.4). The mutation was identified in the homozygous state in 13 of 20 Papillons that had been diagnosed with PRA. Of the phenotypically normal Papillons, none were homozygous for the mutation and 20 were heterozygous for it. This indicates a 16.5% carrier rate, and a mutated allele frequency of ~31% in the Papillon breed, however, ascertainment bias almost certainly falsely inflates these values. In addition, we genotyped 33 dogs from 8 different breeds that had been diagnosed with PRA and 66 dogs from 9 different breeds that were clinically normal, none of the dogs of non-Papillon breeds had the mutation (Supplemental Table 2.S3).

Table 2.4. PRA type 1 genotypes and clinical status for 139 Papillons

Genotype[1]	Clinical Status		
	PRA affected[2]	Unaffected	Total
CNGB1 M/M	13	0	13
CNGB1 M/+	3	20	23
CNGB1 +/+	4	99	103
Total	20	119	139

1. Genotyping results: (+/+) means wild-type CNGB1 sequence. M= mutant (c.2387delA;2389_2390insAGCTAC) genotype
2. Not including colony dogs to avoid inflation of mutation presence in the general population of Papillon dogs

2.4.5 Immunohistochemistry shows lack of detectable full-length CNGB1 protein in affected retina

To confirm that the *CNGB1-fs26* mutation does disrupt CNGB1 expression in the homozygous animal, we performed immunohistochemistry (IHC) on retinal sections from an 8 week-old PRA-affected Papillon from the breeding colony that was homozygous for the *CNGB1-fs26* mutation and compared it to retinal sections from an 8 week-old normal dog that was confirmed not to have the *CNGB1-fs26* mutation.

CNGB1 in other species codes for multiple transcripts via alternative splicing [42,43]. The *CNGB1* locus has been described to code for four sensory transcripts; three retinal transcripts and one olfactory sensory transcript, as well as other splice variants expressed in kidney, brain, testes and spermatozoa [44-47]. The 5' portion of the gene encodes two glutamic acid rich proteins (GARPs) while the full-length transcript encodes the CNGB1 protein. The position of the *CNGB1-fs26* mutation is predicted to

allow normal expression of the two GARPs but to disrupt production of the full-length CNGB1 protein. To test this prediction we used two CNGB1 antibodies: one that targets the amino terminal (GARP region) of CNGB1 and the GARPs and a second antibody that targets the carboxyl end of CNGB1 downstream of both the GARP region and the predicted premature stop codon in the mutant canine *CNGB1* gene. The results from this study showed that while the rod outer segments of the wild-type retina were labeled by both antibodies (Figure 2.5 A, C), the rod outer segments of the PRA-affected Papillon were labeled with the amino terminal antibody but not the carboxyl terminal antibody (Figure 2.5 B, D). This provides strong evidence that the mutation disrupts production of full-length CNGB1 protein while still allowing expression of GARPs as predicted from the *CNGB1-fs26* mutation.

We also performed IHC with a CNGA1 antibody. The rod cGMP-gated channel consists of both CNGA1 and CNGB1 subunits. Studies in mouse models have shown that lack of CNGB1 also disrupts trafficking of CNGA1 to the outer segments resulting in very reduced or absent CNGA1 protein [48,49]. As predicted by the mouse model, the retinal sections for the affected Papillon showed lack of detectable CNGA1 protein while in the retinal sections from the normal dog CNGA1 was appropriately expressed and correctly targeted to the rod outer segments (Figure 2.5 E, F).

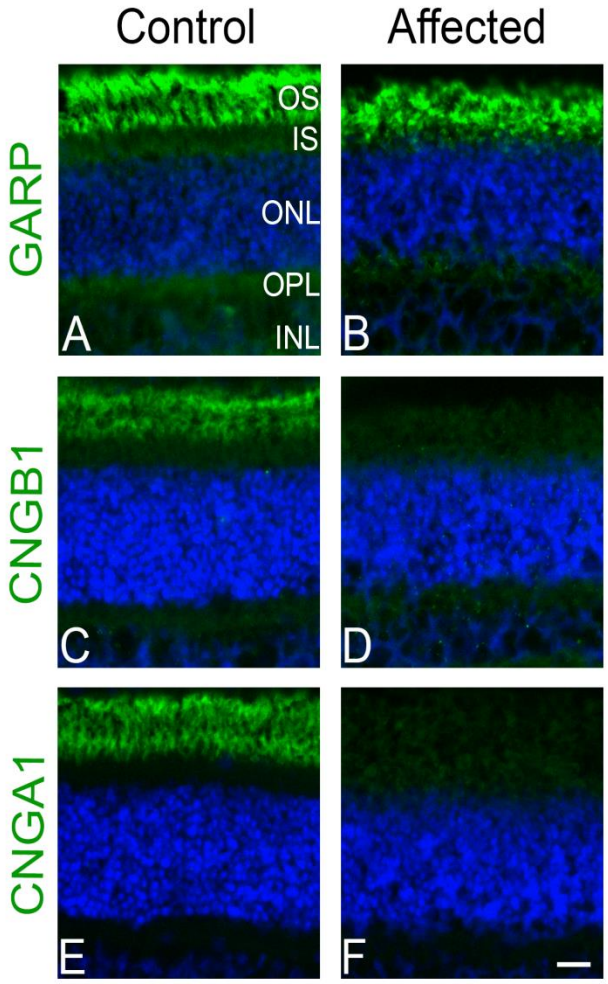

Figure 2.5. Immunohistochemistry on frozen retinal sections from age (8wk) and sex matched (female) control and affected dogs. Images on the left are from the control dog and images on the right are from the affected dog. Panels A and B are stained with GARP-CNGB1 N-terminal antibody (green) and DAPI (blue). GARP proteins are present in both the control and affected samples. Panels C and D were stained with CNGB1 C-terminal antibody (green) and DAPI. CNGB1 full length protein is not detected in the affected sample. Panels E and F are stained with CNGA1 antibody (green) and DAPI. CNGA1 is not detected in the affected sample, presumably due to necessity for CNGB1 to form viable channels and normal trafficking. Size bar: 20 µm. OS- photoreceptor outer segment, IS – photoreceptor inner segment, ONL – outer nuclear layer, IPL – inner plexiform layer, INL – inner nuclear layer

2.5 Discussion

We used homozygosity mapping of SNP microarray genotyping data from PRA-affected Papillons to identify regions where the affected dogs had runs of homozygosity spanning greater than 1.5 Mb and for which control dogs showed allelic variability. Positional candidate genes were identified mapping to those regions and haplotype analysis revealed only one region (on CFA2) in which obligate-carrier dogs had one copy of the haplotype observed in affected dogs, and none of the unrelated control dogs were homozygous for the haplotype observed in affected dogs. *CNGB1* was selected as the most promising positional candidate gene because of its location within the CFA2 region and of the similarity of the phenotype of *CNGB1* retinal dystrophy in mice and humans to that of the PRA-affected Papillons in our breeding colony (early lack of rod function and yet a slow retinal degeneration). The canine genome assembly (CanFam2.0) on the UCSC Genome Browser had incorrect exon predictions for *CNGB1*. We established the normal gene structure by sequencing cDNA from a retinal library developed from a control dog (GenBank KC527595). Sequencing of the confirmed exons and nearby flanking intronic regions of *CNGB1,* in affected and phenotypically normal Papillons, revealed a frameshift mutation *(CNGB1-fs26)* that segregated with disease status in our breeding colony and was not present in the homozygous state in any unaffected Papillons. A missense variation was also detected in the affected dogs (p.P72L). This converts a proline to leucine but at a residue that in some species is a leucine and in others a proline, making it unlikely that this would have a major effect on the function of CNGB1 in the dog [50]. Furthermore, this amino acid change was predicted to be benign by the PolyPhen-2 program [41].

Cyclic nucleotide gated (CNG) channels are necessary for normal phototransduction. There are different CNG channels encoded by paralogous genes specific to the rod and cone photoreceptors [44]. The rod CNG channel is a heterotetrameric protein consisting of three CNGA1 subunits and one CNGB1 subunit [51-53]. In dark conditions, the rod has higher levels of cyclic guanosine monophosphate (cGMP) which act to open a proportion of the CNG channels allowing an influx of cations, resulting in depolarization of the rod photoreceptor. Light stimulation triggers the phototransduction cascade activating the cGMP phosphodiesterase that hydrolyzes cGMP lowering its concentration and leading to closure of the CNG channels. This halts the influx of cations through the channel which, coupled with the continued action of other ion pumps in the cell membrane, results in the light-induced hyperpolarization of the rod photoreceptor.

CNGA1 can form functional channels *in vitro* without CNGB1 [54-56], while CNGB1 on its own does not form a functional channel. However, *in vivo* CNGB1 is important for rod CNG formation and normal functionality of the channel [48,49]. The *CNGB1* gene codes for three splice variants in the retina that encode the soluble glutamic acid rich proteins 1 and 2 (GARP1 and GARP2) and a full length CNGB1 protein [42]. The full length transcript in the retina is known as *CNGB1a*. Full length CNGB1 protein in the retina consists of an N-terminal “GARP region” and a C-terminal “channel domain”. GARP1 is of low abundance whereas GARP2 is more highly expressed [49]. The functions of the GARP subunits are still being explored. GARP2 does bind to PDE6 and may act to reduce dark level noise [57]. It is also postulated to have a structural role in the rod outer segment [49] where it interacts with peripherin-2 at the rod outer segment

disk rim [58]. As discussed further below GARP2 may also play a role in control of the opening of the CNG channel [59]. Other than these three splice variants expressed in the retina, *CNGB1* also has splice variants expressed in the olfactory epithelium (*CNGB1b* –which encodes a shorter protein than expressed in the retina lacking the GARP region), kidney, brain and testes [44-47]. Two mouse gene targeting models, *CNGB1X-1* and *CNGB1X-26*, have been created to study the functions of these proteins in the retina.

The *CNGB1X-1* mouse knockout model, which lacks all retinal *CNGB1* products, has shown that GARPs are necessary in outer segment disk development and the structural integrity of the rod outer segments [49]. Interestingly, the *CNGB1X-1* mice have a weak rod response that is detectable on single cell recording. This activity originates from a low level of homomeric CNGA1 channel formation in the rod outer segments. Despite the presence of the channels and the resulting weak light-induced rod response, these mice have severe rod photoreceptor degeneration. It was suggested that degeneration may be due to rod structural, rather than functional, failure [49]. Another mouse model, *CNGB1X-26,* has an engineered mutation that leads to a deletion of exon 26 resulting in a frameshift that introduces a premature stop codon in the first triplet in exon 27 of *CNGB1.* The *CNGB1X-26* mouse has a complete absence of mRNA for full-length CNGB1 and thus a lack of the CNGB1 protein but still produces GARP proteins [48]. These mice have normal development of the rod outer segments and a slower retinal degeneration than the *CNGB1X-1* mouse.

The premature stop codon in the *CNGB1X-26* mouse is positioned at a site homologous to 10 codons upstream of the premature stop codon predicted in the

CNGB1-fs26 mutation identified in this study. While we anticipate that the premature stop codon in *CNGB1* in the PRA-affected Papillon will lead to nonsense-mediated decay of the abnormal *CNGB1* mRNA and a complete absence of the CNGB1 protein, as was reported for the *CNGB1X-26* mouse [48], rather than production of a truncated protein, further studies are required to confirm this.

IHC using an antibody that binds to the carboxyl end of CNGB1 confirmed the lack of full-length CNGB1 in the rod outer segments of a young affected Papillon prior to photoreceptor degeneration. The *CNGB1-fs26* mutation is not predicted to affect expression of the GARPs, and IHC using an antibody that recognizes GARPs as well as the GARP region of the full-length CNGB1 labeled the rod outer segments of the affected Papillon suggesting that GARPs and/or a truncated CNGB1 product are expressed. If the truncated mRNA avoids degradation and allows the production of a truncated protein, it would be missing domains essential for channel gating and cyclic nucleotide binding and would therefore not be expected to function normally. IHC also showed a lack of detectable CNGA1 protein in the rod outer segments in the young affected Papillon. Similar IHC results were observed in the *CNGB1X-26* mouse. It was suggested that the GARPs may have a dominant-negative effect on the transport of CNGA1 to the outer segment accounting for the lack of homomeric CNGA1 channels in the outer segments of *CNGB1X-26* mice (which have GARPs) contrasted with the presence of low levels of CNGA1 in outer segments of *CNGB1X-1* mice (which lack GARPs) [49]. The reduced level of CNGA1 in the outer segment of the *CNGB1X-1* mouse is probably a reflection of the importance of CNGB1 in transport of CNGA1 to the outer segment [49]. A region in the N-terminal section of the CNGB1 subunit (bovine

amino acids #677-764) has been described to interact and promote protein-protein interactions with the CNGA1 subunit C-terminal region; this region is upstream of the *CNGB1-fs26* mutation and is not predicted to be effected by this mutation [60,61]. As would be expected in animals with a lack of rod CNG channels, the ERG changes in the affected Papillons indicate a lack of rod function. Specifically, prior to a thinning of the outer nuclear layer, there was an elevated dark-adapted ERG threshold with only a recordable response to light intensities above cone response threshold, a marked reduction in a- and b-wave amplitudes for the dark-adapted brighter flashes that elicit a mixed rod cone response in normal dogs.

The *CNGB1X-26* mutation also lacks expression of the *CNGB1* splice variant expressed in the olfactory epithelium (*CNGB1b*). These mice show absence of proper channel localization and delayed olfaction [62]. More detailed phenotypic characterization of the dog model is required to ascertain how closely the canine phenotype, both retinal and olfactory, mimics the *CNGB1X-26* mouse model.

Mutations in *CNGB1* have been identified in human patients with autosomal recessive RP (RP45) and are reported to account for ~4% RP of cases [1]. In 2001, Bariel et al. reported a consanguineous French family with RP that they mapped to an interval containing *CNGB1* [63]. They then identified a missense mutation that converted an evolutionarily conserved glycine to valine (c.2978G>T; p.G993V) which they predicted would alter the cyclic nucleotide-binding domain (CNBD). The effect of this mutation was further elucidated in an elegant study reported by Michalakis et al [59]; they showed that the p.G993V mutation prevented binding of cGMP and that binding is required for removal of an inhibitory effect that the GARP domain and also

GARP2 has on channel opening, such that if cGMP cannot bind to CNGB1 the CNG channel is silent [59]. More recently resequencing of candidate RP genes led to the identification of a simplex RP patient homozygous for a missense substitution in *CNGB1* (c.2957A>T; p.N986I) resulting in substitution of a conserved amino acid 7 codons upstream of the mutation identified by Bariel et al. and also in the CNBD [64]. Kondo et al. used homozygosity mapping to screen known arRP genes in Japanese RP patients and in one patient identified a mutation at the donor site of exon 32 (c.3444+1G>A) of *CNGB1* [65]. Subsequently, Becirovic et al. performed exon trapping experiments to investigate the effect of the mutation. Their studies suggest that the mutation leads to skipping of exon 32 and replacement of the last 170 amino acids by 68 unrelated amino acids [66]. The probands in the Bariel et al. and Kondo et al. studies had night blindness from a young age and were diagnosed with RP in their 30's [63,65].

The *CNGB1-fs26* mutation identified in Papillon dogs was present in 13 of the 20 PRA-affected Papillons tested. This suggests that there is at least one additional PRA locus segregating within the breed. Within-dog breeds genetic heterogeneity for PRA is becoming more evident [13,16]. Additional studies will be required to find the gene mutation(s) responsible for the other form(s) of PRA segregating in Papillons.

The early onset of loss of rod function in the *CNGB1-fs26* mutant dog, coupled with a slow retinal degeneration that we have observed in our colony dogs, seems to accurately parallel the described disease course in human patients as well as the comparable mouse model (*CNGB1X-26*). Recently recombinant adeno-associated viral vector-mediated gene therapy to deliver a normal copy of *CNGB1* to *CNGB1-/-* mice was reported to allow for CNG channel formation, restoration of rod function and retinal

morphological preservation [67]. The early loss of rod function and yet slow rod photoreceptor loss in the animal models suggests that *CNGB1* RP is a good target for gene augmentation therapy. The *CNGB1-fs26* mutant dog promises to be a valuable model for preclinical trials of such therapy.

2.6 Acknowledgements

The authors of this paper would like to thank the Papillon Club of America for their continued support throughout this project. Their effort in acquiring the affected female dog that started the Michigan State University research colony was integral to finding the mutation. We would also like to thank the breeders and owners who donated samples from their dogs. The authors thank Dr. Bob Molday for the CNGA1 antibody and Dr. Stephen Pittler for the N-terminal CNGB1 antibody. The authors would also like to thank Janice Querubin for her help with management of the Papillon research colony and recording the ERGs.

2.7 Supplemental information

```
canine MLSWVQRVLP QPPGTPQKTK VEEEGGADPE ---------- ---------- ---------- ----PEPEPE
human  MLGWVQRVLP QPPGTPRKTK MQEEEEVEPE ---------- ---------- ---------- ----PEMEAE
mouse  MLGWVQRVLP QPPGTPQKT- -VETAGPQPE TESKPEANPQ PEPEPQQEPE PEPEPEPEPE PEPEPEPEPE
rat    MLGWVQRVLP QPPGTPQKT- -EEGAGPQPE TESKPEANPQ PEPEVQ---- ---------- --PEPEPEPE
bovine MLGWVQRVLP QPPGTPQKTK -QEEEGTEPE ---------- ---------- ---------- ----PELEPK
       ********** ****** **    *     **                                    ** *
                     1                              2
canine  VKQEPELEPE TALEKAEQGD SLPPEEPL-- EEVAAADLGP QEIQEAALSP PTSLQAQITV APEVNSSSND
human   VEPEPN--PE EAETESE--- SMPPEESFKE EEVAVADPSP QETKEAALTS TISLRAQGAE ISEMN-SPSR
mouse   PEPEPEPVPE EAPPEVQ--- ALPPEEPMEG EGEAEAGPSL QETQVADPAQ PTS-QAQVAV A-KVN-RPSS
rat     PEPEPEPAPE EAAPEVQ--- TLPPEEPVEG EDVAEAGPSL QETQEADPPQ PTS-QAQVAV V-KVN-RPSS
bovine  PETAPE---E TELEEV---- SLPPEEPCVG KEVAAVTLGP QGTQETALTP PTSLQAQVSV APEAHSSPRG
            *    *              ****        *       *               **

canine  WVLTWLKKSV EKVVPQPVPS SRLAQSTAAG GEGPA-QAGA QVSGQCSTG- --SSDGLGEA --AGDTGSGP
human   RVLTWLMKGV EKVIPQPVHS IT-------- -EDP-----A QILGHGSTGD TGCTDEPNEA LEAQDTRPGL
mouse   WMLSWFWRGM QKVVPQPV-C SNGGQNLAAG ERDPD-QGGA QIPEPCGTGD PGSAEASG-- --TQDTEPSL
rat     WMLSWFWKGM EKVVPQPVYS SSGGQNLAAG EGGPD-QDGA QTLEPCGTGD PGSEDGSDKT SKTQDTEPSL
bovine  WVLTWLRKGV EKVVPQPAHS SRPSQNIAAG LESPDQQAGA QILGQCGTG- --GSDEPSEP SRAEDPGPGP
          * *       ** ***                          * *       *                 *

canine  WLLRWLEQNL EKVLPQPPKT SKDQRDEP-- -ADAALDTEP PGPTLETEPV LQAPESSCVP TAGPLEPQEE
human   RLLLWLEQNL ERVLPQPPKS SEVWRDEPAV ATGAASDPAP PGRPQEMGPK LQARETPSLP TPIPLQPKEE
mouse   WLLRWLEQNL EKVLPQPPPP SLAWKVEP-- -EAAVLDPDP PGTPMQMEPT ----ESPSQP NPGPLEPEEE
rat     WLLRWLELNL EKVLPQPPTP SQAWKVEP-- -EGAVLEPDP PGTPMEVEPT ----ENPSQP NPGPVEPEEE
bovine  WLLRWFEQNL EKMLPQPPKI SEGWRDEP-- -TDAALGPEP PGPALEIKPM LQAQESPSLP APGPPEPEEE
         ** * * ** *  *****   *     **      *     * **      *      *    *    *  * **

canine  ----PPSEPQ LSPQA--SSL LLPSDPARLM AWLLHRLEMA LPQPVLHGKA REQEPDSPVT CDVQTICILP
human   PKEAPAPEPQ PGSQAQTSSL PPTRDPARLV AWVLHRLEMA LPQPVLHGKI GEQEPDSPGI CDVQTISILP
mouse   ----PAAEPQ PGFQS--SSL PPPGDPVRLI EWLLHRLEMA LPQPVLHGKA AEQEPGCPGM CDVQTISILP
rat     ----PAAEPQ PGFQA--SSL PPPGDPVRLI EWLLHRLEMA LPQPVLHGKA AEQEPSCPGT CDVQTISILP
bovine  ----PIPEPQ PTIQA--SSL PPPQDSARLM AWILHRLEMA LPQPVIRGKG GEQESDAPVT CDVQTISILP
            *  ***    *   ***     *  **   * ******* *****  **   ***   *   ****** ***

canine  GGQEEPDLVL EEVDPHWEED EHQDG--GAS PQDSEAAPAY EEENEAVEEM PRKLPWIQEE REDEEEDGEE
human   GGQVEPDLVL EEVEPPW-ED AHQDV--STS PQGTEVVPAY EEENKAVEKM PRELSRIEEE KEDEEEEEEE
mouse   VEQVEHDLVL EEVDSCWEDA QQEDG---AS PQETEVAPAH EEESEAIVEI PRELTKIQEE REDEQEEDEE
rat     VEQAEHDLVL EDVDSCWEDT QQEDG---AS LQETELAPIY EDESEAMVEM PRELPQIQEQ QEEENEEKEE
bovine  GEQEESHLIL EEVDPHWEED EHQEGSTSTS PRTSEAAPAD EEKGKVVEQT PRELPRIQEE KEDEEEEKED
          * *  * * * *   *            *     *  *   *          ** *    *   * * *  *
```

Figure 2.S1. *CNGB1* amino acid alignments. Sequence alignments performed using muscle alignment in SeaView software ([68]. Single nucleotide polymorphism and variants found in Papillon gDNA sequencing are numbered (1: p.E69K, 2: p.P72L, 3: p.L1165P) and the changed amino acid is underlined. 2: p.P72L is the SNV that has only been seen in Papillons with the mutation and is marked with red text. The *CNGB1X-26* mouse stop codon is highlighted in red. The Papillon mutation is highlighted in green. The human mutations are marked in yellow (highlighted N [64] G [63]and arrow which represents a splice mutation [65]). Epitopes for N-terminal antibody (mouse, highlighted in purple) and C-terminal antibody (human, highlighted in teal).

Figure 2.S1. cont'd

```
canine  EGED------ ---------- ---------- ---------- ---------- ---------- ----------
human   EEEE------ ---------- ---------- ---------- ---------- ---------- ----------
mouse   EKEE------ ---------- ---------- -----EKKKG EEEKEKEEEE KEKEKEKEEE KEEEEKEEEE
rat     EEEEKEEKEE KEEEEEKEEE EKREEEKKKE KEEEKKEKEE EENGEEEEKE EKEEKEEEEG KEEKEEKEEK
bovine  GEEEEEEGRE KEE----EEG EEKEEEEGRE KEEEEGEKKE EEGREKEEEE GGEKEDEEGR EKEEEEGRGK
          *

canine  ---------- ---------- ---------- EEEANVLLDS CLEAQAGEDL TGVDRSQPQR AS--------
human   ---------- ---------- --------EE EEVTEVLLDS CVVSQVGVGQ SEEDGTRPQS TSDQKLWEEV
mouse   EEEKEEEEEE KEEEEKEEEE KEEEEEEEEE EEEPIVLLDS CLVVQADVDE CQLERTPSEL AS--------
rat     EEKEEEEKEE KEEEEKEEKE EEEEEEEEEE EEEPIVLLDS CLVVQADVDQ CQLERAQPET AS--------
bovine  EEEEGGEKEE EEGRGKEEVE GREEEEDEEE EQDHSVLLDS YLVPQSEEDR SEESETQDQS EVGGAQAQGE
                                        *    *****     *

canine  ---------- ---------- ---------- ---------- ---------- -----QQELQ EEAVTTSPEV
human   GEEAKKEAEE KAKEEAEEVA ---------- ---------- -EEEAEKEPQ DWAETKEEPE AEAEAASSGV
mouse   ---IQELPEE KEEKEEEK-- ---------- ---------- --EEEKEEEE EKKEEEVEKK EEGEATNSTV
rat     ---IQELPEE EEEKEEEKK- ---------- ---------- -EEEEEKEEE EEKEEEEEKE EEGEATNSTV
bovine  VGGAQALSEE SETQDQSEVG GAQDQSEVGG AQAQGEVGGA QEQDGVGGAQ DQSTSHQELQ EEALADSSGV
                                                                    *   *       *

canine  PATKEHPEVQ VEDVDADSHP LIV-ENTPSP ELPPPSPAKA DTLTVPGSAA GTERKRLPSQ DDEAEELRAL
human   PATKQHPEVQ VEDTDADSCP LMAEENPPST VLPPPSPAKS DTLIVPSSAS GTHRKKLPSE DDEAEELKAL
mouse   PATKEHPELQ VEDTDADSGP LIPEETLPPP ERPPPSPVKS DTLTVPGAAA AGHRKKLPSQ DDEAEELKAL
rat     PATKEHPELQ VEDTDAEAGP LIPEETIPPP ERPPVSPAKS DTLAVPSAA- -THRKKLPSQ DDEAEELKAL
bovine  PATEEHPELQ VEDADADSRP LIAEENPPSP VQLPLSPAKS DTLAVPGSAT GSLRKRLPSQ DDEAEELKML
        ***  *** * *** **   * *   *  *      * ** *  *** **  *     ** ***  *******  *

canine  SPAESPMVAW SDPSSPQGTD GQDRATSTAS QNSAIINDRL QELVKLFKER TEKVKEKLID PDVTSDEESP
human   SPAESPVVAW SDPTTPKDTD GQDRAASTAS TNSAIINDRL QELVKLFKER TEKVKEKLID PDVTSDEESP
mouse   SPAESPVVAW SDPTTPQEAD GQDRAASTAS QNSAIINDRL QELVKMFKER TEKVKEKLID PDVTSDEESP
rat     SPAESPVVAW SDPTTPQEAD GEDRAASTAS QNSAIINDRL QELVKMFKER TEKVKEKLID PDVTSDEESP
bovine  SPAASPVVAW SDPTSPQGTD DQDRATSTAS QNSAIINDRL QELVKLFKER TEKVKEKLID PDVTSDEESP
        *** ** *** ***  *   *   *** ****  ********* ***** **** ********** **********

canine  KPSPAKKAPE PAPVVKPAEV GQAEEEEHYC DMLCCKFKRR PWKTYRFPQS IDPLTNLMYI LWLFFVVLAW
human   KPSPAKKAPE PAPDTKPAEA EPV-EEEHYC DMLCCKFKHR PWKKYQFPQS IDPLTNLMYV LWLFFVVMAW
mouse   KPSPAKKAPE PDPAQKPAEA EVA-EEEHYC DMLCCKFKRR PLKMYRFPQS IDPLTNLMYI LWLFFVVLAW
rat     KPSPAKKAPD SAPAQKPAEA EAA-EEEHYC DMLCCKFKRR PWKMYQFPQS IDPLTNLMYI LWLFFVVLAW
bovine  KPSPAKKAPE PAPEVKPAEA GQV-EEEHYC EMLCCKFKRR PWKKYQFPQS IDPLTNLMYI LWLFFVVLAW
        *********    *  ****      ******  ******* * * * * **** *********  ******* **

canine  NWNCWLIPVR WAFPYQTPNN IHLWLLMDYL CDLIYLLDIT VFQLRLQFVR GGDIITDKKE MRDNYLKSRR
human   NWNCWLIPVR WAFPYQTPDN IHHWLLMDYL CDLIYFLDIT VFQTRLQFVR GGDIITDKKD MRNNYLKSRR
mouse   NWNCWLIPVR WAFPYQRADN IHFWLLMDYL CDFIYLLDIT VFQMRLQFVK GGDIITDKKE MRNNYLKSRR
rat     NWNCWLIPVR WAFPYQRADN IHLWLLMDYL CDFIYLLDIT VFQMRLQFVK GGDIITDKKE MRNNYLKSQR
bovine  NWNCWLIPVR WAFPYQTPDN IHLWLLMDYL CDLIYLLDIT VFQMRLQFVR GGDIITDKKE MRNNYVKSQR
        ********** ******   * ** ******* ** ** **** *** *****  *********  ** ** ** *

canine  FKMDMLCLLP LDFLYLKFGV NPLLRLPRCL KYMAFFEFNS RLESILSKAY VYRVIRTTAY LLYSLHVNSC
human   FKMDLLSLLP LDFLYLKVGV NPLLRLPRCL KYMAFFEFNS RLESILSKAY VYRVIRTTAY LLYSLHLNSC
mouse   FKMDLLCLLP LDFLYLKLGI NPLLRLPRCL KYMAFFEFNN RLEAILSKAY VYRVIRTTAY LLYSLHLNSC
rat     FKMDLLCLLP LDFLYLKLGV NPLLRLPRCL KYMAFFEFNN RLEAILSKAY VYRVIRTTAY LLYSLHLNSC
bovine  FKMDMLCLLP LDLLYLKFGV NPLLRLPRCL KYMAFFEFNN RLESILSKAY VYRVIRTTAY LLYSLHLNSC
        **** * *** ** **** *  ********** *********  *** ****** ********** ****** ***
```

Figure 2.S1. cont'd

```
                                          SS YTGL-
canine  LYYWASAYQG LGSTHWVYDG VGNSYIRCYY WAVKTLITIG GLPDPRTLFE IVFQGLNYFT GVFAFSVMIG
human   LYYWASAYQG LGSTHWVYDG VGNSYIRCYY FAVKTLITIG GLPDPKTLFE IVFQLLNYFT GVFAFSVMIG
mouse   LYYWASAFQG IGSTHWVYDG VGNSYIRCYY WAVKTLITIG GLPDPQTLFE IVFQLLNYFT GVFAFSVMIG
rat     LYYWASAFQG IGSTHWVYDG VGNSYIRCYY WAVKTLITIG GLPDPQTLFE IVFQLLNYFT GVFAFSVMIG
bovine  LYYWASAYEG LGSTHWVYDG VGNSYIRCYY WAVKTLITIG GLPDPRTLFE IVFQGLNYFT GVFAFSVMIG
        *******  *  ********* **********  ********* ***** **** **** ***** **********

canine  QMRDVVGAAT AGQTYYRSCM DSTVKYMNFY KIPRSVQNRV KTWYEYTWQS QGMLDESELM VQLPDKMRLD
human   QMRDVVGAAT AGQTYYRSCM DSTVKYMNFY KIPKSVQNRV KTWYEYTWHS QGMLDESELM VQLPDKMRLD
mouse   QMRDVVGAAT AGQTYYRSCM DSTVKYMNFY KIPRSVQNRV KTWYEYTWHS QGMLDESELM VQLPDKMRLD
rat     QMRDVVGAAT AGQTYYRSCM DSTVKYMNFY KIPRSVQNRV KTWYEYTWHS QGMLDESELM VQLPDKMRLD
bovine  QMRDVVGAAT AGQTYYRSCM DSTVKYMNFY KIPRSVQNRV KTWYEYTWHS QGMLDESELM VQLPDKMRLD
        ********** ********** ********** *** ****** ******** * ********** **********

canine  LAIDVNYNIV SKVALFQGCD RQLIFDMLKR LRSVVYLPND YVCKKGEIGR EMYIIKAGEV QVLGGPDGKA
human   LAIDVNYNIV SKVALFQGCD RQMIFDMLKR LRSVVYLPND YVCKKGEIGR EMYIIQAGQV QVLGGPDGKS
mouse   LAIDVNYSIV SKVALFQGCD RQMIFDMLKR LRSVVYLPND YVCKKGEIGR EMYIIQAGQV QVLGGPDGKA
rat     LAIDVNYNIV SKVALFQGCD RQMIFDMLKR LRSVVYLPND YVCKKGEIGR EMYIIQAGQV QVLGGPDGKA
bovine  LAIDVNYSIV SKVALFQGCD RQMIFDMLKR LRSVVYLPND YVCKKGEIGR EMYIIQAGQV QVLGGPDGKS
        ******* ** ********** ** ******* ********** ********** ***** ** * *********
                                                                                ↓
canine  VLVTLKAGSV FGEISLLAVG GGNRRTANVV AHGFTNLFIL DKKDLNEILV HYPESQKLLR KKARRMLRNN
human   VLVTLKAGSV FGEISLLAVG GGNRRTANVV AHGFTNLFIL DKKDLNEILV HYPESQKLLR KKARRMLRSN
mouse   VLVTLKAGSV FGEISLLAVG GGNRRTANVV AHGFTNLFIL DKKDLNEILV HYPESQKLLR KKARRMLRNN
rat     VLVTLKAGSV FGEISLLAVG GGNRRTANVV AHGFTNLFIL DKKDLNEILV HYPESQKLLR KKARRMLRNN
bovine  VLVTLKAGSV FGEISLLAVG GGNRRTANVV AHGFTNLFIL DKKDLNEILV HYPESQKLLR KKARRMLRNN
        ********** ********** ********** ********** ********** ********** ******** *

canine  NKPKEPKSVL ILPPRAGTPK LFNAALAVAG KMGAKGAKAG KLAHLRARLK ELAALEAAAR QQQLLEQAKS
human   NKPKEEKSVL ILPPRAGTPK LFNAALAMTG KMGGKGAKGG KLAHLRARLK ELAALEAAAK QQELVEQAKS
mouse   NKPKEEKSVL ILPPRAGTPK LFNAALAAAG KMGPRGAKGG KLAHLRARLK ELAALEAAAR QQQLLEQAKS
rat     NKPKEEKSVL ILPPRAGTPK LFNAALAAAG KMGPRGAKGG KLAHLRARLK ELAALEAAAR QQQLLEQAKS
bovine  NKPKE-KSVL ILPPRAGTPK LFNAALAAAG KMGAKGGRGG RLALLRARLK ELAALEAAAR QQQLLEQAKS
        ***** **** ********** *******  * ***  *   *  ** ****** *********  ** * *****
                                    3
canine  SQDAA-GEAG QAAPDQDQPP APEHPESQEP PATRSSP--- -------PAS PPASP-PAS- ERPEEGGEGE
human   SQDVK-GEEG SAAPDQHTHP K-EAATDPPA PRTPPEP--- -------PGS PPSSPPPASL GRPEGEEEGP
mouse   SQEAG-GEEG SGATDQPAPQ EPPEPKDPPK PPGPPEP--- -------SA- -QSSPPPAS- AKPEESTGEA
rat     SQEAG-GEEG SGATDQPAPQ EPSEPKEP-- ----PEP--- -------PA- -PSSPPPAS- AKPEGSTEEA
bovine  SEDAAVGEEG SASPEQPPRP EPPAPEAPAP EPTAPEPLAP EAPAPEAPA- -PSSPPPASQ ERPEGD-KDA
        *     ** *      *                                        ** ***    **

canine  AGPSEPSVLI RMSPGPDPSE QILSVEVPEE KKEAE----- ---------- -------
human   AEPEEHSVRI CMSPGPEPGE QILSVKMPEE REEKAE---- ---------- -------
mouse   AGPPEPSVRI RVSPGPDPGE QTLSVEVLEE KKEGAE---- ---------- -------
rat     AGPPEPSVRI RVSPGPDPGE QTLSVEMLEE KKEEVE---- ---------- -------
bovine  ARPEEHPVRI HVTLGPDPSE QILLVEVPEK QEEKEKKEEE TEEKEEGEEA RKEKEEE
        * * *  * *     ** * * * * *   *    *
```

Table 2.S1. Primers for genomic DNA sequencing

Name	F Primer	R Primer	Amplicon Size
Exon 1	catcgagctcctgttccac	ggaagctccaggtttccag	284
Exon 2	aatgtgtgacccacagaagtg	atgcagaactggcaactgtg	371
Exon 3, 4	tgttcctgcctgaaccag	tgcctgggaatgagtagagac	577
Exon 5, 6, 7	caggacactgtgaatgaagtgc	cttgctcctgaacccaagac	660
Exon 8	tgtgcagatgaggctagagg	ctcatccttcccgatgagc	356
Exon 9	gccaacatacagtacatcataagtttc	agctgatggctaagggcttc	215
Exon 10	ttggtgcctcaaatctggtc	gtgttggacattgggctgag	318
Exon 11	tggggtctgagcagtaggtc	ttgccctcagactttccatc	346
Exon 12	aggagcaactgggtcttcc	tcagggcctggcctagtg	249
Exon 13	tgaatgatcatgggcttcag	tcctgttctatgcccttgg	435
Exon 14	tggtctcagaggtcacaggac	agcctctctgctcagtgctc	325
Exon 15	ttcctcaaatcacccaccac	tctgtccagtcggcatctc	531
Exon 16	gaggactctaacagggtctgg	ggatgagacaggcataggg	250
Exon 17	ccctccaaacatgctttctg	tttaggaccagggagtaggg	358
Exon 18	atctgcaggcgtcaaagtc	cctgctcatccctatccatac	248
Exon 19	tagggccaggtggaatacag	cgtaggcctttctcaagcac	368
Exon 20	tgacagcatgttgtgaggtg	gcttctccctcttgttctgc	358
Exon 21	tccttccctaatcctactgtgg	tgtctcgtctatcgcagcag	391
Exon 22, 23	agcacatgggtctaaggaatg	ctcagggcagagctcaaatg	576
Exon 24	gggctaaggacctctgatttg	agagtgccttgctccgttg	290
Exon 25	ggtggtcttgtttcccacag	atgggacctctttccaggac	269
Exon 26	aagcgtttgcatcttgcac	actcgtgctctttcccagac	361
Exon 27	cgtctgtgtagagtaaacgtgctc	tctcctgacagcccagttg	437
Exon 28	agtgctacagcacagagactgc	ctgtttaggggacgatgtgg	463
Exon 29	ccacatcgtcccctaaacag	cacctcatgccaaacaacc	310
Exon 30	ctttccatcacatcactaactcc	aaccacagtggcctccttc	498
Exon 31	ggtgggaagggacattttag	tcgtttcagcagcacatttc	349
Exon 32	ccattagccaagacgaccac	aaggcatggtccacaatctg	400
Exon 33	aagctgttcaagactcctccag	tggtgggatggactctactg	488

Table 2.S2. Primers for cDNA sequencing

Name	F Primer	R Primer	Amplicon Size
Exon 1-2	ctgcaagtgacagggagaag	tcaggagccacagtgatctg	351
Exon 2-5	ctgcaagtgacagggagaag	ctcaccaagtccatctgagc	538
Exon 3-10	ctggtggtcggcatctgag	caggagccaagccatcaac	819
Exon 9-13	ggcttgagcagaatctggag	ataagctggagctgcctctg	494
Exon 12-18	ttgatggcttggctcctg	tcgtaaacccagtgagtggag	1586
Exon 15-19	tagaggagatgcccaggaag	gagccggtcattgatgatg	551
Exon 19-20	gaagatgttgatgcggacag	gaaagcggtacgtcttccag	526
Exon 19-25	atgaggctgaagagctcagg	ggactgccaggtgtactcg	1226
Exon 20-22	agctcatcgaccctgatgtc	tgtccatcttaaagcgacgag	474
Exon 26-27	ttgaagtttggcgtgaatcc	aaccgcatcttgtctggaag	581
Exon 27-31	tacgatggtgtgggaaacag	ccagaatgaagaggttggtaaac	700
Exon 30-31	accggcagttgatctttgac	cctcaggtgggcaagtttac	500
Exon 31-33	ccaagagctcgcaggatg	tcactcggcctctttctt	287

Table 2.S3. Non-Papillon breeds tested for *CNGB1* mutation

Breed	Clinically PRA affected	Unaffected	Total
Australian Shepherd	4	8	12
Belgian Tervuren	1	12	13
Chinese Crested	1	2	3
Dachsund	2	8	10
Italian Greyhound	10	4	14
Labrador Retriever	0	11	11
Old English Sheepdog	3	8	11
Polish Lowland Sheepdog	8	5	13
Tibetan Terrier	4	8	12

Table 2.S4. The entire region of homozygosity surrounding the site of the *CNGB1* mutation

SNP Name	Chr	Base Position	Pval	A1	A2	A3	C1	C2	U1	U2	U3	U4	U5	U6	U7	U8	U9	U10	U11
TIGRP2P26057_rs8802155	2	60,254,384	0.04	B	A	A	A	A	A	A	A	A	A	A	A	A	A	A	A
			73	B	B	B	B	B	B	A	A	A	A	A	B	A	A	B	B
BICF2S23151662	2	60,273,762	1	B	B	B	B	B	B	B	B	B	B	B	B	B	B	A	A
				B	B	B	B	B	B	B	B	B	B	B	B	B	B	B	B
BICF2P1168980	2	60,548,272	0.02	B	A	A	A	A	A	A	A	A	A	A	A	A	A	A	A
			69	B	B	B	B	B	B	A	A	A	A	A	B	A	A	A	A
TIGRP2P26649_rs9163294	2	60,564,157	0.02	B	A	A	A	A	A	A	A	A	A	A	A	A	A	A	A
			69	B	B	B	B	B	B	A	A	A	A	A	B	A	A	A	A
BICF2S24415286	2	60,735,861	0.02	A	A	A	A	A	A	B	B	B	B	B	A	B	B	B	B
			69	A	B	B	B	B	B	B	B	B	B	B	B	B	B	B	B
TIGRP2P27260_rs8792423	2	60,980,617	0.57	A	A	A	A	A	A	A	A	A	A	A	A	A	A	A	A
			92	A	A	A	A	A	A	A	A	A	A	A	A	A	B	B	B
BICF2P718485	2	61,031,775	0.52	A	A	A	A	A	A	A	A	A	A	A	A	A	A	A	A
			12	A	A	A	A	A	A	A	A	A	A	A	B	A	B	B	B
TIGRP2P27264_rs8807842	2	61,049,489	0.00	B	B	B	A	A	A	A	A	A	A	A	A	A	A	A	A
			22	B	B	B	B	B	B	A	A	A	A	A	A	A	B	B	B
BICF2P319838	2	61,076,087	0.52	A	A	A	A	A	A	A	A	A	A	A	A	A	A	A	A
			12	A	A	A	A	A	A	A	A	A	A	A	B	A	B	B	B
BICF2P488128	2	61,084,643	0.52	B	B	B	B	B	B	B	B	B	B	B	A	B	A	A	A
			12	B	B	B	B	B	B	B	B	B	B	B	B	B	B	B	B
BICF2P845420	2	61,085,185	0.52	A	A	A	A	A	A	A	A	A	A	A	A	A	A	A	A
			12	A	A	A	A	A	A	A	A	A	A	A	B	A	B	B	B
BICF2P845419	2	61,085,481	0.57	B	B	B	B	B	B	B	B	B	B	B	B	B	A	A	A
			92	B	B	B	B	B	B	B	B	B	B	B	B	B	B	B	B
BICF2P352173	2	61,094,748	0.57	A	A	A	A	A	A	A	A	A	A	A	A	A	A	A	A
			92	A	A	A	A	A	A	A	A	A	A	A	A	A	B	B	B

Table2.S4. cont'd

BICF2P544910	2	61,179,425	0.00 22	A A	A A	A A		A B	A B		A B	B B	B B	B B	B B	B B	B B	B B	B B	A B	A B
BICF2P348907	2	61,182,288	0.00 22	B B	B B	B B		A B	A B		A B	A A	A A	A A	A A	A A	A A	A A	A A	A B	A B
BICF2P1349008	2	61,198,715	0.00 22	A A	A A	A A		A B	A B		A B	B B	B B	B B	B B	B B	B B	B B	B B	A B	A B
BICF2S23137837	2	61,206,318	0.00 22	B B	B B	B B		A B	A B		A B	A A	A A	A A	A A	A A	A A	A A	A A	A B	A B
BICF2S23035024	2	61,341,337	0.00 22	B B	B B	B B		A B	A B		A B	A A	A A	A A	A A	A A	A A	A A	A B	A B	A B
BICF2S23238410	2	61,420,765	0.00 22	B B	B B	B B		A B	A B		A B	A A	A A	A A	A A	A A	B B	A A	A A	A A	A A
BICF2P309315	2	61,428,709	0.00 22	B B	B B	B B		A B	A B		A B	A A	A A	A A	A A	A A	A A	A A	A A	A A	A A
BICF2P606415	2	61,556,283	0.00 22	B B	B B	B B		A B	A B		A B	A A	A A	A B	A A	A A	A B	A A	A B	A A	A A
BICF2P548237	2	61,563,742	0.00 22	B B	B B	B B		A B	A B		A B	A A	A A	A B	A A	A A	A B	A A	A B	A A	A A
BICF2S23117344	2	61,604,057	0.00 22	B B	B B	B B		A B	A B		A B	A A	A A	A B	A A	A A	A B	A A	A B	A B	A B
BICF2S23119288	2	61,608,201	0.00 22	A A	A A	A A		A B	A B		A B	B B	B B	A B	B B	B B	A B	B B	A B	A B	A B
BICF2P75954	2	61,645,929	0.00 22	A A	A A	A A		A B	A B		A B	B B	B B	A B	B B	B B	B B	B B	B B	A B	A B
BICF2S23730507	2	61,656,330	0.00 22	B B	B B	B B		A B	A B		A B	A A	A A	A B	A A	A A	A A	A A	A B	A B	A B
BICF2P52239	2	61,677,919	0.00 22	B B	B B	B B		A B	A B		A B	A A	A A	A B	A A	A A	A B	A A	A B	A B	A B
BICF2S23740273	2	61,700,423	0.57 56	B B	B B	B B		B B	B B		B B	B B	B B	A B	B B	B B	A B	B B	A B	B B	B B

Table2.S4. cont'd

			0.00	A	A	A		A	A		B	B	B	A	B	B	B	B	A	A	A
BICF2P57790	2	61,719,834	22	A	A	A		B	B		B	B	B	B	B	B	B	B	B	B	B
BICF2P14457			0.00	A	A	A		A	A		B	B	B	B	B	B	B	B	A	B	B
05	2	61,736,588	22	A	A	A		B	B		B	B	B	B	B	B	B	B	B	B	B
BICF2P65128			0.00	B	B	B		A	A		A	A	A	A	A	A	A	A	A	A	A
3	2	61,761,135	22	B	B	B		B	B		A	A	A	B	A	A	A	A	A	A	A
BICF2P12017			0.58	B	B	B		B	B		B	B	B	A	B	B	B	B	B	A	A
61	2	61,781,060	58	B	B	B		B	B		B	B	B	B	B	B	B	B	B	B	B
BICF2S23256			0.00	A	A	A		A	A		B	B	B	B	B	B	B	B	B	B	B
057	2	61,792,733	22	A	A	A		B	B		B	B	B	B	B	B	B	B	B	B	B
BICF2P70584			0.00	A	A	A		A	A		B	B	B	B	B	B	B	B	B	B	B
1	2	61,822,011	22	A	A	A		B	B		B	B	B	B	B	B	B	B	B	B	B
BICF2S23730				B	B	B		B	B		B	B	B	A	B	B	A	B	B	B	B
081	2	61,830,410	1	B	B	B		B	B		B	B	B	B	B	B	B	B	B	B	B
BICF2P10203			0.00	B	B	B		A	A		A	A	A	A	A	A	A	A	A	A	A
9	2	61,983,959	22	B	B	B		B	B		A	A	A	B	A	A	B	A	B	A	A
BICF2P34022				B	B	B		B	B		B	B	B	B	B	B	B	B	A	B	B
2	2	61,988,808	1	B	B	B		B	B		B	B	B	B	B	B	B	B	B	B	B
BICF2P14303				A	A	A		A	A		A	A	A	A	A	A	A	A	A	A	A
38	2	61,999,276	1	A	A	A		A	A		A	A	A	A	A	A	A	A	B	A	A
BICF2P56788			0.00	B	B	B		A	A		A	A	A	A	A	A	A	A	A	A	A
2	2	62,081,153	22	B	B	B		B	B		A	A	A	A	A	A	B	A	B	B	B
BICF2P35760			0.00	A	A	A		A	A		B	B	B	B	B	B	A	B	A	A	A
8	2	62,097,073	22	A	A	A		B	B		B	B	B	B	B	B	B	B	B	B	B
BICF2P14053			0.00	B	B	B		A	A		A	A	A	A	A	A	A	A	A	A	A
06	2	62,110,938	22	B	B	B		B	B		A	A	A	A	A	A	B	A	B	B	B
BICF2P56190			0.00	A	A	A		A	A		B	B	B	B	B	B	A	B	A	A	A
1	2	62,116,651	22	A	A	A		B	B		B	B	B	B	B	B	B	B	B	B	B
			0.00	A	A	A		A	A		B	B	B	B	B	B	A	B	A	A	A
BICF2P62008	2	62,134,106	22	A	A	A		B	B		B	B	B	B	B	B	B	B	B	B	B

Table2.S4. cont'd

BICF2S23035			0.00	A	A	A		A	A		B	B	B	B	B	B	B	B	B	B	B	B	
175	2	62,150,701	22	A	A	A		B	B		B	B	B	B	B	B	B	B	B	B	B	B	
BICF2S23187			0.00	A	A	A		A	A		B	B	B	B	B	B	B	B	A	A	A		
69	2	62,158,518	22	A	A	A		B	B		B	B	B	B	B	B	B	B	B	B	B		
BICF2P30838			0.00	B	B	B		A	A		A	A	A	A	A	A	A	A	A	A	A		
1	2	62,177,558	22	B	B	B		B	B		A	A	A	A	A	A	A	A	B	A	A		
BICF2P32432			0.39	A	A	A		A	A		A	A	A	A	A	A	A	A	A	B	A		
3	2	62,214,897	33	A	A	A		A	A		A	A	A	A	A	A	B	B	B	B	B		
BICF2P32432			0.39	B	B	B		B	B		B	B	B	B	B	B	A	A	A	A	A		
2	2	62,215,437	33	B	B	B		B	B		B	B	B	B	B	B	B	B	B	A	B		
BICF2P79637			0.64	B	B	B		B	B		B	B	B	B	B	B	B	A	A	A	A		
3	2	62,243,400	61	B	B	B		B	B		B	B	B	B	B	B	B	B	B	A	B		
BICF2P13304			0.64	A	A	A		A	A		A	A	A	A	A	A	A	A	A	B	A		
55	2	62,252,040	61	A	A	A		A	A		A	A	A	A	A	A	A	B	B	B	B		
BICF2P49612				B	B	B		B	B		B	B	B	B	B	B	B	B	B	A	A		
5	2	62,301,315	1	B	B	B		B	B		B	B	B	B	B	B	B	B	B	B	B		
BICF2S23424			0.00	B	B	B		A	A		A	A	A	A	A	A	A	A	A	B	A		
493	2	62,312,743	6	B	B	B		B	B		A	A	A	B	A	A	B	B	B	B	B		
BICF2P87532			0.00	B	B	B		A	A		A	A	A	A	A	A	A	A	A	B	A		
1	2	62,324,397	6	B	B	B		B	B		A	A	A	B	A	A	B	B	B	B	B		
BICF2P10048			0.00	B	B	B		A	A		A	A	A	A	A	A	A	A	A	B	A		
26	2	62,332,319	6	B	B	B		B	B		A	A	A	B	A	A	B	B	B	B	B		
BICF2P10648			0.00	B	B	B		A	A		A	A	A	A	A	A	A	A	A	A	A		
92	2	62,343,676	22	B	B	B		B	B		A	A	A	B	A	A	B	A	B	B	B		
BICF2S23430			0.00	A	A	A		A	A		B	B	B	A	B	B	A	A	A	A	A		
864	2	62,357,680	6	A	A	A		B	B		B	B	B	B	B	B	B	B	B	A	B		
BICF2P10556			0.00	A	A	A		A	A		B	B	B	A	B	B	A	B	A	A	A		
66	2	62,367,351	22	A	A	A		B	B		B	B	B	B	B	B	B	B	B	B	B		
BICF2P51117			0.00	B	B	B		A	A		A	A	A	A	A	A	A	A	A	B	A		
9	2	62,405,199	6	B	B	B		B	B		A	A	A	B	A	A	B	B	B	B	B		

Table2.S4. cont'd

BICF2P21387			0.00	B	B	B		A	A		A	A	A	A	A	A	A	A	A	B	A
1	2	62,413,010	6	B	B	B		B	B		A	A	A	B	A	A	B	B	B	B	B
BICF2P47313			0.00	A	A	A		A	A		B	B	B	B	B	B	B	B	B	A	A
8	2	62,457,372	22	A	A	A		B	B		B	B	B	B	B	B	B	B	B	B	B
			0.00	B	B	B		A	A		A	A	A	A	A	A	A	A	A	A	A
BICF2P88807	2	62,471,732	22	B	B	B		B	B		A	A	A	A	A	A	A	A	A	B	B
BICF2P12207			0.00	B	B	B		A	A		A	A	A	A	A	A	A	A	A	A	A
95	2	62,479,545	22	B	B	B		B	B		A	A	A	B	A	A	B	A	B	B	B
BICF2P72095			0.00	A	A	A		A	A		B	B	B	A	B	B	B	B	A	A	A
1	2	62,500,174	22	A	A	A		B	B		B	B	B	B	B	B	B	B	B	B	B
BICF2P13929				B	B	B		B	B		B	B	B	B	B	B	B	B	B	A	A
15	2	62,524,560	1	B	B	B		B	B		B	B	B	B	B	B	B	B	B	B	B
BICF2S23451			0.00	B	B	B		A	A		A	A	A	A	A	A	A	A	A	A	A
051	2	62,533,775	22	B	B	B		B	B		A	A	A	A	A	A	A	A	A	A	A
BICF2P87894				B	B	B		B	B		B	B	B	B	B	B	B	B	B	A	A
5	2	62,551,012	1	B	B	B		B	B		B	B	B	B	B	B	B	B	B	B	B
BICF2S24428			0.00	A	A	A		A	A		B	B	B	A	B	B	A	A	A	A	A
69	2	62,628,636	6	A	A	A		B	B		B	B	B	B	B	B	B	B	B	A	B
BICF2P10002			0.00	B	B	B		A	A		A	A	A	A	A	A	A	A	A	A	A
52	2	62,696,026	22	B	B	B		B	B		A	A	A	B	A	A	B	A	B	A	A
BICF2S22914				A	A	A		A	A		A	A	A	A	A	A	A	A	A	A	A
690	2	62,806,611	1	A	A	A		A	A		A	A	A	A	A	A	A	A	A	B	B
BICF2S23321				A	A	A		A	A		A	A	A	A	A	A	A	A	A	A	A
75	2	62,819,638	1	A	A	A		A	A		A	A	A	A	A	A	A	A	A	B	B
BICF2S23620				B	B	B		B	B		B	B	B	B	B	B	B	B	B	A	A
100	2	62,826,928	1	B	B	B		B	B		B	B	B	B	B	B	B	B	B	B	B
BICF2P68067			0.43	A	B	B		A	B		B	B	A	A	B	B	A	A	A	A	A
4	2	62,964,565	2	B	B	B		B	B		B	B	B	B	B	B	B	A	B	A	B
BICF2P12893			0.83	A	A	A		A	A		A	A	A	A	A	A	A	A	A	B	A
71	2	63,127,929	8	A	A	A		A	A		A	A	A	A	A	A	A	A	A	B	B

Table2.S4. cont'd

BICF2S23032			0.65	A	A	A		A	A		A	A	B	A	A	A	A	A	A	A	A
857	2	63,150,127	14	A	A	A		B	A		A	A	B	A	A	B	A	B	A	A	A
BICF2S23356			0.65	A	B	B		A	B		B	B	A	A	B	A	B	B	A	A	A
306	2	63,158,699	52	B	B	B		A	B		B	B	B	B	B	B	B	B	B	B	B
BICF2S23551			0.02	B	B	B		B	A		A	A	A	A	A	A	A	A	A	B	A
818	2	63,231,557	1	B	B	B		B	B		A	A	B	B	A	B	B	A	B	B	B

2.7.1 Supplemental methods – *CNGB1* genotyping assay

PCR primers (F primer 5'-AAGCGTTTGCATCTTGCAC-3' and R primer 5'-TGTCCGATCATCACAGAGAAAG-3') were designed to amplify *CNGB1* exon 26 (Figure 2.S2). PCR amplification produces a 239 bp product in unaffected dogs and a larger 244 bp product in affected dogs (due to the 1 bp deletion and 6 bp insertion, Figure 2.S2A; red highlighted text Figure 2.S2B). The enzyme *AluI,* which recognizes the sequence AGCT, can be used to distinguish the normal and mutant alleles. The PCR product is digested for 2 hr at 37°C with 5 units *AluI* enzyme in 1X NEB buffer 4 (New England Biolabs, Ipswitch, MA). There is a common *AluI* site (blue highlighted text Figure 2.S2B) in both unaffected and affected dog DNA that verifies restriction enzyme activity. The unaffected dogs have a 218 bp product and the common 21 bp product (run off the end of this gel; Figure 2.S2A). The affected dogs, due to the 6 bp insertion (AGCTAC) that contains an *AluI* cut site, produce the 21 bp common band and the diagnostic 95 and 128 bp bands (Figure 2.S2A). A heteroduplex band is also seen in carriers, which migrates slightly slower than the 218 bp band. Note that the genotyping assay is designed utilizing the 6 bp insertion, not the 1 bp deletion. It is assumed that these two sequence changes are in complete linkage disequilibrium.

A.

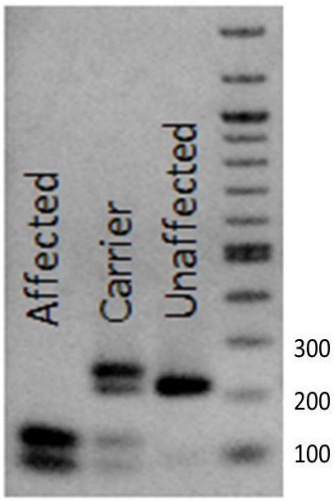

B.

Unaffected dog sequence

aagcgtttgcatcttgcacagctgtcagagccaggccacccaggctcagcagggtggggccttt
gctgaccgaggtccccttcctcttctctctctagTTACATTCGCTGTTACT------ACTGGGC
TGTGAAGACCCTCATCACCATTGGTGGGCTGCCTGACCCCAGAACGCTCTTTGAAATTGTCTTC
CAGGGGCTGAACTATTTCACGGGTGTCTTTGCTTTCTCTGTGATGATCGGACAGgtagctgggt
caccagtctggcttgccacccacccgtctgccagggcccctcccactactgccagaaatgtcac
catctgtggccattccttttggactaagtctgggaaagagcacgagt

Affected dog sequence

aagcgtttgcatcttgcacagctgtcagagccaggccacccaggctcagcagggtggggccttt
gctgaccgaggtccccttcctcttctctctctagTTACATTCGCTGTT CTAGCTACACTGGGC
TGTGAAGACCCTCATCACCATTGGTGGGCTGCCTGACCCCAGAACGCTCTTTGAAATTGTCTTC
CAGGGGCTGAACTATTTCACGGGTGTCTTTGCTTTCTCTGTGATGATCGGACAGgtagctgggt
caccagtctggcttgccacccacccgtctgccagggcccctcccactactgccagaaatgtcac
catctgtggccattccttttggactaagtctgggaaagagcacgagt

Figure 2.S2. *CNGB1* genotyping assay. (A) An agarose gel shows the banding patterns of digested PCR products from *CNGB1* affected, carrier and unaffected Papillons. (B) The unaffected dog *CNGB1* sequence is shown above the affected dog sequence and the primer binding sites are underlined, Intronic sequence is in lower case and exonic sequence is in upper case. The sequence differences are indicated by red highlighting. The AluI enzyme recognition site that is common to both the wildtype and mutant alleles is shown by blue highlighting.

REFERENCES

REFERENCES

1. Hartong DT, Berson EL, Dryja TP (2006) Retinitis pigmentosa. Lancet 368: 1795-1809.

2. Maubaret CG, Vaclavik V, Mukhopadhyay R, Waseem NH, Churchill A, et al. (2011) Autosomal dominant retinitis pigmentosa with intrafamilial variability and incomplete penetrance in two families carrying mutations in PRPF8. Investigative Ophthalmology and Visual Science 52: 9304-9309.

3. Berson EL, Rosner B, Sandberg MA, Weigel-DiFranco C, Dryja TP (1991) Ocular findings in patients with autosomal dominant retinitis pigmentosa and rhodopsin, proline-347-leucine. American Journal of Ophthalmology 111: 614-623.

4. Whitley RD (1988) Focusing on eye disorders among purebred dogs. Veterinary Medicine 83: 50-63.

5. Petersen-Jones SM (1998) Animal models of human retinal dystrophies. Eye 12: 566-570.

6. Aguirre GD, Acland GM (2006) Models, mutants, and man: searching for unique phenotypes and genes in the dog model of inherited retinal degeneration. In: Ostrander EA, Giger U, Lindblad-Toh K, editors. The dog and its genome. Cold Spring Harbor: Cold Spring harbor Laboratory Press. pp. 291-326.

7. Suber ML, Pittler SJ, Quin N, Wright GC, Holcombe N, et al. (1993) Irish setter dogs affected with rod-cone dysplasia contain a nonsense mutation in the rod cGMP phosphodiesterase beta-subunit gene. Proceedings of the National Academy of Sciences of the United States of America 90: 3968-3972.

8. Clements PJ, Gregory CY, Peterson-Jones SM, Sargan DR, Bhattacharya SS (1993) Confirmation of the rod cGMP phosphodiesterase beta subunit (PDE beta) nonsense mutation in affected rcd-1 Irish setters in the UK and development of a diagnostic test. Current Eye Research 12: 861-866.

9. Petersen-Jones SM, Entz DD, Sargan DR (1999) cGMP phosphodiesterase-α mutation causes progressive retinal atrophy in the Cardigan Welsh corgi dog. Investigative Ophthalmology and Visual Science 40: 1637-1644.

10. Dekomien G, Runte M, Godde R, Epplen JT (2000) Generalized progressive retinal atrophy of Sloughi dogs is due to an 8-bp insertion in exon 21 of the PDE6B gene. Cytogenetics and Cell Genetics 90: 261-267.

11. Zhu L, Jang GF, Jastrzebska B, Filipek S, Pearce-Kelling SE, et al. (2004) A naturally occurring mutation of the opsin gene (T4R) in dogs affects glycosylation

and stability of the G protein-coupled receptor. Journal of Biological Chemistry 279: 53828-53839.

12. Kukekova AV, Goldstein O, Johnson JL, Richardson MA, Pearce-Kelling SE, et al. (2009) Canine RD3 mutation establishes rod-cone dysplasia type 2 (rcd2) as ortholog of human and murine rd3. Mammalian Genome 20: 109-123.

13. Downs LM, Bell JS, Freeman J, Hartley C, Hayward LJ, et al. (2012) Late-onset progressive retinal atrophy in the Gordon and Irish Setter breeds is associated with a frameshift mutation in C2orf71. Animal Genetics 44: 169-177.

14. Goldstein O, Kukekova AV, Aguirre GD, Acland GM (2010) Exonic SINE insertion in STK38L causes canine early retinal degeneration (erd). Genomics 96: 362-368.

15. Zangerl B, Goldstein O, Philp AR, Lindauer SJ, Pearce-Kelling SE, et al. (2006) Identical mutation in a novel retinal gene causes progressive rod-cone degeneration in dogs and retinitis pigmentosa in humans. Genomics 88: 551-563.

16. Downs LM, Wallin-Hakansson B, Boursnell M, Marklund S, Hedhammar A, et al. (2011) A frameshift mutation in golden retriever dogs with progressive retinal atrophy endorses SLC4A3 as a candidate gene for human retinal degenerations. PLoS One 6: e21452.

17. Mowat FM, Petersen-Jones SM, Williamson H, Williams DL, Luthert PJ, et al. (2008) Topographical characterization of cone photoreceptors and the area centralis of the canine retina. Molecular Vision 14: 2518-2527.

18. Carter-Dawson LD, LaVail MM (1979) Rods and cones in the mouse retina. I. Structural analysis using light and electron microscopy. Journal of Comparative Neurology 188: 245-262.

19. Acland GM, Aguirre GD, Ray J, Zhang Q, Aleman TS, et al. (2001) Gene therapy restores vision in a canine model of childhood blindness. Nature Genetics 28: 92-95.

20. Bainbridge JW, Smith AJ, Barker SS, Robbie S, Henderson R, et al. (2008) Effect of gene therapy on visual function in Leber's congenital amaurosis. New England Journal of Medicine 358: 2231-2239.

21. Maguire AM, Simonelli F, Pierce EA, Pugh EN, Jr., Mingozzi F, et al. (2008) Safety and efficacy of gene transfer for Leber's congenital amaurosis. New England Journal of Medicine 358: 2240-2248.

22. Cideciyan AV, Hauswirth WW, Aleman TS, Kaushal S, Schwartz SB, et al. (2009) Human RPE65 Gene Therapy for Leber Congenital Amaurosis: Persistence of

Early Visual Improvements and Safety at 1 Year. Human Gene Therapy 20: 999-1004.

23. Acland GM, Aguirre GD, Bennett J, Aleman TS, Cideciyan AV, et al. (2005) Long-term restoration of rod and cone vision by single dose rAAV-mediated gene transfer to the retina in a canine model of childhood blindness. Molecular Therapy 12: 1072-1082.

24. Narfström K, Katz ML, Bragadottir R, Seeliger M, Boulanger A, et al. (2003) Functional and structural recovery of the retina after gene therapy in the RPE65 null mutation dog. Investigative Ophthalmology and Visual Science 44: 1663-1672.

25. Jacobson SG, Acland GM, Aguirre GD, Aleman TS, Schwartz SB, et al. (2006) Safety of recombinant adeno-associated virus type 2-RPE65 vector delivered by ocular subretinal injection. Molecular Therapy 13: 1074-1084.

26. Annear MJ, Bartoe JT, Barker SE, Smith AJ, Curran PG, et al. (2011) Gene therapy in the second eye of RPE65-deficient dogs improves retinal function. Gene Therapy 18: 53-61.

27. Gearhart PM, Gearhart C, Thompson DA, Petersen-Jones SM (2010) Improvement of visual performance with intravitreal administration of 9-cis-retinal in Rpe65-mutant dogs. Archives of Ophthalmology 128: 1442-1448.

28. Beltran WA, Cideciyan AV, Lewin AS, Iwabe S, Khanna H, et al. (2012) Gene therapy rescues photoreceptor blindness in dogs and paves the way for treating human X-linked retinitis pigmentosa. Proceedings of the National Academy of Sciences of the United States of America 109: 2132-2137.

29. Komaromy AM, Alexander JJ, Rowlan JS, Garcia MM, Chiodo VA, et al. (2010) Gene therapy rescues cone function in congenital achromatopsia. Human Molecular Genetics 19: 2581-2593.

30. Mowat FM, Bartoe JT, Bruewer A, Dinculescu A, Boye SL, et al. (2012) Evaluation Of Rod Photoreceptor Function And Preservation Following Retinal Gene Therapy In The PDE6A Mutant Dog. ARVO Meeting Abstracts 53: 1928.

31. Petit L, Lheriteau E, Weber M, Le Meur G, Deschamps JY, et al. (2012) Restoration of vision in the pde6beta-deficient dog, a large animal model of rod-cone dystrophy. Molecular Therapy 20: 2019-2030.

32. Håkanson N, Narfström K (1995) Progressive retinal atrophy in papillon dogs in Sweden: A clinical survey. Veterinary and Comparative Ophthalmology 5: 83-87.

33. Narfström K, Ekesten B (1998) Electroretinographic evaluation of Papillons with and without hereditary retinal degeneration. American Journal of Veterinary Research 59: 221-226.

34. Narfström K, Wrigstad A (1999) Clinical, electrophysiological and morphological changes in a case of hereditary retinal degeneration in the Papillon dog. Veterinary Ophthalmology 2: 67-74.

35. Purcell S, Neale B, Todd-Brown K, Thomas L, Ferreira MA, et al. (2007) PLINK: a tool set for whole-genome association and population-based linkage analyses. American Journal of Human Genetics 81: 559-575.

36. Kent WJ, Sugnet CW, Furey TS, Roskin KM, Pringle TH, et al. (2002) The human genome browser at UCSC. Genome Research 12: 996-1006.

37. Scheet P, Stephens M (2006) A fast and flexible statistical model for large-scale population genotype data: applications to inferring missing genotypes and haplotypic phase. American Journal of Human Genetics 78: 629-644.

38. Mowat FM, Breuwer AR, Bartoe JT, Annear MJ, Zhang Z, et al. (2012) RPE65 gene therapy slows cone loss in Rpe65-deficient dogs. Gene Therapy DOI:10.1038/gt.2012.63.

39. Cook NJ, Molday LL, Reid D, Kaupp UB, Molday RS (1989) The cGMP-gated channel of bovine rod photoreceptors is localized exclusively in the plasma membrane. Journal of Biological Chemistry 264: 6996-6999.

40. Gum GG, Gelatt KC, Samuelson DA (1984) Maturation of the retina of the canine neonate as determined by electroretinography and histology. American Journal of Veterinary Research 45: 1166-1171.

41. Adzhubei IA, Schmidt S, Peshkin L, Ramensky VE, Gerasimova A, et al. (2010) A method and server for predicting damaging missense mutations. Nature Methods 7: 248-249.

42. Colville CA, Molday RS (1996) Primary structure and expression of the human beta-subunit and related proteins of the rod photoreceptor cGMP-gated channel. Journal of Biological Chemistry 271: 32968-32974.

43. Ardell MD, Bedsole DL, Schoborg RV, Pittler SJ (2000) Genomic organization of the human rod photoreceptor cGMP-gated cation channel beta-subunit gene. Gene 245: 311-318.

44. Kaupp UB, Seifert R (2002) Cyclic nucleotide-gated ion channels. Physiological Reviews 82: 769-824.

45. Sautter A, Zong X, Hofmann F, Biel M (1998) An isoform of the rod photoreceptor cyclic nucleotide-gated channel beta subunit expressed in olfactory neurons. Proceedings of the National Academy of Sciences of the United States of America 95: 4696-4701.

46. Chen TY, Peng YW, Dhallan RS, Ahamed B, Reed RR, et al. (1993) A new subunit of the cyclic nucleotide-gated cation channel in retinal rods. Nature 362: 764-767.

47. Wiesner B, Weiner J, Middendorff R, Hagen V, Kaupp UB, et al. (1998) Cyclic nucleotide-gated channels on the flagellum control Ca2+ entry into sperm. Journal of Cell Biology 142: 473-484.

48. Huttl S, Michalakis S, Seeliger M, Luo DG, Acar N, et al. (2005) Impaired channel targeting and retinal degeneration in mice lacking the cyclic nucleotide-gated channel subunit CNGB1. Journal of Neuroscience 25: 130-138.

49. Zhang Y, Molday LL, Molday RS, Sarfare SS, Woodruff ML, et al. (2009) Knockout of GARPs and the beta-subunit of the rod cGMP-gated channel disrupts disk morphogenesis and rod outer segment structural integrity. Journal of Cell Science 122: 1192-1200.

50. Sugimoto Y, Yatsunami K, Tsujimoto M, Khorana HG, Ichikawa A (1991) The amino acid sequence of a glutamic acid-rich protein from bovine retina as deduced from the cDNA sequence. Proceedings of the National Academy of Sciences of the United States of America 88: 3116-3119.

51. Zheng J, Trudeau MC, Zagotta WN (2002) Rod cyclic nucleotide-gated channels have a stoichiometry of three CNGA1 subunits and one CNGB1 subunit. Neuron 36: 891-896.

52. Zhong H, Molday LL, Molday RS, Yau KW (2002) The heteromeric cyclic nucleotide-gated channel adopts a 3A:1B stoichiometry. Nature 420: 193-198.

53. Weitz D, Ficek N, Kremmer E, Bauer PJ, Kaupp UB (2002) Subunit stoichiometry of the CNG channel of rod photoreceptors. Neuron 36: 881-889.

54. Shuart NG, Haitin Y, Camp SS, Black KD, Zagotta WN (2011) Molecular mechanism for 3:1 subunit stoichiometry of rod cyclic nucleotide-gated ion channels. Nature Communications 2: 457.

55. Chen TY, Illing M, Molday LL, Hsu YT, Yau KW, et al. (1994) Subunit 2 (or beta) of retinal rod cGMP-gated cation channel is a component of the 240-kDa channel-associated protein and mediates Ca(2+)-calmodulin modulation. Proceedings of the National Academy of Sciences of the United States of America 91: 11757-11761.

56. Kaupp UB, Niidome T, Tanabe T, Terada S, Bönigk W, et al. (1989) Primary structure and functional expression from complementary DNA of the rod photoreceptor cyclic GMP-gated channel. Nature (London) 342: 762-766.

57. Pentia DC, Hosier S, Cote RH (2006) The glutamic acid-rich protein-2 (GARP2) is a high affinity rod photoreceptor phosphodiesterase (PDE6)-binding protein that modulates its catalytic properties. Journal of Biological Chemistry 281: 5500-5505.

58. Ritter LM, Khattree N, Tam B, Moritz OL, Schmitz F, et al. (2011) In situ visualization of protein interactions in sensory neurons: glutamic acid-rich proteins (GARPs) play differential roles for photoreceptor outer segment scaffolding. Journal of Neuroscience 31: 11231-11243.

59. Michalakis S, Zong X, Becirovic E, Hammelmann V, Wein T, et al. (2011) The glutamic acid-rich protein is a gating inhibitor of cyclic nucleotide-gated channels. Journal of Neuroscience 31: 133-141.

60. Trudeau MC, Zagotta WN (2002) An intersubunit interaction regulates trafficking of rod cyclic nucleotide-gated channels and is disrupted in an inherited form of blindness. Neuron 34: 197-207.

61. Zheng J, Zagotta WN (2004) Stoichiometry and assembly of olfactory cyclic nucleotide-gated channels. Neuron 42: 411-421.

62. Michalakis S, Reisert J, Geiger H, Wetzel C, Zong X, et al. (2006) Loss of CNGB1 protein leads to olfactory dysfunction and subciliary cyclic nucleotide-gated channel trapping. Journal of Biological Chemistry 281: 35156-35166.

63. Bareil C, Hamel CP, Delague V, Arnaud B, Demaille J, et al. (2001) Segregation of a mutation in CNGB1 encoding the beta-subunit of the rod cGMP-gated channel in a family with autosomal recessive retinitis pigmentosa. Human Genetics 108: 328-334.

64. Simpson DA, Clark GR, Alexander S, Silvestri G, Willoughby CE (2011) Molecular diagnosis for heterogeneous genetic diseases with targeted high-throughput DNA sequencing applied to retinitis pigmentosa. Journal of Medical Genetics 48: 145-151.

65. Kondo H, Qin M, Mizota A, Kondo M, Hayashi H, et al. (2004) A homozygosity-based search for mutations in patients with autosomal recessive retinitis pigmentosa, using microsatellite markers. Investigative Ophthalmology and Visual Science 45: 4433-4439.

66. Becirovic E, Nakova K, Hammelmann V, Hennel R, Biel M, et al. (2010) The retinitis pigmentosa mutation c.3444+1G>A in CNGB1 results in skipping of exon 32. PLoS One 5: e8969.

67. Koch S, Sothilingam V, Garcia Garrido M, Tanimoto N, Becirovic E, et al. (2012) Gene therapy restores vision and delays degeneration in the CNGB1(-/-) mouse model of retinitis pigmentosa. Human Molecular Genetics 21: 4486-4496.

68. Gouy M, Guindon S, Gascuel O (2010) SeaView version 4: A multiplatform graphical user interface for sequence alignment and phylogenetic tree building. Molecular Biology and Evolution 27: 221-224

CHAPTER 3

DETAILED DESCRIPTION OF THE RETINAL PHENOTYPE OF *CNGB1* AFFECTED DOGS

3.1 Introduction

Retinitis pigmentosa (RP) is one of the leading causes of inherited retinal degenerations in humans [1]. RP is a well-studied group of retinal diseases in which mutations in over 40 genes have been described. However, detailed phenotypic descriptions of individual types of RP are sometimes lacking in the available literature. For example RP45 patients, caused by mutations in the *CNGB1* gene, have no published ERG or OCT analyses. Understanding the natural course and progression of RP requires detailed ERG, OCT and histological analyses which may aid in the development of potential therapies. For obvious reasons, retinal histology on early stage or pre-degenerate eyes is not a common occurrence for RP characterization. For histological studies, animal models are instrumental. Purpose-bred animals can be studied at early ages and followed throughout the course of the disease.

The *CNGB1* gene produces three retinal proteins in the rod photoreceptor. There are two shorter splice variants that produce glutamic acid-rich proteins that are necessary for structural integrity of the rod photoreceptor and a full length protein (CNGB1a) which is the beta subunit of the rod cyclic nucleotide-gated ion channel that is an integral component of the phototransduction cascade [2,3]. There are two *CNGB1* knockout mouse models which have allowed the characterization of phenotypes resulting from two different mutations in the gene [4,5]. In chapter 2, a complex mutation in *CNGB1* identified in Papillon dogs was described. Dogs homozygous for the *CNGB1* mutation have abnormal rod function from as early as 5 weeks of age, obvious retinal vasculature attenuation within the first year of life and a slow loss of cone function over the next 5-8 years [6].

The purpose of this study was to provide detailed characterization of the progression of the retinal degeneration caused by the mutation identified in the *CNGB1* gene in Papillon dogs. Understanding the natural progression of the disease will provide a baseline for future development of therapies for the disease [7].

3.2 Materials and methods

3.2.1 Animal use

The dogs used in this study were maintained in a colony at the Michigan State University Comparative Ophthalmology Laboratory. Dogs were housed in a 12:12 hour light-dark cycle. The dogs were cared for and all experiments and procedures were in compliance with the ARVO statement for the Use of Animals in Ophthalmic and Vision Research and approved by the Michigan State University Institutional Animal Care and Use Committee (AUF number 05/11-106-00 and 05/14-090-00; Institutional NIH/PHS Animal Welfare Assurance number A3955-01).

3.2.2 Electroretinography

Electroretinograms (ERGs) were recorded following a modified procedure previously described [8]. Briefly, an Espion E2 Electrophysiology system with ColorDome Ganzfeld (Diagnosys LLC, Lowell, MA) with the bandpass set between 0.5 and 500 Hz was used. Dogs were dark-adapted for one hour before being anesthetized with intravenous propofol (10 mg/kg PropoFlo, Abbott Animal Health, North Chicago, IL). They were then intubated and maintained on inhaled 1 to 2% isoflurane (Isoflo, Abbott Laboratories, North Chicago, IL) delivered in oxygen. The anesthesia and manipulations were carried out under a dim red light. The ERG assessment consisted of 11 dark-adapted flash intensities (−2.41, −2.00, −1.60, −1.19, −0.79, −0.39, 0.00, 0.39, 0.85, 1.36, 1.90 log cdS/m^2) and a 5 Hz flicker with flash intensity -1.60 log cdS/m^2 to record rod photoreceptor and mixed rod-cone photoreceptor responses. Following this procedure, dogs were light adapted at 30 cd/m^2 for 10 minutes and 11 light-adapted

flash intensities superimposed over the same 30 cd/m^2 background light (−2.41, −2.00, −1.60, −1.19, −0.79, −0.39, 0.00, 0.39, 0.85, 1.36, 1.90 9 log cdS/m^2) were recorded for cone photoreceptor responses.

To investigate residual rod function scotopic ERGs were recorded from 7 week old *CNGB1* affected dogs (N=5), 8 week old *PDE6A* affected dogs (*PDE6A* affected dogs do not have rod function at this age, N=4) and 7-10 week old phenotypically normal dogs (N=3) [9].

Preservation of cone function was investigated by photopic ERGs recorded from older *CNGB1* affected dogs 1 year, 1.5 years, 3 years, 3.5 years, 4 years and 5.5 years of age (N=2 for each time point). The photopic ERGs of *CNGB1* affected dogs were compared to phenotypically normal controls that were ~1.5 years old (N=3) and 3 years old (N=2).

3.2.3 Spectral domain-optical coherence tomography

Assessment of *CNGB1* affected dog retinal morphology was performed by Spectral Domain-Optical Coherence Tomography (SD-OCT; Spectralis OCT+HRA Heidelberg Engineering Inc., Heidelberg, Germany). Dogs were anesthetized with intravenous propofol (10 mg/kg PropoFlo, Abbott Animal Health, North Chicago, IL), then intubated and maintained on inhaled 1 to 2% isoflurane (Isoflo, Abbott Laboratories, North Chicago, IL) delivered in oxygen. The pupil was dilated with 1% topical tropicamide (Mydriacyl, Alcon Laboratories, Honolulu, HI, USA), a lid speculum fitted and the eye positioned in primary gaze using a stay suture in the inferior perilimbal conjunctiva. High-resolution cross-section images obtained by line and volume scanning and images from the same region of the central retina of *CNGB1* affected and

phenotypically normal dogs were assessed. OCTs were measured from *CNGB1* affected dogs aged 3 months (N=3), 5-7 months (N=4), 1 year (N=1), 1.5 years (N=3), 4 years (N=1) and 5.5-6 years (N=2). Measurements of the central dorsal retina were collected and compared to phenotypically normal dogs 6 months (N=4), 1.5 years (N=1), 3.3 years (N=1), 4.8 years (N=1) and 8 years (N=2) of age.

3.2.4 Vision testing

Vision testing was performed using a previously described four-choice vision testing device [10]. Briefly, dogs were placed in the central box of the vision testing device from which there are four tunnel exits. The far ends of three of the exits were blocked and one was left open. The open exit was randomly chosen for each run. Different light intensities were used to illuminate the room outside of the device (35-45 cd/m^2, 15.0 cd/m^2, 8.0 cd/m^2, 1.0 cd/m^2, 0.4 cd/m^2, 0.2 cd/m^2, 0.02 cd/m^2). The time it takes for the dog to exit the device was recorded, as well as whether the open exit was selected as its first choice. This is a proven method for determining the functional vision of a dog. Increased time and incorrect exit choices indicate decreased vision in the dogs [11]. The mean correct choice and time to exit was calculated over 14 runs per light intensity.

3.2.5 Sample collection and processing

Following humane euthanasia eyes were enucleated from 5 *CNGB1* affected dogs (8 weeks, 5 months, 1 year, 1.5 years, 2.3 years and 2.5 years). The right eyes were fixed with 4% paraformaldehyde (Electron Microscopy Sciences, Hatfield, PA, USA) in phosphate buffered saline (PBS, pH 7.4) with 3% sucrose for 3 hours at 4°C.

The anterior segment of the eye was removed and the eyecup placed back in the fixative for 30 minutes. The eyecup was removed from the fixative, washed with PBS and placed in 30% sucrose in PBS overnight at 4°C. The eye was washed in PBS before embedding in optimal cutting temperature medium (Electron Microscopy Sciences, Hatfield, PA, USA) and frozen with liquid nitrogen. Eyes were stored at -20°C until sectioning. Eyes were sectioned (14 µm) using a cryomicrotome (Leica CM3050-S, Leica Microsystems, Buffalo Grove, IL, USA).

Left eyes from the *CNGB1* affected dogs and one control dog (8 weeks old) were fixed in 3% glutaraldehyde and 2% paraformaldehyde in 0.1 M sodium cacodylate buffer (Electron Microscopy Sciences, Hatfield, PA, USA) for 30 minutes, the anterior segment of the eye removed and the eyecup placed back into the fixative overnight at 4°C. The samples were washed and stored in 0.1 M sodium cacodylate buffer at 4°C until dissected. A 3.0-3.5 mm portion of the retina was dissected about 1-2 mm dorsal to the optic nerve i.e. the central retina. The tissue samples were embedded in 1-2% agarose in 0.1 M sodium cacodylate buffer to facilitate handling of the tissue samples without detachment of the retina during processing. Tissue samples were post-fixed in 2% osmium tetroxide for 15 mins before dehydration in acetone and infusion of Spurr resin [12]. Samples were sectioned with an RMC MTX ultramicrotome (Boeckeler Instruments, Tucson, AZ, USA). Thick sections (500 nm) were stained with epoxy tissue stain (Electron Microscopy Sciences, Hatfield, PA, USA) and imaged with a light microscope (Nikon Eclipse 80i, Nikon Instruments Inc., Melville NY). Thin sections (70-100 nm) were captured on copper grids and stained for 20 min with 4% uranyl acetate and 15 min with Reynolds lead citrate [13]. Thin sections were imaged on a JEOL

100CX transmission electron microscope with a Gatan ORIUS camera (Gatan Inc., Pleasanton, CA, USA).

3.2.6 *CNGB1* transcript quantification and investigation of exon skipping

Retina from 8 week old *CNGB1* affected dogs (N=2), 8 week to 5 month *CNGB1* heterozygous dogs (N=3) and 8 week old mixed breed control dogs (N=3) were dissected from enucleated eyes, placed in an RNA stabilization buffer (RNAlater, Qiagen Sciences, Germantown, MD) and stored in a -80°C freezer until RNA extraction. RNA was extracted according to manufacturer's protocol (RNeasy midi kit, Qiagen Sciences, Germantown, MD). cDNA was made from mRNA using a 3' RACE kit according to manufacturer's protocol (Invitrogen, Carlsbad, CA).

mRNA tissue expression was analyzed via real time quantitative PCR (RT-qPCR) on cDNA templates. An Applied Biosystems StepOne Fast machine (Applied Biosystems Inc., Foster City, CA) was used for the RT-qPCR. The reactions were held for 10 minutes at 95.0° C, then run for 40 cycles at 95.0° C for 15 seconds and 60.0° C for one minute. Samples were run in duplicate and no-template controls were included in each run. The *CNGB1, CNGA1* and *PDE6A* products were normalized to products from the succinate dehydrogenase gene (*SDHA)* (Table 3.1). The ratios of the ddCt values are calculated and compared.

Table 3.1. RT-qPCR primers for retinal tissue expression

Gene	Forward Primer	Reverse Primer	Size[1]
CNGB1	GGACATCACCGTGTTCCAG	TGTCCATCTTAAAGCGACGAG	113
CNGA1	TCCCAATGTGATTGTTCCAG	TCAAACATGGAGGCACTGTC	111
PDE6A	CCACGTGAAGTGTGACAATG	AGCTCTCCTTGCAGGATCTC	117
SDHA	CGGTCCATGACTCTGGAAAT	GCAACTGCAGGTACACATGG	73

1. Amplified cDNA size

Primers were designed flanking *CNGB1* exon 26 (F primer: AGGGTTTTCCCAGTCACGACCGGCCTACCTGCTCTACAGT; R primer: ACCAGGTCTTGACACGGTTC) to investigate exon skipping due to the mutation. Amplicons were purified and sent to Michigan State University's Research Technology Support Facility for Sanger dideoxy-sequencing on an ABI 3730 Genetic Analyzer (Applied Biosystems, Inc., Foster City, CA).

3.2.7 Immunohistochemistry

Immunohistochemistry was performed on frozen retinal sections from *CNGB1* affected dogs and phenotypically normal dogs. The primary and secondary antibodies concentrations, details and protocols are listed in Table 3.2. Protocols 1, 2 and 3 are described below.

Protocol 1: Frozen sections were blocked with 5% horse serum (Sigma-Aldrich, St Louis, MO), 0.5% Triton^{TM} X-100 (Sigma-Aldrich, St Louis, MO) for 1 hour at room temperature. Follow the blocking step the primary antibody was placed on the sections overnight at room temperature.

Protocol 2: Frozen sections were blocked with 5% horse serum, 0.5% Triton^{TM} X-100 for 2 hours at room temperature. Follow the blocking step the primary antibody was placed on the sections overnight at 4°C.

Protocol 3: Frozen sections were blocked with 10% horse serum, 0.1% Triton^{TM} X-100 for 2 hours at room temperature. Follow the blocking step the primary antibody was placed on the sections overnight at 4°C.

Following the primary antibody incubation steps in Protocols 1, 2 and 3, a secondary antibody was placed on the slides for 2 hours in the dark at room

temperature. The nuclear stain DAPI was used as a counterstain for all labeled sections.

Immunolabeled sections were imaged using a fluorescent microscope (Nikon Eclipse 80i, Nikon Instruments Inc., Melville NY) using commercial image capture software (MetaVue, Molecular Devices, Sunnyvale CA). Unless otherwise noted, images were taken using the same exposure settings for both affected and control samples.

Table 3.2. Antibody details and concentrations

Antigen Target	Antibody Details	Source	Secondary Antibody	Protocol
CNGB1 mid' (574-763)	1:2000 rabbit polyclonal	Dr. Frank Müller FPc21K	1:500 AlexaFluor anti-rabbit 488	1
CNGA1	1:10 mouse monoclonal	Dr. Bob Molday	1:500 AlexaFluor anti-rabbit 488	2
Human cone arrestin	1:10,000 rabbit polyclonal	Dr. Cheryl Craft	1:500 AlexaFluor anti-rabbit 488	3
Rhodopsin	1:2 mouse monoclonal	Thermo Scientific MS-1233-R7	1:500 AlexaFluor anti-mouse 488	3

3.2.8 Statistical analysis

P-values were calculated using the statistical software SigmaPlot v12. (Systsat Software, Inc, San Jose, CA, USA). Data were analyzed for normality and equal variance. If the data passed normality and variance tests, a Student t-test was. Nonparametric data was analyzed using a nonparametric t-test (unequal variance) or a Mann-Whitney Sum Test (not normally distributed).

3.3 Results

3.3.1 RT-qPCR and exon skipping

To determine if the *CNGB1* mutation identified in PRA affected dogs decreases the expression of the *CNGB1* transcript a real time quantitative PCR (RT-qPCR) assay was used on samples from 8 week old *CNGB1* affected dogs (N=2), young *CNGB1* heterozygous dogs (N=3) and young control dogs (N=3) (Table 3.3). The level of *CNGB1* transcript was normalized to the gene *SDHA*. The level of expression of mutant *CNGB1* in *CNGB1* affected dogs was significantly lower (42% ± 8.5, p=0.026) than of the wild-type transcript in the control dogs. The mean expression level in the heterozygous dogs was also lower than controls but this difference was not statistically significant (81% ± 22.5, p=0.299). *CNGA1* transcripts were also compared between *CNGB1* affected and control dogs. *CNGB1* affected and heterozygous dogs had lower mean transcript levels of *CNGA1* than the control dogs but the difference was not statistically significant (68.5% ± 4.9; p=0.254 and 74.3% ± 11.9, p=0.226 respectively). *PDE6A* transcript levels were also assessed to see if other phototransduction transcripts were decreased. Mean *PDE6A* transcript levels were lower in the *CNGB1* affected samples than the controls but this difference was not statistically significant (64.5% ± 23.3 p= 0.185).

Table 3.3. RT-q PCR results from retinal extracts

Sample[1]	*CNGB1*[2]	*CNGA1*	*PDE6A*
Aff 1	0.48	0.72	0.81
Aff 2	0.36	0.65	0.48
Het 1	1.04	0.78	1.63
Het 2	0.80	0.61	0.79
Het 3	0.59	0.84	1.39
Unaf 1	1.17	1.40	0.76
Unaf 2	1.05	0.94	1.06
Unaf 3	0.81	0.76	1.24

1. Biological replicates. Aff 1-2, Het 1 and Unaf 1-3: 8 weeks old; Het 2: 12 weeks; Het 3: 5 months
2. Fold change from average of unaffected values.

PCR from retinal cDNA from dogs homozygous for the *CNGB1* mutation using primers in the exons flanking the *CNGB1* mutation in exon 26 (i.e. exon 25 and exon 27) resulted in a product of smaller size (~270 bp) than that from wild-type retinal cDNA (~410 bp) (Figure 3.1A). The heterozygous dog had PCR products of the expected wild-type length and of the length seen in the homozygous *CNGB1* affected dog. Sequencing of the shorter PCR product showed that exon 26 is skipped in the transcripts of *CNGB1* affected dogs. The wild-type dog protein sequence near the mutation site is shown in Figure 3.1B. The skipping of exon 26 alters the previously predicted protein sequence (6 new amino acids before a premature stop codon) (Figure 3.1C) to result in a predicted polypeptide with one altered amino acid before the truncation of the protein in the first codon of exon 27 (Figure 3.1D).

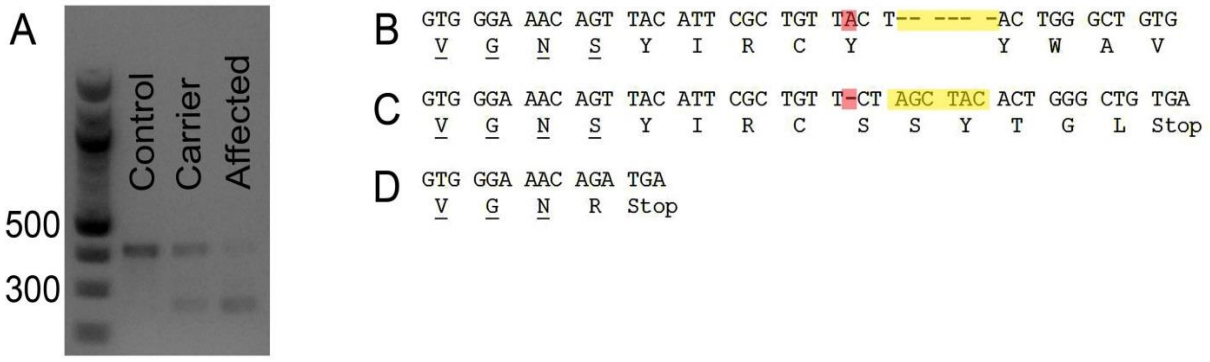

Figure 3.1. Exon 26 is skipped in *CNGB1* affected dogs. (A) Agarose gel showing size difference of PCR amplicon indicating exon skipping. The expected size of the PCR amplicon is 403 base pairs (bps). Exon 26 is 142 bps in control dogs and 137 bps in *CNGB1* affected dogs. The aberrant amplicon is 266 bps as seen in the agarose gel. (B) shows the control protein sequence with yellow dashes and red box indicating the mutation site. (C,D) The evidence of exon skipping has changed the previously predicted alterations of the amino acids and location of the premature stop codon (C) to the protein sequence in panel D. The red dash in panel C is the location of the 1 base pair deletion and the 6 base pair insertion is highlighted in yellow. The 100 bps ladder sizes 300 and 500 bps are labeled.

3.3.2 Presence of truncated CNGB1 protein and low levels of CNGA1 protein in frozen retinal sections

Immunolabeling of frozen retinal sections with a CNGB1 antibody (‘CNGB1mid’) indicates the presence of truncated protein. The CNGB1mid antibody binds to residues 574-763 which are located upstream of the *CNGB1* mutation site and would therefore label a truncated protein [14]. The CNGB1mid antibody labels the inner segments of the rod photoreceptors and not the outer segments. This suggested that the truncated CNGB1 subunit is not incorporated with CNGA1 into channels in the outer segments (Figure 3.2A,B). CNGA1 immunolabeling was not detectable in the rod outer segments of *CNGB1* affected dogs when the same exposure was used as for the sections from

control dogs. However, if the exposre was increased eight times immunolabeling was detectable in the outer segments of the rod photoreceptors of *CNGB1* affected dogs (Figure 3.2B). This low level of CNGA1 in the *CNGB1* affected outer segments may represent CNGA1 homomeric channels. In vitro studies have shown that CNGA1 protein can form homomeric CNG channels with functional but altered channel kinetics

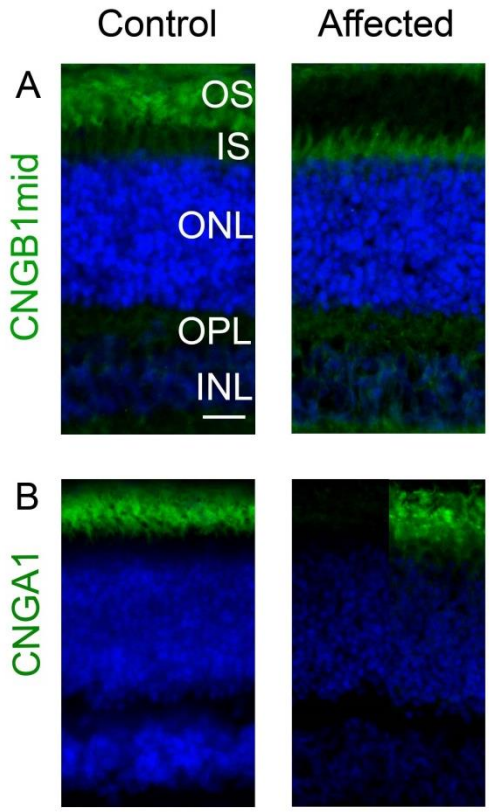

[15-17].

Figure 3.2. Truncated CNGB1 and low levels of CNGA1 are expressed in the retina of *CNGB1* affected dogs. (A) The CNGB1mid antibody (FPc21K) which labels full length CNGB1 protein but does not label the smaller GARP proteins (i.e. located upstream of the *CNGB1* mutation site) indicates the presence of truncated CNGB1 protein in the inner segments of rods. (B) CNGA1 is correctly localized to the rod outer segments at low concentrations in the *CNGB1* affected dog. The *CNGB1* affected dog image in panel B shows CNGA1 antibody labeling with equal exposure to the control dog (left half) and 8x the exposure of the control dog (right half). Size bar 20 µm. OS – outer segments, IS – inner segments, ONL – outer nuclear layer, OPL – outer plexiform layer, INL – inner nuclear layer.

3.3.3 Residual rod function

With the histological evidence suggesting presence of homomeric CNGA1 channels in the rod outer segments, ERGs were carefully analyzed to determine whether residual rod photoreceptor function could be detected in the *CNGB1* affected dogs. Seven week old *CNGB1* affected dogs were compared to 8 week old *PDE6A* affected dogs. At 8 weeks old, the *PDE6A* affected dogs do not have rod function [9]. A-wave intensity-response (I-R) curves show that the *CNGB1* affected dog a-waves are larger than those of the *PDE6A* affected a-waves and are significantly different at 8/11 of the light intensities (Table 3.4, Figure 3.3).

Table 3.4. Scotopic a-wave amplitude comparisons between control, *CNGB1* affected and *PDE6A* affected 7-8 week old dogs

Flash Intensity	Control		*CNGB1* affected		*PDE6A* affected		
Log cdS/m^2	a-wave[1]	SD[2]	a-wave[1]	SD[2]	a-wave[1]	SD[2]	*P*-value[3]
-2.41	0.65	0.81	0.56	0.40	0.08	0.08	0.095
-2.00	2.18	1.06	0.49	0.60	0.34	0.17	0.690
-1.60	3.18	1.81	0.56	0.40	0.08	0.08	0.032
-1.19	7.80	1.95	1.34	0.52	0.50	0.22	0.008
-0.80	17.63	5.04	1.42	0.86	0.30	0.20	0.008
-0.40	35.24	6.29	2.03	0.91	1.02	0.21	0.151
0.00	57.29	14.87	5.80	1.41	2.06	0.97	0.008
0.39	80.41	15.93	11.25	3.71	3.11	1.56	0.008
0.86	98.59	22.52	17.52	5.29	5.35	1.90	0.008
1.36	120.42	30.11	22.77	8.47	3.36	2.43	0.008
1.90	141.80	31.60	28.84	12.42	5.60	2.43	0.008

1. Average a-wave from control (N=3), *CNGB1* affected (N=5), *PDE6A* affected (N=5) dogs
2. Standard deviation of a-wave means
3. *P*-value of *CNGB1* affected dogs compared to *PDE6A* affected dogs, calculated using Mann-Whitman rank sum test

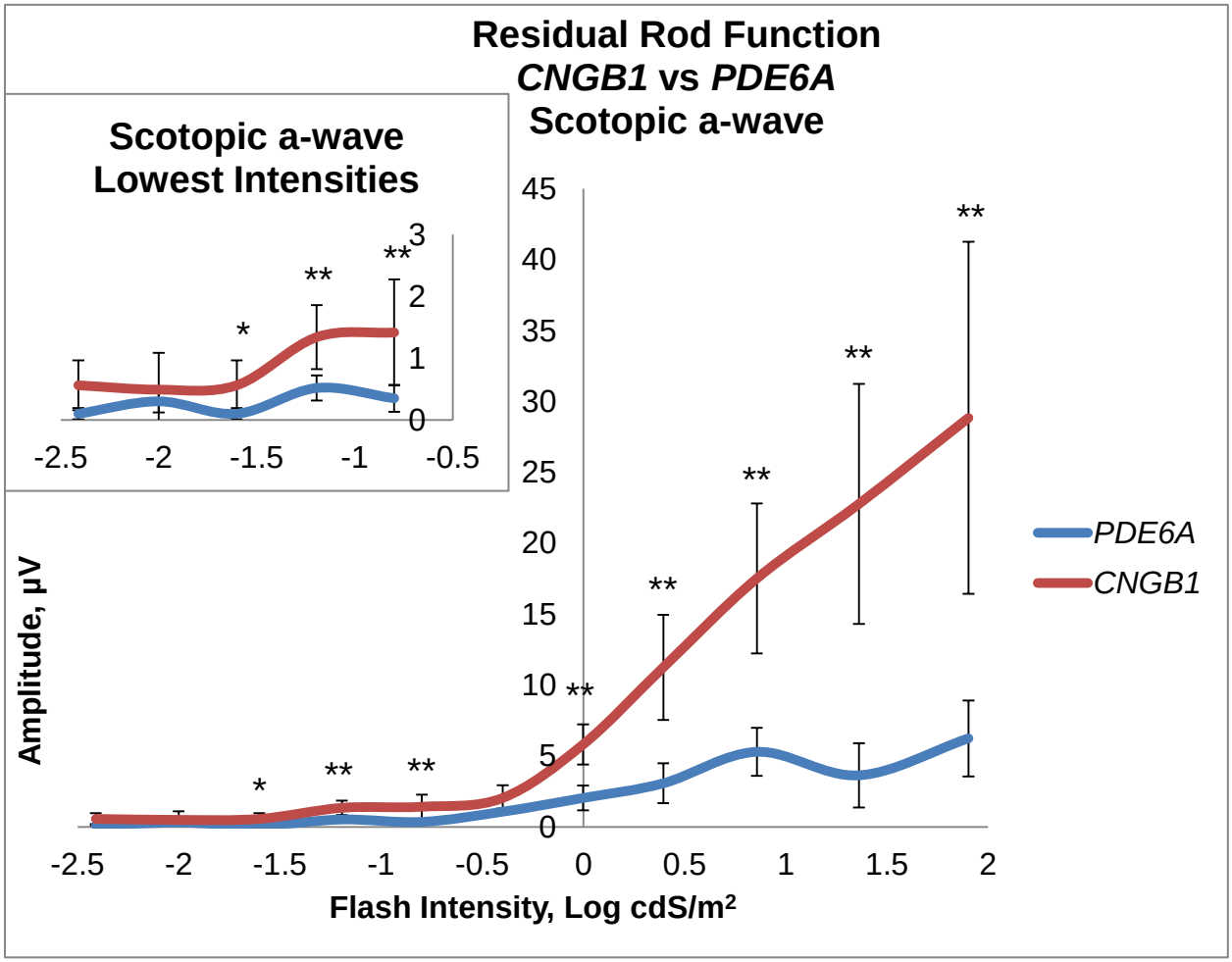

Figure 3.3. Scotopic intensity-response a-wave curves of *PDE6A* and *CNGB1* affected dogs. 7-8 week old *CNGB1* and *PDE6A* affected dog scotopic amplitudes. *PDE6A* dogs do not have rod function at this age. The inset graph shows the lowest light intensities. The *CNGB1* dogs have significantly larger scotopic a-waves at brighter light intensities. * - $p \leq 0.05$, ** - $p \leq 0.01$.

Plotting mean ERG tracings from *CNGB1* and *PDE6A* affected dogs on the same graph shows an abnormal second positive wave following the initial a- and b-waves peaking around 170 msec (Figure 3.4). This wave occurs in scotopic ERGs at the lower light intensities, where the ERG is primarily rod driven.

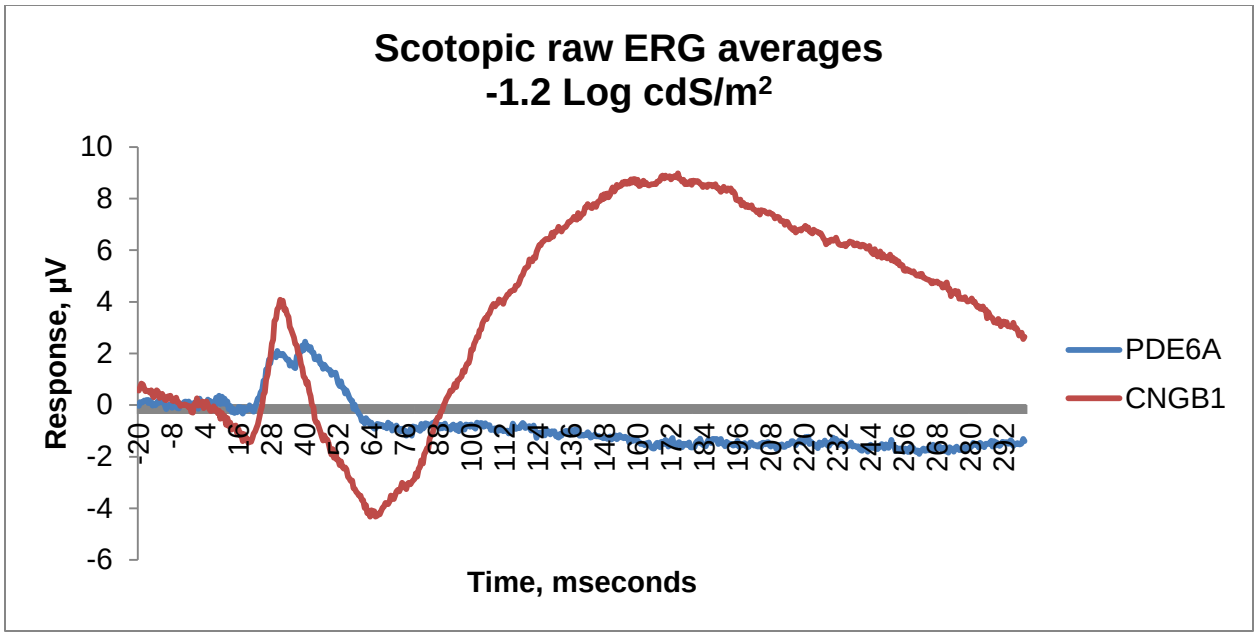

Figure 3.4. *CNGB1* affected dogs have an abnormal second slow positive waveform that is present after the normal b-wave. The *CNGB1* affected dogs (red line) have a slow additional wave peaking at around 170 msec. The *PDE6A* affected dogs (blue line) do not have a similar peak nor do control dogs (data not shown).

3.3.4 Retinal morphology of *CNGB1* affected dogs

To assess the morphological changes during the course of the retinal degeneration we used OCT for *in vivo* analysis and measured the thickness of retinal layers from a consistent region of the dorsal retina. The photoreceptor layers were measured from images taken 5000 µm dorsal to the optic nerve. Figure 3.5 shows the photoreceptor thickness ("Rec+"; measured from the outer plexiform layer to the photoreceptor outer segments) on a series of dogs over ~6 years of disease progression (red squares) compared to control dog photoreceptor thickness (blue diamonds, 6 months to 96 months of age). At 3 months of age the thickness of the photoreceptor layer is normal. There is only a slight decrease in thickness by 7 months of age. There is a significant difference in thickness of the photoreceptor layer starting

at 1.5 years of age (p<0.001). By 4 years of age, there is a substantial decrease in photoreceptor layer thickness. The photoreceptor layer continues to decline until the last time point was measured ~6 years of age (66-69 months). Supplemental Table 3.S1 shows the data, p-values and statistical test used that correspond with Figure 3.5.

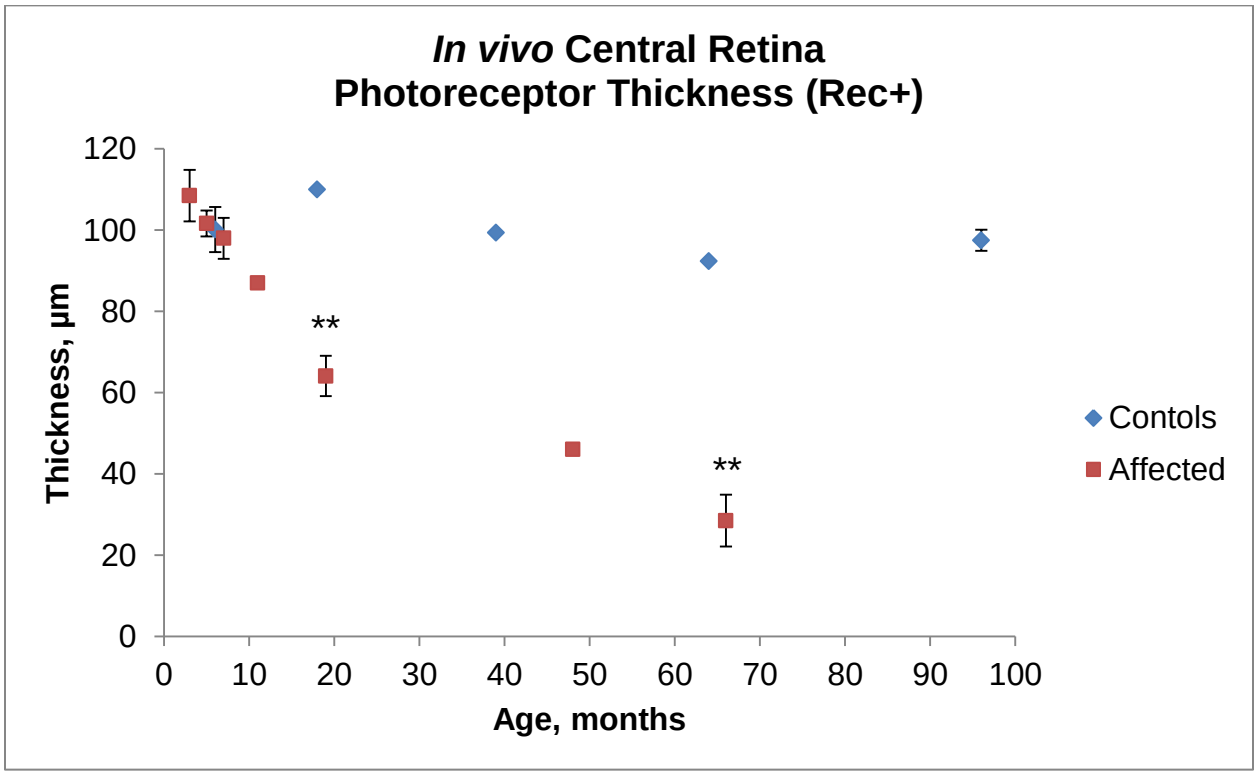

Figure 3.5. OCT measurements show *CNGB1* affected dog Rec+ thickness decreases slowly. The blue diamonds indicate the photoreceptor thickness in control dogs from 6 months to 8 years of age. The *CNGB1* affected dog (red squares) Rec+ layer decreases as the disease progresses. There is a significant decrease (**) in thickness of *CNGB1* affected dogs at 19 and 66 months of age compared to the control dogs. There was no significant difference between young control dog (6 months) Rec+ thickness and old control dogs (18 – 96 months) * - $p \leq 0.05$, ** - $p \leq 0.01$. Control dogs: 6 months (N=4), 18 months (N=1), 39 months (N=1), 64 months (N=1), 96 months (N=2). *CNGB1* affected dogs: 3 months (N=2), 5 months (N=2), 6-7 months (N=3), 12 months (N=1), 19 months (N=3), 66 months (N=2).

Semi-thin plastic embedded sections from *CNGB1* affected dogs were compared to control dog sections using light microscopy. Figure 3.6 shows representative images from the central dorsal regions of a control dog and an age series of *CNGB1* affected

dogs. At 8 weeks of age the *CNGB1* affected dog retina looks relatively normal, although the cone inner segments appear within the outer segments of the rods (as shown by arrows in Figure 3.6) due to shortening of the rod inner segments. From 5 months to 1 year of age, the outer nuclear layer has thinned slightly and the outer segments have shortened, thinned and are disorganized. The cone and rod inner segments are still apparent. By 1.5 years of age the outer nuclear layer of the retina has thinned considerably, being reduced from a normal of 10-12 nuclei thick to only 4-5 nuclei thick. There are still some remnants of rod outer segments and the cones have started to lose their shape and begun to shorten. At 2.3 years, the outer nuclear layer shows little further change in thickness but rod inner segments are very reduced in size and the cone inner segments have a round and stunted shape.

Figure 3.7 shows representative transmission electron microscopy images from the central dorsal regions of a control dog and the age series of *CNGB1* affected dogs. Control dogs show tightly packed rod outer segments and the disks of the rod outer segments are organized. The 8 week *CNGB1* affected dog shows disorganized outer segments but the disks appear to be stacked relatively normally. At 5 months of age, the rod outer segments are variable in size and the disks are not stacked uniformly. The 1 year *CNGB1* affected dog shows less tightly packed rod outer segments. The rod outer segments are very disorganized, stunted and highly variable in appearance.

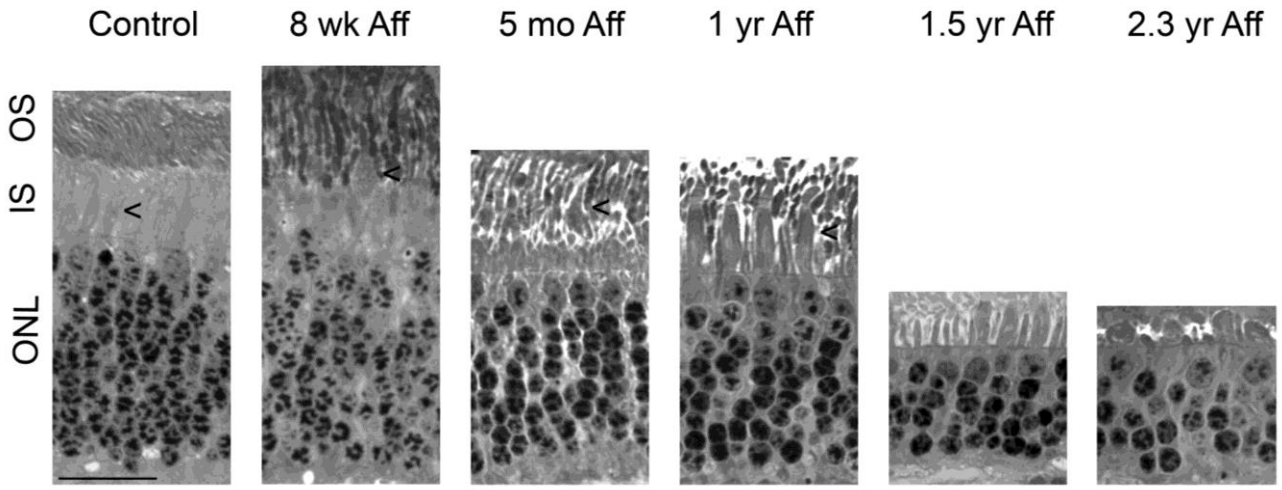

Figure 3.6. Plastic embedded semi-thin sections of control and *CNGB1* affected retinal tissue show slow retinal thinning and changes in inner and outer segment structure. Plastic embedded tissue samples from an 8 week old control dog compared to 8 week, 5 month, 1 year, 1.5 year and 2.3 year *CNGB1* affected dogs. The black arrow heads in the sections point to cone inner segments. The inner segments of cones are located adjacent to the inner segments of rods in the control dogs. Shortening of the rod inner segments in the *CNGB1* affected dogs means that cone inner segments extend to the level of the rod outer segments. Rod outer segments appear disorganized and deteriorate over the course of the first 2 years of life. Initially, cone inner segments appear grossly normal then, with rod loss, initially appear enlarged (1 year *CNGB1* affected) but then become shortened and atrophied (see 2.3 years of age). 500 nm sections were stained with epoxy tissue stain. Size bar 20 µm. OS – outer segments, IS – inner segments, ONL – outer nuclear layer.

Interestingly, as seen in the bottom panel of the 1 year old affected dog (Figure 3.7), some relatively normal looking rod outer segments are still present. By 2.3 years, there are inner segments of rods and cones present and scattered remnants of outer segments remain.

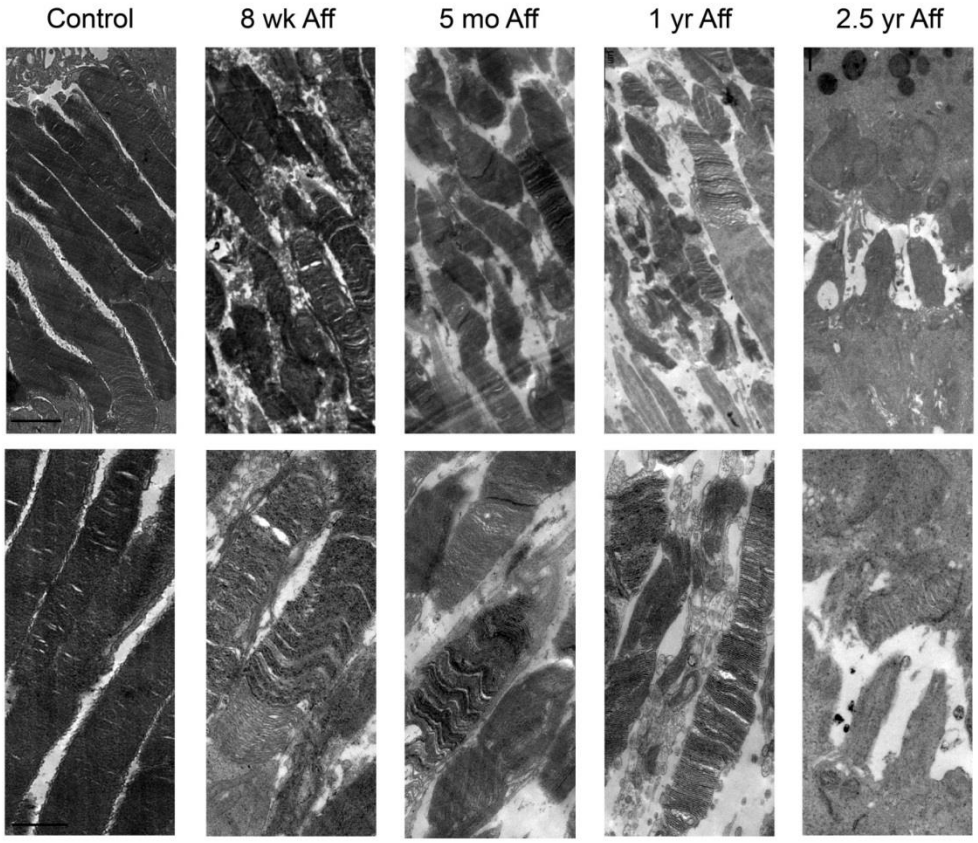

Figure 3.7. Transmission electron microscopy shows disorganized rod outer segments in *CNGB1* affected retinal tissue. 8 week control dog retinal tissue shows organized rod outer segments and organized, horizontally stacked disks. The rod outer segments are tightly packed. 8 week old *CNGB1* affected retinal tissue shows increasing levels of disorganization as the retina degenerates. Note that even at 2.3 years, there are still stubs of inner segments and remnants of outer segments (bottom). Top – 5000X, size bar 2 µm. Bottom – 10000X, size bar 1 µm.

Frozen retinal sections were immunolabeled with rod photoreceptor (rhodopsin, Figure 3.8) and cone photoreceptor markers (PNA, M/L opsin and cone arrestin Figure 3.9). Rhodopsin is correctly localized to the outer segments at 1 year of age (Figure 3.8) but at 2.5 years old, there is mislocalization of rhodopsin with the protein appearing in the remnants of the outer segments but also in the photoreceptor cell body. Co-labeling with PNA and M/L opsin stains the cone extracellular matrix (peanut agglutinin, PNA) and the outer segments of medium/long wavelength cones (M/L opsin) (Figure 3.9). These antibodies are correctly localized confirming the preservation of cone morphology seen in the plastic sections. Up to 1 year of age, the *CNGB1* affected dogs show near normal cone morphology and protein labeling. At 1.5 years of age the cone outer segments appear shorter and less defined. By 2.5 years of age, the cone outer segments are severely shortened (Car, Figure 3.9).

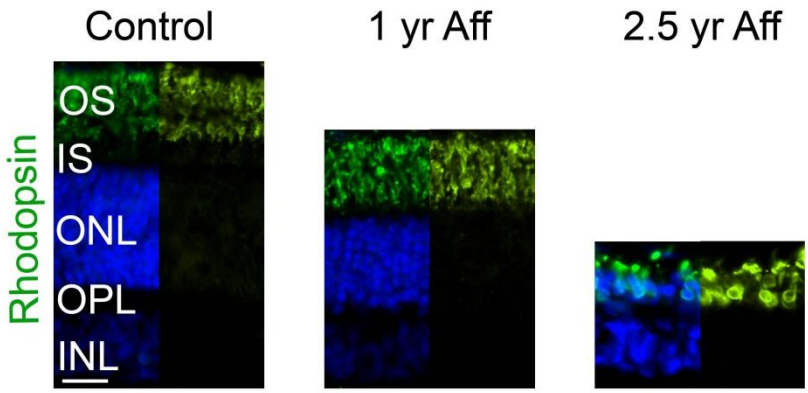

Figure 3.8. Rhodopsin is mislocalized in older *CNGB1* affected dogs. Rhodopsin is correctly localized to the outer segments in control dogs and 1 year old *CNGB1* affected dogs. At 2.5 years of age, there is mislocalization of the rhodopsin protein. DAPI/rhodopsin overlays are displayed in the left panels while the rhodopsin-only stain is on the right panel, highlighting the mislocalization in the older dog. Size bar 20 µm. OS – outer segments, IS – inner segments, ONL – outer nuclear layer, OPL – outer plexiform layer, INL – inner nuclear layer.

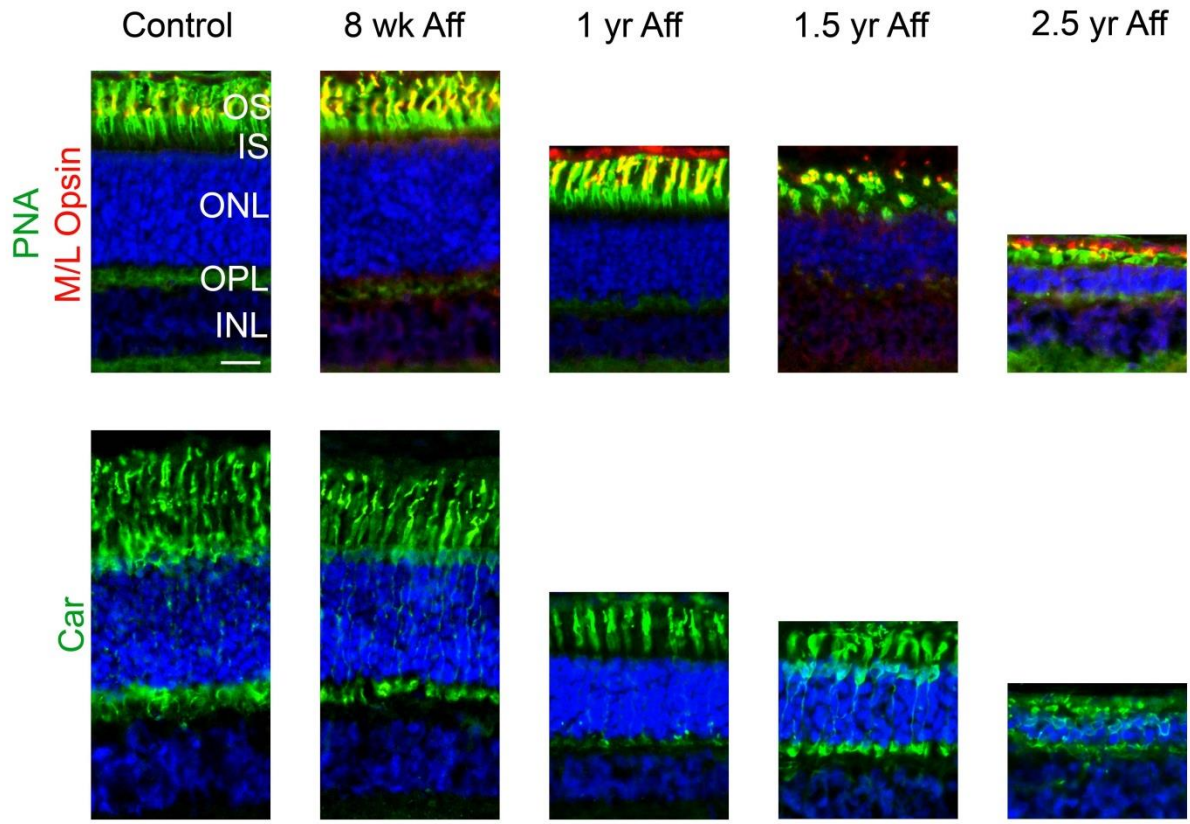

Figure 3.9. Cones show near normal morphology until 1 year of age and are still present at 2.5 years of age. Normal morphology of cones is shown until 1 year of age in the *CNGB1* affected dogs. (Top) PNA and M/L opsin shows correct localization throughout the time span shown but the outer segments degenerate and are shortened by 2.5 years. (Bottom) Human cone arrestin (Car) labels the cone sheath and shows the shortening of the cone outer segments. In the older *CNGB1* affected dogs (1.5 and 2.5 years) the cones are still visible, albeit shortened. Size bar 20 µm. OS – outer segments, IS – inner segments, ONL – outer nuclear layer, OPL – outer plexiform layer, INL – inner nuclear layer.

3.3.5 Preservation of cone function

Histological sections revealed that the cones have well preserved morphology until 1 year of age in the *CNGB1* affected dogs. ERG analysis of photopic ERGs showed decreased but measurable function until at least 5.5 years of age. A-wave amplitudes of the *CNGB1* affected dogs were significantly lower than controls at 3.5 and 5.5 years of age (p=0.02 and 0.018, respectively).

The *CNGB1* affected b- wave amplitudes were significantly lower than controls at 5.5 years of age (p=0.003) but there was not a significant difference at the other ages (Figure 3.10, 3.11). These data support the observation that there was near normal levels of cone function until between 3.5 and 5.5 years of age when the ERG cone b-wave decreased from a~30 µV (b-wave mean at 4 years of age) to ~6 µV (b-wave mean at 5.5 years of age) (Figure 3.11).

Vision testing using a four-choice device was conducted on *CNGB1* affected dogs (4 months to 6 years of age) to assess visual function. There was no significant difference of correct exit choice and time to exit between young *CNGB1* affected dogs (4 months - 1.5 years) and old *CNGB1* affected dogs (2 - 5.5 years) (data not shown). The young and old *CNGB1* affected dog results were combined and compared to controls dogs resulting in a significant difference at the dimmer light intensities (Figure 3.12). The time to exit increases as the *CNGB1* affected dogs become unsure of which exit to choose. The *CNGB1* affected dogs have no significant differences in the time it takes them to choose an exit compared to control dogs except at the dimmer light intensities (Figure 3.12). Supplemental Table 3.S1 shows the data, p-values and statistical test used that correspond with Figure 3.10 through 3.12.

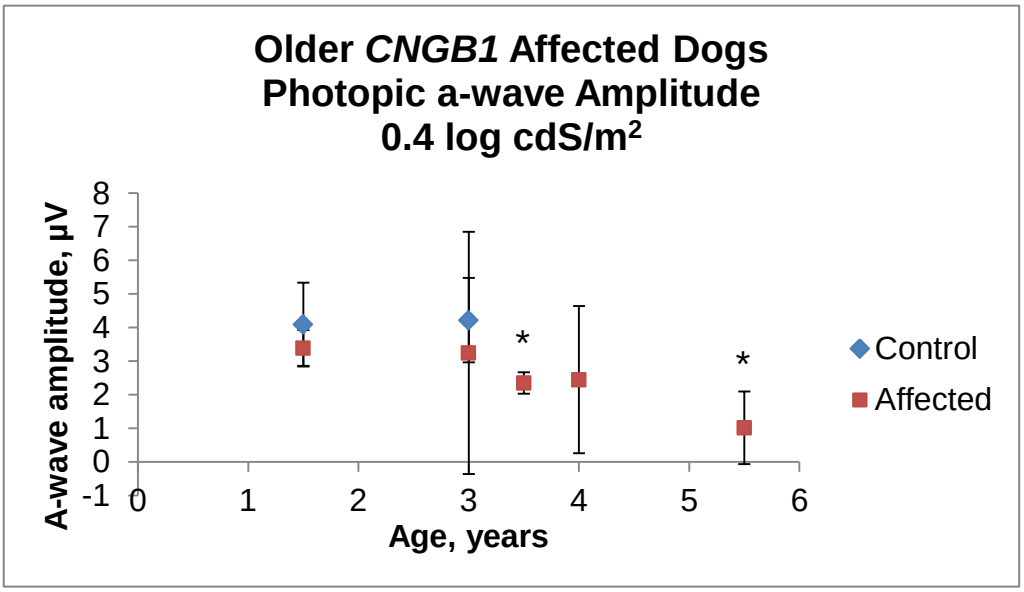

Figure 3.10. A-wave amplitudes in *CNGB1* affected dogs are maintained until 5.5 years of age. Photopic a-wave amplitude difference between *CNGB1* affected and control dogs is significantly lower at 3.5 and 5.5 years at a flash intensity of 0.4 log cdS/m^2. * - $p \leq 0.05$

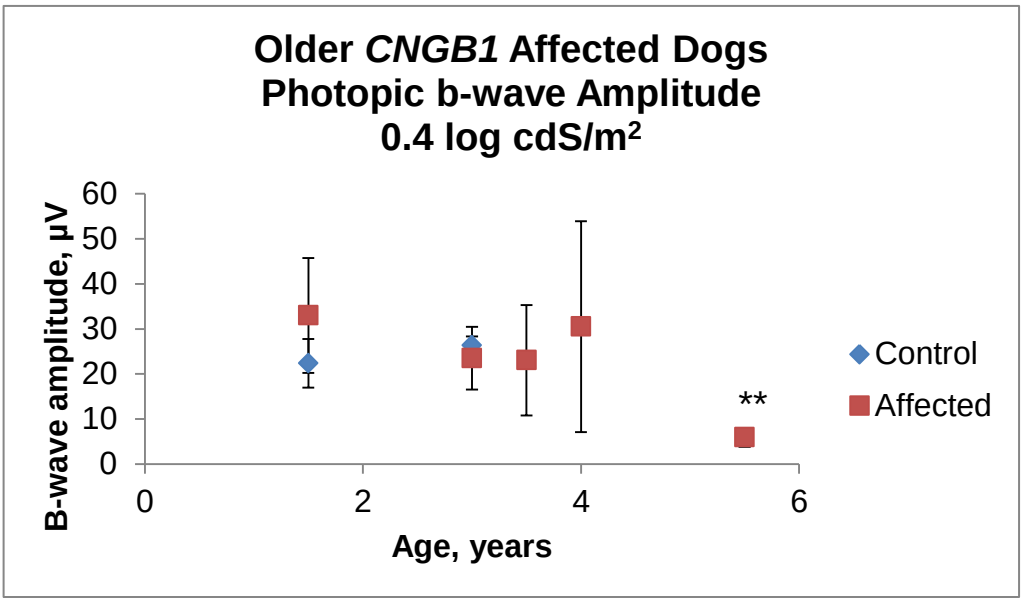

Figure 3.11. B-wave amplitudes in *CNGB1* affected dogs are maintained until 5.5 years of age. There is no significant difference in b-wave amplitudes at photopic flash intensity 0.4 log cdS/m^2 between *CNGB1* affected dogs and control dogs until 5.5 years of age by which time the b-wave amplitude was significantly decreased. This suggests that *CNGB1* affected dogs have near normal cone function until 5.5 years of age. * - $p \leq 0.05$, ** - $p \leq 0.01$

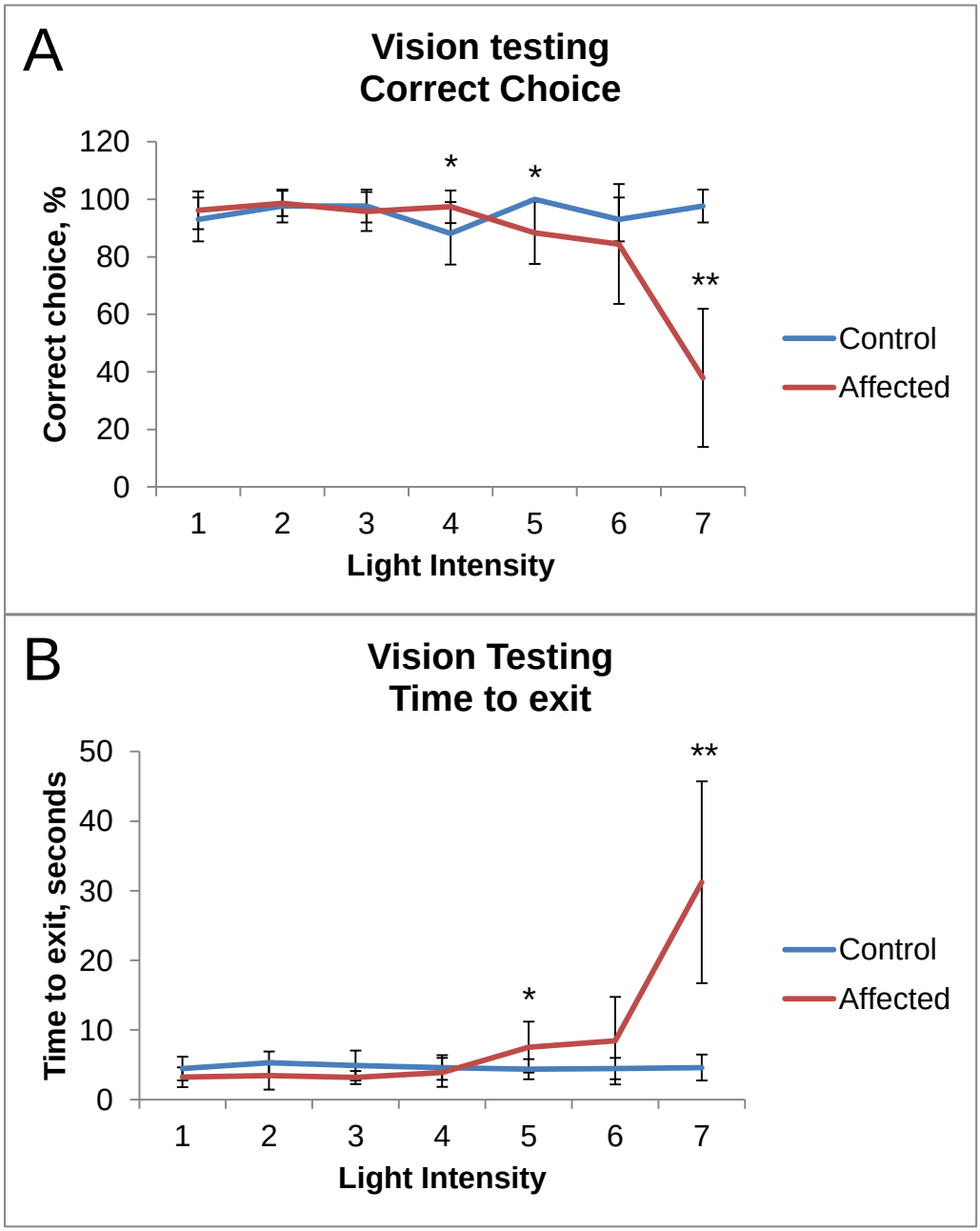

Figure 3.12. Vision testing *CNGB1* affected dogs shows functional cone vision despite retinal degeneration. Light intensity: 1 – Full light (i.e. 35-45 cd/m^2), 2 – 15.0 cd/m^2, 3 – 8.0 cd/m^2, 4 – 1.0 cd/m^2, 5 – 0.4 cd/m^2, 6 – 0.2 cd/m^2, 7 – 0.02 cd/m^2 (very dim light). (A) *CNGB1* affected dogs (4 months to 6 years of age, N=7) show significant signs of inability to choose the correct exit at the lower light intensities. (B) The time it takes for a dog to exit the device is significantly increased at the lower light intensities. These graphs show that affected dogs up to 5.5 years of age have enough cone function despite advance retinal degeneration and very low a- and b-wave amplitudes (at 5.5 years of age) to navigate the vision testing device at all intensities except at dim light levels below cone threshold. * - $p \leq 0.05$, ** - $p \leq 0.01$.

3.4 Discussion

In this study, we provide a description of the retinal phenotype of the *CNGB1* affected dog. The *CNGB1* affected dogs have a slow retinal degeneration in which rods initially have abnormal function and then slowly generate. The cone photoreceptors retain their structure until about 2 years of age after which they develop morphological changes. However, the *CNGB1* affected dogs retain measurable photopic (cone-mediated) ERGs and functional vision until at least 6 years of age.

An interesting finding of this study was the level of *CNGB1* transcript expression observed in the *CNGB1* affected retinal tissue. Nonsense-mediated mRNA decay (NMD) typically reduces transcript levels that contain a premature stop codon to 5-25% of normal wild-type levels although it has been shown that there can be tissue variability of transcript expression in knockout animals that varies from the mean values of 16-36% [18,19]. Premature stop codons typically initiate NMD when they are located more than ~55 nucleotides before the last exon-exon junction of the transcript. The *CNGB1* mutation occurs in exon 26 which is well before the last exon-exon junction of the gene (33 exons in canine *CNGB1*). The *CNGB1* transcript levels observed in the *CNGB1* affected dogs (42%) are at the higher end of the reported NMD values but the reduced levels may still be due to NMD related processes.

There are cellular mRNA quality control mechanisms that recognize premature stop codons and degrade the transcript so that aberrant proteins are not produced [18,20]. In translation, the ribosomes move along the transcript elongating the polypeptide. In the first round or translation, the ribosome displaces exon-junction complexes. If the ribosome successful reaches the end of the transcript, additional

ribosomes can bind and begin translation and are not hindered by any remaining exon-junction complexes. However, if the first ribosome encounters a premature stop codon it will stop translation and any remaining exon-junction complexes will remain on the transcript and interfere with the elongation of future ribosomes [21,22]. As a result the mRNA will then be destabilized and degraded. Another mechanism that triggers NMD is known as nonsense-associated alternative splicing (NAS). This mechanism is poorly understood and there are many hypotheses of the function of NAS [22]. In this process an exon containing a premature stop codon is skipped. The exon skipping could be due to the mutation disrupting exon-splicing enhancing sites, a process to ensure that mutant proteins are not produced or alternatively it can act as a mechanism to restore the reading frame by skipping the exon with the premature stop codon (and allow the production of a protein which may be semi-functional) [22]. Future studies will be needed to elucidate the mechanism behind the alternative splicing but this is beyond the scope of this chapter. The skipping of exon 26 in the CNGB1 affected dog results in essentially the same mutation that was engineered in the *CNGB1-X26* mouse model.

The presence of truncated CNGB1 protein observed in the inner segments of rods shows that, no matter the mechanism responsible for the lower levels of *CNGB1* transcript in affected dogs, some *CNGB1* transcript escapes NMD and an aberrant truncated protein is produced. Based on the predicted protein sequence of the *CNGB1* affected dog this protein would be missing the pore region and so would not be functional as a channel. Immunolabeling of the *CNGB1* affected retina with an antibody that would label the truncated protein (and not the shorter alternatively spliced GARP protein) revealed that the truncated protein remains localized to the inner segments and

is not trafficked to the rod outer segment. Further work will be needed to investigate if the truncated protein is produced at near normal levels or if it produced at lower levels. In 1 year old *CNGB1* affected dogs, the truncated protein is not detected by immunolabeling (data not shown). This suggests that an abnormal accumulation of the truncated CNGB1 protein in the inner segments is not the cause of retinal degeneration.

We did not directly investigated the association of CNGA1 and truncated CNGB1 in the inner segments of *CNGB1* affected dogs but a comparison of the inner segments from the retinal sections of the young *CNGB1* affected dog in Figure 3.2 (anti-CNGA1) to the sections in 3.8 (anti-rhodopsin), shows that the anti-rhodopsin antibody only labels the outer segments and there is no rhodopsin labeling in the inner segments. The anti-CNGA1 antibody does have some labeling in the inner segments when viewed with increased exposure. If heteromeric CNG channels are formed in the inner segment in the *CNGB1* affected dogs they would be at very low levels based on the low levels of CNGA1 observed. Additional support of the evidence of the truncated protein can be observed in the N-terminal CNGB1 (GARP) IHC conducted in Chapter 2 (Figure 2.5). There is no clear delineation of inner and outer segments (based on N-terminal CNGB1 antibody localization). This was originally attributed to disorganization of the inner and outer segments of rod photoreceptors due to the disease but further investigation (Figure 3.8; anti-rhodopin only labeling rod outer segments and having clear inner segment - outer segment morphology) would suggest that in fact the inner segment immunolabeling with the N-terminal CNGB1 antibody was due to the labeling of the truncated CNGB1 protein retained in the inner segment.

The significantly greater dark-adapted ERG a-wave amplitude in the pre-degenerate retinas of *CNGB1* affected dogs compared to the *PDE6A* affected dogs suggests that there is greater photoreceptor function in the *CNGB1* affected dogs, perhaps due to residual rod function. However, the very small amplitudes of the dark-adapted a-waves in both of these models are difficult to measure and just above the signal to noise ratio. The b-wave of the ERG is driven by the secondary neurons of the retina. There is no significant difference in the b-waves of *CNGB1* affected and *PDE6A* dogs at the dim light intensities. The b-wave in the *PDE6A* dog is led by cone bipolar cells because the *PDE6A* dogs do not have functional rods. We interpret this to mean that the first positive peak seen in the *CNGB1* affected dog is the cone bipolar cell b-wave. The second positive peak in the young *CNGB1* affected dog ERG could be driven by abnormal rod kinetics due to homomeric CNGA1 channels in the rod outer segments. Homomeric CNGA1 channels have decreased Ca^{2+} permeability and cellular current and abnormal single channel flickering behavior (specifically, the channels remain open for longer when exposed to low levels of cGMP compared to native single channel flickers which open and close transiently) [2,23]. Additional studies will be needed to understand this peak and how, or if, CNGA1 homomeric channels are involved. Specifically, tracking the implicit time and amplitude of the second positive peak at increasing scotopic light flashes will help determine the origin of the wave. Alternatively, rods are 1000 times more sensitive to blue light than cones so the use of blue colored light flashes can help elicit rod-only responses [24]. This ERG study is ongoing in young *CNGB1* affected and *PDE6A* affected dogs.

The slow retinal degeneration, as made evident by OCT measurements and the semi-thin retinal sections (Figures 3.5 and 3.6), is comparable to that described in the *CNGB1-X26* mouse [4]. Transmission electron microscopy showed that at young ages (in both the *CNGB1* affected dog [8 weeks, Figure 3.7] and mouse [6 weeks, [4]]) there is some degree of degeneration and disorganization (more so in the mouse) but the outer segment disks were still normally stacked in many of the rods. This indicates that the rods likely develop essentially normally and then degenerate over the course of the disease. Semi-thin sections show that the rate of decline of the ONL is similar between the dog and mouse model (at relative disease stages). At 4 months of age the *CNGB1* mouse model has about 8 layers of nuclei in the outer segments (control mice have 10-12 nuclei) with a decrease to 5-6 by 6 months of age. Between 6 months and 1 year of age, the nuclear layer thickness decreases to only 1 nucleus thick. We see similar slow progression in the *CNGB1* affected dog and decrease of Rec+ thickness between 1 and 1.5 years of age. We do not have any histological samples from time points after 2.5 years of age so we do not have a clear indication of when the retina degenerates to the equivalent of the 11 month old *CNGB1-X26* mouse [4]. In the *CNGB1-X26* mouse model there was occasional rod function (3/35 rod photoreceptors responded to light in single-cell recording studies) [4]. The investigators did not use the CNGB1mid antibody to detect truncated protein and it is unclear from their N-terminal CNGB1 antibody sections if there is inner segment labeling [4]. It is possible that this is a species difference and the presence of CNGA1 in the outer segments and the truncated CNGB1 protein is unique to the *CNGB1* dog phenotype. Alternatively, the CNGA1 and

CNGB1mid proteins might only be expressed in the rod outer segments for a short period of time and were not observed in the mouse.

The *CNGB1-X26* mouse model has normal cone function (as determined by ERG) until 6 months of age; ERGs after this time point were not displayed [4]. The *CNGB1* dog model has near normal cone function until at least 4 years of age. There is a significant drop in photopic b-wave amplitudes between 4 and 5.5 years of age. However, the *CNGB1* affected dogs still have normal functional vision at the brighter light intensities when tested with the vision testing device. In fact, anecdotal observations indicate that a 9 year old *CNGB1* affected dog (the female that founded the MSU research colony from Chapter 2) still has enough functional day light vision to maneuver around furniture and locate toys. Future work will use OCT to focus on the *area centralis* to assess the preservation of this photoreceptor dense region.

Descriptions of human RP45 patients have indicated an initial loss or lack of rod vision and a slow disease progression leading to progressive constriction of visual fields. The slow progression of the disease provides a window of opportunity for gene supplementation therapy. This is important as often the patients are not diagnosed until they already have a degree of retinal degeneration. Recently, the *CNGB1-X26* mouse phenotype was rescued in a gene supplementation therapy trial [25]. The similarities between the RP45 patients, *CNGB1-X26* mouse and the *CNGB1* affected dog model indicate that the dog will be an ideal model for pre-clinical large animal trials.

3.5 Supplemental information

Table 3.S1. Comprehensive table of data, statistical analyses and *p*-values corresponding to Figures 3.5, 3.10, 3.11 and 3.12

Figure 3.5 Photoreceptor thickness (Rec+) *CNGB1* affected age means compared to all control mean				
Age, months	Controls[1]	*CNGB1* Affected[1]	Statistical Analysis[2]	Pval
3		108.5	ST	0.088
5		101.7	ST	0.946
6 to 7	100.2	98.0	ST	0.662
11.00		87[$]		
18 to 19	110[$]	64.1	ST	<0.001
39	99.3[$]		-	
48		46[$]	-	
56			-	
64	92.3[$]		-	
66		28.5	ST	<0.001
96	97.5		-	
Figure 3.10 Photopic a-wave amplitudes *CNGB1* affected age means compared to all control mean				
Age, years	Controls[1]	*CNGB1* Affected[1]	Statistical Analysis[2]	Pval
1.5	4.1	3.4	NT	0.284
3.0	4.2	3.3	NT	0.785
3.5		2.4	NT	0.020
4.0		2.5	ST	0.201
5.5		1.0	ST	0.018
Figure 3.11 Photopic b-wave amplitudes *CNGB1* affected age means compared to all control mean				
Age, years	Controls[1]	*CNGB1* Affected[1]	Statistical Analysis[2]	Pval
1.5	26.3	33.0	NT	0.494
3.0	22.4	23.5	NT	0.978
3.5		23.1	ST	0.882
4.0		30.5	NT	0.759
5.5		5.9	ST	0.003

Table 3.S1 cont'd

Figure 3.12A Vision testing correct choice
Wild-type control mean compared to all affected mean

Light Intensity (cd/m^2)	Controls[1]	*CNGB1* Affected[1]	Statistical Analysis[2]	Pval
35-45	93.0	95.8	M-W	0.478
15.0	97.7	98.4	M-W	0.842
8.0	97.7	95.3	M-W	0.539
1.0	88.2	98.6	M-W	0.023
0.4	100.0	88.6	M-W	0.027
0.2	93.0	84.3	M-W	0.514
0.02	97.7	41.7	M-W	0.002

Figure 3.12B Vision testing, time to exit
Wild-type control mean compared to all affected mean

Light Intensity (cd/m^2)	Controls[1]	*CNGB1* Affected[1]	Statistical Analysis[2]	Pval
35-45	4.5	3.3	ST	0.168
15.0	5.3	3.7	ST	0.135
8.0	4.9	3.2	ST	0.060
1.0	4.6	4.1	ST	0.618
0.4	4.4	7.7	M-W	0.030
0.2	4.5	7.1	ST	0.194
0.02	4.6	28.3	M-W	0.001

1. Mean values unless otherwise noted. $ - N=1 values
2. Statistical analysis: ST – Student t-test; NT – nonparametric t-test; M-W – Mann-Whitney Rank Sum Test

REFERENCES

REFERENCES

1. Hartong DT, Berson EL, Dryja TP (2006) Retinitis pigmentosa. Lancet 368: 1795-1809.

2. Kaupp UB, Seifert R (2002) Cyclic nucleotide-gated ion channels. Physiological Reviews 82: 769-824.

3. Biel M, Michalakis S (2009) Cyclic nucleotide-gated channels. Handbook of experimental pharmacology 191:111-36.

4. Huttl S, Michalakis S, Seeliger M, Luo DG, Acar N, et al. (2005) Impaired channel targeting and retinal degeneration in mice lacking the cyclic nucleotide-gated channel subunit CNGB1. Journal of Neuroscience 25: 130-138.

5. Zhang Y, Molday LL, Molday RS, Sarfare SS, Woodruff ML, et al. (2009) Knockout of GARPs and the beta-subunit of the rod cGMP-gated channel disrupts disk morphogenesis and rod outer segment structural integrity. Journal of Cell Science 122: 1192-1200.

6. Winkler PA, Ekenstedt KJ, Occelli LM, Frattaroli AV, Bartoe JT, et al. (2013) A Large Animal Model for CNGB1 Autosomal Recessive Retinitis Pigmentosa. PLoS One 8: e72229.

7. Petersen-Jones SM, Komaromy AM (2015) Dog models for blinding inherited retinal dystrophies. Human Gene Therapy Clinical Development 26: 15-26.

8. Annear MJ, Bartoe JT, Barker SE, Smith AJ, Curran PG, et al. (2011) Gene therapy in the second eye of RPE65-deficient dogs improves retinal function. Gene Therapy 18: 53-61.

9. Tuntivanich N, Pittler SJ, Fischer AJ, Omar G, Kiupel M, et al. (2009) Characterization of a canine model of autosomal recessive retinitis pigmentosa due to a PDE6A mutation. Investigative Ophthalmology & Visual Science 50: 801-813.

10. Gearhart PM, Gearhart CC, Petersen-Jones SM (2008) A novel method for objective vision testing in canine models of inherited retinal disease. Investigative Ophthalmology & Visual Science 49: 3568-3576.

11. Annear MJ, Gornik KR, Venturi FL, Hauptman JG, Bartoe JT, et al. (2013) Reproducibility of an objective four-choice canine vision testing technique that assesses vision at differing light intensities. Veterinary Ophthalmology 16: 324-328.

12. Spurr AR (1969) A low-viscosity epoxy resin embedding medium for electron microscopy. Journal of Ultrastructure Research 26: 31-43.

13. Reynolds ES (1963) The use of lead citrate at high pH as an electron-opaque stain in electron microscopy. Journal of Cell Biology 17: 208-212.

14. Bonigk W, Bradley J, Muller F, Sesti F, Boekhoff I, et al. (1999) The native rat olfactory cyclic nucleotide-gated channel is composed of three distinct subunits. Journal of Neuroscience 19: 5332-5347.

15. Shuart NG, Haitin Y, Camp SS, Black KD, Zagotta WN (2011) Molecular mechanism for 3:1 subunit stoichiometry of rod cyclic nucleotide-gated ion channels. Nature Communications 2:457

16. Chen TY, Illing M, Molday LL, Hsu YT, Yau KW, et al. (1994) Subunit 2 (or beta) of retinal rod cGMP-gated cation channel is a component of the 240-kDa channel-associated protein and mediates Ca(2+)-calmodulin modulation. Proceedings of the National Academy of Sciences of the United States of America 91: 11757-11761.

17. Kaupp UB, Niidome T, Tanabe T, Terada S, Bönigk W, et al. (1989) Primary structure and functional expression from complementary DNA of the rod photoreceptor cyclic GMP-gated channel. Nature (London) 342: 762-766.

18. Isken O, Maquat LE (2007) Quality control of eukaryotic mRNA: safeguarding cells from abnormal mRNA function. Genes & Development 21: 1833-1856.

19. Zetoune AB, Fontaniere S, Magnin D, Anczukow O, Buisson M, et al. (2008) Comparison of nonsense-mediated mRNA decay efficiency in various murine tissues. BMC Genetics 9: 83.

20. Maquat LE (1995) When cells stop making sense: effects of nonsense codons on RNA metabolism in vertebrate cells. RNA 1: 453-465.

21. Ishigaki Y, Li X, Serin G, Maquat LE (2001) Evidence for a pioneer round of mRNA translation: mRNAs subject to nonsense-mediated decay in mammalian cells are bound by CBP80 and CBP20. Cell 106: 607-617.

22. Cartegni L, Chew SL, Krainer AR (2002) Listening to silence and understanding nonsense: Exonic mutations that affect splicing. Nature Reviews Genetics 3: 285-298.

23. Korschen HG, Illing M, Seifert R, Sesti F, Williams A, et al. (1995) A 240 kDa protein represents the complete beta subunit of the cyclic nucleotide-gated channel from rod photoreceptor. Neuron 15: 627-636.

24. Perlman I (1995) The Electroretinogram: ERG. In: Kolb H, Fernandez E, Nelson R, editors. Webvision: The Organization of the Retina and Visual System. Salt Lake City UT.

25. Koch S, Sothilingam V, Garrido MG, Tanimoto N, Becirovic E, et al. (2012) Gene therapy restores vision and delays degeneration in the CNGB1-/- mouse model of retinitis pigmentosa. Human Molecular Genetics 21: 4486-4496.

CHAPTER 4

AAV5 GENE THERAPY RESCUE OF VISION IN A LARGE ANIMAL MODEL OF AUTOSOMAL RECESSIVE RETINITIS PIGMENTOSA

4.1 Introduction

Retinitis pigmentosa (RP) is the leading cause of inherited blindness, affecting ~1 in 4000 people [1]. It is a genetically heterogeneous disease with mutations described in over 60 genes [1]. Retinitis pigmentosa 45 (RP45) patients present with typical RP symptoms; night blindness at school-age and loss of peripheral vision, RP diagnosis around the age of 30 and blindness by the age of 60 [2,3]. RP45 is caused by mutations in the *CNGB1* gene. Currently, there is no cure for RP although gene therapy treating similar retinal degenerations is showing promising results [4-7].

The *CNGB1* gene codes for the B subunit (CNGB1a) of the rod photoreceptor cyclic nucleotide-gated (CNG) ion channel and additional splice variants that are expressed in the retina (GARP1 and GARP2), olfactory sensory neurons (CNGB1b) and other tissues. CNG channels in the photoreceptors are nonspecific cation channels the closure of which are responsible for the hyperpolarization of the photoreceptor due to exposure to light. Rod photoreceptor CNG channels consist of three CNGA1 subunits and one CNGB1a subunit (encoded by *CNGA1* and *CNGB1*, respectively) [8,9].

Two mouse models of RP45 have been generated for research. The *CNGB1X-1* mouse model was engineered to remove the upstream promoter region and exon 1 and 2 from the *CNGB1* gene, effectively knocking out all *CNGB1* products in the retina. The *CNGB1X-1* mouse has a severe retinal degeneration that is primarily the result of structural deficits due to the lack of *CNGB1* products [10]. The second mouse model, *CNGB1X-26*, excised exon 26 from the *CNGB1* gene resulting in loss of only the full length CNGB1b protein. The *CNGB1X-26* mouse shows a significant decrease of rod function and a slow retinal degeneration, similar to RP45 human patients [11].

CNGB1X-26 mice were used in a successful gene therapy study that not only restored vision but also delayed the progression of the retinal degeneration [12].

Recently, a spontaneous canine model has been described [13]. The *CNGB1* affected dogs show abnormal rod function and a slow retinal degeneration making them ideal candidates for a gene therapy trial. Here we report the first results of a successful gene therapy trial in 4 *CNGB1* affected dogs.

4.2 Materials and methods

4.2.1 Animal use

The dogs used in this study were maintained in a colony at the Michigan State University Comparative Ophthalmology Laboratory as described in Chapter 3.

4.2.2 Gene therapy

Recombinant AAV5 vectors (modified AAV2 genomes pseudotyped with an AAV5 capsid) were manufactured using previously published methods [14-16]. The AAV5 vectors were packaged with a construct containing the canine *CNGB1* cDNA with a G protein-coupled receptor kinase 1 (*GRK1*)-promoter (AAV5-cCNGB1) (Supplemental Figure 4.S1). Eight eyes in 4 dogs were subretinally injected with the construct as described in Petersen-Jones et al. [17]. Initially, one eye was injected with AAV5-cCNGB1 at a titer of $1x10^{12}$ ("low titer") in a pilot study. Subsequently a further 6 eyes were injected with a titer of $5x10^{12}$ ("high titer). As an injection control one eye was injected with an AAV5-GFP construct at a titer of $1.5x10^{11}$. The injection blebs were targeted to dorsal regions of the retina. Ages of the dogs at the time of injection ranged from 3 months to 6 months of age (Table 4.1).

Table 4.1. Treated dogs and injection details

Dog	Sex	Age (months)	OD[1] - titer	Volume (µl)	OS[1] - titer	Volume (µl)
1	M	3	cCNGB1 - $5x10^{12}$	300	GFP - $1.5x10^{11}$	250
2	F	5	cCNGB1 - $5x10^{12}$	300	cCNGB1 - $5x10^{12}$	250
3	F	5	cCNGB1 - $5x10^{12}$	300	cCNGB1 - $5x10^{12}$	300
4	M	4	cCNGB1 - $1x10^{12}$	175	NA	
4	M	6.5	NA		cCNGB1 - $5x10^{12}$	200

1. OD – right eye, OS – left eye, NA – not injected at that time

4.2.3 Electroretinography

Electroretinograms (ERGs) were recorded as described in Chapter 3 of this dissertation.

ERGs from *CNGB1* affected AAV5-cCNGB1 injected (low and high titer) treated dogs were recorded 1, 2, 3, 4, 5, 6, 7 and 9 months post-injection (7 eyes) and compared to AAV5-GFP injected (1 eye), age matched untreated *CNGB1* affected dogs (N=2 for each age) and phenotypically normal 14 month old dogs (N=3).

4.2.4 Vision testing

Vision testing was performed using the four-choice vision testing device described previously in Chapter 3.

CNGB1 affected dogs treated with AAV5-cCNGB1 (low and high titer) were tested with the device. Each eye was tested individually by placing an opaque contact lens on one eye, allowing only one eye to be used during each run. Vision testing was performed 1, 2, 3, 4 ,5, 7 and 9 months post-treatment.

4.2.5 Sample collection and processing

Dogs were humanely euthanized at 3 months (Dog 3), 6 months (Dog 1) and 9 months (Dog 4) post-injection and the eyes were enucleated and processed following the procedure described in Chapter 3. Dog 2 is being maintained for long term assessment of therapeutic outcomes.

4.2.6 Immunohistochemistry

Frozen tissue sections were labeled with C-terminal CNGB1, CNGA1 and peanut agglutinin lectin (PNA). Protocol 2 or Protocol 3 (described in Chapter 3) was used to label the sections (see Table 4.2 for the antibody information and protocol used). Immunolabeling protocols and imaging of sections were as described in Chapter 3.

Table 4.2. Antibody details and concentrations

Antigen Target	Antibody Details	Source	Secondary Antibody	Protocol
CNGB1 C-terminal 1144-1238	1:500 rabbit polyclonal	Sigma-Aldrich HPA039159	1:500 AlexaFluor anti-rabbit 488 or 596	3
CNGA1	1:10 mouse monoclonal	Dr. Bob Molday	1:500 AlexaFluor anti-rabbit 488	2
Cone matrix	Peanut agglutin lectin (PNA) biotinylated 1:500	Vector Laboratories B-1075	1:500 AlexaFluor streptavadin 405	3

4.2.7 Statistical analysis

Statistical analysis was performed as described in Chapter 3. Paired t-tests and paired nonparametric tests (Wilcoxon Signed Rank Test) were used when comparing pre- to post-treatment values.

4.3 Results

4.3.1 Gene therapy injections

Eight eyes from 4 *CNGB1* affected dogs were injected with an AAV5 vector with a *GRK1* promoter (Table 4.1). One eye was injected with AAV5-GFP to serve as a vehicle control. Subretinal injection blebs of the vector were targeted to the dorsal regions of the eyes. Functional rescue was analyzed via ERGs and vision testing collected 1, 2, 3, 4, 5, 6, 7 and 9 months post injection.

4.3.2 Full length CNGB1 protein is expressed in photoreceptors in treated regions

Frozen retinal sections from Dog 3 and 4 (3 and 9 months post-injection, respectively) were labeled with a C-terminal CNGB1 antibody, which labels full length CNGB1 protein but not the alternatively spliced retinal variants, nor the truncated CNGB1 protein produced in *CNGB1* affected dogs. Full length CNGB1 protein was detected in the outer segments of the rod photoreceptors in the injected region. Figure 4.1A shows an injected region of the eye highlighting the presence of full length CNGB1 which was correctly targeted to the photoreceptor outer segments. The untreated regions of the 3 month post-injected dog (as well as previous IHC study of untreated CNGB1 affected dogs, Figure 2.5) showed that full length CNGB1 was not present in the absence of treatment.

In the treated regions, there was detectable levels of CNGA1 expression in the rod outer segments in both the 3 month and 9 month post-injected eyes while there was

no detectable CNGA1 in the untreated region of the *CNGB1* affected retina when the sections were imaged using the same exposure as the control retina (Figure 4.1B).

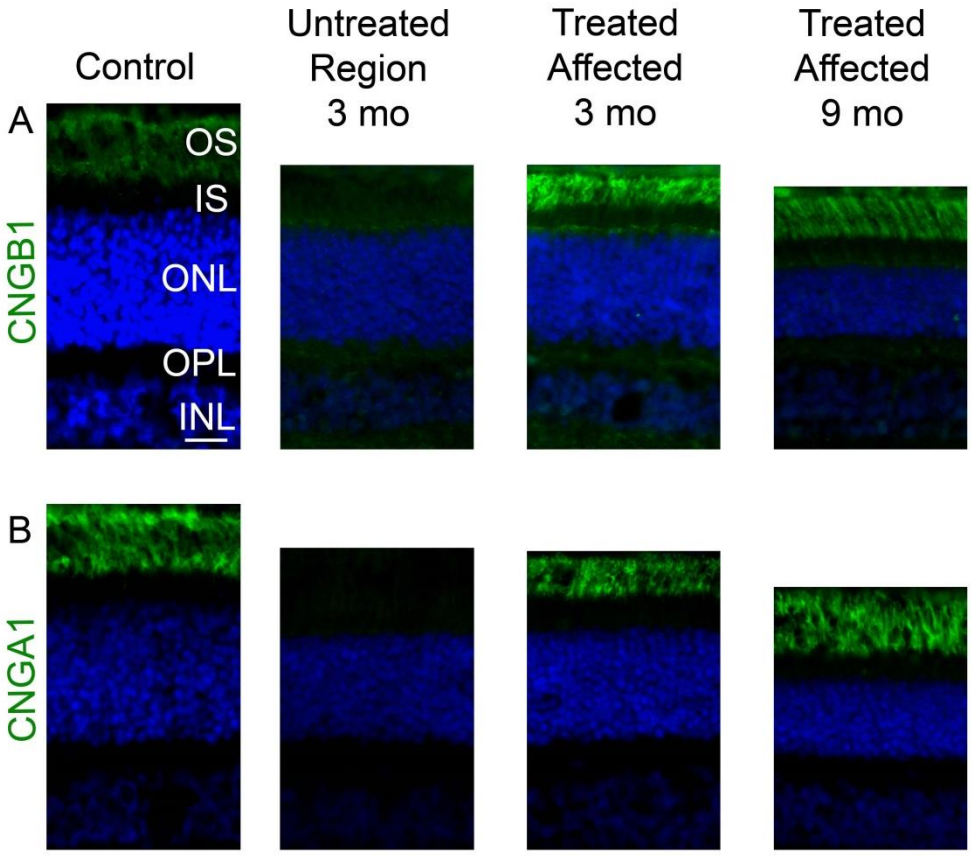

Figure 4.1. CNGB1 and CNGA1 are expressed in the AAV5-cCNGB1 high titer treated regions of *CNGB1* affected retinas. (A) CNGB1 (green) is expressed in the outer segments of the treated regions of the 3 and 9 month post-injected retinas. The untreated region from the 3 month post-injected retina does not express full length CNGB1. (B) CNGA1 (green) is expressed and correctly targeted to the photoreceptor outer segments in the treated regions of the 3 month and 9 month post-treatment retinas but is not detectable in the untreated region. Size bar 20 µm. OS – outer segments, IS – inner segments, ONL – outer nuclear layer, OPL – outer plexiform layer, INL – inner nuclear layer.

The expression of the cCNGB1 cDNA was driven by a *GRK1* promoter which has previously been shown to function in both rod and cone photoreceptors [18]. To investigate whether the vector led to CNGB1 expression in cone photoreceptors, C-terminal CNGB1 and PNA (peanut agglutinin) were co-labeled on high titer AAV5-

cCNGB1 treated sections to check for CNGB1 expression in cones (Figure 4.2). The control dog shows no apparent overlap of the CNGB1 and PNA, as expected. There did not appear to be extensive co-labeling with PNA and CNGB1 in the 3 and 9 month post-treated eyes. However, with the close proximity and the overlapping of rod and cone OS it is difficult to definitively say that CNGB1 is not expressed in cones.

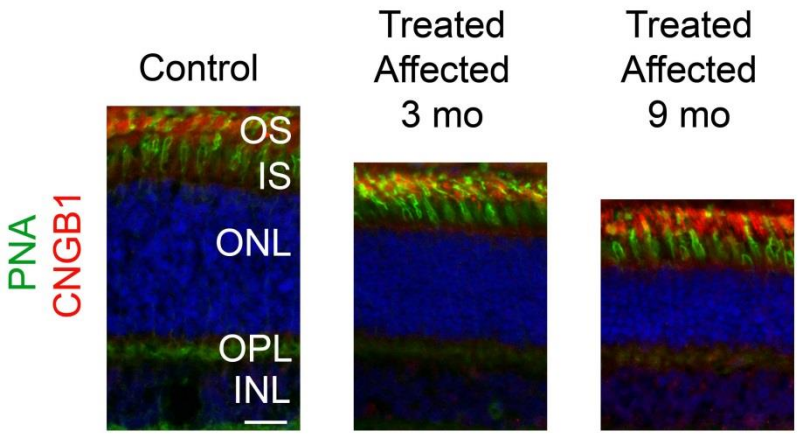

Figure 4.2. CNGB1 is not extensively expressed in cones in AAV5-cCNGB1 high titer treated regions of *CNGB1* affected retinas. CNGB1 (red) and peanut agglutinin (PNA, green) were co-labeled to detect if there was co-expression of CNGB1 and the cone-specific PNA antibody. The majority of cones do not appear to be co-labeled. Size bar 20 µm. OS – outer segments, IS – inner segments, ONL – outer nuclear layer, OPL – outer plexiform layer, INL – inner nuclear layer.

4.3.3 Gene therapy rescues vision in *CNGB1* affected dogs

Subretinal injection of the AAV5-cCNGB1 vector successfully rescued vision in all treated eyes. Phenotype values for all eyes injected with the higher titer of the AAV5-cCNGB1 ($5x10^{12}$) were averaged for analyses. The lower AAV5-cCNGB1 titer ($1x10^{12}$) and the AAV5-GFP vector were analyzed separately.

As a pilot study right and left eyes of CNGB1 affected dog #4 were injected with low titer ($1x10^{12}$) and high titer ($5x10^{12}$) AAV5-cCNGB1 respectively, although at different times. Both eyes showed increased scotopic b-wave amplitudes compared to 6 month old non-treated *CNGB1* affected dogs (Figure 4.3). Scotopic b-wave rescue in the eye injected with the higher titer showed greater rescue than the eye injected with the lower titer. Vision testing showed functional rescue in both high and low titer eyes; the dog chose the correct exit 100% of the time with each eye, at all light intensities (Figure 4.4A). The dog was able to exit the device quickly with using either the high or low titer injected eye (Figure 4.4B). Dogs with normal vision are able to choose the correct exit nearly 100% of the time and leave the vision testing device quickly.

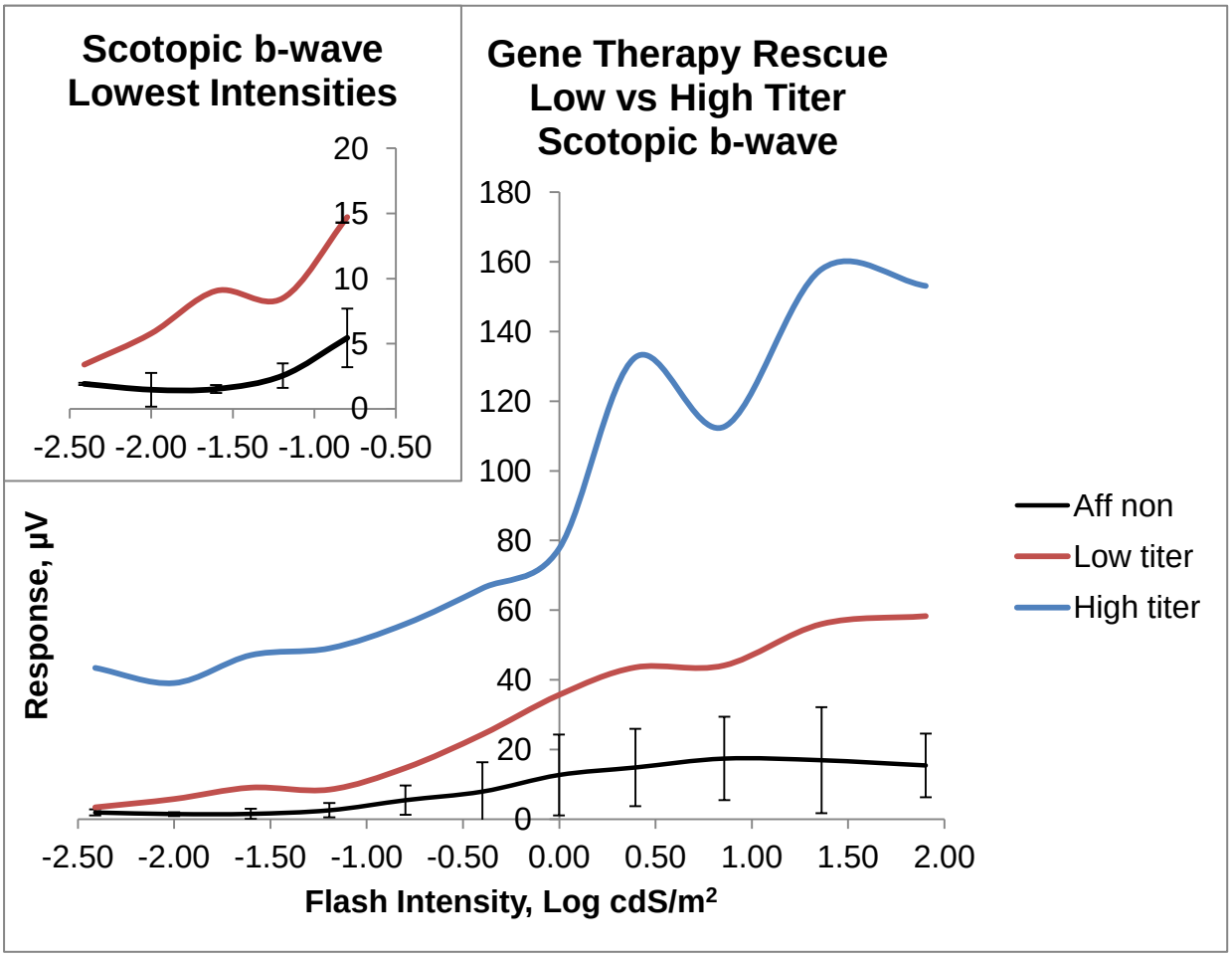

Figure 4.3. Scotopic b-wave amplitudes were increased in the eye injected with a higher titer of AAV5-cCNGB1. Dog 4 had a low titer of AAV5-cCNGB1 injected into one eye ($1x10^{12}$) and a high titer injected into the other eye ($5x10^{12}$). There was an increase in scotopic ERG b-waves for both eyes when compared to untreated *CNGB1* affected dogs (N=4, 6 months old). The high titer eye had a much more dramatic increase in amplitude compared to the low titer eye. The inset graph shows the lowest flash intensities comparing the low titer and untreated *CNGB1* affected scotopic b-waves.

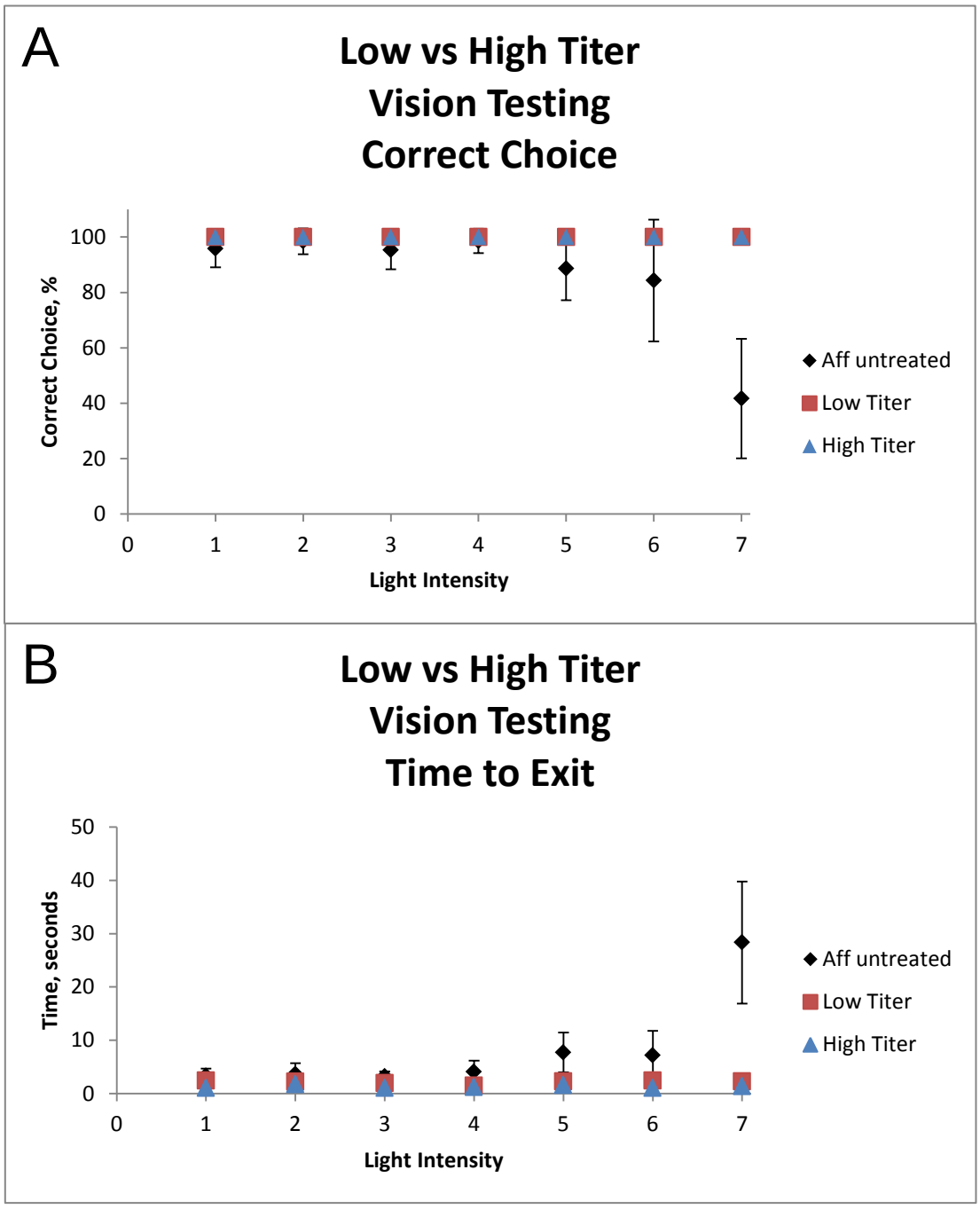

Figure 4.4. Low and high titer injected eyes both showed improved functional vision. (A) Dog 4 chose the correct exit 100% of the time with both eyes (each eye tested separately) at all light intensities with both the AAV5-cCNGB1 low titer ($1x10^{12}$) and high titer ($5x10^{12}$) eyes. (B) The dog was able to exit the vision testing device quickly with both eyes (each tested separately). Untreated *CNGB1* affected dogs were unable to choose the correct exit at dim light intensities and took longer to exit the device. Light intensity: 1 – Full light (i.e. 35-45 cd/m^2), 2 – 15.0 cd/m^2, 3 – 8.0 cd/m^2, 4 – 1.0 cd/m^2, 5 – 0.4 cd/m^2, 6 – 0.2 cd/m^2, 7 – 0.02 cd/m^2 (very dim light).

In one dog (#1), one eye was treated with the high titer AAV5-cCNGB1 while the other was treated with AAV5-GFP. The AAV5-GFP eye was injected as a control to assess the procedural and vector related effects of injection. Scotopic ERG tracings from the AAV5-cCNGB1 treated eye 3 months post-injection showed increased threshold and amplitudes compared to the AAV5-GFP eye (Figure 4.5A). The rod flicker amplitude in the treated eye was ~4.5X larger than the AAV5-GFP treated eye (Figure 4.5B). At the 3 month post-injection time point there was rescue of rod function due to treatment of AAV5-cCNGB1 and there was no apparent effect of the AAV5-GFP treatment on the other eye.

Figure 4.6A shows the mean scotopic b-wave intensity-response (I-R) curves (red line) of the eyes administered the high titer of AAV5-cCNGB1. At 6 months post-injection the b-wave amplitudes were significantly higher than pre-injection (black line). The eye treated with AAV5-GFP had similar b-wave amplitudes at 6 months post-injection to the b-waves prior to treatment (green line). Control dog mean scotopic b-waves (14 months old, N=3) were significantly higher than the *CNGB1* affected dogs treated with the high titer of AAV5-cCNGB1 (blue line). This was anticipated because only a proportion of the retina was treated. The photopic b-wave I-R curve (Figure 4.6B) was not significantly different between the *CNGB1* affected dogs pre-injection ERGs, the 6 month post AAV5-cCNGB1 injection (except at one point: -1.6 Log cdS/m^2, p=0.5) and control dogs. The photopic ERGs are indicative of cone function and as expected that remains normal in the *CNGB1* affected dogs at this age. The fact that the subretinal injections did not reduce the photopic b-wave indicates that there were no detrimental effects of the subretinal injection or viral vector on cone photoreceptor function.

There was a significant increase in the scotopic b-wave amplitude in response to dim flashes (e.g. at -2 log cdS/m^2) which is indicative of restored rod function (Figure 4.7A). At this flash stimulus the b-wave amplitudes were significantly increased compared to pre-injection in the high titer AAV5-cCNGB1 treated eyes at 1 month post-injection. This improvement was maintained to the last time point measured at 9 months post-injection (Figure 4.7A) showing that the rescue was sustained. Note that the 7 and 9 month measurements are not significant due to low number of dogs followed to these time points but the trend of rescue remains evident. The AAV5-GFP injected eye b-wave amplitudes remained comparable to pre-injection amplitudes and age matched untreated *CNGB1* affected dogs. The 5 Hz low intensity flicker (-1.6 log cdS/m^2), which predominantly represents rod responses was significantly increased in amplitude in the high titer AAV5-cCNGB1 treated eyes compared to the pre-injection ERGs and the AAV5-GFP treated eye (Figure 4.5 and 4.7B).

At brighter light flashes in the scotopic ERG, in which the a- and b-waves are driven by mixed rod and cone responses (e.g. 0.4 log cdS/m^2) there were significant increases of the a-wave at 4 and 6 months post injection. The b-wave was significantly increased at 2 months post-injection in the AAV5-cCNGB1 treated dogs compared to their pre-injection amplitudes. These increased amplitudes were maintained until the last time point measured at 9 months (Figure 4.8A,B). Note that the 7 and 9 month measurements are not significant due to the low number of dogs followed to these time points but the trend of rescue remains evident.

Functional vision was also rescued in the high titer AAV5-cCNGB1 treated eyes as determined by the four-choice device (Figure 4.9). Untreated *CNGB1* affected dogs

and dog #1 when the AAV5-GFP injected eye was exposed (and the AAV5-cCNGB1 treated eye covered) had difficulty choosing the correct exit at the dimmest light intensity whilst when using the AAV5-cCNGB1 treated eyes the injected dogs at 6 months post-treatment chose the correct exit nearly 100 percent of the time (Figure 4.9A, p=0.005). The untreated *CNGB1* affected dogs also took longer to exit the device at the lowest light intensity compared to the AAV5-cCNGB1 6 month post-treatment dogs and the AAV5-GFP injected eye (Figure 4.9B, p=0.006). Supplemental Table 4.S1 shows the data, p-values and statistical test used that correspond to Figures 4.6 through 4.9.

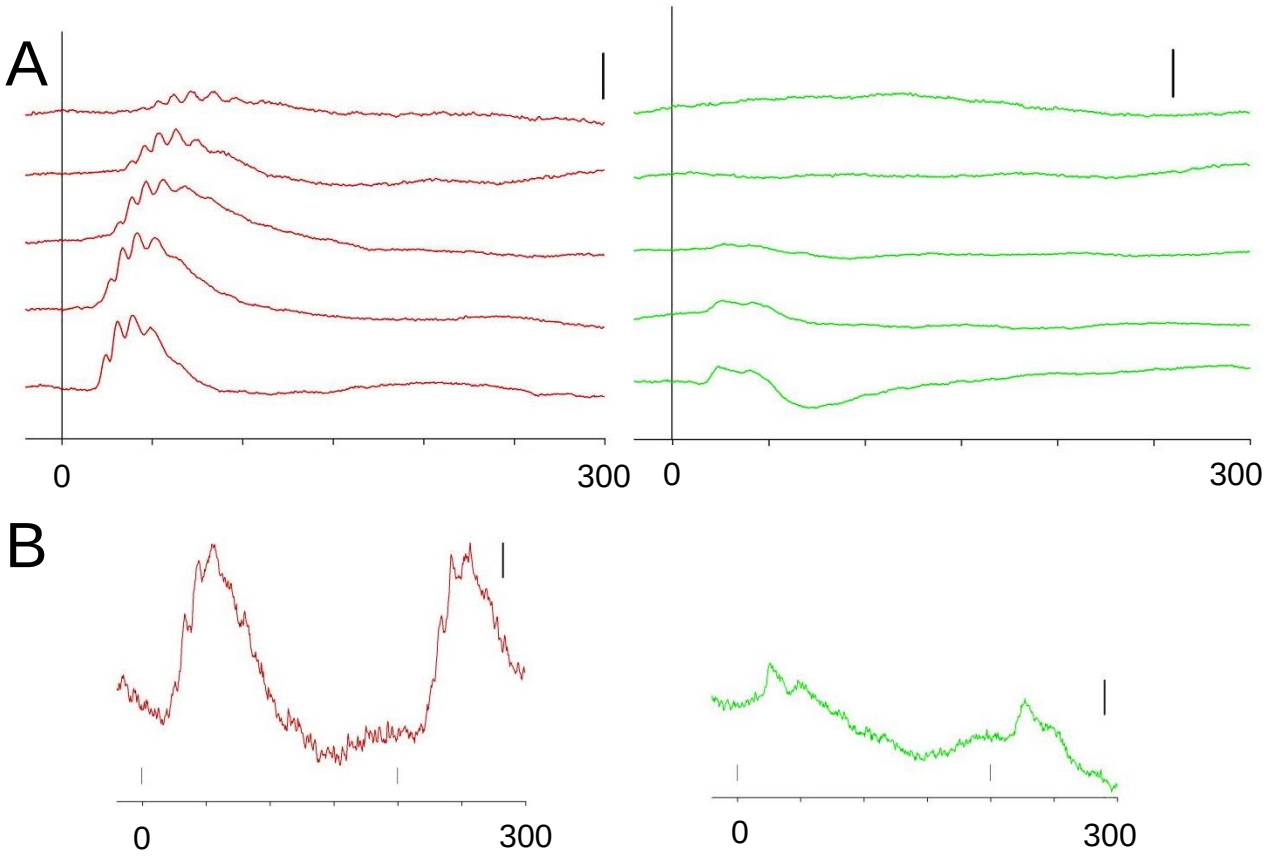

Figure 4.5. Representative scotopic ERG tracings from AAV5-cCNGB1 treated eye and AAV5-GFP treated eye (dog #1). Three month scotopic post-injected ERG tracings from the high titer AAV5-cCNGB1 eye (red tracings) and AAV5-GFP eye (green tracings) shows decreased response threshold and increased amplitudes in the AAV5-cCNGB1 treated eye. (A) Scotopic single flash ERGs from intensity: -2.6, -2.4, -2.0, -1.6, -1.2 log cdS/m^2 (from top to bottom); size bar 20 µV. (B) Scotopic flicker ERG tracing: 5 Hz -1.6 log cdS/m^2; size bar 4 µV, vertical gray bars indicate flash timing.

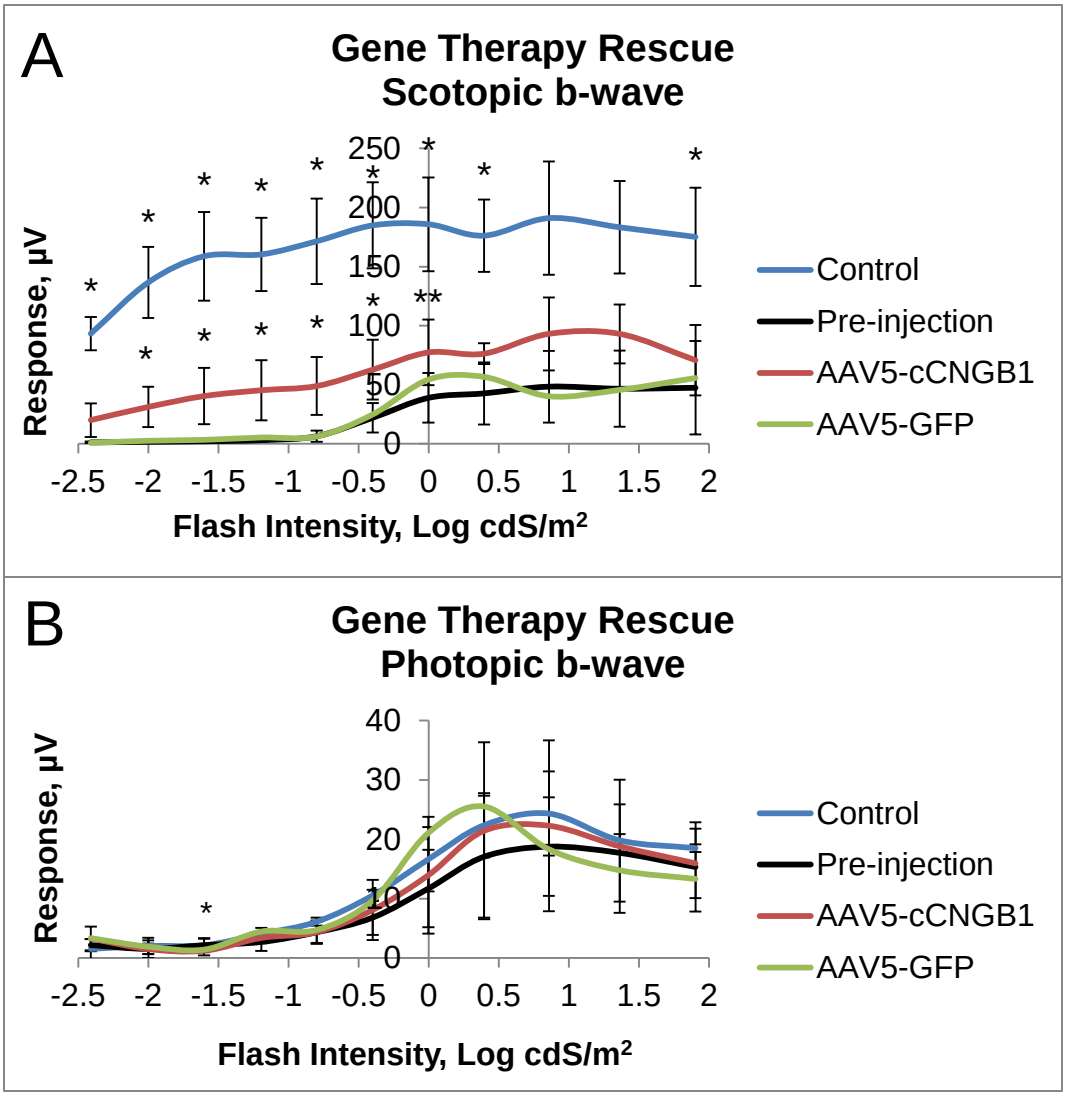

Figure 4.6. Scotopic and photopic b-wave amplitude plotted against stimulus intensity. Gene therapy rescues rod function resulting in increased scotopic ERG b-wave amplitudes and has no detrimental effects on cone function as assessed by the photopic ERG 6 months post-injection. (A) There is a significant increase in the mean scotopic b-wave amplitude at 6 months post-treatment (AAV5-cCNGB1, high titer) compared to the pre-injection mean response. The increase in the scotopic b-wave amplitude, specifically at the low light intensities (rod only responses), highlights the rescue of rod function. However, the scotopic b-wave amplitude of treated CNGB1 affected dogs 6 months post-injection were significantly smaller than the mean control b-waves. This is expected because only a portion of the retina was treated. (B) The pre-injection, 6 month post-treated *CNGB1* affected dogs and control dogs were not statistically different indicating that there was no detrimental effect from the treatment. * - $p \leq 0.05$, ** - $p \leq 0.01$, Pre-injection – 7 eyes, 6 month post-injection high titer AAV5-cCNGB1 – 4 eyes, 6 month post-injection AAV5-GFP – 1 eye., 14 month old control dogs – 3 eyes.

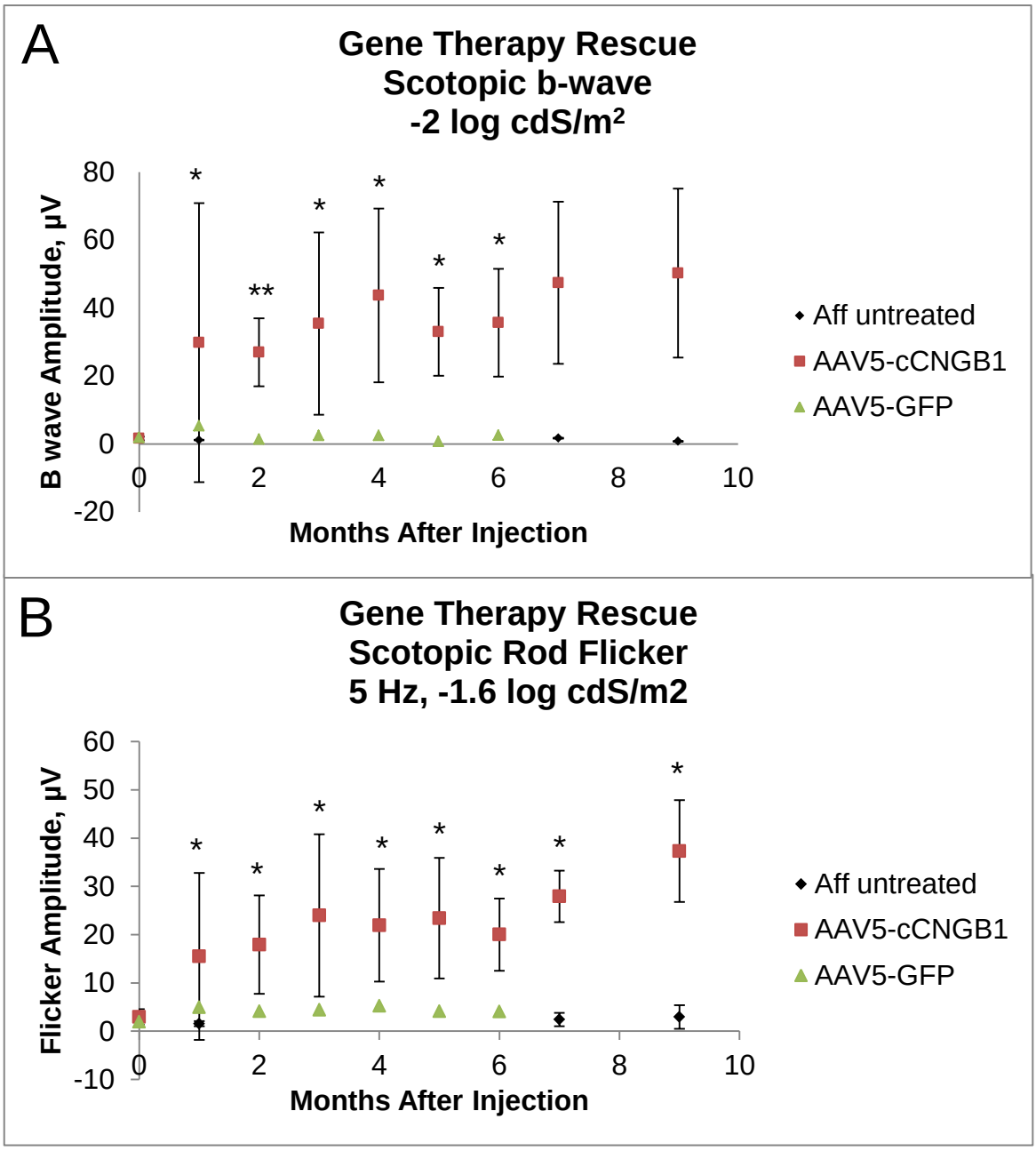

Figure 4.7. The improvement in rod-mediated ERG responses was maintained to 9 months post-injection. (A) Shows the scotopic b-wave amplitude in response to a dim-light flash (-2 log cdS/m^2) for up to 9 months after treatment with the high titer of AAV5-cCNGB1. (B) Similarly, rod flicker amplitudes are increased within 1 month of treatment and are maintained for 9 months. * - $p \leq 0.05$, ** - $p \leq 0.01$, pre-injection – 7 eyes, age-matched untreated CNGB1 affected – 2 eyes,1-3 month post-injection – 6 eyes, 4-6 month post-injection – 4 eyes, 7 and 9 months post-injection 3 eyes, AAV5-GFP – 1 eye.

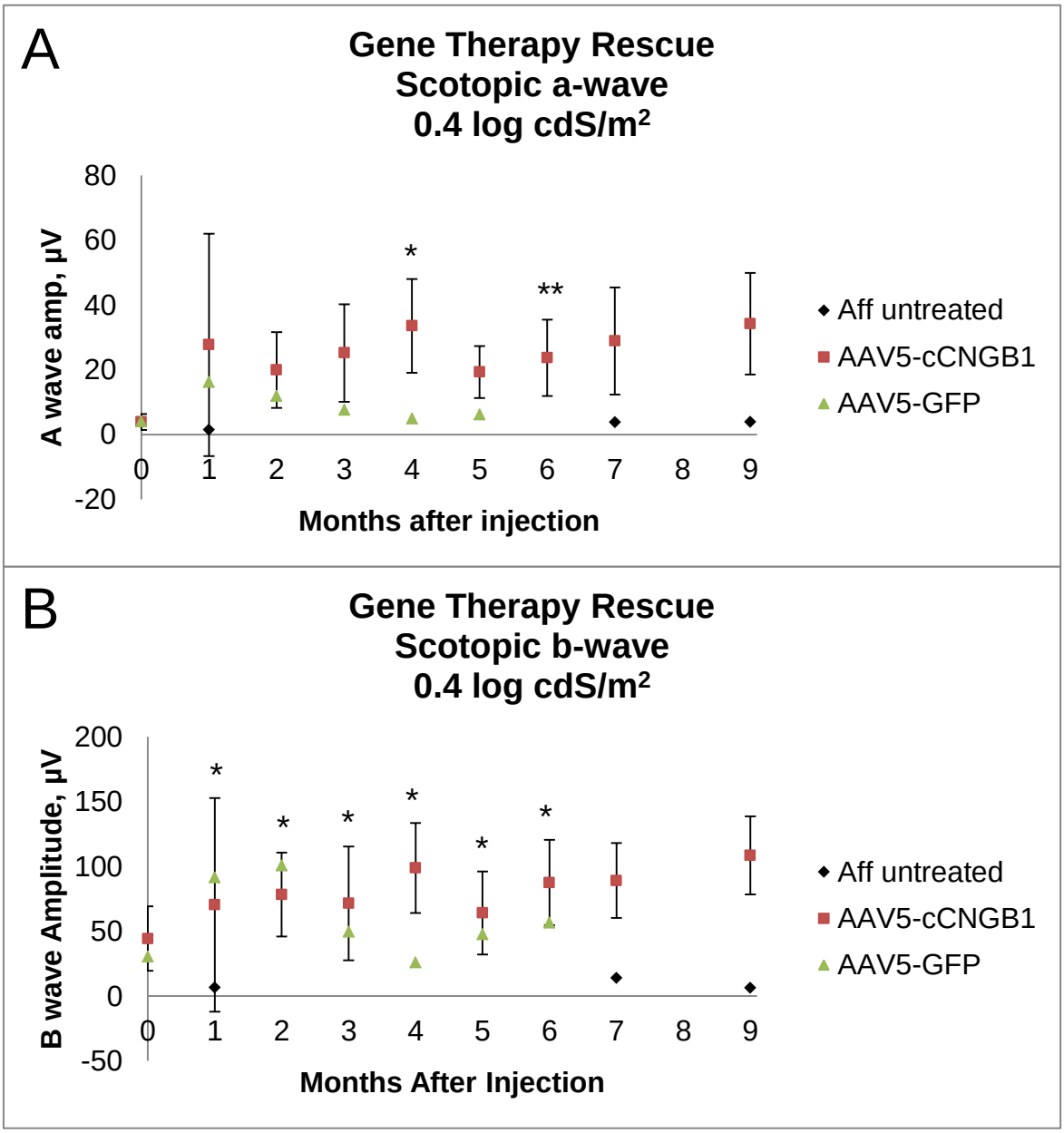

Figure 4.8. Scotopic mixed rod and cone ERG amplitudes were increased in AAV5-cCNGB1 treated dogs. Scotopic ERGs with bright light flashes elicit mixed cone and rod responses. (A) A-wave amplitudes were increased in the AAV5-cCNGB1 treated dogs and this was maintained up to 9 months post-injection. (B) B-wave amplitudes are increased in the AAV5-cCNGB1 treated dogs compared to the pre-injection b-wave amplitudes. * - $p \leq 0.05$, ** - $p \leq 0.01$, pre-injection – 7 eyes, age-matched untreated CNGB1 affected – 2 eyes,1-3 month post-injection – 6 eyes, 4-6 month post-injection – 4 eyes, 7 and 9 months post-injection 3 eyes, AAV5-GFP – 1 eye.

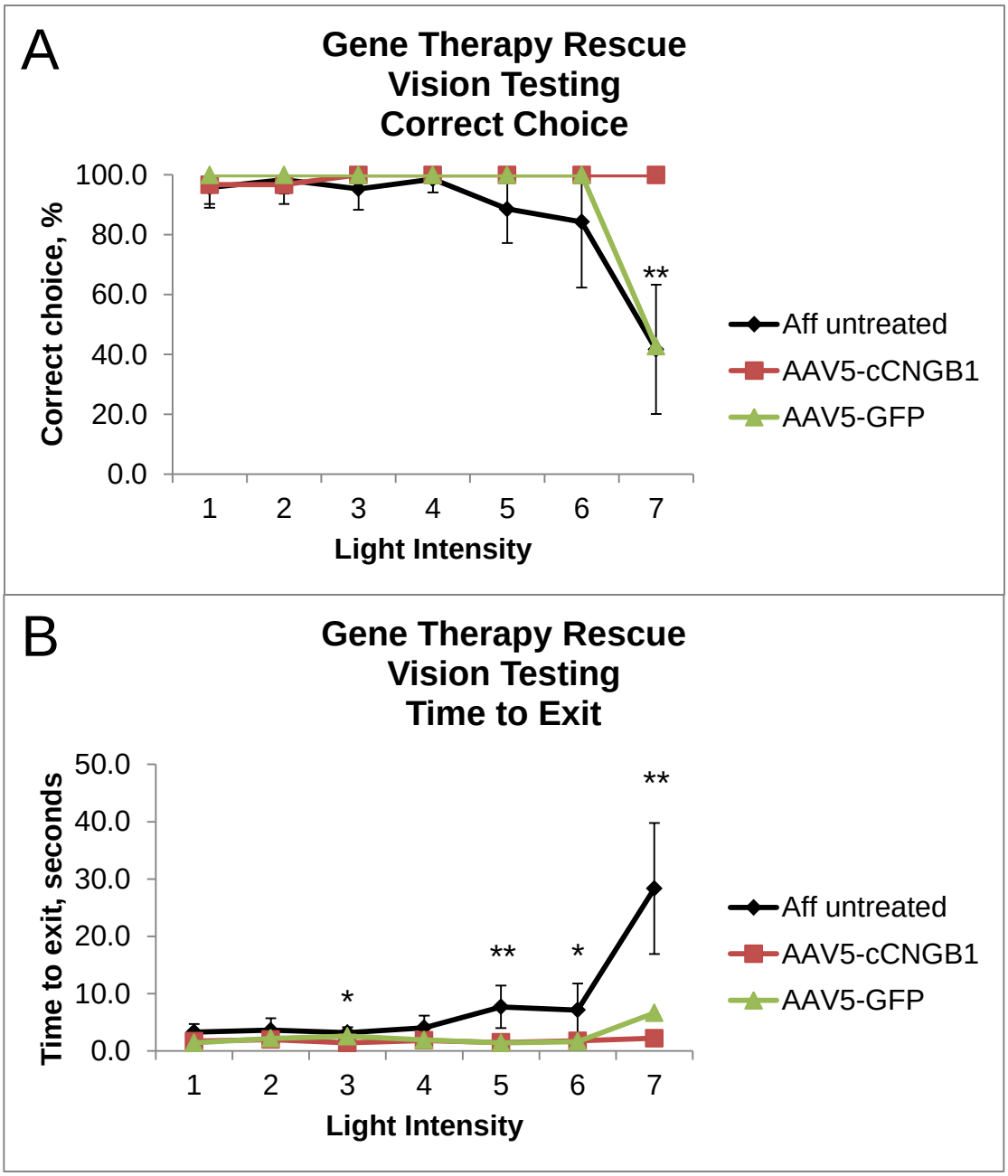

Figure 4.9. Functional vision is restored in the treated *CNGB1* affected eyes. (A) The *CNGB1* affected dogs that were treated with AAV5-cCNGB1 have more correct exit choices at the lowest light levels when compared to untreated *CNGB1* affected dogs. (B) The AAV5-cCNGB1 treated dogs are faster to exit the device at dim light intensities than the untreated *CNGB1* affected dogs. Light intensity: 1 – Full light (i.e. 35-45 cd/m^2), 2 – 15.0 cd/m^2, 3 – 8.0 cd/m^2, 4 – 1.0 cd/m^2, 5 – 0.4 cd/m^2, 6 – 0.2 cd/m^2, 7 – 0.02 cd/m^2 (very dim light). * - $p \leq 0.05$, ** - $p \leq 0.01$. Untreated *CNGB1* affected dogs (4 months to 6 years of age) – N=7, 6 month AAV5-cCNGB1 post-injection – 4 eyes, 6 month AAV5-GFP – 1 eye.

4.4 Discussion

We treated a total of 8 eyes (4 dogs) with an AAV5 vector; 6 eyes (4 dogs) with high titer ($5x10^{12}$) AAV5-cCNGB1, one eye with low titer ($1x10^{12}$) AAV5-cCNGB1 and one eye was treated with AAV5-GFP as a vehicle control. All vectors held a photoreceptor-specific *GRK1* promoter (the encoded protein for *GRK1* is also known as rhodopsin kinase). All eyes treated with AAV5-cCNGB1 showed some degree of ERG rescue and complete vision testing rescue.

Full length CNGB1 protein was expressed in the regions of the *CNGB1* affected retina treated with the AAV5-cCNGB1 vector. The CNGB1 protein was correctly targeted to the outer segments where it, presumably, incorporated with CNGA1 subunits to form functional CNG channels (Figure 4.1). CNGA1 levels are increased to give normal appearing IHC within the treated regions. While CNGA1 channels are capable of forming homomeric CNG channels *in vitro*, we have shown that CNGA1 protein expression is reduced in the untreated retina of 8 week old *CNGB1* affected dogs (Chapter 3) [8,9,13,19]. However, in vitro studies have shown that CNGB1 does not form channels without the presence of CNGA1 [20,21]. The recovery of detectable levels of the CNGA1 subunits, and the incorporation of the CNGB1 subunit to form functional channels, is integral to the rescue just reported. This same recovery of detectable levels of CNGA1 is seen in the *CNGB1-X26* mouse model when treated with AAV-mediated gene therapy [12].

The *GRK1* promoter has been shown to function in both rods and cones and can be transduced with the AAV5 vector [22]. To assess if CNGB1 was expressed in cones in the treated regions we co-labeled with antibodies for cone-sheath protein (PNA) and

CNGB1. While we did not conduct any quantification analyses our results show that there are at least some cones in the treated regions that do not have detectable levels of CNGB1 protein (Figure 4.2). Additionally, there did not appear to be any CNGB1 expression in the inner segments of the cones. More investigation of the CNGB1 expression in cones must be done before making more definitive remarks on the extent of cone transduction. It is possible that the cones are transduced by the vector but the protein is not utilized and/or degraded. The CNG channels expressed in cones contain subunits from the *CNGA3* and *CNGB3* genes [23]. CNGB1 and CNGB3 proteins share about 48% sequence identity but the CNGB3 subunit lacks the GARP domain of the full length protein [9]. It is possible that the presence of the GARP domain or the difference in protein sequence of the CNGB1 protein inhibits the incorporation of the CNGB1 protein into the cone CNG channels.

We conducted a pilot study treating one eye with a low titer ($1x10^{12}$) and one eye with a high titer ($5x10^{12}$) of AAV5-cCNGB1. Neither injected eye showed evidence of inflammatory or immune responses to the treatment. Both eyes showed increased scotopic b-wave amplitudes compared to untreated *CNGB1* affected dogs. However, the low titer treated eye showed only marginal scotopic ERG rescue compared to the high titer treated eye. Functional vision was rescued in both eyes; the dog was able to choose the correct exit 100% of the time with each eye, at all light intensities. This preliminary study showed that there is a dose response to the ERG rescue and that issuing an increased dose improved rescue and did not illicit any detrimental effects on the dog.

After the pilot study, three additional dogs were treated (6 eyes). Five eyes were treated with high titer AAV5-cCNGB1 and one eye was treated with AAV5-GFP ($1.5x10^{11}$). The eye treated with AAV5-GFP was used as a vehicle/procedural control; the titer of AAV5-GFP was chosen because it had been previously reported to not elicit an inflammatory response in the dog [22]. The AAV5-GFP injected eye showed no rescue of visual function and also did not have detrimental effects on the retina. The scotopic intensity-response plots of b-wave amplitudes showed the AAV5-GFP treated eye had similar responses to pre-injection values when measured at 6 months post-treatment. Additionally, the photopic intensity-response curves of the AAV5-GFP eye were comparable to pre-injection and control values. The five eyes treated with the high titer ($5x10^{12}$) of AAV5-cCNGB1 (5 eyes) showed significant scotopic ERG rescue. The AAV5-cCNGB1 treated dogs had a statistically significant increase in scotopic b-wave amplitudes when compared to pre-injection ERGs. The increase in amplitudes did not result in a- or b-waves comparable to control dogs but this was expected because only a portion of the retina was treated. Increasing the surface area treated in an eye could increase rescue but because the subretinal injection causes a retinal detachment one must weigh the risks of increasing the size of the treated region [17]. There was no significant difference in the photopic responses in the eyes treated with the vector compared to control dogs, showing that there were no long lasting detrimental effects on cone photoreceptor function due to the treatment. This is particularly important in *CNGB1* retinopathies where the cones are preserved until late stages of the disease. It would not be advantageous to harm the cones while delivering the vector.

The slow retinal degeneration, seen in the *CNGB1* affected dogs and RP45 patients, is ideal for gene supplementation therapy. In the *CNGB1* dogs the rod outer segments have started to degenerate and the outer nuclear layer has thinned slightly by around 5 months of age. The *CNGB1* affected eyes were treated with AAV5-cCNGB1 between 3 and 6 months of age and showed significant rescue. Future studies will elucidate the extent of this treatment window and how it may impact human clinical trials.

The long-term goal of retinal gene supplementation therapy is to permanently rescue vision. For permanent rescue to be accomplished the therapy must rescue functional vision (by ERG and by vision testing) and halt, or significantly slow, the loss of retinal degeneration. We have shown that in the *CNGB1* affected dog model that functional vision was rescued and maintained for at least 9 months. Preliminary results investigating photoreceptor layer thickness as measured *in vivo* with OCT, has shown that the retina continues to degenerate but at a slower rate (data not shown). However, the time course for this study was not long enough to appreciate the modification of the rate of photoreceptor loss. Some continued loss of rods in the treated are is to be expected because although the AAV5 transduction efficiency is good not every rod is transduced. It remains to be determined if once the untreated rods in the injected area have died that the progression of cell loss is halted. It is our hypothesis that the photoreceptor layer will thin as the untreated cells die and then retinal thickness will remain constant within the treated regions preserving functional vision and ERGs. Dog 2 was kept for future monitoring of retinal thickness and maintained rescue.

This first report showed that gene supplementation therapy using AAV5-cCNGB1 restored functional vision in *CNGB1* affected dogs. This rescue was statistically significant by 2 months of age and was maintained over 9 months. The success of this trial will pave the way for future clinical trials human patients with mutations in the *CNGB1* gene.

4.5 Supplemental information

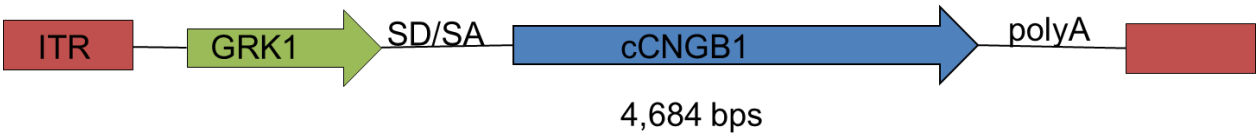

Figure 4.S1. AAV2/5 viral vector genome. The AAV2/5 vector is constructed using the inverted terminal repeats (ITR) from an AAV2 virus and the capsid of the AAV5 virus. The promoter is a portion of the human *GRK1* promoter (292 bps). SD/SA is the splice donor/acceptor signal from the SV40 virus. The canine *CNGB1* cDNA is 3,360 bps in size. The GFP cDNA is 717 bps in size. Total vector size is 4,684 bps for the AAV5-cCNGB1 vector and 2,041 bps for AAV5-GFP vector.

Table 4.S1. Comprehensive table of data, statistical analyses and *p*-values corresponding to Figures 4.6 through 4.9

Figure 4.6A Scotopic b-wave amplitudes
Pre-injection mean compared to 6 month AAV5-cCNGB1 mean

Flash Intensity (Log cdS/m^2)	Pre-injection[1]	AAV5-cCNGB1[1]	Statistical Analysis[2]	Pval
-2.41	1.4	20.1	PT	0.084
-2.00	1.6	31.2	PT	0.040
-1.60	1.8	40.4	PT	0.049
-1.19	2.7	45.3	PT	0.041
-0.80	4.6	48.9	PT	0.034
-0.40	20.4	62.7	PT	0.024
0.00	42.9	77.3	PT	0.004
0.39	49.7	76.3	PT	0.104
0.86	55.5	93.1	PT	0.241
1.36	55.5	93.1	PT	0.172
1.90	56.3	70.7	WSR	0.875

Figure 4.6A Scotopic b-wave amplitudes
Wild-type control mean compared to 6 month AAV5-cCNGB1 mean

Flash Intensity (Log cdS/m^2)	Wild-type Control[1]	AAV5-cCNGB1[1]	Statistical Analysis[2]	Pval
-2.41	93.3	20.1	M-W	0.036
-2.00	136.6	31.2	M-W	0.036
-1.60	158.8	40.4	M-W	0.036
-1.19	160.3	45.3	M-W	0.036
-0.80	171.5	48.9	M-W	0.036
-0.40	184.9	62.7	M-W	0.036
0.00	185.8	77.3	M-W	0.036
0.39	176.2	76.3	M-W	0.036
0.86	191.1	93.1	M-W	0.250
1.36	183.3	93.1	M-W	0.143
1.90	175.1	70.7	M-W	0.036

Table 4.S1 cont'd

Figure 4.6B Photopic b-wave amplitudes
Pre-injection mean compared to 6 month AAV5-cCNGB1 mean

Flash Intensity (Log cdS/m^2)	Pre-injection[1]	AAV5-cCNGB1[1]	Statistical Analysis[2]	Pval
-2.41	2.2	3.3	PT	0.522
-2.00	1.5	1.5	PT	0.836
-1.60	2.2	1.2	PT	0.050
-1.19	2.7	3.4	PT	0.106
-0.80	4.3	4.3	PT	0.641
-0.40	6.8	8.1	PT	0.258
0.00	11.7	14.0	PT	0.297
0.39	17.1	21.4	WSR	0.125
0.86	18.8	22.3	PT	0.337
1.36	17.7	18.8	PT	0.471
1.90	15.3	15.9	PT	0.286

Figure 4.6B Photopic b-wave amplitudes
Wild-type control mean compared to 6 month AAV5-cCNGB1 mean

Flash Intensity (Log cdS/m^2)	Wild-type Control[1]	AAV5-cCNGB1[1]	Statistical Analysis[2]	Pval
-2.41	1.5	3.3	M-W	0.229
-2.00	2.0	1.5	M-W	0.400
-1.60	2.1	1.2	M-W	0.229
-1.19	4.1	3.4	M-W	0.400
-0.80	6.1	4.3	M-W	0.400
-0.40	10.5	8.1	M-W	0.400
0.00	16.6	14.0	M-W	0.400
0.39	22.4	21.4	M-W	0.629
0.86	24.3	22.3	M-W	0.400
1.36	19.8	18.8	M-W	0.400
1.90	18.5	15.9	M-W	0.400

Table 4.S1 cont'd

Figure 4.7A Gene therapy rescue, scotopic b-wave
Pre-injection mean compared to AAV5-cCNGB1 mean

Months Post Injection	Pre-injection[1]	AAV5-cCNGB1[1]	Statistical Analysis[2]	Pval
0	1.6	-	-	-
1		29.8	WSR	0.031
2		27.0	PT	0.002
3		35.5	PT	0.026
4		43.7	PT	0.044
5		23.8	PT	0.022
6		35.7	PT	0.022
7		47.5	PT	0.079
8		-	-	-
9		52.0	PT	0.071

Figure 4.7B Gene therapy rescue, scoptic rod flicker
Pre-injection mean compared to AAV5-cCNGB1 mean

Months Post Injection	Pre-injection[1]	AAV5-cCNGB1[1]	Statistical Analysis[2]	Pval
0	3.0	-	-	-
1		15.5	WSR	0.031
2		17.9	PT	0.020
3		24.0	PT	0.029
4		22.0	PT	0.033
5		23.4	PT	0.036
6		20.0	PT	0.011
7		27.9	PT	0.014
8		-	-	-
9		37.3	PT	0.026

Table 4.S1 cont'd

Figure 4.8A Scotopic mixed rod and cone ERG a-wave amplitudes
Pre-injection mean vs AAV5-cCNGB1 mean

Months Post Injection	Pre-injection[1]	AAV5-cCNGB1[1]	Statistical Analysis[1]	Pval
0	3.9		-	-
1		27.7	WSR	1.000
2		19.9	PT	0.164
3		25.2	PT	0.156
4		33.6	PT	0.020
5		19.3	PT	0.583
6		23.7	PT	0.008
7		28.9	PT	0.308
8			-	-
9		34.2	PT	0.136

Figure 4.8B Scotopic mixed rod and cone ERG b-wave amplitudes
Pre-injection mean vs AAV5-cCNGB1 mean

Months Post Injection	Pre-injection[1]	AAV5-cCNGB1[1]	Statistical Analysis[1]	Pval
0	44.4		-	-
1		70.5	WSR	0.031
2		78.3	PT	0.014
3		71.6	PT	0.017
4		98.9	PT	0.024
5		64.1	PT	0.019
6		87.6	PT	0.025
7		89.1	PT	0.117
8			-	-
9		108.6	PT	0.075

Figure 4.9A Vision testing, correct choice
Untreated *CNGB1* affected vs AAV5-cCNGB1

Light Intensity (cd/m^2)	Untreated Affected[1]	AAV5-cCNGB1[1]	Statistical Analysis[1]	Pval
35-45	95.8	96.8	M-W	0.721
15.0	98.4	96.8	M-W	0.713
8.0	95.3	100.0	M-W	0.246
1.0	98.6	100.0	M-W	0.635
0.4	88.6	100.0	M-W	0.067
0.2	84.3	100.0	M-W	0.068
0.02	41.7	100.0	M-W	0.005

Table 4.S1 cont'd

Figure 4.9B Vision testing, time to exit
Untreated *CNGB1* affected vs AAV5-cCNGB1

Light Intensity (cd/m^2)	Untreated Affected[1]	AAV5-cCNGB1[1]	Statistical Analysis[1]	Pval
35-45	3.3	1.7	M-W	0.056
15.0	3.7	2.0	M-W	0.143
8.0	3.2	1.4	M-W	0.017
1.0	4.1	1.9	M-W	0.103
0.4	7.7	1.5	M-W	0.006
0.2	7.1	1.8	M-W	0.044
0.02	28.3	2.2	M-W	0.006

1. Mean values
2. Statistical analysis: PT – paired t-test; WSR – Wilcoxon Rank Sum Test; M-W – Mann-Whitney Rank Sum Test

REFERENCES

REFERENCES

1. Hartong DT, Berson EL, Dryja TP (2006) Retinitis pigmentosa. Lancet 368: 1795-1809.

2. Bareil C, Hamel CP, Delague V, Arnaud B, Demaille J, et al. (2001) Segregation of a mutation in CNGB1 encoding the beta-subunit of the rod cGMP-gated channel in a family with autosomal recessive retinitis pigmentosa. Human Genetics 108: 328-334.

3. Kondo H, Qin MH, Mizota A, Kondo M, Hayashi H, et al. (2004) A homozygosity-based search for mutations in patients with autosomal recessive retinitis pigmentosa, using microsatellite markers. Investigative Ophthalmology & Visual Science 45: 4433-4439.

4. Bainbridge JW, Mehat MS, Sundaram V, Robbie SJ, Barker SE, et al. (2015) Long-term effect of gene therapy on Leber's congenital amaurosis. New England Journal of Medicine 372: 1887-1897.

5. Bainbridge JW, Smith AJ, Barker SS, Robbie S, Henderson R, et al. (2008) Effect of gene therapy on visual function in Leber's congenital amaurosis. New England Journal of Medicine 358: 2231-2239.

6. Maguire AM, Simonelli F, Pierce EA, Pugh EN, Jr., Mingozzi F, et al. (2008) Safety and efficacy of gene transfer for Leber's congenital amaurosis. New England Journal of Medicine 358: 2240-2248.

7. Cideciyan AV, Hauswirth WW, Aleman TS, Kaushal S, Schwartz SB, et al. (2009) Human RPE65 Gene Therapy for Leber Congenital Amaurosis: Persistence of Early Visual Improvements and Safety at 1 Year. Human Gene Therapy 20: 999-1004.

8. Shuart NG, Haitin Y, Camp SS, Black KD, Zagotta WN (2011) Molecular mechanism for 3:1 subunit stoichiometry of rod cyclic nucleotide-gated ion channels. Nature Communications 2:457.

9. Kaupp UB, Seifert R (2002) Cyclic nucleotide-gated ion channels. Physiological Reviews 82: 769-824.

10. Zhang YW, Molday LL, Molday RS, Sarfare SS, Woodruff ML, et al. (2009) Knockout of GARPs and the beta-subunit of the rod cGMP-gated channel disrupts disk morphogenesis and rod outer segment structural integrity (vol 122, pg 1192, 2009). Journal of Cell Science 122: 1927-1927.

11. Huttl S, Michalakis S, Seeliger M, Luo DG, Acar N, et al. (2005) Impaired channel targeting and retinal degeneration in mice lacking the cyclic nucleotide-gated channel subunit CNGB1. Journal of Neuroscience 25: 130-138.

12. Koch S, Sothilingam V, Garcia Garrido M, Tanimoto N, Becirovic E, et al. (2012) Gene therapy restores vision and delays degeneration in the CNGB1(-/-) mouse model of retinitis pigmentosa. Human Molecular Genetics 21: 4486-4496.
13. Winkler PA, Ekenstedt KJ, Occelli LM, Frattaroli AV, Bartoe JT, et al. (2013) A Large Animal Model for CNGB1 Autosomal Recessive Retinitis Pigmentosa. PLoS One 8: e72229.

14. Petrs-Silva H, Dinculescu A, Li Q, Deng WT, Pang JJ, et al. (2011) Novel properties of tyrosine-mutant AAV2 vectors in the mouse retina. Molecular Therapy 19: 293-301.

15. Petrs-Silva H, Dinculescu A, Li Q, Min SH, Chiodo V, et al. (2009) High-efficiency transduction of the mouse retina by tyrosine-mutant AAV serotype vectors. Molecular Therapy 17: 463-471.

16. Zhong L, Li B, Mah CS, Govindasamy L, Agbandje-McKenna M, et al. (2008) Next generation of adeno-associated virus 2 vectors: point mutations in tyrosines lead to high-efficiency transduction at lower doses. Proceedings of the National Academy of Sciences of the United States of America 105: 7827-7832.

17. Petersen-Jones SM, Bartoe JT, Fischer AJ, Scott M, Boye SL, et al. (2009) AAV retinal transduction in a large animal model species: comparison of a self-complementary AAV2/5 with a single-stranded AAV2/5 vector. Molecular Vision 15: 1835-1842.

18. Khani SC, Pawlyk BS, Bulgakov OV, Kasperek E, Young JE, et al. (2007) AAV-mediated expression targeting of rod and cone photoreceptors with a human rhodopsin kinase promoter. Investigative Ophthalmology & Visual Science 48: 3954-3961.

19. Biel M, Michalakis S (2009) Cyclic nucleotide-gated channels. Handbook of experimental pharmacology 191: 111-36.

20. Chen TY, Peng YW, Dhallan RS, Ahamed B, Reed RR, et al. (1993) A new subunit of the cyclic nucleotide-gated cation channel in retinal rods. Nature 362: 764-767.
21. Matulef K, Zagotta WN (2003) Cyclic nucleotide-gated ion channels. Annual Review of Cell and Developmental Biology 19: 23-44.

22. Beltran WA, Boye SL, Boye SE, Chiodo VA, Lewin AS, et al. (2010) rAAV2/5 gene-targeting to rods:dose-dependent efficiency and complications associated with different promoters. Gene Therapy 17: 1162-1174.

23. Peng C, Rich ED, Varnum MD (2004) Subunit configuration of heteromeric cone cyclic nucleotide-gated channels. Neuron 42: 401-410.

CHAPTER 5

THE HISTOLOGICAL AND BEHAVIORAL OLFACTORY PHENOTYPES OF *CNGB1* AFFECTED DOGS

5.1 Introduction

Cyclic nucleotide-gated (CNG) ion channels are nonselective cation channels that are gated by the cyclic nucleotides, cAMP and cGMP [1]. CNG channels have been described in many tissues and are well understood for their role in the sensory transduction in vision and the sense of smell. The CNG channels of the olfactory epithelium are expressed in the olfactory sensory neurons (OSNs). The *CNGB1* gene has three splice variants expressed in rod photoreceptors (GARP1, GARP2 and CNGB1a) and one expressed in the OSNs (CNGB1b) [2]. CNG channels play a key role in olfaction, aiding in the initial depolarization of the OSNs in response to an odorant.

The CNG channels in the OSNs are heterotetrameric proteins consisting of a 2:1:1 ratio of CNGA2, CNGA4 and CNGB1b respectively [3]. The channels localize to the OSN cilia where they are in close proximity to the odorant receptor and a Ca^{2+}-dependent Cl^- channel. When an odorant binds to a receptor a G-protein (G_{olf}) is activated. G_{olf} then activates adenylate cyclase III which converts ATP to cAMP. cAMP binds to and opens the CNG channel which allows the influx of cations, most importantly Ca^{2+}, resulting in an initial depolarization of the cell. Ca^{2+} plays two additional roles; first it binds to and opens the Ca^{2+}-dependent Cl^- channel resulting in an efflux of Cl^- ions and a further depolarization of the cell. The CNG channel only carries about 15% of the depolarization of the OSN, the rest is due to the Ca^{2+}-dependent Cl^- channel [2]. Second, the Ca^{2+} binds to calmodulin which both desensitizes the CNG channel to cAMP and initiates cAMP hydrolysis; this plays a key role in odor adaptation. Depolarization of the cell results in the release of an action potential which travels through the axons of the OSNs to the olfactory bulb where the

OSNs synapse with mitral cells [2]. The signal is processed through multiple cell types in the olfactory bulb and is further processed in the brain.

The *CNGB1-X26* mouse has olfactory impairment due to its mutation in the *CNGB1* gene. The mice have decreased olfactory responses as measured by electro-olfactograms and behavioral testing but are not completely anosmic. The olfactory epithelium (OE) and olfactory bulbs (OB) of *CNGB1-X26* mice have normal morphology although the OE is 15-20% thinner and the OBs are markedly reduced in size [4].

A mutation in *CNGB1* has been described in a canine model of retinitis pigmentosa [5]. This mutation is in an almost identical exonic location compared to the *CNGB1-X26* mouse. In this study, we investigated the effect of mutation in *CNGB1* affected dogs on the olfactory system.

5.2 Materials and methods

5.2.1 Animal use

The dogs used in this study were maintained in a colony at the Michigan State University Comparative Ophthalmology Laboratory as described in Chapter 3.

5.2.2 Behavioral testing

We developed a method for assessing behavioral olfactory function which included food being randomly placed in one of four boxes inside a large pen (modified from a buried food test used for phenotyping mice) [6].

This method required little hands-on training and reduced the effect of handler bias although there was a long conditioning period [7]. Each dog was placed in a 7 foot by 7 foot square pen with four boxes. Dogs became comfortable with the room, experiment pen and boxes by being placed alone in the pen for 20 minutes 3-5 days a week for five weeks. Inside the experiment pen were four open boxes with food placed in one box. The boxes were placed in a line in the middle of the pen with meat baby food (ham or turkey; Gerber Inc., Florham Park, NJ) in one randomly selected box. The boxes were recycled pipette tip boxes (Biohit, Bohemia, NY) that were opaque and any contents could not easily be seen but the food could be smelled. Two different amounts of food were tested; 2 grams and 20 grams. Dogs were allowed 2 minutes in the test pen per test and the box containing the food was randomly assigned for each test. Dogs were fasted overnight but had access to drinking water.

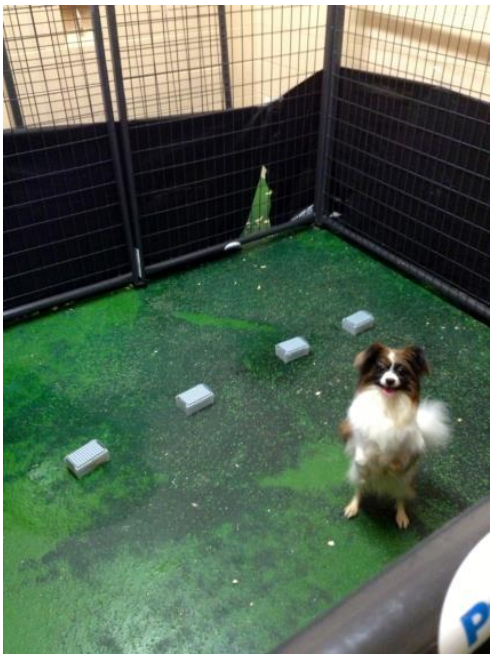

Figure 5.1. Olfaction behavior testing pen layout. The dogs are placed in a pen with four covered boxes in a line. In one of the boxes there is food. The dogs are given 2 minutes to investigate the boxes.

Dogs did not observe the researcher placing the food into the box. The dogs were alone in the room and recorded while the investigator waited quietly in another room, so as not to distract the dog or give any clues as to which box contained the food. After each test, the box was opened and the dog was shown that there was food in the box and the dog was allowed a taste of the baby food. As a positive control, dogs were also placed in the pen while all four boxes were open and food was placed in one box.

After the test, an observer blinded to which box contained the food watched the recorded videos and did a quantitative and qualitative assessment. For the quantitative assessment the observer used a timer to record the time the dog spent at each box. If the dog obviously smelled a box but spent less than 1 second at the box, this was counted as 1 second. After this assessment, videos in which the dog did not spend at least 5 seconds investigating the boxes were removed from the analysis. For the qualitative assessment, a blinded observer watched the video and recorded which box

they thought the food was in based on the dog's behavior. Four *CNGB1* affected Papillons and two control Papillons were tested.

5.2.3 Sample collection and processing

Following humane euthanasia, the nasal cavities and olfactory bulbs from several *CNGB1* affected and controls dogs (see the following sections for numbers and ages) were collected for further processing. First, the head was removed from the carcass. The skin, musculature and lower jaw were removed from the head. The calvarium was carefully removed. The olfactory bulbs (OB) were removed and fixed in 1% paraformaldehyde and 0.1% glutaraldehyde (pH 7.4) for at least 24 hours at 4°C.

The nasal cavity was sagitally sectioned 1-2 mm to the right of the midline, yielding an intact left nasal cavity and a right nasal lateral wall. The ethmoturbinate 4 (ET4) of the right nasal cavity was collected and flash frozen in liquid nitrogen and stored at -80°C for later extraction of RNA. ET4 was specifically selected for RNA isolation because it is known to be lined with an abundance of olfactory mucosa [8]. The left side of the nasal cavity was fixed in 1% paraformaldehyde and 0.1% glutaraldehyde (pH 7.4) for at least 24 hours at 4°C.

Each left nasal cavity specimen was decalcified in 10% ethylenediaminetetraacetic acid (EDTA) in 0.1M sodium cacodylate buffer (pH 7.4) for 120 days and then rinsed with distilled water. Transverse sections of the nasal cavity were cut using dental and palatine landmarks in a plane perpendicular to the hard palate and nasal septum to obtain 8 (8-week old dogs) or 12 (5 month old dogs) sections. These tissue sections (~5 mm thick) and the OBs were paraffin embedded with the anterior face sectioned at 5 µm. Paraffin embedded sections were stained with

hematoxylin and eosin (H&E, nasal cavities and OBs) and Alcian blue/periodic acid Schiff (AB/PAS, nasal cavities only) and evaluated for histopathology and morphometric assessments. Additional sections were labeled for immunohistochemical analyses as described in section *5.2.5 Immunohistochemistry*.

5.2.4 *CNGB1* transcript quantification

Olfactory ET4 from 8 week old *CNGB1* affected dogs (N=2), 8 week old *CNGB1* heterozygous dogs (N=1) and 8 week old mixed breed control dogs (N=3) were dissected as described in the previous section (5.5.2 Sample Collection and Processing). RNA was extracted and cDNA was made following the manufacturer's protocols (RNeasy midi kit Qiagen Sciences, Germantown, MD and 3' RACE, Invitrogen, Carlsbad, CA). Real time quantitative PCR (RT-qPCR) was conducted as described in Chapter 3 using the primers listed in Table 5.1.

Table 5.1. RT-qPCR primers for olfactory epithelium tissue expression

Gene	Forward Primer	Reverse Primer	Size[1]
CNGB1	GGACATCACCGTGTTCCAG	TGTCCATCTTAAAGCGACGAG	113
CNGA2	CCGCTGGCTATTTGTCATTG	GTCACTGAAGCAGGCTCTGG	76
CNGA4	ACCCAAGGCCAGGAAGTTG	TCGTGTTCAGCCACCAGTAG	71
OMP	ACATGACCTTGCGGATCTTG	GCCATGGATTGGAACGAG	79

1. Amplified cDNA size

5.2.5 Immunohistochemistry

Additional 5 µm sections were obtained from all tissue blocks containing olfactory mucosa. Unstained and hydrated paraffin embedded sections were blocked and incubated with specific dilutions of primary polyclonal antibodies (Table 5.2). Paraffin embedded sections were labeled with antibodies against CNGB1 C-terminal peptide,

olfactory marker protein (OMP) to identify mature OSNs, or the pan-neuronal marker protein gene product 9.5 (PGP 9.5) to identify all OSNs. Immunohistochemistry on paraffin embedded sections was conducted by Michigan State University Diagnostic Center for Population and Animal Health Histology Laboratory (Lansing, MI 48910) and the Investigative Histopathology Laboratory in the Division of Human Pathology at Michigan State University (East Lansing, MI 48824). Primary and secondary antibody concentrations are listed in Table 5.2.

Table 5.2. Antibody details and concentrations

Antigen Target	Antibody Details	Source	Secondary Antibody
CNGB1 C-terminal[1] (1144-1238)	1:200 rabbit polyclonal	Sigma-Aldrich HPA039159	EnVision FLEX K8000
OMP - olfactory marker protein	1:2000 goat polyclonal	Wako 544-10001	Vector Labs Biotinylated anti-rabbit IgG
PGP 9.5 - neuronal marker	1:500 rabbit polyclonal	Abcam ab15503	EnVision FLEX K8000

1. Protein detected with this antibody is assumed to be full-length

5.2.6 Stereology

OE sections from the rostral and caudal aspects of the dorsal medial meatus of the rostral and caudal nasal cavity were labeled with OMP and used for morphometry measurements. The thickness of the OE and the volume density of OSNs (as determined by volume fraction of OMP-positive staining within the OE) were calculated using the following procedure (modified from [9]). Serial photomicrographs of the OE lining the dorsal medial meatus were obtained at a final magnification of 1,710x using a light microscope (Olympus BX-40, Olympus America, Melville, NY) coupled to a 3.3-

megapixel digital color camera (Q-color 3, Quantitative Imaging Corporation, Burnaby, British Columbia, CA) The images were loaded into a software package that automatically overlays a 136-point cycloid grid (containing 136 points and 35 intercepts) onto the image (Stereology Toolbox, Moprhometrix, Davis, CA). Each point represents 1 μm^3 of olfactory tissue. The software is calibrated using a micrometer image taken using the same microscope, camera and magnification as the tissue images. The length of the cycloid (used in further calculations) is calculated by the equation: $Cycloid\ arc = \frac{1}{10}X$ where X is the calibrated width of the grid; for example: $Cycloid\ arc = \frac{1}{10}510.5$ the cycloid arc is 51.05 µm. Using the software, points that were touching OSNs, cilia or OE were counted as *points* and placed into a table organized by each category. The number of cycloid arcs intersecting with the basal lamina were counted as *intercepts.*

A series of equations are used to calculate the percent of that total volume of OSNs in the OE:

1. The length per points (l/P) is calculated with the equation:

   $$l/P = \frac{\#\ intercepts\ x\ cycloid\ arc}{total\ points\ on\ grid}$$

   For example: $l/P = \frac{35\ x\ 51.05}{136}$ the l/P = 13.14.

2. The total tissue thickness is calculated by the equation:

   $$Lt = \frac{l}{P}\ P_{tissue}$$

   For example: Lt = (13.14)(Total # of points counted in an image)

3. Finally, volume density for the object of interest (T) (for example the OSNs) is calculated with the equation: $T = \left(\frac{Pob}{Ptis}\right)\left(\frac{Lt}{2(Int)}\right)$

   Where P_{ob} are the points touching your tissue of interest, P_{tis} are the total points counted in the tissue, and Int are the number of intercepts of the basal lamina counted.

These calculations result in an estimate of volume per surface area of a tissue of interest (Vs, μ^3/μ^2) (for example, volume of OSNs per unit of OE basal lamina). T was calculated for all images taken for four dogs; one 8 week old *CNGB1* affected, one 5 month old *CNGB1* affected and two age matched (8 week and 5 month) control dogs.

5.2.7 Statistical analysis

Statistics were calculated as described in Chapter 3.

5.3 Results

5.3.1 *CNGB1* transcript is reduced in *CNGB1* affected dogs

CNGB1 transcript levels were assessed in 8 week old *CNGB1* affected (N=2), heterozygous (N=1) and control dogs (N=3) using RT-qPCR. The *CNGB1* transcripts were normalized to the mature OSN-specific gene *OMP* (olfactory marker protein). This gene was used for normalizing (as opposed to a housekeeping gene) because CNGB1b is only expressed in the mature OSNs of the OE tissue reducing the variability caused by the inclusion of other tell types in the sample. Mean *CNGB1* transcript levels were significantly reduced in *CNGB1* affected dogs compared to the age matched control dogs (20.2% ± 2.8, $p< 0.001$; Table 5.3). The transcript levels of *CNGA2* and *CNGA4* in the *CNGB1* affected dogs were also assessed. *CNGA2* and *CNGA4* levels were not significantly different between *CNGB1* affected and control dogs (107% ± 0.07, $p=0.634$; 115% ± 14.3, $p=0.186$).

Table 5.3. RT-qPCR results from olfactory epithelial extracts

Sample[1]	*CNGB1*[2]	*CNGA2*	*CNGA4*
Aff 1	0.22	1.07	1.25
Aff 2	0.18	1.07	1.04
Het 1	1.03	0.79	1.01
Unaf 1	1.00	1.04	0.99
Unaf 2	1.06	1.14	1.06
Unaf 3	0.95	0.84	0.96

1. Biological replicates. Aff 1-2, Het 1 and Unaf 1-3: 8 weeks old
2. Fold change from mean of unaffected *CNGB1* transcript levels.

5.3.2 Full length CNGB1 protein is not expressed in the olfactory epithelium

To confirm that the reduced *CNGB1b* transcript expression due to the mutation results in altered CNGB1b protein expression, we conducted IHC on caudal sections of the OE in 8 week old *CNGB1* affected and control dogs. The sections labeled with the C-terminal CNGB1 antibody showed that the full length CNGB1b protein is not detectable in the *CNGB1* affected dogs while it is correctly localized to the cilia of the OSNs in the control dog (Figure 5.2). Additional IHC will be needed to investigate the presence of a truncated CNGB1 protein, as seen in the retina.

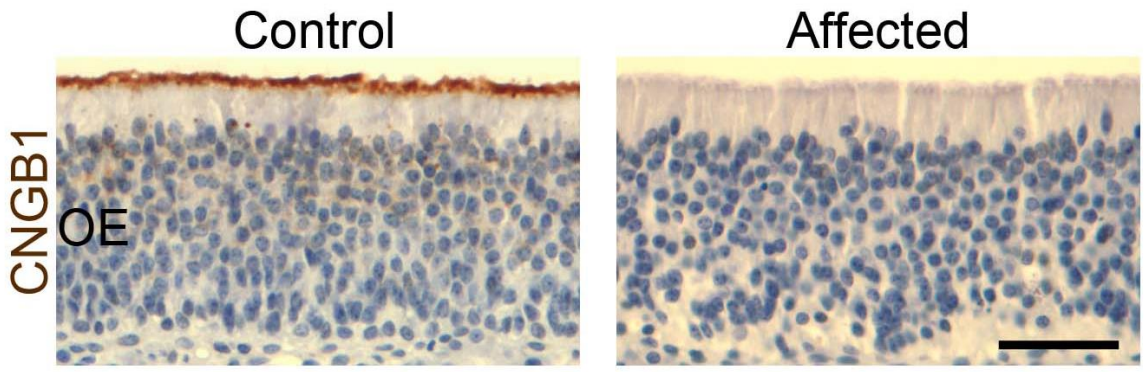

Figure 5.2. Full length CNGB1 protein is not detectable in the *CNGB1* affected dog. The full length CNGB1 protein (brown) is localized to the cilia of the OSNs in the 8 week old control dog but is not detectable in the *CNGB1* affected dog. The counterstain (blue) is hematoxylin. Size bar – 50 µm.

5.3.3 Olfactory epithelium morphology in the *CNGB1* affected dogs

The morphology of *CNGB1* affected dogs compared to age-matched control dogs was assessed using stereological methods applied to serial images from rostral and caudal sections. The 8 week old *CNGB1* affected dog had thinner OE than the 8 week control dog (Table 5.4, Figure 5.3). However, the OE from a 5 month old *CNGB1*

affected dog was thicker than the respective OE from a 5 month old control dog and from both of the 8 week old dogs. The volume of OMP positive OSNs per surface area of OE basal lamina was less in the 8 week old *CNGB1* affected dog compared to the control dogs while the 5 month old *CNGB1* affected dog had less volume of OMP positive OSNs per surface area of OE than the control dogs in the rostral section but more in the caudal section.

Table 5.4. Morphometric description of *CNGB1* affected and control dog OSNs in the OE

Sample	Location[1]	OE[2] (μ)	OSNs[3] (μ^3/μ^2)
8 week control	Rostral	140.1	36.4
	Caudal	174.0	37.4
8 week affected	Rostral	123.0	26.8
	Caudal	108.8	22.3
5 month control	Rostral	131.6	37.1
	Caudal	131.0	36.6
5 month affected	Rostral	221.7	19.8
	Caudal	197.3	49.2

1. Two sections of the olfactory cavity were analyzed per dog, the rostral and caudal sections of the dorsal medial meatus
2. The mean thickness of the OE in microns
3. The mean volume per surface area of OMP positive-stained OSNs

Mature OSNs are labeled with the OMP antibody while PGP 9.5 is a pan OSN marker. The *CNGB1* affected dogs have very few OMP positive axons compared to the control dogs (Figure 5.3A). However, there are PGP 9.5 positive axons in the *CNGB1* affected dogs (as well as the control dogs) (Figure 5.3B, arrow heads). This indicates that there are less mature OSNs in the *CNGB1* affected dogs.

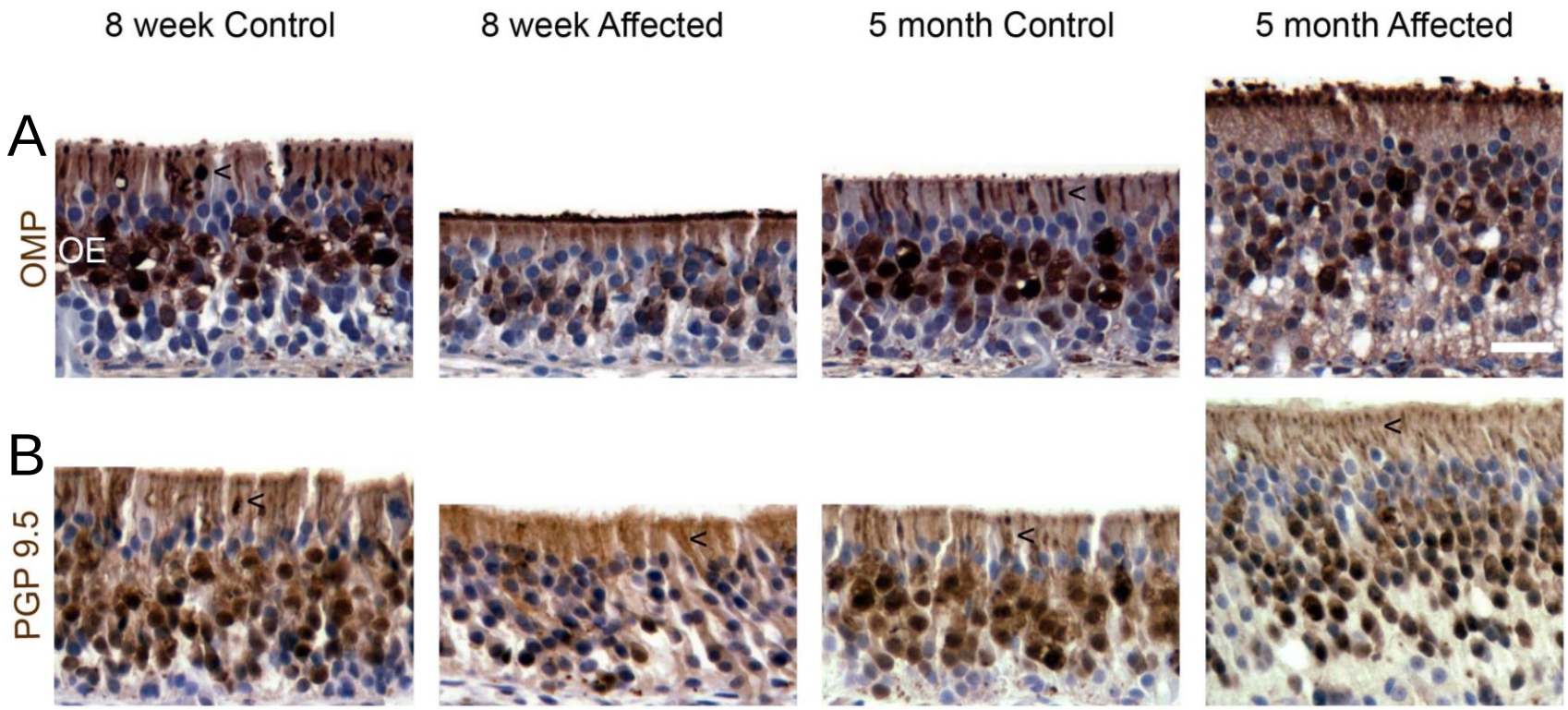

Figure 5.3. OMP and PGP 9.5 labeling in *CNGB1* affected dogs and age matched controls. Representative sections of the OE in the sections showed differences in the OE thickness between the *CNGB1* affected and age-matched control dogs. The OE of the 8 week old *CNGB1* affected dog is thinner than that of the 8 week old control dog while the 5 month *CNGB1* affected dog has thicker OE than both control dogs. (A) The sections are labeled with OMP which labels mature OSNs. The *CNGB1* affected dogs have less OMP positive stained OSNs than the control dogs, as determined by stereology. (B) The sections are labeled with PGP 9.5 which labels all OSNs. Note the increased number of OSN axons labeled with PGP 9.5 in the *CNGB1* affected dogs compared to the axons labeled with OMP (black arrow heads). The counterstain (blue) is hematoxylin. Size bar – 50 µm.

5.3.4 Olfactory bulbs in *CNGB1* affected dogs are morphologically normal

The OBs in the *CNGB1* affected dogs have normal morphology compared to control dogs (Figure 5.4). Labeling OB sections of the 8 week old *CNGB1* affected dog with OMP showed defined olfactory nerve, glomerular, external plexiform, mitral cell and inner plexiform layers, similar to the control dog. This data indicates that the 8 week old *CNGB1* affected dogs have normal development of the OBs.

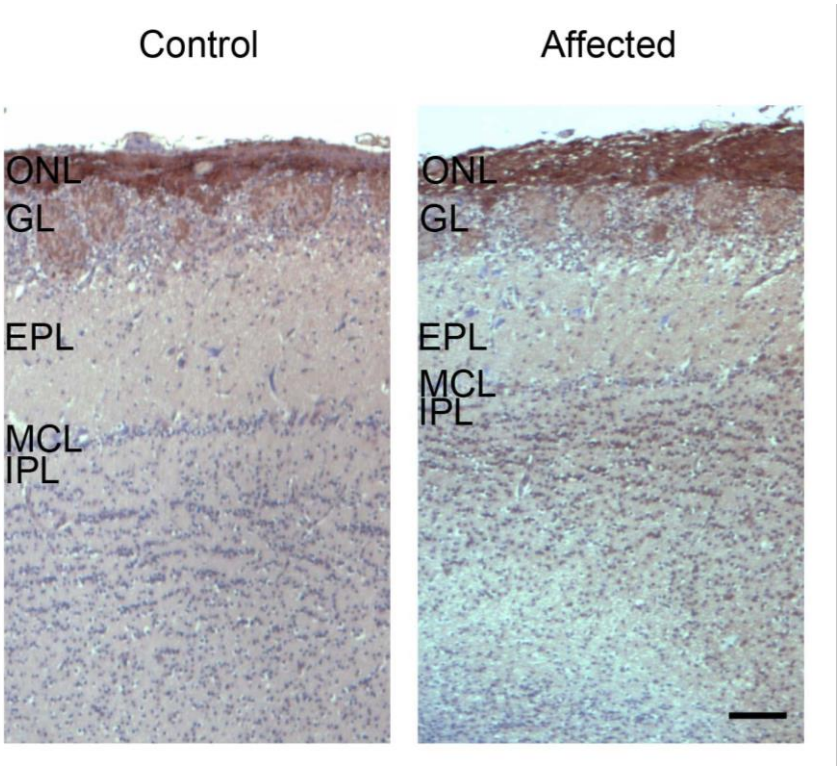

Figure 5.4. The olfactory bulb in the 8 week old *CNGB1* affected dog has normal morphology. The olfactory bulb has 5 layers which are visible in the control and *CNGB1* affected dog histological sections. The OSN axons are labeled with OMP (brown). The *CNGB1* affected dog has normal morphology of the OB. The counterstain (blue) is hematoxylin. Size bar 100 µm. ONL – outer nerve layer; GL – glomerular layer, EPL – external plexiform layer; MCL – mitral cell layer; IPL – inner plexiform layer.

5.3.5 Functional olfaction is reduced in *CNGB1* affected dogs

We developed a behavioral assay to test olfactory function in the *CNGB1* affected dogs. Only purebred Papillon dogs were tested (9 months to 6 years of age). The volume of food (2 g or 20 g) did not significantly impact the amount of time spent at the correct box for the *CNGB1* affected dogs and the controls dogs (p=0.685 and p=0.667 respectively). *CNGB1* affected dogs spent less time investigating the box containing the food than control dogs (2 g: p=0.004; 20 g: p=0.009; Figure 5.5A). A qualitative assessment was also conducted by a blinded observer. The observer would infer which box held the food based on the dog's behavior. For example, the control dogs would often paw or lick at the correct box, making it clear to the observer which box the food was in. The *CNGB1* affected dog behavior was significantly less likely to indicate which box the food was in (2 g: p=0.01; 20 g: p=0.002; Figure 5.5B). This means that about 30% of the time the *CNGB1* dogs indicated the correct box (compared to the controls dogs ~87%). Supplemental Table 5.S1 shows the mean values, p-values and statistical test used for the data presented in Figure 5.5. This data supports that the hypothesis that *CNGB1* affected dogs have decreased but not absent olfactory function.

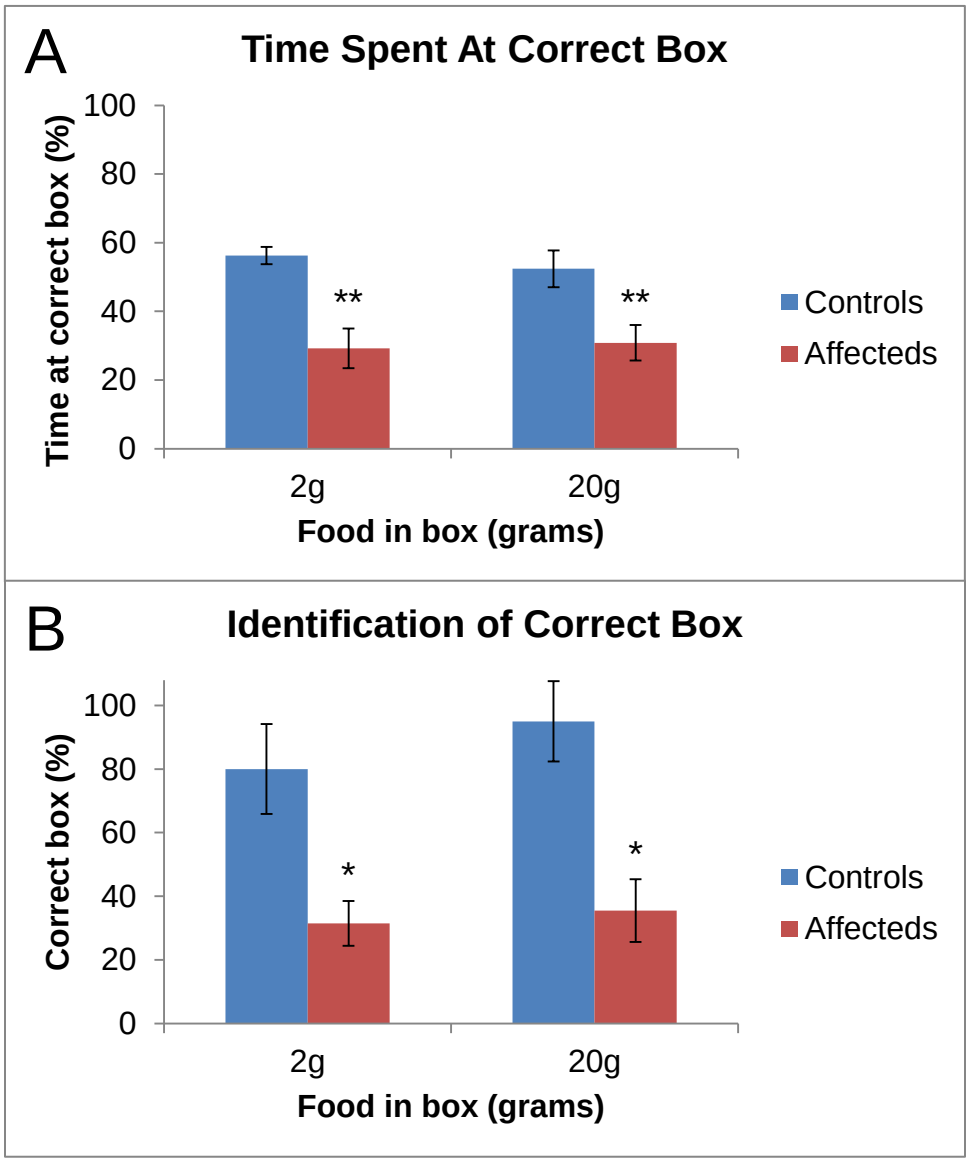

Figure 5.5. *CNGB1* affected dogs have decreased olfactory function. (A) The CNGB1 affected dogs spend significantly less time investigating the correct box than the control dogs at both amounts of food (2 g and 20 g). (B) The *CNGB1* affected dog's behavior indicated the correct box significantly fewer times than control dog behavior at both amounts of food. * - $p \leq 0.05$, ** - $p \leq 0.01$.

5.4 Discussion

In this study we showed that there is a significant decrease in *CNGB1* transcript expression in the OE, lack of detectable full length CNGB1 protein in the OSN cilia and decreased olfactory function as determined by a behavioral assay. Additionally, we showed that there is normal morphology of OE and OB but there is a difference in epithelial height and OSN volume.

The decrease in the *CNGB1* transcript to ~20% of wild type levels is within published values of nonsense-mediated mRNA decay (NMD; 5-36%) [10,11]. The levels of *CNGB1* transcript in the retina (42%, Chapter 3 Section 3.3.1) is about twice that of the OE levels but NMD efficiency between tissues of mouse knockout models have shown to be variable (16-36%) [11,12]. PCR amplification of OE cDNA showed the same exon skipping as was seen in the *CNGB1* affected retinal tissue (data not shown; see the discussion in Chapter 3 for more details about NMD and nonsense-associated alternative splicing). Future studies will be needed to understand the difference in NMD efficiency between the retina and the OE but are beyond the scope of this chapter.

Full length CNGB1b was not detectable in the 8 week old *CNGB1* affected OE but was localized correctly in the age-matched control dog. The C-terminal CNGB1 antibody will not detect the presence of a truncated CNGB1b in *CNGB1* affected dogs. A CNGB1 antibody is available that is targeted to the N-terminal region of CNGB1b (FPc21K, referred to as CNGB1 mid in Chapter 3) [3]. Initial attempts with this antibody in the OE were not successful. We have shown that the antibody labels the canine CNGB1 protein (Chapter 3) but it remains to be optimized in the paraffin-embedded fixed OE. In the *CNGB1-X26* mouse model full length CNGB1b was not expressed in OE but the CNGA2 and CNGA4 subunits were expressed. The OSNs in the *CNGB1-*

X26 mouse showed characteristics of abnormal channel behavior similar to heterologously expressed CNGA2 and CNGA4 channels [4]. Attempts to immunolabel canine tissue with the CNGA2 and CNGA4 antibodies were not successful. Comparisons of the canine CNGA2 and CNGA4 predicted protein sequences and the immunogens for CNGA2 and CNGA4 indicated that the antibodies should probably identify the canine proteins (>90% sequence similarity, http://blast.ncbi.nlm.nih.gov). Future work to optimize immunohistochemistry using the N-terminal CNGB1b, CNGA2 and CNGA4 antibodies in the canine OE tissue is needed.

The OE is morphologically normal but OE thickness differs between the *CNGB1* affected and control dogs. The OE is thinner in the 8 week old *CNGB1* affected dog compared to the control dog. The OE thickness is directly related to the volume of OSNs present in the OE, therefore, the thinner OE in the *CNGB1* affected dog may be due to the decreased volume of OMP positive OSNs in the OE [13]. However, the 5 month old *CNGB1* affected dog had a thicker OE than the age-matched control but the number of OMP positive OSNs in the rostral section was similar to the 8 week old *CNGB1* affected dog. The thickness seen in the rostral section of the 5 month old *CNGB1* affected dog is not explained by an increased number of OMP positive OSNs. The 5 month old *CNGB1* affected dog's caudal section had a much higher volume of OMP positive OSNs, which could explain the increased OE thickness in this section. One dog at each time point was investigated for the descriptive analysis of OE thickness and the OSN volume. Additional age-matched control and *CNGB1* affected dogs will be needed to do statistical assessments of these data. Figure 5.3B showed the *CNGB1* affected dog OEs had very few OMP positive axons and there were more

positive PGP 9.5 axons. This indicates that there are lower numbers of mature OSNs in the *CNGB1* affected dogs compared to the control dogs. OSNs need stimulation to mature, so the decreased number of OMP positive OSNs and labeled axons could be the result of decreased function in the OSNs [14-16]. Further work using the same stereological and morphological techniques used for the OMP positive volume assessments can be used with PGP 9.5 (to assess if the OE thickness is a factor of increased immature OSNs in the caudal section of the 5 month old *CNGB1* affected dog) and basal cell markers (to see if the 5 month old *CNGB1* affected dog has increased basal cells compared to control dogs).

Comparing the OBs of the 8 week old *CNGB1* affected and control dogs showed that the OBs have normal morphology at this age. Future work will be needed to assess how or if the OB changes over time. Preliminary work assessing the volumes of OB in *CNGB1* affected and controls dogs indicated that there may be a difference in OB volumes in older *CNGB1* affected dogs, however, this data may have been confounded by the physical characteristics of the control dogs used in the study (data not shown). Additional work investigating the OB volumes in *CNGB1* affected dogs will take into account skull shape and body size to decrease variables that could alter the results.

The developed behavior test to assess olfaction showed that the *CNGB1* affected dogs have decreased but not completely absent olfactory capabilities. The behavior test required little hands on training but was time consuming during the conditioning phase. The fact that the test did not require that the dogs were trained to complete it was important under the assumption that a *CNGB1* affected dogs were anosmic because training an anosmic dog to signal if it was able to smell would not be

possible. Additionally, handler bias in canine behavior can be a concern [7]. Previous studies have indicated that if a dog can smell, it will find food hidden in its pen [17]. The research Papillons were not as food oriented as one might anticipate. An assortment of food options were offered to the dogs until we found that the meat baby food was palatable to all of the Papillons in the study. We used 4 *CNGB1* affected dogs and 2 control dogs for the behavioral assessment and we did not use any Papillon crosses as controls to decrease any across breed variability there might be on olfaction or food motivation. Preliminary trials with a Beagle/Papillon cross showed that (at least with the single dog tested) there was a behavioral difference between the purebred Papillons and the Beagle/Papillon cross (data not shown). The assessment showed that the *CNGB1* affected Papillons occasionally identified the box containing the food but were not as successful as the control Papillons. We did not test for significance between the *CNGB1* affected dogs and random chance so we cannot conclude from this data whether the *CNGB1* affected dogs are completely anosomic. However, anecdotal evidence from *CNGB1* affected dogs outside the testing procedure indicates that the dogs are capable of smelling at least to some degree.

Recent studies have shown successful adenoviral vector gene therapy in mouse OSNs as a model for ciliopathies [18]. With the characterization of the *CNGB1* affected dog olfactory phenotype and the development of a behavioral assessment the *CNGB1* affected dog model is optimal for any future large animal OSN gene therapy trials.

5.5 Supplemental information

Table 5.S1. Comprehensive table of data, statistical analyses and *p*-values corresponding to Figure 5.3

Figure 5.3A Quantitative Olfaction Testing				
Food	Control[1]	*CNGB1* Affected[1]	Statistical Analysis[2]	Pval
2 g	56.3	29.2	ST	0.004
20 g	52.4	30.9	ST	0.009
Figure 5.3B Qualitative Olfaction Testing				
Food	Control[1]	*CNGB1* Affected[1]	Statistical Analysis[2]	Pval
2 g	80.0	31.4	M-W	0.018
20 g	95.0	35.5	M-W	0.011

1. Mean values of the percentage of time the dog spent (Figure 5.3A) or indicated (Figure 5.3B) at the box containing the food
2. Statistical analysis: ST – Student t-test; M-W – Mann-Whitney Rank Sum Test

REFERENCES

REFERENCES

1. Kaupp UB, Niidome T, Tanabe T, Terada S, Bönigk W, et al. (1989) Primary structure and functional expression from complementary DNA of the rod photoreceptor cyclic GMP-gated channel. Nature (London) 342: 762-766.

2. Kaupp UB, Seifert R (2002) Cyclic nucleotide-gated ion channels. Physiological Reviews 82: 769-824.

3. Bonigk W, Bradley J, Muller F, Sesti F, Boekhoff I, et al. (1999) The native rat olfactory cyclic nucleotide-gated channel is composed of three distinct subunits. Journal of Neuroscience 19: 5332-5347.

4. Michalakis S, Reisert J, Geiger H, Wetzel C, Zong XG, et al. (2006) Loss of CNGB1 protein leads to olfactory dysfunction and subciliary cyclic nucleotide-gated channel trapping. Journal of Biological Chemistry 281: 35156-35166.

5. Winkler PA, Ekenstedt KJ, Occelli LM, Frattaroli AV, Bartoe JT, et al. (2013) A large animal model for CNGB1 autosomal recessive retinitis pigmentosa. PLoS One 8: e72229.

6. Yang M, Crawley JN (2009) Simple behavioral assessment of mouse olfaction. Current Protocols in Neuroscience Chapter 8: Unit 8 24.

7. Lit L, Schweitzer JB, Oberbauer AM (2011) Handler beliefs affect scent detection dog outcomes. Animal Cognition 14: 387-394.

8. Craven BA, Neuberger T, Paterson EG, Webb AG, Josephson EM, et al. (2007) Reconstruction and morphometric analysis of the nasal airway of the dog (Canis familiaris) and implications regarding olfactory airflow. The Anatatomical Record (Hoboken) 290: 1325-1340.

9. Carey SA, Plopper CG, Hyde DM, Islam Z, Pestka JJ, et al. (2012) Satratoxin-G from the black mold Stachybotrys chartarum induces rhinitis and apoptosis of olfactory sensory neurons in the nasal airways of rhesus monkeys. Toxicologic Pathology 40: 887-898.

10. Maquat LE (1995) When cells stop making sense: effects of nonsense codons on RNA metabolism in vertebrate cells. RNA 1: 453-465.

11. Zetoune AB, Fontaniere S, Magnin D, Anczukow O, Buisson M, et al. (2008) Comparison of nonsense-mediated mRNA decay efficiency in various murine tissues. BMC Genetics 9: 83.

12. Isken O, Maquat LE (2007) Quality control of eukaryotic mRNA: safeguarding cells from abnormal mRNA function. Genes & Development 21: 1833-1856.

13. Graziadei PPC, Montigraziadei GA (1979) Neurogenesis and neuron regeneration in the olfactory system of mammals. I. Morphological aspects of differentiation and structural organization of the olfactory sensory neurons. Journal of Neurocytology 8: 1-18.

14. Farbman AI, Brunjes PC, Rentfro L, Michas J, Ritz S (1988) The effect of unilateral naris occlusion on cell dynamics in the developing rat olfactory epithelium. Journal of Neuroscience 8: 3290-3295.

15. Suh KS, Kim SY, Bae YC, Ronnett GV, Moon C (2006) Effects of unilateral naris occlusion on the olfactory eptihelium of adult mice. Neuroreport 17: 1139-1142.

16. Kikuta S, Sakamoto T, Nagayama S, Kanaya K, Kinoshita M, et al. (2015) Sensory deprivation disrupts homeostatic regeneration of newly generated olfactory sensory neurons after injury in adult mice. Journal of Neuroscience 35: 2657-2673.

17. Houpt KA, Shepherd P, Hintz HF (1978) Two methods for producing peripheral anosmia in dogs. Lab Anim Sci 28: 173-177.

18. McIntyre JC, Davis EE, Joiner A, Williams CL, Tsai IC, et al. (2012) Gene therapy rescues cilia defects and restores olfactory function in a mammalian ciliopathy model. Nature Medicine 18: 1423-1429.

CHAPTER 6

DISCUSSION AND FUTURE DIRECTIONS

While much of the work in this dissertation is basic research, it also has some very practical applications. Both the basic research and the practical applications will be described in a primarily historical context of this final chapter.

In 2009 the Papillon Club of America (PCA) located intact male and female Papillons that were affected with PRA. The pair was bred and two members of the PCA Health and Genetics Committee flew to Sweden to pick up the pregnant female Papillon. The female and her two offspring were the foundation stock of the research colony used for this dissertation. These three dogs were the small family group of cases used to identify the region of homozygosity containing the *CNGB1* gene. The *CNGB1* gene had not been directly sequenced in the canine genome and many of the exons were incorrectly predicted. Fortunately, the mutation was in a correctly predicted exon and was identified early in the process of Sanger sequencing the gene. It took an additional few months to piece together the intron/exon boundaries and the mRNA sequence of the canine *CNGB1* gene. The additional effort put into sequencing the *CNGB1* transcript prepared us for an easy transition into the gene therapy trials, in which the coding region that I pieced together was used to synthesize the AAV5-cCNGB1 vector genome. The early identification of the mutation enabled us to grow our research colony. Papillons are small dogs and have litters of 1-3 very small puppies, which is less than ideal for a research setting. We were able to cross the Papillons with beagles and choose the larger and heartier offspring to expand our research colony. To repay the PCA and the many breeders who helped us with sample collection, we developed a genotyping assay for the breeders. Since the development of the genotyping assay over 2,600 Papillons have been tested for the *CNGB1* mutation

(http://www.pcagenetics.com/). The use of this test for informed breeding decisions may eradicate this form of PRA in Papillons dogs.

The *CNGB1* mutation accounts for about 70% of Papillons affected with PRA. The number of unaccounted PRA cases exceeds what would be expected from phenocopies, misdiagnoses and sample mix-ups. It is likely that the ~30% of the non-*CNGB1* PRA-affected Papillons have a mutation in different gene causing their form of PRA. It has been of great interest to the Comparative Ophthalmology (CO) lab and the PCA to account for the other form(s) of PRA within the Papillon breed. On the original SNP array (used to locate the region of homozygosity harboring the *CNGB1* mutation, Chapter 2) we had 4 PRA-affected dogs that did not have the *CNGB1* mutation. With the help of the PCA, our lab and the lab at Optigen, LLC (Ithaca, Ney York) we recruited an additional 6 non-*CNGB1* affected DNA samples. These additional 6 samples were genotyped using the same protocol as the original samples and the two data sets were merged for analyses. A genome-wide association analyses and model testing was conducted by the genome analysis toolset, PLINK. No regions reached genome-wide significance. Any regions near genome-wide significance did not harbor any candidate genes. We will continue to recruit samples from non-*CNGB1* affected Papillons to add to our current genotyped dogs. The PCA is actively searching for non-CNGB1 affected Papillons which are intact to breed the CO lab a research litter. With the continued support and dedication of the PCA, I am confident that the CO lab will be able to identify the additional form(s) of PRA within the Papillon breed.

The establishment of the *CNGB1* affected dog research colony allowed us to characterize the phenotype of the mutation in the retina and olfactory system. The

CNGB1 transcript was significantly decreased in retinal and olfactory epithelial tissues. Sequencing the *CNGB1* transcript isolated from *CNGB1* affected retinal tissue showed that our initial prediction of the location of the premature stop codon was incorrect. The identified mutation (a 6 bp insertion and a 1 bp deletion) results in skipping of the exon harboring the mutation. This exon skipping created a premature stop codon creating a shorter open reading frame, making the *CNGB1* affected dog mutation and the *CNGB1-X26* mouse mutation nearly identical. Despite the premature stop codon, decreased transcript levels and predicted loss of function of the *CNGB1* protein there is presence of truncated CNGB1 protein in the retina. The *CNGB1* affected dogs have decreased and abnormal rod function at the earliest age tested although histological evidence supports normal development of the rod photoreceptors. Immunohistochemistry on retinal sections show presence of rod-associated proteins until 2.5 years. The retina degenerates slowly over the 6 years we have followed the mutation, with functional day-light vision being maintained in the *CNGB1* affected dogs for at least 6 years.

Future work characterizing the retinal phenotype will involve detailed early rod ERG analysis to understand the origin of the second positive peak in the scotopic ERG. We hypothesize that this wave is residual rod function, possibly coming from homomeric CNGA1 channels. It would be interesting to carefully track the second peak amplitude and collect retinal tissues at different stages of its development to see if it corresponds with CNGA1 levels in the rod outer segments. However, the number of *CNGB1* affected dogs that would be needed for this type of study outweighs the information that could be gleaned from such a study. Currently, we are using intricate ERG protocols and analyses to understand the residual rod function in the *CNGB1* affected dogs.

The olfactory phenotype of the *CNGB1* affected dogs is more subtle than the retinal phenotype. In the 8 week old *CNGB1* affected dogs the olfactory epithelium (OE) appears thinner while at 5 months the OE is much thicker than control dogs. These observations were from one *CNGB1* affected and control dog at each time point, future work will be needed to confirm that these differences are due to the *CNGB1* mutation and not normal variation seen in dog OE. The olfactory bulb (OB) to brain ratio is smaller in *CNGB1* affected dogs than in control dogs, suggesting that the OBs are affected by the *CNGB1* mutation. Additional immunohistochemistal and morphological studies on the OBs will be needed to investigate the effect of the *CNGB1* mutation on this tissue. A behavioral test was developed to investigate the functional olfactory phenotype of the *CNGB1* affected dog. For this study, we only used purebred Papillons which limited our sample size. However, we saw a significant decrease in olfaction in the *CNGB1* affected dogs although the dogs were not anosmic.

CNGB1 splice variants are also present in testes and the flagellum of sperm. The *CNGB1* affected dogs and mice are able to produce offspring so little work has been conducted on either of these models characterizing the effect of a *CNGB1* mutation in this tissue. Testicular tissue has been collected from all *CNGB1* affected and heterozygous male dogs that have been euthanized. Tissue has been flash frozen or fixed in paraformaldehyde for future studies. In very limited observations, we have noticed that the semen from a *CNGB1* affected Papillon could not be frozen and stored; the sample was not usable after thawing. Our male breeding Papillon has decreased sperm count (although he was obviously still able to produce offspring). Additionally, many of the male *CNGB1* affected dogs are cryptorchid. Whether these observations

are unrelated or due to the *CNGB1* mutation is purely speculative at this point but may be of interest as the research colony expands.

One of the benefits of the detailed retinal phenotyping was to understand the natural history of the disease so that when gene therapy was developed and utilized we would know how the disease was altered due to the therapy. *CNGB1* affected dogs were treated with an adeno-associated viral (AAV) vector containing a wildtype copy of the canine *CNGB1* transcript (AAV5-cCNGB1). All dogs treated with AAV5-cCNGB1 showed vision rescue. Significant ERG rescue was seen and maintained in eyes injected with a higher titer of AAV5-cCNGB1 ($5x10^{12}$) and no detrimental effects of the therapy was noted. Full length CNGB1 was expressed in the rod outer segments of the treated regions. The slow retinal degeneration and the success of the first gene therapy trial highlights the *CNGB1* affected as a useful model in future optimization of gene therapy for translation into human patients.

Recent collaborations with clinicians and patients (containing mutations in the *CNGB1* gene) have shown that there is great interest in developing and optimizing gene therapy for the treatment of retinitis pigmentosa 45 (RP45). These groups are working together to form a foundation to locate and recruit additional RP45 patients for future gene therapy clinical trials. The *CNGB1* affected dog will be used to optimize the AAV vector that will be utilized for the human gene therapy clinical trials.